รายงานสรุปความก้าวหน้าของโครงการในรอบ 3 ปี

โครงการวิจัย: การศึกษาตัวเร่งปฏิกิริยาสำหรับใช้ในอุตสาหกรรมปิโตรเคมีและใช้กำจัดมลพิษทางอากาศ

A study of catalysts for petrochemical industry and for air pollution abatement

(สัญญาเลขที่ RTA/02/2540)

โดย ศ.ดร. ปิยะสาร ประเสริฐธรรม

จุฬาลงกรณ์มหาวิทยาลัย

สัญญาเลขที่ RTA/02/2540.

โครงการวิจัย: การศึกษาตัวเร่งปฏิกิริยาสำหรับใช้ในอุตสาหกรรมปิโตรเคมีและใช้กำจัดมลพิษทางอากาศ

A study of catalysts for petrochemical industry and for air pollution abatement

รายงานสรุปความก้าวหน้าของโครงการในรอบ 3 ปี

ชื่อหัวหน้าโครงการ ศ.ดร. ปิยะสาร ประเสริฐธรรม

รายงานในช่วงเวลาตั้งแต่วันที่ 1 ธันวาคม พ.ศ. 2541 **ถึง** 30 พฤศจิกายน พ.ศ. 2543

1. กิจกรรมที่ได้ดำเนินการ

1.1 ด้านการประสานงานระหว่างผู้ดำเนินการ

- เนื่องจากคณะผู้ดำเนินการประกอบด้วยอาจารย์จากหลายสถาบัน ดังนั้นการปรึกษางานจึงทำด้วยวิธีต่อไปนี้

- อ.ดร. นุรักษ์ กฤษดานุรักษ์ จากมหาวิทยาลัยขอนแก่น ใช้การติดต่อทางโทรศัพท์ และเดินทางมาจุฬาลงกรณ์มหาวิทยาลัย
- ผศ.ดร. ชาคริต ทองอุไร จากมหาวิทยาลัยสงขลานครินทร์ ใช้การติดต่อทางโทรศัพท์ และเดินทางมาจุฬาลงกรณ์มหาวิทยาลัย
- อ.ดร. วรากรณ์ ธนะกุลรังสรรค์ จากสถาบันเทคโนโลยีราชมงคล วิทยาเขตเทคนิค-กรุงเทพ ใช้การติดต่อทางโทรศัพท์ และเดินทางมาจุฬาลงกรณ์มหาวิทยาลัย

1.2 ด้านการเข้าร่วมประชุมทางวิชาการระดับนานาชาติ

1.2.1 การสัมมนาทางวิชาการ 15th Canadian Symposium on Catalysis" ที่ประเทศคานาดา ในวันที่ 17-20 พฤษภาคม พ.ศ. 2541

1. "Effect of NO on Coke Formation for Propane and Propene Conversion via Cu/Na-ZSM-5 Catalyst"

2. "Determination of Coke Propagation on Metal and Support of Pt/Al2O3 by Using Schulz-Flory Distribution Theory"
3. "Comparative Study of Coke Deposition on Pt Catalysts in Reactions with and with out Oxygen"

1.2.2 Regional Symposium on Chemical Engineering ณ ประเทศมาเลเซีย (2540)

1. "Determination of high temperature coke deposition on metal active sites of propane dehydrogenation catalysts"
2. "Adsorption study on Cu/ZSM-5 of NO Reduction by Hydrocarbon using Transient Technique"

1.2.3 Regional Symposium on Chemical Engineering ณ ประเทศฟิลิปปินส์ (2541)

1. "The Effect of NO on Coke Formation over Pt Catalyst in NO Reduction by Propene under Lean-Burn Condition"
2. "Determination of Coke Propagation on Metal and Support of Pt/Al_2O_3 by Using Schulz-Flory Distribution Theory"

1.2.4 Miami 2nd World Congress on Environmental Catalysis ณ ประเทศสหรัฐอเมริกา (2541)

1. "Removal of Automotive Emissions By Co/Pd Three-way Catalysts"
2. "Relationship Between Coke Formation , Hydrocarbon and NO Conversion on Selective Catalytic Reduction of NO by Propene on Cu/Na –ZSM-5 with Excess Oxygen",
3. "Role of NO Propene and NO Conversion over Pt/ Al_2O_3 Catalyst under Lean-Burn Condition at low temperature"

1.2.5 The 8th Congress of Asian Pacific Conference of Chemical Engineering ที่เมืองโซล ประเทศเกาหลี ระหว่างวันที่ 16 – 19 สิงหาคม พ.ศ. 2542

1. "Influence of Fe and Zn loading method over MFI- type zeolite catalysts on toluene methylation"
2. "Aromatization of light paraffins over metal-containing MFI-type catalysts"
3. "Catalytic cracking of n-octane over Y-type zeolite catalyst"
4. "Isomerization of n-Hexane over beta zeolite"

1.2.6 งานประชุมทางวิชาการระดับนานาชาติ The Regional Symposium on Chemical Engineering 1999 ที่จังหวัดสงขลา ระหว่างวันที่ 22 – 24 พฤศจิกายน พ.ศ. 2542

1. "Synergistic effect in catalytic hydrogenation on modified supported nickel catalyst by platinum"
2. "Oxidation of C_3H_8, C_3H_6 and CO over V-Mg-O/TiO_2 catalyst"

3. "Oxidation of C_3H_8, C_3H_6 and CO over Co-Mg-O/TiO_2 catalyst"
4. "The use of infrared-spectroscopy in studies of metal oxide surfaces: experience on experimental procedure"
5. "Dehydrogenation of propane in a palladium membrane reactor"
6. "Oxidative dehydrogenation of butane in a ceramic membrane reactor"

1.2.7 การสัมมนาทางวิชาการ 2nd Asia Pacific Congress on Catalysis APCAT 2000" ที่ประเทศออสเตรเรีย ในวันที่ 31 มกราคม – 3 กุมภาพันธ์ พ.ศ. 2543

1. "Activation of acetylene selective hydrogenation catalysis using oxygen containing compound"
2. "Influence of Fe or Zn loading method over MFI type zeolite catalysts on toluene methylation"
3. "Determination of coke propagation on metal and support of Pt/Al_2O_3 using Schulz-Flory distribution theory"
4. "Effect of Lantana on SiO_2-supported Pd catalyst over catalytic coversion of ethanol to syngas"
5. "Non oxidative methane coupling over Co-ion exchanged Y type zeolite"

1.3 การประชุมทางวิชาการระดับนานาชาติที่กำลังจะเข้าร่วม

1.3.1 งานประชุมทางวิชาการระดับนานาชาติ The Regional Symposium on Chemical Engineering 2000 ที่ National University of Singapore ระหว่างวันที่ 10 – 12 ธันวาคม พ.ศ. 2543

1. "Ethanol and 1-propanol oxidation over supported cobolt oxide catalyst"
2. "Monocyclopentadienyl Metallocene catalyst with methylaluminoxane as cocatalyst for styrene polymerization"
3. "Kinetics of Liquid Phase Synthesis of Ethyl *tert*-Butyl Ether from *tert*-Butyl Alcohol and Ethanol Catalyzed by β-Zeolite"

1.3.2 งานประชุมวิชาการระดับนานาชาติ Bangkok International Conference on Catalysis จัดที่ โรงแรมมณฑียรริเวอร์ไซด์ วันที่ 7-9 มกราคม 2544

1. "Design of Electrode Catalyst for Solid Oxide Fuel Cell Type Reactor"
2. "Application of a palladium membrane reactor to the dehydrogenation of ethylbenzene to styrene"
3. "Cumene synthesis from benzene and isopropanol over zeolite"

4. "Oxidation of alcohol's to aldehyde over V-MgO/TiO_2 catalyst"
5. "Effect of the preparation with O_2 and/or O_2-containing compounds on the catalytic performance of Pd-Ag/Al_2O_3 for the selective hydrogenation of acetylene"

1.4 การเสนอผลงานในที่ประชุมวิชาการในประเทศไทย

1.4.1 การประชุมทางวิชาการวิศวกรรมเคมีและเคมีประยุกต์แห่งประเทศไทย ครั้งที่ 8 ณ มหาวิทยาลัยมหิดล วันที่ 17 – 18 ธันวาคม พ.ศ. 2541

1. "Role of External Electron Donor in Supported Ziegler-Natta Catalyst on Isotacticity of Polypropylene"
2. "ผลของตัวรองรับที่มีต่อคุณสมบัติในการออกซิเดชันของโคบอลต์ออกไซด์"
3. "ผลของลำดับการเติมทังสเตนบนตัวเร่งปฏิกิริยาวานาเดียมออกไซด์บนตัวรองรับไททาเนียมออกไซด์ที่ใช้ในการเลือกกำจัดแก๊สไนตริกออกไซด์"
4. "บทบาทความเป็นกรดของพื้นผิวตัวเร่งปฏิกิริยาวานาเดียม (V) ออกไซด์บนไททาเนียม (IV) ออกไซด์ต่อความว่องไวในการเกิดปฏิกิริยาการเลือกรีดิวซ์ไนตริกออกไซด์ด้วยแอมมอเนีย"
5. "คุณสมบัติในการออกซิเดชันของตัวเร่งปฏิกิริยาวาเนเดียมแมกนีเซียออกไซด์บนตัวรองรับไทเทเนียมออกไซด์"

1.4.2 การประชุมทางวิชาการครั้งที่ 37 ณ มหาวิทยาลัยเกษตรศาสตร์ วันที่ 23 กุมภาพันธ์ พ.ศ. 2542

1. "Dehydrogenation of Propane in a Palladium Membrane Reactor: ii) Determination of the rate law for the dehydrogenation of propane on Pt-Sn-K/Al_2O_3 catalyst"

1.4.3 การประชุมทางวิชาการครั้งที่ 38 ณ มหาวิทยาลัยเกษตรศาสตร์ วันที่ 1-4 กุมภาพันธ์ พ.ศ. 2543

1. "การศึกษาปฏิกิริยาออกซิเดทีฟดีไฮโดรจีเนชันของบิวเทนในเครื่องปฏิกรณ์แบบอินเนอร์ทเมมเบรน"

1.4.4 การประชุมทางวิชาการวิศวกรรมเคมีและเคมีประยุกต์แห่งประเทศไทย ครั้งที่ 10 ณ BITECH วันที่ 24-25 ตุลาคม พ.ศ. 2543

1. "Photocatalytic Decomposition of 2-propanol over TiO_2 catalyst"
2. "Surface basicity characterization using probe molecule adsorption"
3. "การผลิตซินดิโอแทคติคพอลิสไตรีนโดยใช้ไตรเอทิลอะลูมินัมเป็นสารกระตุ้น"

2. ผลงาน

2.1 บทความวิจัยในวารสารระดับนานาชาติ จำนวน 18 ผลงาน

1. "Determination of coke Deposition on Metal Active sites of Propane Dehydrogenation Catalysts" *Stud. Surf. Sci. Catal.* vol. 111 (1997) 153. (เอกสารแนบ 1)
2. "Comparative study of Coke Deposition on Catalysts in Reactions with and without oxygen" *Res.Chem.Intermed.* Vol. 24 No 5 (1998) 605. (เอกสารแนบ 2)
3. "Role of Pt and Alumina during the oxidation of Coke Deposits on Propane Dehydrogenation Catalysts" *Korean Journal of Chemical Engineering*, vol. 15(1998) 486. (เอกสารแนบ 3)
4. "Transient study of the effect of residual cation in in Cu/ZSM-5 for SCR of NO by hydrocarbon" *Chemical Engineering Science* vol. 55 (2000) 2249. (เอกสารแนบ 4)
5. "Influence of Fe or Zn loading Methane, over MFI Type Zeolite Catalysts on Toluene Methylation," *Korean Journal of Chemical Engineering* vol. 17 (2000) 414. (เอกสารแนบ 5)
6. "Activation of Pd-Ag Catalyst for selective hydrogenation of acetylene via nitrous oxide addition," *Reaction Kinetics and Catalysis Letters* vol. 70 (2000) 125. (เอกสารแนบ 6)
7. "Coke formation over Pt-Sn-K/Al_2O_3 in C_3, C_5, C_5-C_8 alkane dehydrogenation" *Chemical Engineering Journal* vol. 77(2000) 215. (เอกสารแนบ 7)
8. "Oxidative Coupling of Methane in a Ceramic Membrane Uniform oxygen Permeation Pattern, *J. Chin. Inst. Chem. Engrs*, vol. 31 (2000) 19. (เอกสารแนบ 8)
9. "Kinetics for the dehydrogenation of propane on Pt-Sn-K/Al2O3 catalyst" *Journal of Chemical Engineering of Japan* vol. 33 No. 3 (2000) 529. (เอกสารแนบ 9)
10. "Dependence of hydrogen pressure on the permeation rate of hydrogen through a composite palladium membranes" *Journal of Chemical Engineering of Japan* vol. 33 No. 2 (2000) 330. (เอกสารแนบ 10)
11. "The effect of direction of hydrogen permeation on the rate through a composite palladium membrane" *Journal of Membrane Science* vol. 175 (2000) 19. (เอกสารแนบ 11)
12. "Synthesis of large-surface area silica-modified titania ultrafine particles by the glycothermal method" *J. of Materials Science Letters* vol. 19 (2000) 1439. (เอกสารแนบ 12)
13. " Selective Oxidation of Ethanol and 1-Proponol over V-Mg-O/TiO_2 catalyst", Chemistry Letter (2000) 968-969. (เอกสารแนบ 13)
14. "Deactivation of the metal and acedic function for Pt, Pt-Sn, Pt-Sn-K using physically mixed catalyst" *Korean J. of Chem. Eng.* vol. 17 (2000) 548. (เอกสารแนบ 14)

15. "Activation of Acetylene Selective Hydrogenation Catalysts using oxygen containing Compounds" *Catalysis Today* (accepted 29 August 2000). (เอกสารแนบ 15)
16. "Effect of organic solvents on the thermal stability of porous silica-modified alumina powders prepared via one pot solvothermal synthesis" *Inorg. Chem. Commu.* (accepted Aug 16, 2000). (เอกสารแนบ 16)
17. "Effect of Pd on the stability improvement of Cu/H-MFI for NO removal under hydrothermal pretreatment condition" *J. Molecular Catalysis* (accepted September 30, 2000). (เอกสารแนบ 17)
18. Isomerization of n-hexane over Pt ion exchanged β zeolite. Reaction Kinetics and Catalysis Letters 2000 (accepted October, 2000) (เอกสารแนบ 18)

2.2 จำนวนผลงานที่อยู่ในขั้นตอนการแก้ไข จำนวน 5 ผลงาน

1. "Selective oxidation of achohols over Co-Mg-O catalyst" นำเสนอในวารสาร Journal of the Chinese Institute of Chemical Engineers ขณะนี้อยู่ในขั้นตอนการพิจารณาต้นฉบับที่ผ่านการแก้ไขแล้ว
2. " The catalytic performance for NO elimination of Co- and Cu-species in MFI zeolite and the effect of high temperature calcination on the state of copper" เสนอในวารสาร Microporous and Mesoporous Material ขณะนี้อยู่ในขั้นตอนการพิจารณาต้นฉบับที่ผ่านการแก้ไขแล้ว
3. "Cooperative effect of Pt and alumina on catalyst deactivation for dehydrogenation reaction" เสนอในวารสาร Reaction Kinetics and Catalysis Letters ขณะนี้อยู่ในขั้นตอนการแก้ไข
4. "Role of Sn and K on Hydrogen Spillover on Pt/γ-Al_2O_3 Catalyst" นำเสนอในวารสาร Journal of the Chinese Institute of Chemical Engineers ขณะนี้อยู่ในขั้นตอนการแก้ไข
5. "Effect of organic solvent on the synthesis of silica modified titanium (IV) oxide นำเสนอในวารสาร Journal of the Chemical Engineering of Japan ขณะนี้อยู่ในขั้นตอนการแก้ไข

2.3 ผลงานที่อยู่ระหว่างการพิจารณา จำนวน 3 ผลงาน

1. "Effect of pretreatment of O_2 and O_2-containing compounds on the catalytic performance of Pd-Ag/Al_2O_3 for acetylene dehydrogenation" เสนอในวารสาร Applied Catalysis A เมื่อ 9 กันยายน 2543
2. "The nature and distribution of coke on the metal sites and the support sites for Pt, Pt-Sn and Pt-Sn-K catalysts applied a physical mixture" เสนอในวารสาร Canadian Journal of Chemical Engineering เมื่อ 20 กรกฎาคม 2543

3. "Application of Ceramic Membrane Reactor to Oxidative Dehydrogenation of *n*-Butane" นำเสนอในวารสาร Chemical Engineering Journal เมื่อ 2 ตุลาคม 2543

2.5 จำนวนนิสิตที่จบ

2.5.1 ดุษฎีบัณฑิต สำเร็จการศึกษาแล้ว 3 คน

1. นาย นครินทร์ มงคลศิริ
2. นาย ธนา พูลทรัพย์สวัสดิ์
3. น.ส. สุนีย์ ศรีหิรัญพัลลภ

2.5.2 มหาบัณฑิต สำเร็จการศึกษาแล้ว 21 คน

1. น.ส. ภาวิณี สินทรโก
2. น.ส. สุภาภรณ์ ขอบุญส่งเสริม
3. น.ส. พูนทรัพย์ ตรีภพนาถกูล
4. นาย อาทิตย์ เนรมิตตกพงษ์
5. นาย เกรียงศักดิ์ ไกรวัฒนวงศ์
6. น.ส. หฤทัย ตั้งอุดมวงษา
7. น.ส. อรวรรณ กนกรัตนา
8. น.ส. นิษฐกานต์ ฉัตรเท
9. น.ส. วิไลวรรณ เยื้องสวัสดิกูล
10. นางสาว ระพีพรรณ เล็กเลิศสุนทร
11. นาย นิพนธ์ คนองชัยยศ
12. นางสาว วนิดา ยังวนิชเศรษฐ
13. นางสาว เพียงพร ล้ออัศจรรย์
14. นางสาว วราภรณ์ มากพูน
15. นาย วิโรจน์ จรลีชาญชัย
16. นาย ศักดิ์ชัย กิตติเกิดกุลชัย
17. นาย สุวัฒน์ ลิ้มตระกูล
18. นางสาว ภูริดา พิมานมาศ
19. นาย พงศ์พรหม เฉลิมวรรณพงศ์
20. นาย ศิพิระ กุหลาบแก้ว
21. นางสาว สุดศิริ เหมศรี

2.6 จำนวนผู้ช่วยศาสตราจารย์ที่ได้

1. ดร. ธราธร มงคลศรี
2. ดร. นุรักษ์ กฤษดานุรักษ์
3. ดร. สุทธิชัย อัสสะบำรุงรัตน์

2.7 จำนวนรองศาสตราจารย์

ผศ.ดร. ธราธร มงคลศรี ได้ยื่นเอกสารเพื่อขอรับการพิจารณาตำแหน่งรองศาตราจารย์เมื่อวันที่ 2 มิถุนายน 2543

2.8 การจัดสัมมนาทางวิชาการ

1. ได้มีการจัดสัมมนาทางวิชาการเมื่อวันที่ 27 พฤศจิกายน พ.ศ. 2541 โดยการสัมมนามีหัวข้อว่า "Recent Development of Catalysis in Thailand" ซึ่งจัดที่ชั้นที่ 12 อาคาร 4 คณะวิศวกรรมศาสตร์ จุฬาลงกรณ์มหาวิทยาลัย
2. ได้มีการจัดสัมมนาทางวิชาการในหัวข้อ "ตัวเร่งปฏิกิริยากับสิ่งแวดล้อม" เมื่อวันที่ 29 พฤศจิกายน 2542 ณ ห้อง 209 ตึก 3 คณะวิศวกรรมศาสตร์ จุฬาลงกรณ์มหาวิทยาลัย
3. ได้มีการจัดสัมมนาทางวิชาการเมื่อวันที่ 6 ตุลาคม พ.ศ. 2543 โดยการสัมมนามีหัวข้อว่า "ตัวเร่งปฏิกิริยากับอุตสาหกรรมปิโตรเคมี" ซึ่งจัดที่ชั้นที่ห้อง 209 ตึก 3 คณะวิศวกรรมศาสตร์ จุฬาลงกรณ์มหาวิทยาลัย

2.9 สรุปผลงาน

ตารางที่ 1 สรุปผลงานตามข้อเสนอโครงการและผลงานในปัจจุบันประจำปี พ.ศ. 2541 - 2543

ผลงาน	ข้อเสนอ	ผลงาน
1. บทความลงวารสารระดับนานาชาติ	17	18 + (5)[1] + (3)[2]
2. ประชุมทางวิชาการระดับนานาชาติ	-	33
3. ประชุมทางวิชาการระดับชาติ	-	10
4. ดุษฎีบัณฑิต	3	3
5. มหาบัณฑิต	21	21
6. รองศาสตราจารย์	1	(1)[3]
7. ผู้ช่วยศาสตราจารย์	2	3
8. การจัดสัมมนาทางวิชาการ	3	3

หมายเหตุ [1] จำนวนบทความลงวารสารระดับนานาชาติที่อยู่ในขั้นตอนการแก้ไข (revised manuscripts)

[2] จำนวนบทความลงวารสารระดับนานาชาติที่อยู่ในขั้นตอนการพิจารณา

[3] ยื่นเอกสารเพื่อขอตำแหน่งรองศาสตราจารย์เมื่อวันที่ 9 มิถุนายน 2543 ขณะนี้อยู่ในขั้นตอนการพิจารณา

ลงนาม .....

(ศ.ดร. ปิยะสาร ประเสริฐธรรม)

หัวหน้าโครงการ

Catalyst Deactivation 1997
C.H. Bartholomew and G.A. Fuentes, editors

Determination of Coke Deposition on Metal Active Sites of Propane Dehydrogenation Catalysts

P.Praserthdam*, T.Mongkhonsi, S.Kunatippapong, B.Jaikaew and N.Lim

Petrochemical Engineering Laboratory, Department of Chemical Engineering,
Faculty of Engineering, Chulalongkorn University, Bangkok 10330 THAILAND.
e-mail : fengpps@chulkn.car.chula.ac.th

Sn and alkali metals (Li, Na and K) can reduce coke covering on the Pt active site of a propane dehydrogenation catalyst, Pt/γ-Al_2O_3. The role of the alkali metals is to increase excess mobile electrons of the catalyst surface. Sn and Sn-alkali metal promoted catalysts show higher excess mobile electrons than unpromoted ones. The excess mobile electrons enhance hydrogen spillover on the catalyst surface, thus reducing the amount of coke deposits.

1. INTRODUCTION

Coking is a common deactivation mode in hydrocarbon conversion processes, involving the deposition of carbonaceous materials on the catalyst surface. Materials deposit may include elemental carbon, high molecular weight polymer and polycyclic aromatics [1,2]. Coke formation involves the metallic and acidic functions of the catalyst with the steps of dehydrogenation, condensation, alkylation and cyclization [3]. The structure of coke is rather complex, containing several different growth forms, which can be grouped into amorphous, filamentous and graphitic platelets [4-6]. The surface on which coke is deposited and their effects on coking can also vary widely. Most metallic catalysts are supported and the metal, the support and metal-support interaction can affect the coking.

The thermodynamics of the dehydrogenation reaction of propane to propene are such that it is desirable to operate at high temperature and low pressure. But these conditions are the conditions that favour coke formation. Therefore, there are many attempts trying to improve the performance of the present catalyst, based on Pt/γ-Al_2O_3, and to develop new catalyst compositions that yield the desired results. Sn and alkali metals are examples of promoter that can increase catalyst resistance to coking [7-11].

In the present work, the effect of Sn and the alkali metals (Li, Na and K) is presented. The main objective is to clarify their role in enhancing coking resistance of the resulting catalyst.

2. EXPERIMENT

Pt/γ-Al_2O_3 (0.3wt%Pt), Pt-Sn/γ-Al_2O_3 (0.3wt%Pt, 0.3wt%Sn), Pt-Sn-Li/γ-Al_2O_3 (0.3wt%Pt, 0.3wt%Sn, 0.6wt%Li), Pt-Sn-Na/γ-Al_2O_3 (0.3wt%Pt, 0.3wt%Sn, 0.6%wtNa), and

Pt-Sn-K/γ-Al_2O_3 (0.3wt%Pt, 0.3wt%Sn, 0.6wt%K) were used in the research. The catalysts were prepared by a conventional dry impregnation method using H_2PtCl_6, $SnCl_2$ and alkali metal nitrates as salt precursors. All chemicals used are normally analytical grade.

Coked catalyst was prepared from the dehydrogenation reaction of C_3H_8 to C_3H_6. 0.1 mg of the catalyst was packed in a quartz reactor. 20% C_3H_8, balanced with N_2 was used as reactant gas. To study the effect of H_2, H_2 was mixed with the reactant gas at a Hydrogen/Hydrocarbon (H/HC) ratio equal to 1. All gas reactants were supplied by Thai Industrial Gas Co.Ltd. and were passed through oxygen and moisture traps before entering the reactor. The reaction was performed at near atmospheric pressure with gas hourly space velocity (GHSV) 25000 hr^{-1}.

Temperature programmed oxidation (TPO) was performed by burning the obtained coked catalyst in 1%O_2 in an He atmosphere. The heating rate was 10°C/min. CO_2 produced was measured using a gas chromatograph equipped with a TCD and an on-line gas sampling valve.

To measure the amount of metal active sites, a CO adsorption technique was used. In the case of fresh or coked samples, the measurement was performed by monitoring the amount of CO adsorbed at room temperature. The % active site covered by coke was defined as (active site lost due to coke coverage)/(active site of fresh catalyst) x 100

The electrical conductivities of all catalyst samples were measured using a Philips PM 6303 automatic RCL meter. The catalyst was first ground to a fine powder and packed into a die. Then the sample was reduced with H_2 for 1 hour. At the end of the reduction period, the powder was pressed at 13.3 MPa for 5 min. The measurement was performed under these condition. This measurement was used only for qualitative guidance.

3. RESULTS AND DISCUSSION

3.1. Temperature programmed oxidation and metal active site measurement

Figure 1 shows the TPO profiles of 0.3%Pt/γ-Al_2O_3, 0.3%Pt-0.3%Sn/γ-Al_2O_3 and 0.3%Pt-0.3%Sn-0.6%Li/γ-Al_2O_3 catalysts. Each sample shows a TPO peak around 460°C. In addition, a small peak around 100°C was observed for all catalysts used in this work. For the same operating conditions, the amount of coke deposit can be arranged in the following order: Sn-promoted > unpromoted > Sn-Li-promoted. However, when based on propane conversion, the following order was found ; unpromoted > Sn-promoted > Sn-Li-promoted. Sn-Na- or Sn-K-promoted catalysts also have less coke than unpromoted and Sn-promoted.

BET surface area and metal active site measured by CO adsorption of the promoted and unpromoted fresh catalysts are shown in Table 1. The addition of Sn significantly reduced the

Table 1 BET surface area and metal active site

Catalyst	Surface area (m^2/g cat)	Metal active site (site/g cat)
γ-Al_2O_3	316	-
0.3%Pt/γ-Al_2O_3	366	1.63×10^{18}
0.3%Pt-0.3%Sn/γ-Al_2O_3	351	0.73×10^{18}
0.3%Pt-0.3%Sn-0.6%Li/γ-Al_2O_3	282	1.17×10^{18}
0.3%Pt-0.3%Sn-0.6%Na/γ-Al_2O_3	289	1.53×10^{18}
0.3%Pt-0.3%Sn-0.6%K/γ-Al_2O_3	304	1.50×10^{18}

number of surface Pt atom. In this case, more than half of the surface Pt atoms disappear. However, the incorporation of the alkali metals can the increase number of surface Pt atoms again. The percentage of metal active site covered by coke is shown in Figure 2. The figure demonstrates that in the low reaction temperature region ,*i.e.* < 550°C, Sn does reduce coke deposits on the metal active site. At higher reaction temperatures, however, adding only Sn does not yield any benefit. The addition of alkali metals to Sn-promoted catalysts significantly increases the metal surface available in both low and high reaction temperature regions.

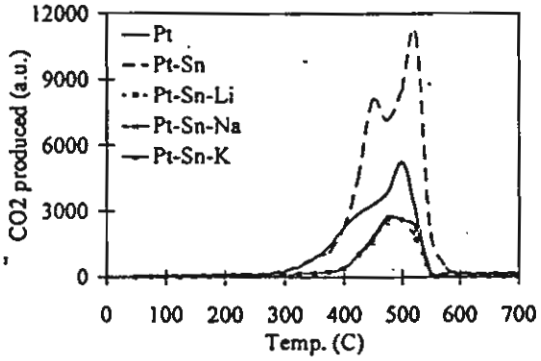

Figure 1 Effect of Sn and alkali metals on TPO spectra. Reaction Temperature 600°C.

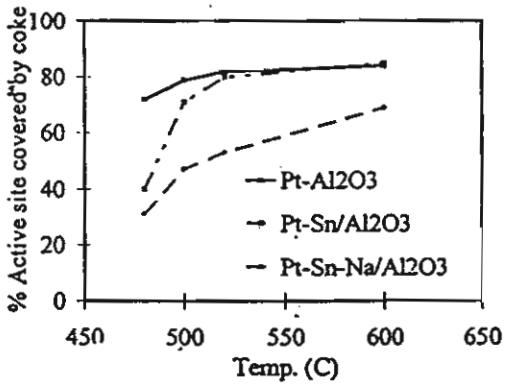

Figure 2 Total coke deposited on the metal active site of various catalysts at different reaction temperatures. H/HC = 0

The effect of hydrogen partial pressure on % active site covered by coke is shown in Figure 3. For Pt/γ-Al_2O_3 catalyst, H_2 decreases coke deposits only in the initial period. On the other hand, on Sn or Sn-Na promoted samples, higher H_2 pressure results in less coke on the metal active sites throughout the reaction period. This underlines the role of Sn and the alkali metals in enhancing the activity of H_2 in the coke elimination process. It should be noted here that coke can cover a fraction of the metal active sites, in accordance with the literature [12,13].

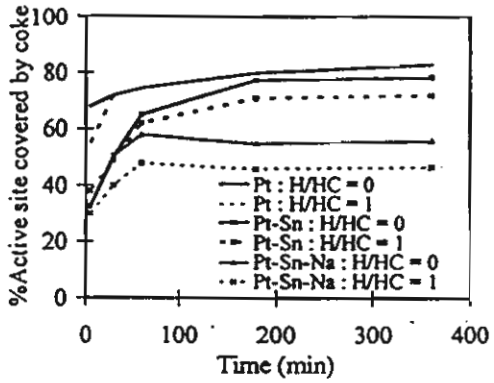

Figure 3 Coke deposit on the metal active site of 0.3%Pt/γ-Al_2O_3, 0.3%Pt-0.3%Sn/γ-Al_2O_3 and 0.3%Pt-0.3%Sn-0.6%Na/γ-Al_2O_3 catalysts at reaction temperature 500°C, H/HC = 0,1.

3.2 Electrical conductivity

Table 2 shows electrical conductivity data of the catalysts and the support. A is the electrical conductivity of alumina. B is the electrical conductivity of Sn and alkali metals promoted alumina. C is the electrical conductivity of Pt catalyst while D is the electrical conductivity of Pt-Sn catalyst. E is the electrical conductivity of Pt-Sn-Alkali metals catalyst. The data shows that the addition of metal to alumina increases electrical conductivity. The addition of Sn to Pt catalyst augments electrical conductivity approximately three times. Further incorporation of the alkali metals results in an order of magnitude further increases.

Since electrical conductivity reflects the mobility of electrons in the bulk solid (14), the data in Table 2 can be used to compare the amount of mobile electrons in each sample. Table 3 shows the amount of excess mobile electrons (in conductivity unit) of the catalysts shown in table 2. The value (B-A) is the electrical conductivity of 0.3wt%Sn added to γ-Al_2O_3 support. The value (D-C) is the electrical conductivity of 0.3wt%Sn added to 0.3%Pt/γ-Al_2O_3 catalyst. If Sn does not have any electronic effect on the Pt site, the value (B-A) should be equal to the value (D-C). The calculation, however, clearly indicates that 0.3wt%Sn loaded on 0.3%Pt/γ-Al_2O_3 catalyst does provide more mobile electrons to the catalyst than its presence on γ-Al_2O_3 support. The addition of alkali metals also shows an interesting result. The value (E-D) is the increase in electrical conductivity of 0.3%Pt-0.3%Sn/γ-Al_2O_3 after 0.6wt% of the alkali metals was added. The result demonstrates that the alkali metals greatly increase the amount of the excess mobile electrons in the bulk catalysts.

By decreasing the amount of coke, Sn functions by creating an ensemble effect and forming a solid solution with Pt in electron-rich Pt sites [15]. The proposed synergistic model for Sn addition is exhibited in Figure 4. The presence of Sn on Pt surface results in a dilution in the number of large active ensembles of Pt. Thus, it is more difficult for coke molecules to deposit on the metal surface. In addition, Sn also provides some additional electron to Pt site. Not only do the alkali metals not only act as electron donors to Pt [16], but their addition also decreases the acidity of the catalyst, which results in less coke forming on the support. Moreover, the alkali metals also promote hydrogen spillover, which can eliminate some coke already formed on the metal site. The alkali metals also act as textural promoters by reducing

Pt-Sn alloy formation. The synergistic mechanism model for Sn and the alkali metal addition are shown in Figure 5.

Table 2 Electrical conductivity data of catalysts and support

Code	Catalyst	Electrical conductivity ($Ohm^{-1}cm^{-1}$)
A	γ-Al_2O_3	2.15×10^{-6}
B	0.3%Sn/γ-Al_2O_3	3.05×10^{-6}
	0.6%Li/γ-Al_2O_3	5.58×10^{-6}
	0.6%Na/γ-Al_2O_3	5.23×10^{-6}
	0.6%K/γ-Al_2O_3	4.04×10^{-6}
C	0.3%Pt/γ-Al_2O_3	3.25×10^{-6}
D	0.3%Pt-0.3%Sn/γ-Al_2O_3	9.43×10^{-6}
E	0.3%Pt-0.3%Sn-0.6%Li/γ-Al_2O_3	20.3×10^{-6}
	0.3%Pt-0.3%Sn-0.6%Na/γ-Al_2O_3	26.6×10^{-6}
	0.3%Pt-0.3%Sn-0.6%K/γ-Al_2O_3	74.7×10^{-6}

Table 3 Amount of excess mobile electrons on the surface of bulk catalysts (in conductivity units)

Catalysts	Equations	excess mobile electrons ($Ohm^{-1}cm^{-1}$)
0.3%Pt-0.3%Sn/γ-Al_2O_3	(D-C) - (B-A)	5.28×10^{-6}
0.3%Pt-0.3%Sn-0.6%Li/γ-Al_2O_3	(E-D) - (B-A)	7.44×10^{-6}
0.3%Pt-0.3%Sn-0.6%Na/γ-Al_2O_3	(E-D) - (B-A)	14.1×10^{-6}
0.3%Pt-0.3%Sn-0.6%K/γ-Al_2O_3	(E-D) - (B-A)	63.4×10^{-6}

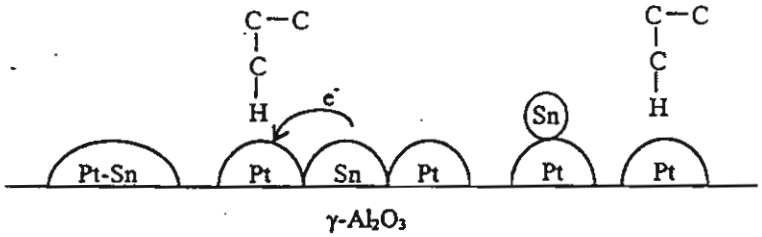

Figure 4 Synergistic mechanism model for Sn addition

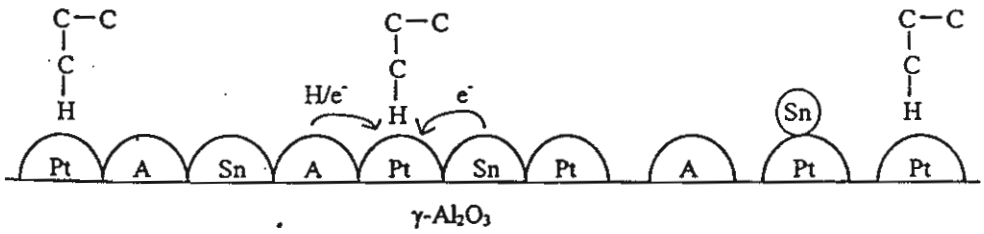

Figure 5 Synergistic mechanism model for Sn and alkali metal (A) addition

4. CONCLUSIONS

Test results reveal that the addition of only Sn or Sn + alkali metals (Li, Na and K) can reduce coke covering on Pt active sites of propane dehydrogenation catalyst, Pt/γ-Al_2O_3. Sn reduces the coke coverage area on the metal active site by creating an ensemble effect and providing additional electrons to Pt atoms. The role of the alkali metals is to increase excess mobile electrons of the catalyst surface and reduce Pt-Sn alloy formation. Sn and Sn-Alkali metal promoted catalysts show higher excess mobile electrons than the unpromoted ones. The additional excess mobile electrons enhance hydrogen spillover on the catalyst surface, thus, reducing the amount of coke deposits on the catalyst surface.

REFERENCES

1. F.Caruso, E.L.Jablonski, J.M.Graw and J.M.Parera, Appl. Catal., 51 (1989) 195.
2. B.C.Gates, J.R..Katzer and G.C.Schuit, Chemistry of Catalytic Processes, McGraw Hill, New York, 1979.
3. J.M.Parera, R.J.Venderone and C.A.Querini in Catalyst Deactivation 1987, B.Delmon and G.F.Froment (eds.), p135, Amsterdam, 1987.
4. H.B.Palmer and C.F.Cullis, Chemistry and Physics of Carbons (vol. 1) p265, Dekker, New York, 1965.
5. R.T.K.Baker and P.S.Harris, Chemistry and Physics of Carbons (vol. 14) p83, Dekker, New York, 1978.
6. B.W.Gainey, U.S. Energy Research and Development Admin. Report. GA-Al 3982, UC-77.
7. J.Barbier in B.Delmon and G.F.Froment (eds.), Catalyst Deactivation 1987 p135, Amsterdam, 1987.
8. J.Barbier, P.Marecot, N.Martin, L.Elassal and R.Maurel in Catalyst Deactivation 1987, B.Delmon and G.F.Froment (eds.),p135, Amsterdam, 1987.
9. R.D.Corright and J.A.Dumesic, J.Catal., 157 (1995) 576.
10. O.A.Barias, A.Holmen and E.A.Blekkan, J.Catal., 158 (1996) 1.
11. S.de Migues, A.Castro, O.Scelza, J.L.G.Fierro and J.Sorin, Catal. Lett., 36 (1996) 201.
12. J.Barbier, G.corro, P.Marecot, J.P.Bournonville and J.P.Frank, React. Kinet. Catal. Lett., 28 (1985) 245.
13. J.Barbier, E.Churin, J.M.Parera and Riviere, React. Kinet. Catal. Lett., 29 (1985) 323.
14. F.W.Sears, M.W.Zemansky and H.D.Yound, University Physics, 5th ed. p784, Addison-Wesley Publishing Company 1981.
15. R..Burch, J. Catal., 71 (1981) 348.
16. J.Oudar, in J. Oudar (ed.), Deactivation and Poisoning of Catalysts, New York, Dekker, 1986.

Res. Chem. Intermed., Vol. 24, No. 5, pp. 605-612 (1998)

COMPARATIVE STUDY OF COKE DEPOSITION ON CATALYSTS IN REACTIONS WITH AND WITHOUT OXYGEN

P. PRASERTHDAM, C. CHAISUK and P. KANCHANAWANICHKUN
Petrochemical Research Laboratory, Department of Chemical Engineering, Chulalongkorn University, Bangkok 10330, Thailand

Received 1 December 1997; accepted 27 November 1997

Abstract—Two types of catalysts, i.e. Pt/γ Al_2O_3 and Cu/Na-ZSM-5, were used to investigate the catalyst activity and amount of coke formation on the spent catalysts. The reactions of particular interest were the hydrocarbon oxidation and the SCR of NO with and without O_2. Propane and propene were used as the hydrocarbon sources. The reaction conditions were as follows: reaction temperature = 170-500°C, GHSV = 4,000 hr^{-1}, TOS = 2 hr, feed composition depending on each reaction, but the composition of gases were fixed as HC = 3,000 ppm, NO = 1,000 ppm and O_2 = 2.5%, using He balance. It was found that both the case of Pt/γ Al_2O_3 and the case of Cu/Na-ZSM-5, propene provided higher conversion and coke deposition than propane in the presence or the absence of O_2 and/or NO. For Pt/γ Al_2O_3 catalyst, in case of the absence of oxygen reactions, the propene conversion dropped more rapidly than the propane conversion. Finally the reaction of propene gave a lower percent of hydrocarbon conversion than the reaction of propane. Additionally, propene had a higher percent selectivity of coke formation for the reaction with the absence of oxygen, but propane had a higher percent selectivity of coke formation for the reaction with the presence of oxygen. For Cu/Na-ZSM-5, in the system with absence and presence of oxygen, the addition of oxygen caused a significant change in % coke selectivity. With the presence of NO_x, the percent conversion of both propane and propene decreased and that the % coke selectivity of propane decreased, whereas that of in propene increased.

INTRODUCTION

Coke deposition is an important deactivation mode in the hydrocarbon conversion process In general, most researchers [1-5] have emphasized only coke formation in reducing atmospheres e.g. dehydrogenation, cracking, reforming etc. Nevertheless, in oxidizing atmospheres, coke deposition can also take place on the catalyst surface. Therefore, in the present work, it is set up to compare the amount of coke formed on Pt/Al_2O_3 and Cu/Na-ZSM-5 catalysts for reactions with the absence and presence of oxygen. The catalytic activity and the amount of coke on the spent Pt/Al_2O_3 and Cu/Na-ZSM-5 catalysts were investigated for reactions with oxygen, *i.e.* hydrocarbon combustion and reduction of NO_X, and without oxygen, *i.e.* dehydrogenation or aromatization and reduction of NO_X. Propane and propene were used as the hydrocarbon sources for all four reactions.

EXPERIMENTAL

Pt/Al_2O_3 (0.3 wt.% Pt) catalyst in this study was prepared by a dry impregnation method using H_2PtCl_6 as the salt precursor. The parent Na-ZSM-5 zeolite with Si/Al ratio of 50 was hydrothermally synthesized from gel and decant solution in an autoclave. The structure of ZSM-5 was confirmed by X-ray diffraction (XRD). Cu/Na-ZSM-5 zeolite was prepared by exchanging Cu^{2+} into Na-ZSM-5 sample in the aqueous solution. The catalytic reactions were carried out at atmospheric pressure in a fixed bed reactor. A 0.5 g of catalyst was packed in a quartz tube reactor. In the case of Cu/Na-ZSM-5, before the reaction, the catalyst was heated under He flow from room temperature to 500°C in 1 hr., and held for 1 hr. before being cooled down. In the case of Pt/Al_2O_3, the catalyst was reduced to 500°C for 1 hr using hydrogen as the reductant gas. The 50 cc./min. of mixed gas feed consisting of 100 ppm NO, 3000 ppm hydrocarbon, 2.5% vol. oxygen and He was introduced to the reactor at a space velocity of 4000 hr^{-1}. The temperatures of the reaction with and without oxygen were 170°C and 350°C (in the case of Pt/Al_2O_3) or 500 °C (in the case of Cu/Na-ZSM-5) respectively. The outlet gases were analyzed by SHIMADZU GC-8APT gas chromatograph with MS-5A column for nitrogen, oxygen and carbon monoxide and with SHIMADZU GC-8AIT porapak QS column for carbon dioxide, propane and propene. Coke deposited on the catalysts was characterized by temperature programmed oxidation (TPO). Before starting the TPO, 0.5 g of the spent catalysts was heated to 130°C at 10°C/min. under He atmosphere and held for 3 hr. The heat treatment removed any air and water that was adsorbed on the catalyst. Then the pretreated sample was heated from 50°C to 700°C with a heating rate of 5°C/min. then in a 30 cc./min. stream of 1% O_2 in helium gas. The carbon dioxide formed was determined by SHIMADZU GC-8AIT gas chromatograph using a thermal conductivity detector with parapak QS column. The percentage of carbon in coke can be calculated from TPO curves. CO_2 area is divided by a internal time in which CO_2 flows through the sampling loop (1 cc.). The rate of CO_2 formation is, hence, obtained. The area under the curve of CO_2 formation rate versus time gives the value of total CO_2 formation. Finally, this value is converted to milligram carbon or percentage of carbon by using a calibration curve.

RESULTS AND DISCUSSION

For the Case of Pt/Al_2O_3

The experimental results were shown in Table 1, Figure 1 and Figure 2. In all four reactions, it was observed that the reactions with propene as a reactant gave a larger percent of hydrocarbon conversion in the initial interval of time on stream and also

Table 1
Hydrocarbon conversion, amount of coke and coke selectivity of 0.3% Pt/Al_2O_3.

Reaction	Reactant	Temperature (°C)	% HC conversion (at 5 min.)	% Carbon in coke	% Selectivity of coke formation
HC	Propane	350	59.36	0.17	0.22
	Propene	350	98.88	0.32	0.27
HC+NO	Propane	350	46.17	0.13	0.19
	Propene	350	66.14	0.16	0.34
$HC+O_2$	Propane	170	11.71	0.13	1.13
	Propene	170	100.00	0.48	0.29
$HC+NO+O_2$	Propane	170	5.59	0.12	1.07
	Propene	170	40.12	0.33	0.54

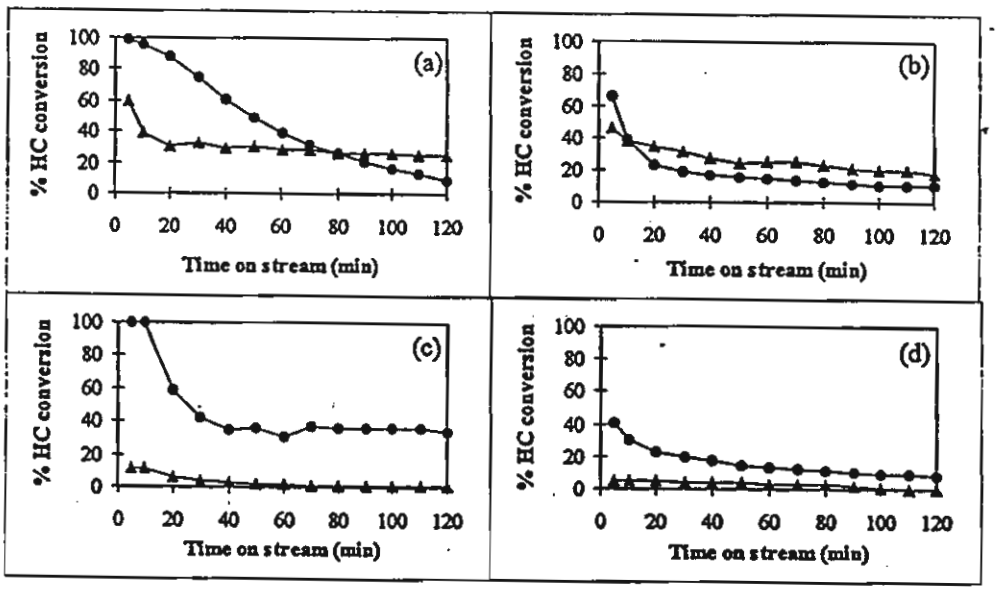

Figure 1. Relationship between % HC conversion versus time on stream. (a) Feed: 3000 ppm HC + He balance, Temperature = 350°C. (b) Feed: 3000 ppm HC + 1000 ppm NO + He balance, Temperature = 350°C. (c) Feed: 3000 ppm HC + 2.5 vol.% O_2 + He balance, Temperature = 170°C. (d) Feed: 3000 ppm HC + 1000 ppm NO + 2.5 vol.% O_2 + He balance, Temperature = 170°C.: (♦) Propane, (●) Propene.

had a larger amount of coke than the reactions with propane as a reactant. However, in the dehydrogenation reaction and NO_x reduction under the absence of oxygen condition, the propene conversion dropped more rapidly than the propane

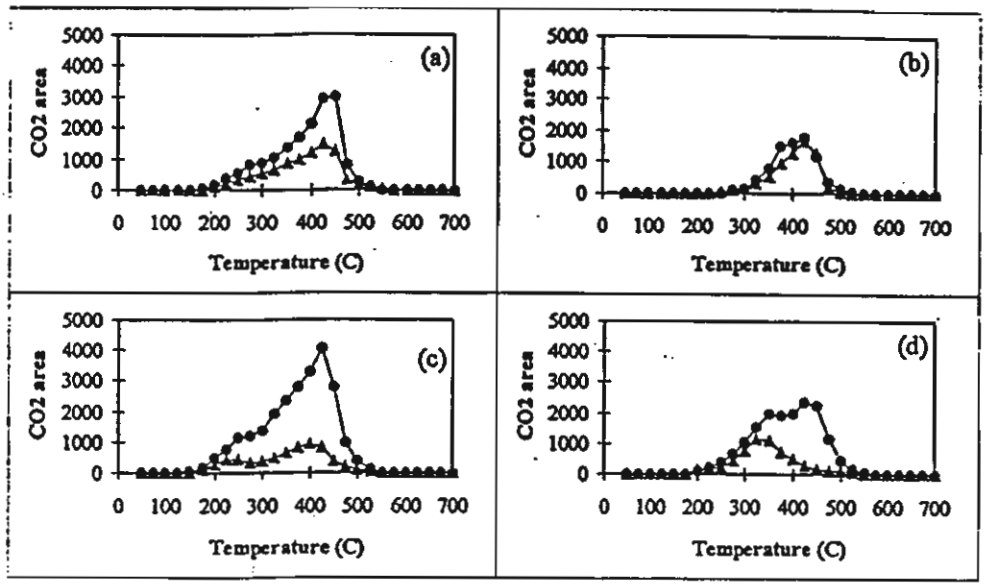

Figure 2. TPO profiles of 0.3 g coked catalyst from reaction. (a) Dehydrogenation, Temperature = 350°C. (b) Reduction of NO_x under absence of oxygen condition, Temperature = 350°C. (c) Combustion, Temperature = 170°C. (d) Reduction of NO_x under absence of oxygen condition, Temperature = 170°C.: (♦) Propane, (●) Propene.

conversion. Finally the reaction of propene gave a lower percent of hydrocarbon conversion than the reaction of propane. It meant that propene is more active than propane [6]. Since propene reacted more, there was more opportunity to convert to coke precursor. Additionally, it was clarified that the product of propene from the reaction with the absence of oxygen, propadiene which is converted irreversibly to ethylidyne leading to coke deposition [7,8], was more reactive than propene [6]. Thus the catalysts in the reaction using propene as a reactant were rapidly covered by carbonaceous deposits. The TPO profiles of 0.3% Pt/Al_2O_3 catalysts are indicated in Figure 2. Each sample showed a TPO peak around 425°C except the TPO profiles of spent catalyst from reduction of NO_X in the presence of oxygen condition. This TPO profiles showed a TPO peak at a temperature of around 325°C for the reaction with propane as a reactant and two peaks at the temperature around 325°C and 425°C for that with propene as a reactant. Barbier *et al.* [3] suggested that the first peak is the coke on metal and the second peak is the coke on the support. In this paper, we define the selectivity of coke formation as the ratio of carbon atom in coke to carbon atom of feed hydrocarbon converted. It was found that propene had a higher percent of selectivity of coke formation for the reaction with the absence of oxygen, but propane had a higher percent of selectivity of coke

formation for the reaction with the presence of oxygen. Under the presence of oxygen, it suggested that coke is formed in parallel with carbon dioxide formation. Propene or coke precursor is more effectively reacted with oxygen to carbon dioxide [9]. Additionally, for the reaction with the presence of oxygen using propane as a reactant, it was observed that the reaction with the absence of NO gave a higher percent of selectivity of coke formation than the reaction with the presence of NO. On the other hand, in the case of propene, the reactant with the presence of NO gave higher percent selectivity of coke formation. It suggests that propane or propene is first reacted with adsorbed oxygen to be converted to intermediates [10,11]. In the case of propane [10,11], these intermediates are preferably reacted with NO which result in, when NO was added in feed, propane producing less selectively of coke formation. However, in the case of propene [12], NO hardly reacted with the intermediates but it preferred to dissociate into dinitrogen. Thus, since the dissociation of NO hinders the reaction of carbon dioxide formation, the intermediates prefer produce coke rather than carbon dioxide for the case of the presence of NO reaction.

For the Case of Cu/Na-ZSM-5

The experimental results were summarized in Figure 3. It was found that the propene conversion was higher than that of propane. This is particularly obvious for the reaction with the presence of oxygen and absence of NO_x as shown in Figure 3(b). Propane conversion was only 10 % ,whereas propene conversion is about 100 %. Figure 3(c),(d) (reduction of NO_x with and without O_2) exhibited the effect of NO_x on the reaction. It was found that the % of propene conversion decreased when NO_x was added, however the % of propene conversion was still higher than that of propane. It means that propene is more active than propane [6]. The temperature program oxidation (TPO) results were shown in Figure 4. It was found that the amount of coke from the four reactions of propene was greater than propane over Cu/Na-ZSM-5 zeolite. The results in Table 2 can suggest that in aromatization, the percentage of propene conversion was greater than that of propane; however, on the other hand, the % coke selectivity of propene was less than that of propane, because propene was converted to product more than to coke while propane formed product less than coke. In the system with absence and presence of oxygen it was found that the addition of oxygen caused a significant change in % of coke selectivity [13-15]. With the presence of NO_x, it was found that the percent conversion of both propane and propene decrease and that the % of coke selectivity of propane decreased whereas that of in propene increased. From this result in the case of propene, we can propose that NO_x was adsorbed on the surface of the catalyst to form an intermediate which is strongly adsorbed and, hence, the desorption rate is slow [16-21]. As a result, the intermediate can not selectively form the product but can be further

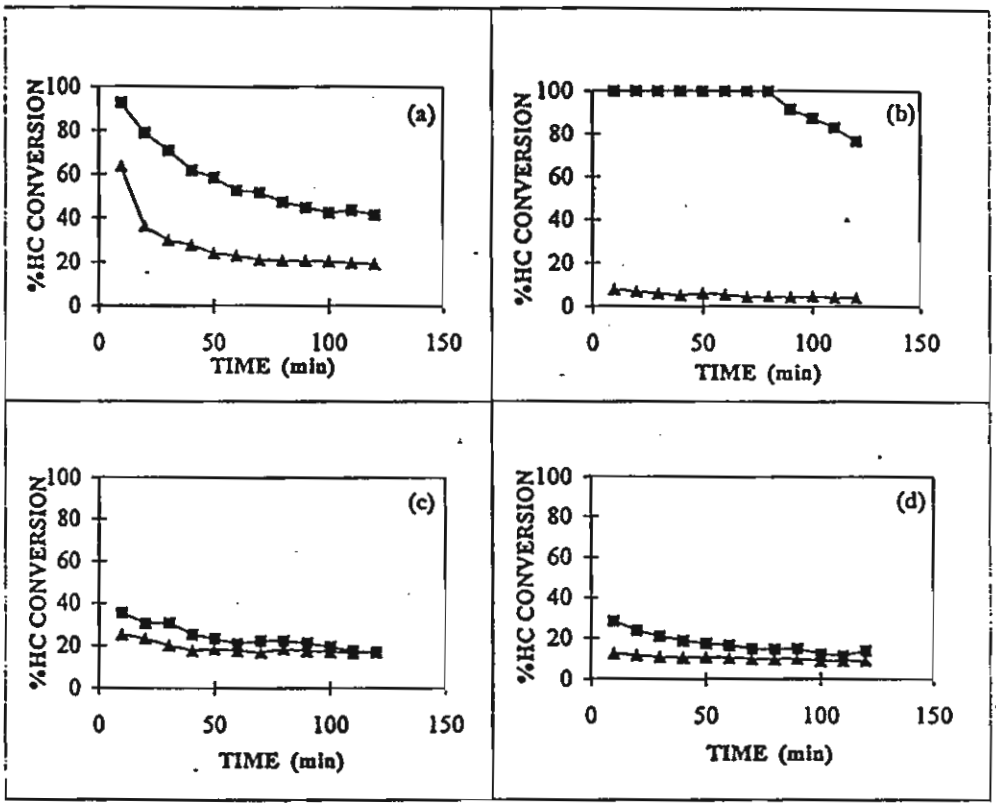

Figure 3. Relationship between % HC conversion versus time over 1.58% Cu/Na-ZSM-5; (a) Feed: 3000 ppm HC + He balance, Temperature = 500°C. (b) Feed: 3000 ppm HC + 2.5 vol.% O_2 + He balance, Temperature = 170°C. (c) Feed: 3000 ppm HC + 1000 ppm NO + He balance, Temperature = 500°C. (d) Feed: 3000 ppm HC + 1000 ppm NO + 2.5 vol.% O_2 + He balance, Temperature = 170°C: (▲) C_3H_8, (■) C_3H_6

converted to coke.

CONCLUSION

Both in the case of Pt/γ Al_2O_3 and in the case of Cu/Na-ZSM-5, propene provided both higher conversion and coke deposition than propane in the presence or the absence of O_2 and/or NO. For Pt/γ Al_2O_3 catalyst, in the case of the absence of oxygen reactions, the propene conversion dropped more rapidly than the propane conversion. Finally, the reaction of propene gave a lower percentage of hydrocarbon conversion than the reaction of propane. Additionally, propene had a higher

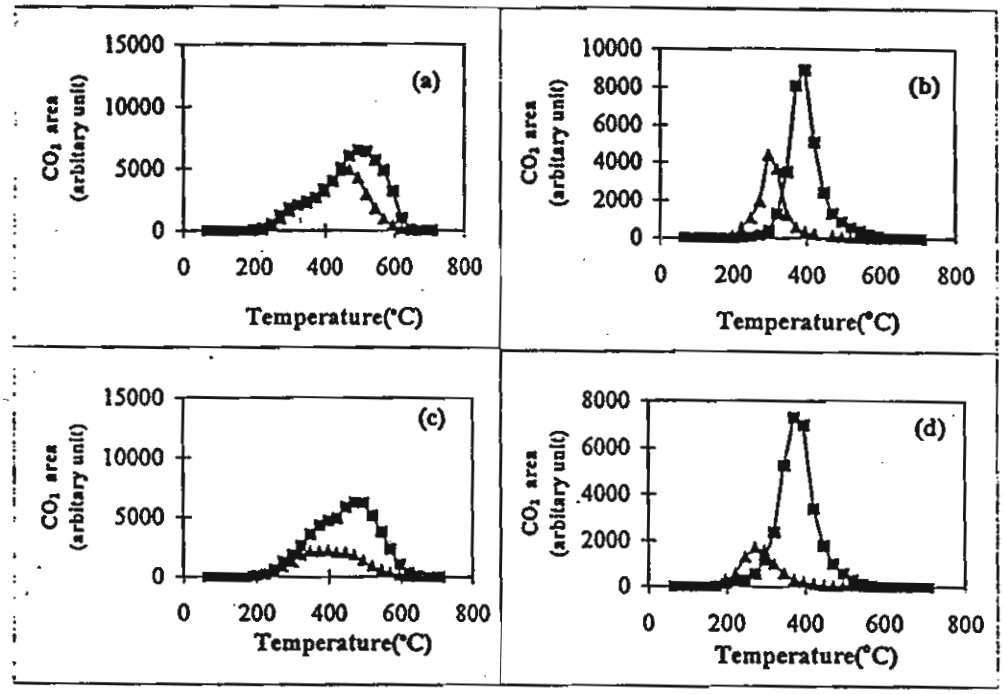

Figure 4. TPO curve of 1.58% Cu/Na-ZSM-5 after the reaction; (a) HC at 500 °C, (b) HC+O_2 at 170 °C, (c) HC+NO at 500 °C, (d) HC+NO+O_2 at 170 °C; (▲) C_3H_8, (■) C_3H_6; In the case of propene (b,d), amount of coked catalyst for TPO is five times than that of propane.

Table 2
Percentage HC conversion and selectivity of coke over 1.58%Cu/Na-ZSM-5

Reaction	Reactant	Temperature (°C)	% HC conversion (at 5 min.)	% Carbon in coke	% Selectivity of coke formation
HC	propane	500	75	0.45	0.74
	propene	500	98	0.68	0.51
HC+O_2	propane	170	9	0.17	1.43
	propene	170	100	2.03	0.86
HC+NO_x	propane	500	26	0.25	0.45
	propene	500	38	0.67	1.51
HC+NO_x+O_2	propane	170	15	0.10	0.39
	propene	170	38	1.82	2.80

percentage of selectivity of coke formation for the reaction with the absence of oxygen but propane had higher percent selectivity of coke formation for the reaction with the presence of oxygen. For Cu/Na-ZSM-5, in the system with absence and presence of oxygen, the addition of oxygen caused a significant change in the % of coke selectivity. With the presence of NO_x, the percent conversion of both propane and propene decreased and that of the % coke selectivity of propane decreased, whereas that in propene increased.

REFERENCES

1. W.G. Appleby, J.W. Gibson, and G.M. Good, *I & EC Process Design and Development* 1, 102 (1962).
2. J.N. Beltramini, E.E. Martinelli, E.J. Churin, N.S. Figoli, and J.M. Parera, *Applied Catalysis* 7, 43 (1983).
3. J. Barbies, *Catalyst Deactivation* 1 (1987).
4. J. Biswas, P.G. Gray, and D.D. Do, *Applied Catalysis* 32, 249 (1987).
5. Mikael Larsson, Magnus Hulten, Edd A Blekkan, and Bengt Andersson, *Journal of Catalysis* 164, 44 (1996).
6. Morrison and Boyd, *Organic Chemistry (sixth edition)*: 122, 287, 410. .
7. Gabor A. Somorjai, *Introduction to Surface Chemistry and Catalysis*: 420.
8. B.J. McIntyre, M. Salmeron, and G.A. Somorjai, *Journal of Catalysis* 164, 184 (1996).
9. R. Burch and T.C. Watling, *Catalysis Letters* 43, 19 (1997).
10. Motoi Sasaki, Hideaki Hamada, Yoshiaki Kintaichi, and Takehiko Ito, *Catalysis Letters 15*, 297 (1992).
11. Megumu Inaba, Yoshiaki Kintaichi, and Hideaki Hamada, *Catalysis Letters* 36, 223 (1996).
12. R. Burch, P.J. Millington, and A.P. Walker, *Applied Catalysis* B4, 65 (1994).
13. J.L. d' Itri and W.M.H. Sachtler, *Catal. Lett.*. 15, 289 (1992).
14. H. Hamada, Y. Kintaichi, M. Sasaki, T. Ito, and M. Tabata, *Appl. Catal*. 64, L1 (1990).
15. A.Yu Stakheev, C.W. Lee, S.P. Park, and P.J.Chong, *Progess in Zeolite and Microporous Materials.*, Vol 105 , 1579 (1997).
16. H. Hamada, Y. Kintaichi, M. Sasaki, M. Tabata, and T. Ito, *Appl. Catal.*, 70, L15 (1991).
17. C.J. Bennett, P.S. Bennett, S.E. Golunski, J.W. Hayes, and A.P. Walliker, *Appl. Catal. A*, 86 L1 (1992).
18. R.Burch and P.J. Millington , *Appl. Catal B:Env*, 2. 101 (1993).
19. M. Iwamoto, H. Yahiro, H. Khin, M.Watanabe, J Gue, M. Konno, T. Chikabisa and T. Murayama, *Appl. Catal* B5., L1 (1994).
20. Chikafumi Yokotama and Makoto Misono, *Journal of Catalysis.*160, 95 (1996).
21. Janos Szanyi and Mark T. Paffett, *Journal of Catalysis.*164 232 (1996).

Korean J. Chem. Eng., 15(5), 486-490 (1998)

ROLES OF Pt AND ALUMINA DURING THE COMBUSTION OF COKE DEPOSITS ON PROPANE DEHYDROGENATION CATALYSTS

Tharathon Mongkhonsi†, Piyasan Prasertdham, Atchara Saengpoo, Nonglak Pinitniyom and Bualom Jaikaew

Department of Chemical Engineering, Faculty of Engineering, Chulalongkorn University, Bangkok 10330, Thailand
(*Received 2 November 1997 • accepted 26 June 1998*)

Table 1. Catalyst composition, surface area and Pt active site

Catalysts	wt% of metal loading					Surface area	Pt active site
	Pt	Sn	Li	Na	K	m^2/g cat	molecule CO/g cat
$Pt/\gamma\text{-}Al_2O_3$	0.3	-	-	-	-	330	5.55×10^{18}
$Pt\text{-}Sn/\gamma\text{-}Al_2O_3$	0.304	0.292	-	-	-	320	3.17×10^{18}
$Pt\text{-}Sn\text{-}Li/\gamma\text{-}Al_2O_3$	0.299	0.266	0.528	-	-	248	3.26×10^{18}
$Pt\text{-}Sn\text{-}Na/\gamma\text{-}Al_2O_3$	0.288	0.269	-	0.590	-	289	4.26×10^{18}
$Pt\text{-}Sn\text{-}K/\gamma\text{-}Al_2O_3$	0.283	0.311	-	-	0.577	304	4.17×10^{18}

by CO adsorption technique on the basis that one CO molecule is adsorbed per one Pt atom [Biswas et al., 1987]. The actual catalyst compositions, surface areas and number of Pt active sites of fresh samples are reported in Table 1. The catalysts were coked using the dehydrogenation reaction of propane to propene at different reaction temperatures and H_2/HC ratios. 20% vol C_3H_8 balanced with N_2 was used as reactant gas. In order to change H_2/HC ratio, an appropriate amount of N_2 was replaced by H_2. All results reported here are based on the following reference conditions unless otherwise stated: reaction temperature 600 °C, time on stream 40 minutes, H_2/HC=0. The reactor was operated at atmospheric pressure and the gas hourly space velocity (GHSV) was 25,000 hr^{-1}. Coke deposited on the catalyst was studied by Temperature Programmed Oxidation (TPO). Thermogravimetric analysis (TGA), Shimadzu model TG-50, was also used to cross check some TPO results. In the TPO experiment, 1% O_2 in He was used as the oxidizing gas. About 90 mg of coked catalyst sample was used in each experiment unless otherwise stated. The coked catalyst sample was packed in a quartz tube, supported by glass wool and burnt at a constant heating rate of 5 °C/min from 50 °C to 700 °C. The effluent gas was directed to a gas chromatograph Shimadzu model GC-8A equipped with a 1 ml gas sampling loop and a thermal conductivity detector. The gas sampling was performed every 5 minutes (or 25 °C). Our experience on TGA and results reported in some literatures [e. g. Barbier et al., 1980, 1985] have shown that the main TPO peaks usually distance from the adjacent peak(s) by about 100 °C. Therefore, this sample interval is considered appropriate. In addition, it can be seen later that there are other factors affecting locations of TPO peaks apart from C/H ratio of coke.

Separation of coke from the coked catalysts was achieved by dissolving the coked catalyst sample in a warm mixture of HCl and HNO_3. $\gamma\text{-}Al_2O_3$ and Pt can dissolve in this acid solution, but SiO_2 which is present as the major impurity (up to about 20 wt%) cannot dissolve in this manner. Several drops of HF have to be added to the solution to dissolve the remaining SiO_2 particle but coke. Separation of coke from the solution was performed by using a centrifuge. After each centrifuge, the clear solution was pipetted out and distilled water was added instead. This step was to wash any remaining acid and dissolve solid from the coke sample. The centrifugal and washing steps were repeated until most of the acids added were removed. The obtained coke sample then was dried in air at 110 °C overnight. Further details of experimental system and experimental procedures are described elsewhere [Atchara, 1995; Bualom, 1995; Nonglak, 1996].

RESULTS AND DISCUSSION

Effects of H_2/HC ratio and reaction temperature are shown in Figs. 1 and 2, respectively. From the TPO spectra, despite the differences in H_2/HC ratio and reaction temperature, we can categorise coke into three groups. The first group appears in a very small amount and burns around 110 °C (in the small boxed area). Since this coke appears in a very small amount, there will be no further discussion on this coke. The second coke is the one that can be removed at around 450 °C and the last one must use temperatures higher than 450 °C. Location of the second coke on the coked catalyst was determined by the CO adsorption technique. The CO adsorption results obtained from coked catalysts regenerated at different temperature show that burning the coked catalyst at 450 °C can recover all Pt active

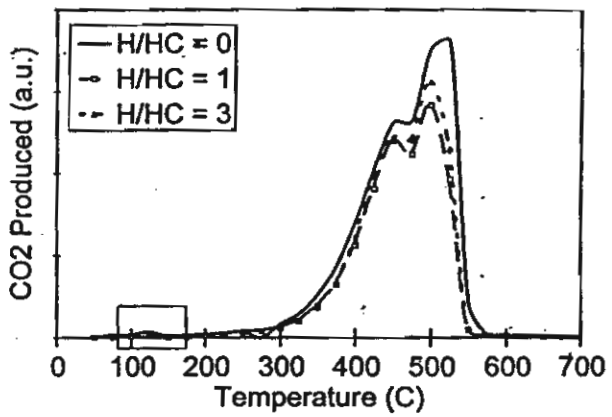

Fig. 1. TPO spectra of $Pt\text{-}Sn/\gamma\text{-}Al_2O_3$ at different H_2/HC ratios.

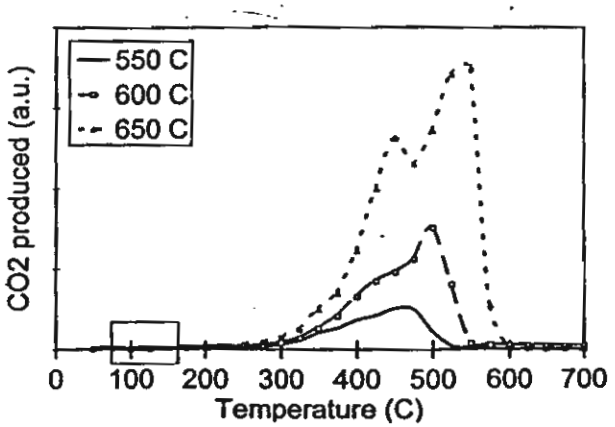

Fig. 2. TPO spectra of $Pt\text{-}Sn/\gamma\text{-}Al_2O_3$ at different reaction temperatures.

es. The TPO spectra of the coked catalyst regenerated at ·0 °C (not shown here) did not show the peak of the sec- d coke while the peak of the third coke still remained. ierefore, it can be identified that the second coke is the ke on metal site and the last is the coke on alumina sup- t. The TPO results clearly show that both H_2/HC ratio and ction temperature can alter the amount of coke formed. The rning characteristic of the coke on the coked catalysts is "l the same. Reaction temperature rather than H_2/HC ratio a stronger effect on the amount of coke. The slight shift of PO peaks in both figures is the effect of the amount of coke n each sample. The sample with a larger amount of coke ex- its a higher temperature of TPO peak for the same group coke.

Fig. 3 shows TPO spectra of coked Pt-Sn/γ-Al_2O_3 after be- used at different time on stream. The TPO peak of the coke the metal site still appears around 450 °C and seems not depend on the total amount of coke. The location of the eak of coke on the support shifts to a higher temperature the total amount of coke increases. At a high coke con- t the peaks of the coke on the metal site and on the sup- ort lump together into one large peak.

The effect of promoters (Sn, Li, Na, K) on propene yield demonstrated in Fig. 4. Fig. 4 shows that addition of Sn o the Pt catalyst significantly enhances propene yield. Addi- on of Li, Na and K further increases yield of propene. TPO ectra of the unpromoted and promoted catalysts are shown Fig. 5. Despite the differences in catalyst compositions and

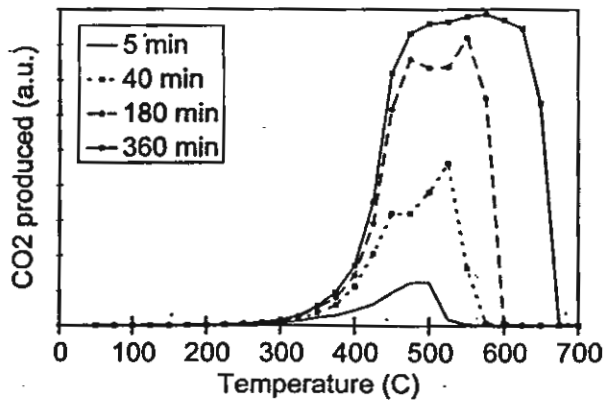

g. 3. TPO spectra of Pt-Sn/γ-Al_2O_3 at different time on stream.

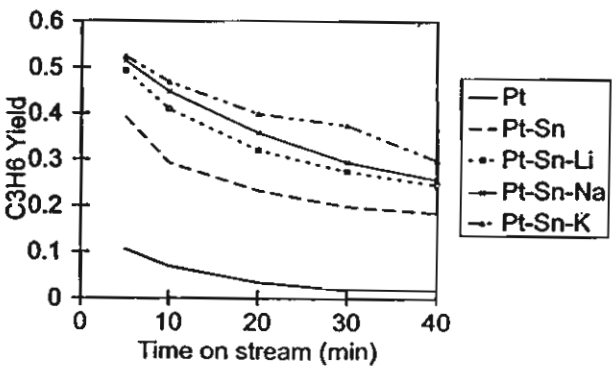

ig. 4. Effect of promoters on propene yield.

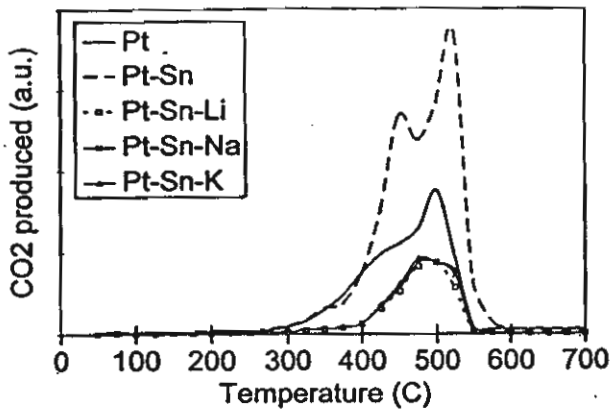

Fig. 5. Effect of promoters on TPO spectra of Pt based catalyst.

reaction conditions, all TPO spectra exhibit similar behaviour. It is found that Pt-Sn catalyst produced more coke per unit mass of catalyst more than the unpromoted one. This is because propane conversion is higher on Pt-Sn catalyst, and if propane conversion is taken into account it will be found that selectivity to coke on Pt-Sn catalyst is lower. Addition of alkali metals suppresses the formation and accumulation of coke on metal sites and catalyst support by reducing acidity of the catalyst surface. However, no significant effect on locations of TPO peaks is observed.

The roles of Pt and γ-Al_2O_3 during coke combustion were clarified by separating the coke from the coked catalyst and performing a TPO study on the carbonaceous compound obtained. Since the results shown previously indicate that the structure of coke formed does not likely to depend on reaction condition and catalyst composition, only the coke formed on Pt-Sn/γ-Al_2O_3 at the reference condition was studied. Fig. 6 demonstrates the comparison between TPO spectra of the coked catalyst and the coke sample. The figure shows that the absence of the metal and the support has an obvious effect on the characteristics of coke combustion. Only one CO_2 evolution peak was detected from the coke sample. This peak also appears at a higher combustion temperature than that of the coked catalyst. This result suggests that the appearance of two CO_2 evolution peaks of the coked catalyst relates to the

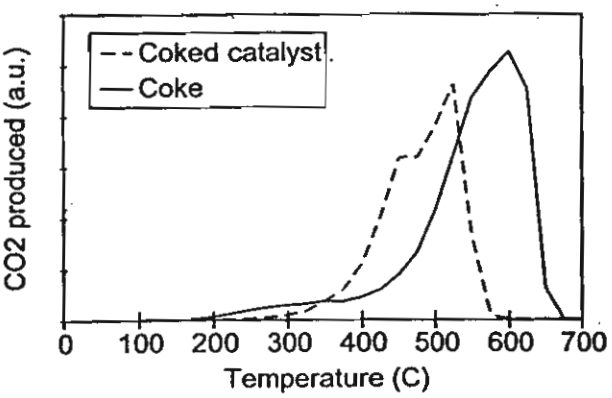

Fig. 6. Comparison between TPO spectra of coked Pt-Sn/γ-Al_2O_3 catalyst and coke separated from Pt-Sn/γ-Al_2O_3 catalyst.

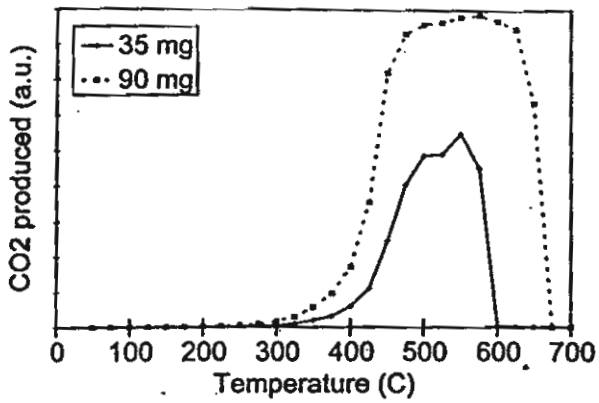

Fig. 7. Effect of weight of coked catalyst (Pt-Sn/γ-Al_2O_3) on TPO profiles.

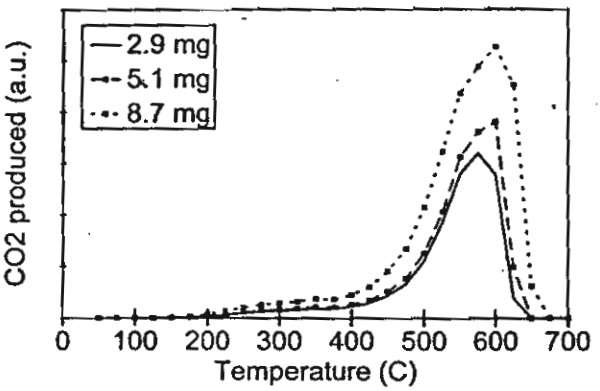

Fig. 8. Effect of weight of coke separated from coked Pt-Sn/γ-Al_2O_3 on TPO profiles.

presence of the metal and the support. The high surface area and porosity of the support promote the combustion of coke by increasing coke surface area contact to oxygen. In addition, Pt may also be involved in the combustion process by acting as a catalyst since CO_2 evolved from the coked catalyst at a lower temperature than the coke sample.

The effect of sample weight on the resolution of TPO spectra is shown in Fig. 7. TPO spectra of 90 mg coked catalyst sample show only one large peak but it cannot be determined whether it consists of only one large peak or several small peaks lumped together. Using a smaller sample amount shows a different result, *i.e.*, better resolution. Here, when the amount of coked catalyst sample was reduced to 35 mg a shoulder near 500 °C becomes distinct from the peak at 550 °C.

Fig. 8 shows TPO spectra of a coke sample by using different sample weights. The spectrum patterns do not show any obvious difference. Only one combustion peak can be observed independent from sample weight. When the TPO spectrum of the coke sample is superimposed on the TPO spectrum of coked catalyst (Fig. 6), one can see that the coke on the catalyst can be burned off at a lower temperature. This result provides further support for the hypothesis that both the metal site (in this case Pt) and the support should play some role in coke burning process.

CONCLUSIONS

At least three groups of coke can be present on the Pt based dehydrogenation catalyst. The first group, which appears in a very small amount, is the coke that can be removed at a temperature only around 110 °C. The second group, the amount of which increases with time on stream but up to a limit, can be burned using higher combustion temperatures, *i.e.*, >450 °C. These two groups are determined to be the coke that deposits on metal sites. The third coke, which keeps increasing with time on stream and can be removed by using further higher temperature, *i.e.*, 550 °C, is the coke that deposits on alumina support. Experiments also show that changing dehydrogenation reaction temperature, variation of H_2/HC ratios, addition of Sn or alkali metals (Li, Na and K) significantly affect mainly the amount of each coke formed.

TPO is a powerful technique widely used in coke characterization. However, one must be careful in interpreting the obtained spectra since the amount of sample used can lead to a different explanation. An optimal sample weight which is a compromise between sensitivity and resolution of the technique should be determined.

ACKNOWLEDGEMENT

T. Mongkhonsi and P. Praserthdam wish to acknowledge The Thailand Research Fund (TRF) for their support.

REFERENCES

Atchara Saengpoo, "Combustion of Coke on Dehydrogenation Catalysts", M. Eng. Theses, Chulalongkorn University (1995).

Barbier, J. B., Corro, G. and Zhang, Y., "Coke Formation on Platinum-Alumina Catalyst of Wide Varying Dispersion", *Appl. Catal.*, 13, 245 (1985).

Barbier, J. B., Marecot, P., Martin, N., Elassal, L. and Maurel, R., "Selective Poisoning by Coke Formation on Pt/Al_2O_3", Catalyst Deactivation (Delmon, B. and Froment, G. F. eds), Elsevier, Amsterdam, p.53 (1980).

Bartholdy, J., Zenthen, P. and Masooth, F. E., "Temperature-Programmed Oxidation Studies of Aged Hydroprocessing Catalysts", *Appl. Catal. A*, 129, 33 (1995).

Biswas, J., Gray, P. G. and Do, D. D., "The Reformer Line-out Phenomenon and Its Fundamental Importance to Catalyst Deactivation", *Appl. Catal.*, 32, 249 (1987).

Bualom Jaikaew, "Effect of Alkali Metals in Dehydrogenation Catalysts for Coke Reduction", M. Eng. Theses, Chulalongkorn University (1995).

Carlos, L. P. and Jose, M. P., "Comparison of Coke Burning on Catalysts Coked in a Commercial Plant and in the Laboratory", *Ind. Eng. Chem. Res.*, 28, 1785 (1989).

Larsson, M., Hulten, M., Blekkan, E. and Andersson, B., "The Effect of Reaction Conditions and Time on Stream on the Coke Formed During Propane Dehydrogenation", *J. Catal.*, 164, 44 (1996).

Liwu, L., Tao, Z., Jingling, Z. and Zhusheng, Z., "Dynamic

Process of Carbon Deposition on Pt and Pt-Sn Catalysts for Alkane Dehydrogenation", *Appl. Catal.*, **67**, 11 (1990).

Marecot, P., Akhachane, A. and Barbier, J., "Coke Deposition on Supported Palladium Catalysts", *Catal. Lett.*, **36**, 37 (1996).

Nonglak Pinitniyom, "Characterization of Coke on Dehydrogenation Catalysts", M. Eng. Theses, Chulalongkorn University (1996).

Pieck, C. L., Jablonski, E. L., Verderone, R. J. and Parera, J. M., "Selective Regeneration of Catalytic Functions of Pt-Re-S/Al_2O_3-Cl During Coke Burning", *Appl. Catal.*, **56**, 1 (1989).

Querini, C. A. and Fung, S. C., "Coke Characterisation by Temperature Programmed Techniques", *Catal. Today*, **37**, 277 (1997).

Querini, C. A. and Fung, S. C., "Temperature-Programmed Oxidation Technique: Kinetics of Coke-O_2 Reaction on Supported Metal Catalysts", *Appl. Catal. A*, **117**, 53 (1994).

Reyes, P., Oportus, M., Pecchi, G., Frety, R. and Moraweck, B., "Influence of the Nature of the Platinum Precursor on the Surface Properties and Catalytic Activity of Alumina-Supported Catalysts", *Catal. Lett.*, **37**, 193 (1996).

Silipoln Kunatippapong, "Determination of Irreversible Coke Deposition of Platinum Active Site of Propane Dehydrogenation Catalyst", D. Eng. Theses, Chulalongkorn University (1995).

Tao, Z., Jingling, Z. and Liwu, L., "Relation Between Surface Structure and Carbon Deposition on Pt/Al_2O_3 and Pt-Sn/Al_2O_3 Catalysts", Studies in Surface Science and Catalyst, Elsevier, Amsterdam, **34**, 143 (1991).

PERGAMON

Chemical Engineering Science 55 (2000) 2249–2256

Chemical Engineering Science

Transient study of the effect of residual cations in Cu/ZSM-5 for SCR of NO by hydrocarbon

Nakarin Mongkolsiri[a], Piyasan Praserthdam[a,*], P.L. Silveston[b], R.R. Hudgins[b]

[a]*Department of Chemical Engineering, Chulalongkorn University, Bangkok, 10330, Thailand*
[b]*Department of Chemical Engineering, University of Waterloo, Ontario, Canada, N2L 3G1*

Received 4 December 1997; accepted 16 August 1999

Abstract

A step change technique was used to investigate individual reactions in the reduction of NO by hydrocarbon on Na-ZSM-5, H-ZSM-5, Cu/Na-ZSM-5 and Cu/H-ZSM-5 catalysts. Na-ZSM-5 is not active in NO decomposition and NO reduction by propane both in the presence and in the absence of oxygen. On the other hand, H-ZSM-5 is active in the oxidation of NO to NO_2 and in the reduction of NO. Zeolite does not adsorb NO but preferentially adsorbs O_2 which, subsequently, reacts with NO in the gas phase to produce NO_2. In the absence of oxygen, Cu/H-ZSM-5 is more active than Cu/Na-ZSM-5 in both the decomposition of NO and the reduction of NO by propane since Cu/H-ZSM-5 can produce more NO_2 in the absence of oxygen. Differences in the Cu/H and Cu/Na forms of ZSM-5 result from residual H^+ or Na^+ in these zeolites. These residual cations either affect catalytic sites directly or control the Cu^+/Cu^{2+} ratios. Differences in these ratios were observed.

Keywords: SCR of NO; Transient experiments; NO oxidation; Cu-exchanged ZSM-5

1. Introduction

The selective catalytic reduction (SCR) of NO by hydrocarbon has been a topic of interest during the last decade (Held, Konig, Richter & Puppe, 1990; Iwamoto & Hamada, 1991). Unlike the reaction over conventional three-way catalysts normally used on gasoline engine exhaust, SCR of NO by hydrocarbon can occur even under a highly oxidizing atmosphere. Consequently, this reduction may be promising for the removal of NO from diesel and other lean burn engines. A number of catalysts have been proposed in literature; however, among them, Cu/ZSM-5 is one of the most active ones. It has been the most widely studied.

In general, Cu/ZSM-5 zeolite can be prepared by ion-exchanging Cu ion with either the Na- or H- forms of ZSM-5. The choice of the primary form of ZSM-5 used by a researcher seems to be arbitrary. Na-ZSM-5 is used because it can be exchanged with Cu ion more easily than the H^+ form. In other cases, H-ZSM-5 is used in order to avoid the effect of Na^+ ion (Shelef, 1995). Although overexchanged Cu/ZSM-5, the most active catalyst for SCR of NO by hydrocarbon (Iwamoto, Mizuno & Yahiro, 1992), has a degree of Cu^{2+} exchange above 100%, based on the assumption that one Cu^{2+} ion exchanges with two Na^+ ions or two protons, this sample retains a significant amount of cations on the surface (Shelef, 1995). This was confirmed by Zhang, Leo, Salofim and Hu (1995) who found that some Na^+ ion still existed in 165% Cu-exchanged ZSM-5. Therefore, there should be some residual Na^+ ions left in Cu/Na-ZSM-5 whereas some protons should still remain in Cu/H-ZSM-5. These residual ions could result in different activities between Cu/ZSM-5 zeolites formed from the H^+ and Na^+. Alternatively, they could result in different Cu^+/Cu^{2+} ratios which would then affect activity.

In order to study the effect of the residual ions, the activities of Na-ZSM-5, H-ZSM-5, Cu/Na-ZSM-5 and Cu/H-ZSM-5 for NO removal in the absence and presence of oxygen were investigated by transient methods. The performance of these catalysts was compared for the various reactions making up the reduction process. In addition, the state of copper on Cu-ZSM-5 catalysts was characterized.

* Corresponding author.

0009-2509/00/$ - see front matter
PII: S0009-2509(99)00476-5

2. Experimental

The parent Na-ZSM-5 zeolite was synthesized by the method described elsewhere (Inui et al., 1984). The given zeolite was analysed by XRD to confirm the structure of ZSM-5. Na-ZSM-5 was exchanged with ammonium nitrate solution at 80°C twice and then calcined in air at 540°C for 3.5 h in order to form H-ZSM-5. Cu/ZSM-5 was prepared by exchanging either Na-ZSM-5 or H-ZSM-5 with a copper (II) nitrate solution overnight by controlling the pH of the solution at about 9. The solid obtained was washed with fresh batches of deionized water 5 times. Finally, the catalysts were dried at 110°C in an oven overnight and then calcined in air at 540°C for 3.5 h. The catalyst powder was pelletized using a press. Then the zeolite pellet was crushed into a granular form and sieved to select a particle size between 10 and 20 mesh. This granular sample was used in the experiments of this study.

The GC switching valve was modified to alternate flows of reactant or inert gas passing through the reactor. A 10 mm diameter quartz tube reactor was filled with 1.2 g of catalyst and also glass beads to reduce void volume as much as possible. This bed of catalyst was pretreated in N_2 at 400°C for 1 h before use. The reactor operated at 300–400°C. Outlet gas was passed through a specially designed IR gas cell (Khodadadi, 1994) placed in a FT-IR (Mattson Galaxy series 5022) to continuously measure the composition of the outlet stream. The FT-IR measured NO, NO_2, N_2O, CO_2 and propane simultaneously but neither N_2 nor O_2 could be detected. The band of each gas used in this study is summarized in Table 1. No other species besides those mentioned in Table 1 were detected, of course, with the exception of water. From a blank test, the retention time for a total gas flow of around 50 ml/min at 350°C was approximately 12 s from the switching valve to the detector.

The amount of total Cu, Al, Si and Na in catalysts was determined by AAS and XRF methods. Tetrahedral alumina in ZSM-5 zeolite was investigated by Al NMR. Cu^{1+} sites on the Cu/ZSM-5 surface were quantified by CO adsorption (Iwamoto, Yahiro, Tanda, Mizuno, Mine & Kagawa, 1991). For this measurement, 0.2 g of the catalyst sample was packed in an 4 mm stainless-steel tube. The catalyst bed was pretreated in 50 ml/min of He at 450°C for 1 h. Then, the catalyst bed was cooled to room temperature for adsorption. Injections of 0.2 ml of CO to the bed were carried out until adsorption was complete. Unabsorbed CO downstream of the catalyst bed was detected by TCD. Further details of equipment and procedure are found in a Ph.D. Thesis (Mongkolsiri, 1998).

3. Results and discussion

Amounts of total copper and Na in the catalysts used in this study were determined and the result shown in Table 2. In order to avoid the effect of copper content on the activities of catalysts, the same amount of copper was loaded into the Cu/Na-ZSM-5 and Cu-H-ZSM-5 samples. Na was not found in H-ZSM-5 and there was very little in Cu/H-ZSM-5. However, a significant amount of Na was detected in Cu/Na-ZSM-5. Because of the remaining Na in the Cu/Na-ZSM-5, we expect that the Cu/H-ZSM-5 will contain significant residual protons as well.

The signals of NO absorbance with time following a switch from a N_2 to a NO feed to the reactor are shown in Fig. 1 for various catalysts. It is likely that Na-ZSM-5 and H-ZSM-5 are not active for direct decomposition of NO because the retention time and trend of the NO response were similar to those from a blank experiment. Moreover, only NO was observed for these samples. With the Cu-loaded zeolites, N_2O and NO_2 are seen. It is known that Cu/ZSM-5 shows a remarkably high activity for NO decomposition (Iwamoto, 1991,1994). Although both N_2 and O_2 are the main products of the decomposition, these cannot be detected by IR measurement. NO_2 and N_2O are intermediate or side products in decomposition reaction. There are both similarities and differences between transient responses over Cu/Na-ZSM-5 and Cu/H-ZSM-5. The absorbance signal first appeared at about the same time in both experiments; however, the retention time indicated by these signals was much longer than the time for the experiment without catalyst or with the Na-ZSM-5 and H-ZSM-5 samples. The signal for N_2O overshot the steady-state level

Table 1
IR band of gases used for transient studies[a]

Gas species	Appearance peak (cm^{-1})
NO	1905(xl), 1850(l)
NO_2	1630(xl), 1600(xl), 1750(l), 1263(l)
N_2O	2225(xl), 1290(l)
C_3H_8	2970
CO_2	2362

[a]*Note*: xl = extra large, l = large.

Table 2
Si/Al, Na/Al, Cu/Al weight ratio and Cu and Na contents in catalysts

Catalyst	Si/Al	Na/Al	Cu/Al	Cu content (wt%)	Na content (wt%)
Na-ZSM-5	40.4	0.79	—	—	1.84
H-ZSM-5	40.0	—	—	—	—
Cu/Na-ZSM-5	37.2	0.15	0.42	1.06	0.38
Cu/H-ZSM-5	39.0	0.04	0.44	1.09	< 0.09

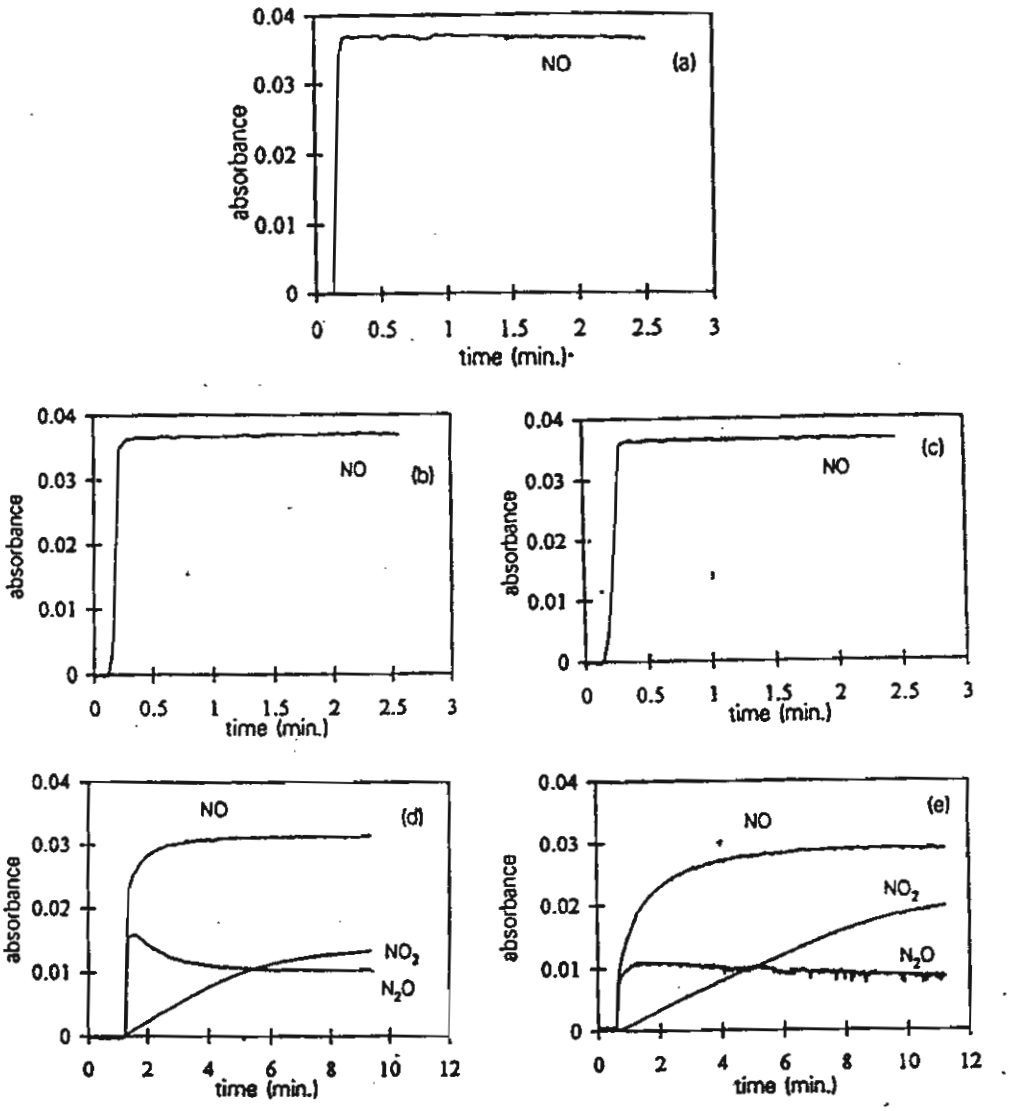

Fig. 1. Absorbance of gaseous species after switching from N_2 to 1.2% NO + N_2 350°C over (a) without catalyst; (b) Na-ZSM-5; (c) H-ZSM-5; (d) Cu/Na-ZSM-5; (e) Cu/H-ZSM-5.

in the first few minutes and then gradually decreased to this level. By contrast, NO_2 signal increased slowly after appearing in the reactor outlet. These phenomena were also observed by Li and Hall (1990) and Iwamoto et al. (1992). Pirone, Ciambelli, Morrette and Russo (1996) mentioned that at a temperature below 300°C NO disproportionation to N_2O and NO_2 occurs in parallel with NO decomposition. Furthermore, O_2 formed by NO decomposition might further oxidize NO to produce NO_2 (Iwamoto, 1991). NO consumption seems to be slightly greater for Cu/H-ZSM-5 than for Cu/Na-ZSM-5. In addition, the experiment on Cu/H-ZSM-5 produced more NO_2 whereas the one on Cu/Na-ZSM-5 produced more N_2O.

Fig. 2 shows results of a step change from N_2 gas to a gas mixture of 0.5% NO + 12% O_2. NO_2 formation in homogeneous NO oxidation at 25°C (Fig. 2a) was more than that at 350°C (Fig. 2b). This indicates that NO can be oxidized in the gas phase but preferably at a low temperature and that the net homogeneous oxidation rate decreases as the temperature increases because the reverse reaction becomes important. Occurrence of this homogeneous reaction was also reported by Chajar, Primet, Praliaud, Cherrier, Gauthier and Mathis (1994). The activity of Na-ZSM-5 in the oxidation of NO to NO_2 is very low compared to H-ZSM-5 (Fig. 2(c) and (d)). Halasz, Brenner and Simon (1995) also observed the activity of H-ZSM-5 in NO oxidation. The activity of H-ZSM-5 in NO oxidation to NO_2 was quite similar to Cu/H-ZSM-5 and Cu/Na-ZSM-5, but, surprisingly, the lag time of the appearance of NO_x in the system with Cu catalyst was much longer than the system with

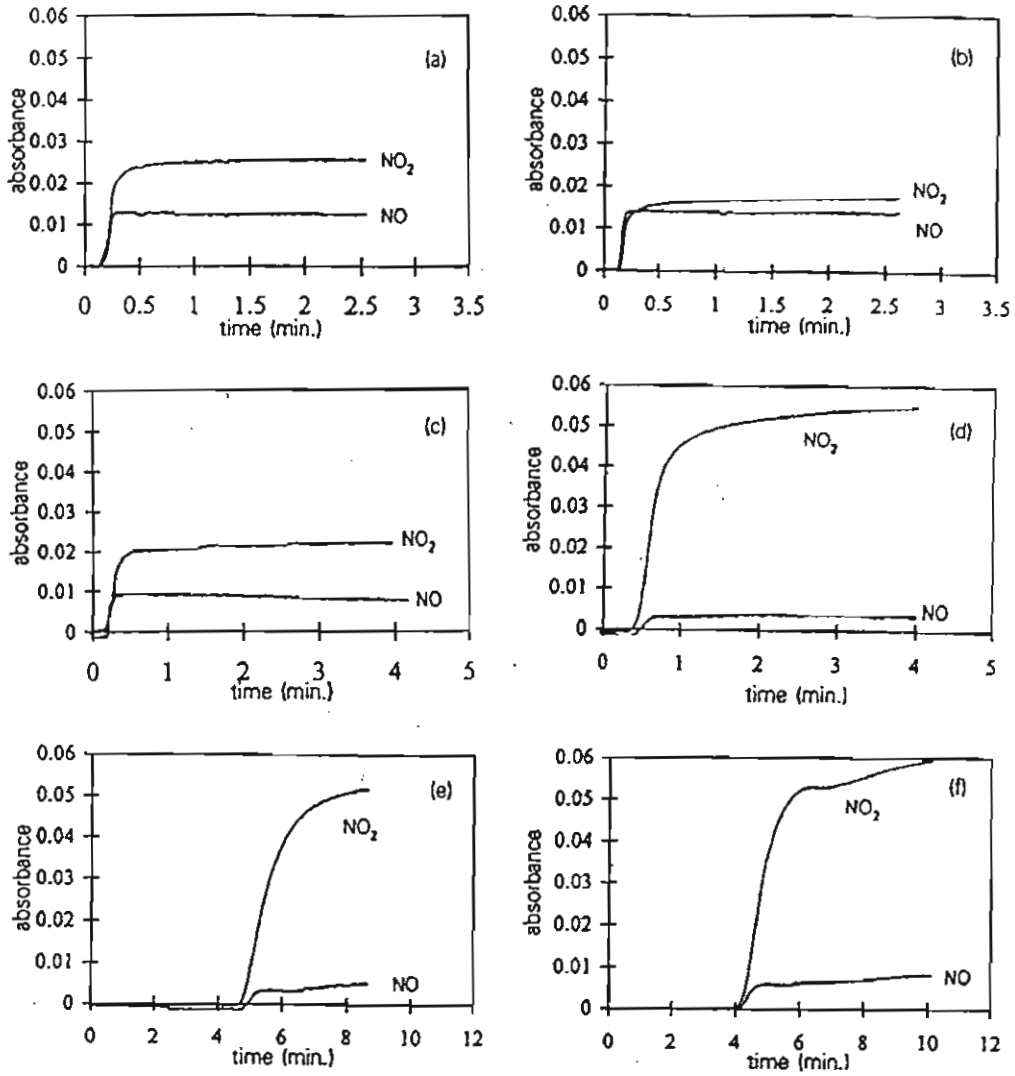

Fig. 2. Absorbance of gaseous species after switching from N_2 to 0.5% NO + 12% O_2 + N_2 at 350°C over (a) without catalyst at 30°C; (b) without catalyst at 350°C; (c) Na-ZSM-5 at 350°C; (d) H-ZSM-5 at 350°C; (e) Cu/Na-ZSM-5 at 350°C; (f) Cu/H-ZSM-5 at 350°C.

H-ZSM-5. NO_x signals in the experiment on H-ZSM-5 appeared, after switching, in about half a minute (Fig. 2(d)) whereas, in the Cu/ZSM-5 experiments, NO_x was first detected at around 4 min after switching (Fig. 2(f) and (e)). This indicates the high NO_2 adsorption capacity of Cu/ZSM-5.

The delay in the appearance of NO in Fig. 2(e) and (f) may be explained by the rapid oxidation of NO to NO_2 in the presence of O_2 in the feed. NO_2 appears only when the catalyst is saturated with NO_2. This condition interferes with NO oxidation allowing the appearance of some NO in the product gas. The lag of about 4 min in Fig. 2(e) and (f) compared to about 1 min in Fig. 1(d) and (e) is due to the concentration of NO in the feed. It is 1.2% in the latter and 0.5% in the former.

The slow rise in NO_2 in Fig. 1(d) and (e) appears to be due to the strong adsorption of NO_2 on the copper. Differences between Fig. 1(d) and (e) and Fig. 2(e) and (f) probably reflect the reduction of the Cu catalyst by NO when O_2 is not present in the feed.

Neither Na-ZSM-5 nor H-ZSM-5 is active in NO decomposition, but, in the case of the oxidation of NO by O_2, Na-ZSM-5 is not active whereas H-ZSM-5 is quite active. Possibly, the active site in H-ZSM-5 does not adsorb NO; instead it preferably adsorbs O_2. In NO oxidation over H-ZSM-5, we believe NO_2 was produced by the interaction between the adsorbed oxygen and NO in the gas phase. This hypothesis is supported by temperature-programmed desorption (TPD) measurements for NO. We did not find any desorption peak of NO during the temperature programming over Na-ZSM-5 and H-ZSM-5. Pirone et al. (1996) also noticed that H-ZSM-5 hardly adsorbed NO.

Absorbances of gases with time on stream shown in Fig. 3 were obtained from the experiments without oxygen in the feed gas over CU/H-ZSM-5 and

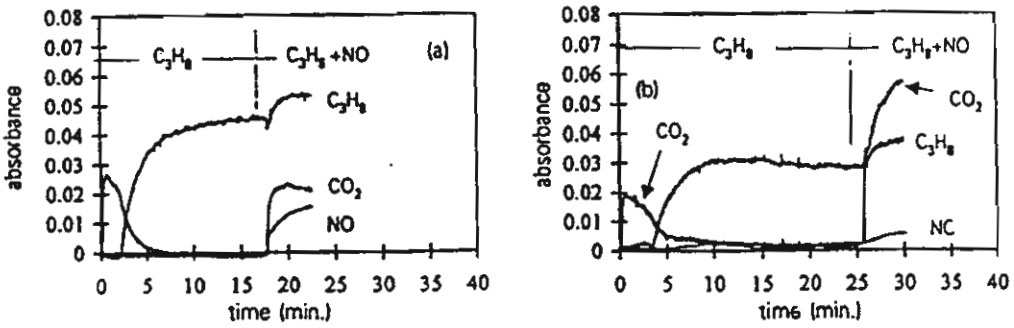

Fig. 3. Absorbance of gas products after switching from 0.4% C_3H_8 to 0.4% C_3H_8 + 0.5% NO at 400°C over (a) Cu/Na-ZSM-5, (b) Cu/H-ZSM-5.

Cu/Na-ZSM-5 zeolites. After switching from N_2 to C_3H_8, formation of CO_2 in the first few minutes after a step change from N_2 to C_3H_8 comes from the reaction between C_3H_8 and adsorbed oxygen or extra lattice oxygen in the catalyst (Valyon & Hall, 1993). When this oxygen was exhausted, the CO_2 signal disappeared. After CO_2 formation ended the response of the propane signal in the reactor outlet gradually increased until a constant level was reached after about 10 min. This could result from a chromatographic effect due to competitive adsorption of CO_2 and light hydrocarbon over Cu/ZSM-5 (Cho, 1995; Burch & Millington, 1993). After NO was added to the reactor feed, NO consumption and CO_2 production in the experiment over Cu/H-ZSM-5 was higher than for Cu/Na-ZSM-5. The C_3H_8 signal in the experimental over both catalysts is enhanced after addition of NO because NO adsorption competes with preadsorbed hydrocarbon and causes some hydrocarbon desorption. Hoost, Laframboise and Otto (1995) noticed that propane adsorption decreases in the presence of NO_x. CO, N_2O and NO_2 were not observed during NO reduction by propane in the absence of oxygen over both catalysts.

The first step of the reaction after introduction of NO would be the decomposition of NO (Burch & Scire, 1994). Oxygen generated will react further to form NO_2 or to oxidize propane. The NO_2 formed would be further reduced by propane to form CO_2, H_2O and N_2. NO_2 has been considered as the key intermediate of SCR of NO by hydrocarbon because it is more easily reduced by hydrocarbon than NO (Petunchi & Hall, 1993; Shelef, Montreuil & Jen, 1994; Chajar et al., 1994; Centi & Perathoner, 1996). Because for NO decomposition, Cu/H-ZSM-5 produces more NO_2 than Cu-Na-ZSM-5 (Fig. 1(d) and (e)), we believe that with propane in the feed, more NO_2 is formed and this leads to a higher rate of CO_2 formation over the Cu-H-ZSM-5 catalyst.

When the gas stream was changed from N_2 to a gas mixture of C_3H_8 and O_2, only CO_2 was observed with Cu/Na-ZSM-5 and Cu/H-ZSM-5 (Fig. 4(d) and 4(e)). This means that complete combustion took place. On the other hand, C_3H_8 and CO_2 signals appear with Na-ZSM-5 and H-ZSM-5 (Fig. 4(b) and 4(c)). The intensities of the absorbance of C_3H_8 and CO_2 in the experiment on Na-ZSM-5 are about the same as those for H-ZSM-5. The low-C_3H_8 conversion of H-ZSM-5 indicates low activity of the acid site in hydrocarbon oxidation at 350°C, which is in line with the report of Sasaki, Hamada, Kintaichi and Ito (1992). In comparison, propane is completely oxidized over Cu/Na-ZSM-5 and Cu/H-ZSM-5. The different oxidative performance between Cu/H-ZSM-5 and H-ZSM-5 must be the result of the presence of copper in the catalyst. Copper in zeolites is known to be very active in hydrocarbon oxidation (Neyestanaki, Kumar & Lindfors, 1995; Kucherov, Hubbard, Kucherova & Shelef, 1996). The pulse of the C_3H_8 signals on switching, observed in the experiments over Na-ZSM-5 and H-ZSM-5 (Fig. 4(b) and (c)), is due to the fluctuation of gas flow during switching rather than an adsorption phenomenon. Later, when NO is abruptly added to the feed, CO_2 formation rose rapidly and then gradually declined until a steady state was reached. This overshoot is observed in all zeolite runs (Fig. 4(b) to (e)). This is probably due to the competitive adsorption between NO_x and CO_2. The appearance of NO forces CO_2 on catalyst surface to desorb until a new balance of adsorption rate is reached. NO_2 was observed only in the experiment on Na-ZSM-5. NO and C_3H_8 were not detected in the experiment on Cu/H-ZSM-5 and Cu/Na-ZSM-5. In the H-ZSM-5 experiment, after NO was added into the system, C_3H_8 conversion increased enormously and NO signal was not observed. This observation indicates that NO reduction proceeds readily over the H-ZSM-5 samples. NO reduction, however, is not able to account for the drop in concentration of C_3H_8 leaving the reactor or for the large increase in CO_2 formation.

Even though the responses cannot be converted to concentrations because the IR signals were not calibrated, Fig. 4(c) can be analyzed by noting that the IR response at the low concentrations used is proportional to concentration. Stoichiometric considerations that 3 mol of CO_2 are formed per mol of C_3H_8 combusted mean that total oxidation of propane by O_2 over the

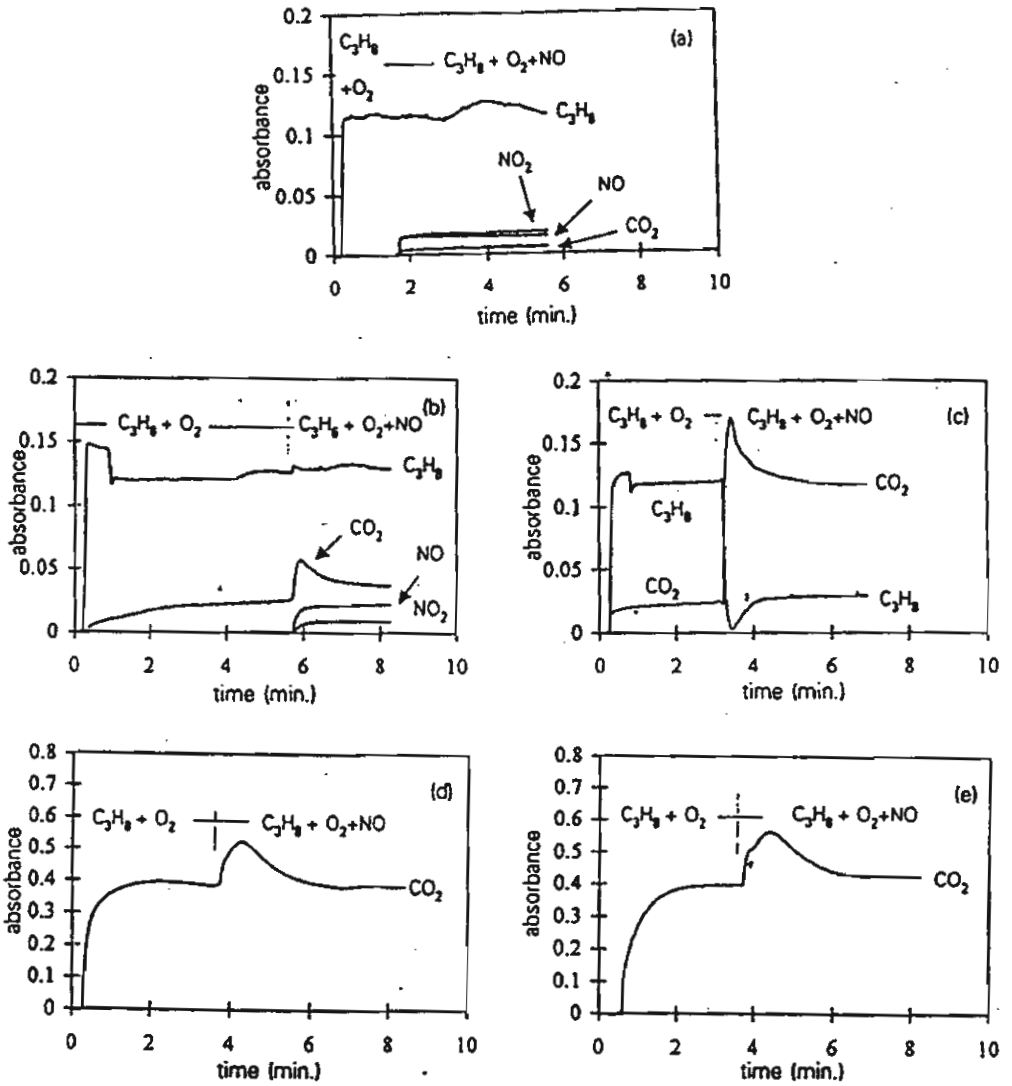

Fig. 4. Absorbance of gas products after switching from 0.4% C_3H_8 + 12% O_2 to 0.4% C_3H_8 + 12% O_2 + 0.5% NO over (a) without catalysts; (b) Na-ZSM-5 at 350°C; (c) H-ZSM-5 at 350°C; (d) Cu/Na-ZSM-5 at 300°C; (e) Cu/H-ZSM-5 at 300°C.

H-ZSM-5 sample must be promoted by the presence of NO in the reactor feed. Only this assumption can account for the response after NO introduction shown in Fig. 4(c). H-ZSM-5 is very active for NO oxidation by O_2 (see Fig. 2(d)) but does not adsorb NO strongly. Thus, we speculate that NO oxidation proceeds through

$$O_2\,(ad) + NO \rightarrow NO_2\,(ad) + O\,(ad)$$

In the presence of C_3H_8, the reactive O (ad) on the surface results in combustion. This is in addition to O_2 oxidation of the C_3H_8 that probably occurs at a different surface site. The promotion of hydrocarbon oxidation by O_2 in the presence of NO appears to have occurred for zeolite catalysts.

When activities between Cu/H-ZSM-5 and Cu/Na-ZSM-5 were compared in various transient experiments, it was found that Cu/H-ZSM-5 and Cu/Na-ZSM-5 have the same activity in the NO oxidation and NO reduction in the excess oxygen system. On the other hand, Cu/H-ZSM-5 is more active than Cu/Na-ZSM-5 in NO decomposition and NO reduction by propane without oxygen. The experiment with only NO in the feed produces more NO_2 for Cu/H-ZSM-5 than for Cu/Na-ZSM-5. More CO_2 was produced and more NO was converted in NO reduction by propane in the absence of oxygen over Cu/H-ZSM-5 than over Cu/Na-ZSM-5. However, the reactions are much faster with excess oxygen than in the absence of oxygen. The activity of both Cu/Na-ZSM-5 and Cu/H-ZSM-5 is nearly identical in NO oxidation.

The difference in the performance between Cu/Na-ZSM-5 and Cu/H-ZSM-5 observed in this study seems to be due to different residual cations, Na^+ or H^+, in the catalysts. Why this difference affects performance is

Table 3
Amount of Cu^{1+} in catalysts estimated by CO adsorption

Catalyst	Amount of CO Adsorbed (μmol/g.cat)	Number of Cu^{1+} ($\times 10^{19}$ site/g.cat)
Cu/Na-ZSM-5	1.121	1.35
Cu/H-ZSM-5	2.247	2.71

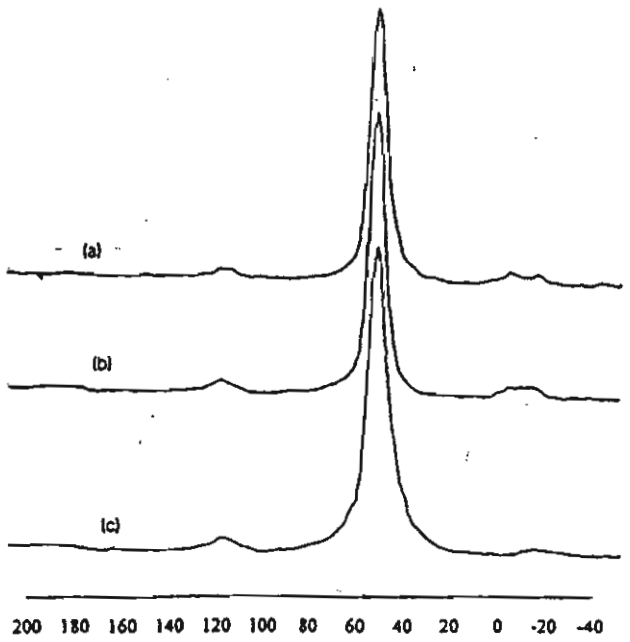

Fig. 5. Al-NMR spectra of (a) fresh H-ZSM-5; (b) spent H-ZSM-5 and (c) spent Cu/H-ZSM-5.

uncertain. It could be that these residual cations influence catalyst site directly. On the other hand, they may affect the Cu^{+}/Cu^{2+} ratio in the copper exchanged and calcined zeolites. Although the total copper content on both Cu/ZSM-5 zeolites was carefully controlled to be about the same, differences in the copper state may have occurred. It is generally accepted that several oxidation states of Cu can exist on Cu/ZSM-5 surface (Valyon & Hall, 1993; Gruinert, Hayes, Joyner, Shpiro, Siddiqui & Baeva, 1994). The residual cations could affect the distribution of states in each of the zeolite. Thus, the copper oxidation state was examined. CO adsorption is a simple method to determine the amount of Cu^{1+} (Iwamoto et al., 1991). The amount of CO adsorbed on the catalyst surface represents the amount of Cu^{1+}. Our measurements are shown in Table 3. The amount of Cu^{1+} in Cu/H-ZSM-5 appears to be about double in Cu/Na-ZSM-5. Since the total copper content of the two catalysts was equal, Cu/H-ZSM-5 had a higher Cu^{1+}/Cu^{2+} ratio. The difference in Cu^{1+}/Cu^{2+} could have an effect on the activity in the copper exchanged zeolites. One possibility for the different ratio is that the reducibility of Cu in the zeolites is affected by the residual cations.

Another explanation of the zeolite differences observed in our study is different extents of formation of Lewis acid sites through dealumination of the zeolite. This possibility was examined by carefully measuring the alumina content of our zeolite samples. Fig. 5 shows Al-NMR pattern of H-ZSM-5 and Cu/H-ZSM-5. Only one peak at around 50 ppm was observed in all samples. This peak is assigned to tetrahedral aluminum. The intensity of the peak was not reduced in spent catalysts indicating that dealumination did not occur in this study. This is supported by Torre-Abreu, Ribeiro, Henriques, Ribeiro and Delahay (1997). The dealumination of H-ZSM-5 and Cu/ZSM-5 was observed only in severely steamed samples (Tabata, Kokitsu, Okada, Nakayama, Yasumatsu & Sakane, 1994; Budi, Curry-Hyde & Howe, 1996). Therefore, dealumination of catalyst is not involved in the different activities observed among the zeolites in this study.

4. Conclusions

Among catalysts in this study, Na-ZSM-5 is not active in any reaction involving NO, O_2 and C_3H_8. H-ZSM-5 is not active in the decomposition of NO but is active in the oxidation of NO of NO_2. This probably implies that H-ZSM-5 does not adsorb NO but preferentially adsorbs O_2 which subsequently reacts with NO in the gas phase to form NO_2. The difference in activity between Cu/Na-ZSM-5 and Cu/H-ZSM-5 was not evident when oxygen was present in feed. When only NO was present, Cu/H-ZSM-5 produced more NO_2 but less N_2O than Cu/Na-ZSM-5. In addition, Cu/H-ZSM-5 was found to be more active than Cu/Na-ZSM-5 in the reduction of NO by propane in the absence of oxygen. NO_2 was produced more rapidly over Cu/H-ZSM-5 especially in the absence of oxygen compared with Cu/Na-ZSM-5. Promotion of O_2 oxidation of propane of H-ZSM-5 in the presence of NO was observed. The different activities of Cu/Na-ZSM-5 and Cu/H-ZSM-5 might be due to either the different residual cations or the Cu^{1+}/Cu^{2+} ratio on catalysts surface which was probably cause by these same cations. Differences in this ratio were found. Further study is needed to identify as to which of these explanations of the residual cations effect is correct.

Acknowledgements

These experiments were performed at The Reactor Engineering Laboratory of Prof. P.L. Silveston, Chemical Engineering Department, University of Waterloo. The research was supported financially by the Thailand Research Fund.

References

Budi, P., Curry-Hyde, E., & Howe, R. F. (1996). Stabilization of Cu/ZSM-5 NO_x reduction catalysts with lanthanum. *Catalysis Letters, 41*, 47–53.

Burch, R., & Millington, P. J. (1993). Role of propane in the selective reduction of nitrogen monoxide in copper-exchanged zeolites. *Applied Catalysis B. Environment, 2*, 101–116.

Burch, R., & Scire, S. (1994). Selective catalytic reduction of nitric oxide with ethene and methane on some metal exchanged ZSM-5 zeolite. *Applied Catalysis B. Environment, 3*, 295–318.

Centi, G., & Perathoner, S. (1996). Role and importance of oxidized nitrogen oxide adspecies on the mechanism and dynamics of reaction over copper-based catalysts. *Catalysis Today, 29*, 117–122.

Chajar, Z., Primet, M., Praliaud, H., Cherrier, M., Gauthier, G., & Mathis, F. (1994). Nitrogen dioxide effect in the reduction of nitric oxide by propane in oxidizing atmosphere. *Catalysis Letters, 28*, 33–40.

Cho, B. K. J. (1995). Nitric oxide reduction by ethylene over Cu-ZSM-5 under lean conditions: study of reaction dynamics by transient experiment. *Journal of Catalysis, 155*, 184–195.

Grunert, W., Hayes, N. W., Joyner, R. W., Shpiro, E. S., Siddiqui, R. H., & Baeva, G. N. (1994). Structure, chemistry, and activity of Cu-ZSM-5 catalysts for the selective reduction of NO_x in the presence of oxygen. *Journal of Physical Chemistry, 98*, 10832–10846.

Halasz, I., Brenner, A., & Simon Ng, K. Y. (1995). Active sites of H-ZSM-5 catalysts for the oxidation of nitric oxide by oxygen. *Catalysis Letters, 34*, 151–161.

Held, W., Konig, A., Richter, T., & Puppe, L. (1990). Catalytic NO_x reduction in net oxidizing exhaust gas. *SEA, 900496*, 13–19.

Hoost, T. E., Laframboise, K. A., & Otto, K. (1995). Co-adsorption of propane and nitrogen oxides on Cu-ZSM-5: An FTIR study. *Applied Catalysis B. Environment, 7*, 79–93.

Inui, T., Vamase, O., Fuguda, K., Itoh, A., Tarumoto, J., Morinage, N., Hagiwara, T., & Takegami, Y. (1984). *Proceedings of the Eighth International Congress on Catalysis*, Berlin, vol. 3, (p. 569).

Iwamoto, M. (1991). Copper ion-exchanged zeolites as active catalysts for direct decomposition of nitrogen monoxide. *Studies on Surface Science Catalysis, 60*, 327–334.

Iwamoto, M., & Hamada, H. (1991). Removal of nitrogen monoxide from exhaust gases through novel catalytic processes. *Catalysis Today, 10*, 51–71.

Iwamoto, M., Yahiro, H., Tanda, K., Mizuno, N., Mine, Y., & Kagawa, S. (1991). Removal of nitrogen monoxide through a novel catalytic process. 1. decomposition on excessively copper ion exchanged ZSM-5 Zeolites. *Journal of Physical Chemistry, 95*, 3727–3730.

Iwamoto, M., Mizuno, N., & Yahiro, H. (1992). Selective catalytic reduction of NO by hydrocarbon in oxidizing atmosphere. *Proceedings of the 10th International Congress on Catalysis*, Budapest (pp. 213–215).

Iwamoto, M. (1994). Heterogenous catalyst for removal of NO in excess oxygen: Progress in 1994. *Catalysis Today, 29*, 29–35.

Khodadadi, A. A. (1994). *Transient studies of the Fisher–Tropsch synthesis over a cobalt catalyst*. Ph.D. thesis, Univ. of Waterloo, Waterloo, Ontario, Canada.

Kucherov, A. V., Hubbard, C. P., Kucherova, T. N., & Shelef, M. (1996). Stabilization of the ethane oxidation catalytic activity of Cu-ZSM-5. *Applied Catalysis B. Environment, 7*, 285–298.

Li, Y., & Hall, W. K. (1990). Stoichiometric catalytic decomposition of nitric oxide over Cu-ZSM-5 catalysts. *Journal of Physical Chemistry, 94*, 6145–6147.

Mongkolsiri, N. (1998). *Effect on remaining cations in copper ion exchanged ZSM-5 zeolite for selective reduction on nitric oxide*. Ph.D. Thesis Chulalongkorn Univ. Bangkok, Thailand (Contact authors for a copy).

Neyestanaki, A. K., Kumar, N., & Lindfors, L. -E. (1995). Catalytic combustion of propane and natural gas over Cu and Pd modified ZSM-5 zeolite catalysts. *Applied Catalysis B. environment, 7*, 95–111.

Petunchi, J. O., & Hall, W. K. (1993). On the role of nitrogen dioxide in the mechanism of the selective reduction of NO_x over Cu-ZSM-5 zeolite. *Applied Catalysis B. Environment, 2*, L17–L26.

Pirone, R., Ciambelli, P., Morrette, G., & Russo, G. (1996). Niric oxide decomposition over Cu-exchanged ZSM-5 with high Si/Al ratio. *Applied Catalysis B. Environment, 8*, 197–207.

Sasaki, M., Hamada, H., Kintaichi, Y., & Ito, T. (1992). Role of oxygen in selective reduction of nitrogen monoxide by propane over zeolite and alumina-based catalysts. *Catalysis Letters, 15*, 297–304.

Shelef, M., Montreuil, C. N., & Jen, H. W. (1994). NO_2 formation over Cu/ZSM-5 and the selective catalytic reduction of NO. *Catalysis Letters, 26*, 277–284.

Shelef, M. (1995). Selective catalytic reduction of NO_x with N-free reduction. *Chemical Review, 95*, 209–225.

Tabata, T., Kokitsu, M., Okada, O., Nakayama, T., Yasumatsu, T., & Sakane, H. (1994). Deterioration mechanism of Cu/ZSM-5 as a catalyst of selective reduction of NO_x by hydrocarbons from the exhaust of stationary natural gas-fueled engine. *Studies on Surface Science and Catalysis, 88*, 409–417.

Torre-Abreu, C., Ribeiro, M. F., Henriques, C., Ribeiro, F. R., & Delahay, G. (1997). Deactivation of Cu-MFI catalysts under NO selective catalytic reduction by propane: influence of zeolite form, Si/Al ratio and copper content. *Catalysis Letters, 43*, 31–36.

Valyon, J., & Hall, W. K. (1993). Studies of species formed NO on copper zeolites. *Journal of Physical Chemistry, 97*, 1204–1212.

Zhang, Y., Leo, K. M., Salofim, A. F., & Hu, Z. (1995). Preparation effects on the activity of Cu-ZSM-5 catalyst for NO decomposition. *Catalysis Letters, 31*, 75–89.

Influence of Fe or Zn Loading Method on the Toluene Methylation over MFI-Type Zeolite Catalysts

*Suphot Phatanasri, Piyasan Praserthdam, and Thana Punsupsawat

Petrochemical Engineering Laboratory, Department of Chemical Engineering, Faculty of Engineering, Chulalongkorn University, Bangkok 10330, Thailand.

Fax: (+662)2186890, (+662)6390449, e-mail: suphot@thaibeginner.com

ABSTRACT Toluene methylation with methanol was investigated on MFI-type zeolite catalysts containing Fe or Zn within the range of 0 - 2 % by weight as an active component. The catalytic performances were compared on catalysts to which Fe or Zn was introduced by different methods, i.e. ion-exchanged and incorporation methods. The prepared catalysts were characterized by XRD, XRF, BET, FTIR and pyridine adsorption technique on in-situ FTIR. The results showed that the incorporated samples, H-Fe,Al-silicate(Si/Fe=150) and H-Zn,Al-silicate(Si/Zn=150), exhibited catalytic activity and xylene selectivities approximately equivalent to those from the ion-exchanged samples, Fe(0.8)/H-MFI and Zn(1.0)/H-MFI, containing nearly the same amount of Fe or Zn. The higher *p*-xylene selectivity was achieved with H-Fe,Al-silicate (Si/Fe=150) and H-Zn,Al-silicate (Si/Zn=150) because of the Brönsted acid strengths weaker than Fe(0.8)/H-MFI and Zn(1.0)/H-MFI. Therefore, the isomerization of *p*-isomer produced primarily was suppressed on the incorporated catalysts better than the ion-exchanged ones.

Running Title: Influence of metal loading methods on toluene methylation over MFI zeolites

Keywords: ion-exchange method, incorporation method, modified MFI zeolites, toluene methylation, characterization

---

* *To whom correspondence should be made.*

INTRODUCTION

MFI zeolites are known as a noteworthy material which have been used as catalysts in many commercial processes. Among their properties, shape selectivity, the presence of strong acid sites, and the resistance to deactivation by coking are the main causes of the unique catalytic behavior. The alkylation of benzene or toluene with light hydrocarbons over acidic catalysts for production of alkylaromatics is an important industrial process [Weitkamp, 1982]. The alkylation over solid catalysts usually has been employed. Initially, protonated or rare earth exchanged faujasites were used in the alkylation of benzene with various olefins [Venuto et al., 1966]. For instance, Yashima et al. [Yashima et al., 1981] focused attention on the distribution of xylene isomers produced by alkylation of toluene with methanol over a variety of cation exchanged Y-zeolites. Consequently, MFI has been used as an alkylation catalyst for the methylation of toluene with methanol [Kaeding et al., 1981]. Many researchers tried to modify MFI in order to alter the selectivities of the alkylaromatics products. Kaeding et al. [Kaeding et al., 1984] proposed that the higher para-selectivity was achieved with MgO, P_2O_5, B_2O_3 or SiO_2 modified MFI. Papa ratto et al. [Papa ratto et al., 1989] reported that the improvement in para-selectivity by the modification of MFI was due to the inactivation of the acid sites on the external surfaces. Sotelo et al. [Sotelo et al., 1993] reported that the impregnation of MFI with Mg or Ni also increases the para-selectivity.

The influence of the preparation methods, however, i.e. ion-exchange or incorporation method on the location of loading metals and their role for the catalytic properties were only briefly reported so far [Yashima et al., 1981, Inui et al., 1992, Parikh et al., 1992]. Therefore, we tried to obtain a more specific relation between the structural properties and the catalytic activity of the modified H-MFI catalysts in

toluene methylation with methanol. To this end, we investigated the catalytic activity of Fe- and Zn-MFI zeolites which were prepared by applying various loading methods in an attempt to change the location of the metals.

EXPERIMENTAL SECTION

Catalyst Preparation

The MFI-type catalysts were prepared by adopting the rapid crystallization method [Inui, 1989] using TPABr as a template. The Na-form MFI-type obtained was converted to its protonated form by four times ion-exchange with 1 M NH_4NO_3 solutions at 80 °C for 1 h, then washed with distilled water, dried overnight at 110 °C, and finally calcined in air at 540 °C for 3.5 h.

H-MFI zeolites incorporated with Fe or Zn, H-Fe,Al-silicate or H-Zn,Al-silicate were prepared by the rapid crystallization method similar to H-MFI synthesis but adding both Al and Fe or Zn during the stage of gel formation before crystallization.

H-MFI materials ion-exchanged with Fe or Zn, Fe/H-MFI or Zn/H-MFI catalyst were prepared by ion-exchange H-MFI with an aqueous solution of $Fe(NO_3)_3.9H_2O$ or $Zn(NO_3)_2.6H_2O$ followed by drying at 110 °C and calcined in air at 350 °C for 2 h. The loading amount of Fe and Zn was in the range of 0-2 % by weight. All the catalysts were tableted, crushed and sieved to 8-16 mesh for the reaction.

Catalyst Characterization

The prepared catalysts were characterized by employing the techniques of XRD (SIEMENS D5000 diffractometer) to confirm MFI framework structure; BET measurement (micromeritics ASAP2000 analyzer) to determine catalyst surface areas;

XRF (Fisons ARL-8410 spectrometer) to determine bulk compositions; FTIR (Nicolet Impact 400 spectrometer) to determine the vibrational modes in the structure sensitive region; and pyridine adsorption on in-situ FTIR to determine the zeolite acidities.

Pyridine adsorption technique on in-situ FTIR was described as following procedure: The prepared catalysts were pressed into self-supporting wafer, mounted in a vacuum apparatus containing cell for IR measurements fitted with potassium bromide windows. The wafer was pretreated by heating to 300 °C for 1 h under vacuum. Then, pyridine was allowed to expose the wafer for 2 h at room temperature. The wafer was then evacuated at 50 °C for 10 min and heated from 50 °C to 450 °C at a heating rate of 5 °C/min to desorb pyridine. In order to measure acid concentration and compare acid strength, the spectra were collected in the temperature range 150-450°C. Infrared spectra were collected on the spectrometer stated above with a resolution of 4 cm^{-1} and typically 500 interferograms were used as an average value.

Catalysis

The toluene methylation with methanol was carried out in a fixed bed tubular quartz reactor under atmospheric pressure. A portion of 0.25 g catalyst was packed in 6.0 mm inner diameter quartz reactor. The feed mixture of toluene and methanol was vaporized before it was contacted with the catalyst bed. The products were analyzed by a SHIMADZU GC-14A gas chromatograph using the flame ionization detector with silicon OV-1 and bentone column. The product selectivities were calculated on the carbon number basis.

RESULTS AND DISCUSSIONS

Catalyst Characterization

The X-ray diffraction (XRD) patterns of the prepared catalysts are shown in Fig. 1. All the prepared catalysts had substantially the structure identical to MFI-type zeolite. The MFI-type framework structure has been further confirmed by FTIR spectra using the KBr technique (0.5 % by weight catalyst) for studying vibrational modes in the structure-sensitive region [Karge, 1998]. As shown in Fig. 2, all the prepared catalysts provided the similar asymmetric stretching vibrations at 1220-1230 and 1100-1110 cm^{-1}; symmetric stretching vibration at 795-800 cm^{-1}; double ring vibration at 540-555 cm^{-1}; and the T-O stretching vibration at 440-450 cm^{-1}. Metal loading did not significantly affect the structure and shape of crystals. BET surface areas and other physical properties of catalysts are shown in Table 1.

From Table 1, the loading of Fe or Zn on H-MFI with incorporation method provided BET surface areas and external surface areas approximately the same as H-MFI. On the other hand, in case of small amounts loading of metal, Fe(0.2)/H-MFI, and Zn(0.2 %)/H-MFI , the external surface areas decreased and micropore areas increased when compared with those of H-MFI. By contrast, the external surface areas increased and micropore areas decreased with the high amounts loading of metal, Fe(0.8)/H-MFI and Zn(1.0)/H-MFI. This suggests that the aggregation of Fe and Zn on the external surface preferably occurred in case of the high amount loaded samples and only small amounts of Fe and Zn could be ion-exchanged with H^+. The aggregation of Fe and Zn on the external surface of catalyst may hinder the passage of N_2 and its adsorption on micropore areas resulting to the lower micropore areas in case of Fe(0.8)/H-MFI and Zn (1.0)/H-MFI.

The pyridine adsorption technique on in-situ FTIR was adopted for the assessment of Brönsted and Lewis acidities. The bands at about 1540 cm^{-1} and 1450 cm^{-1} were reportedly assigned to pyridine adsorbed on Brönsted and Lewis acid sites, respectively [Connerton et al., 1995, Campbell et al., 1996, Karge 1998]. The FTIR spectra of pyridine adsorbed on the prepared catalysts are shown in Fig. 3. The Brönsted and Lewis acid site concentrations of each zeolite sample were determined by measurement of peak areas of these bands at the reference temperature of 150 °C while the relative acid strengths were determined by measurement of the temperature required for reduce a half of pyridine adsorbed; the higher the temperature, the stronger the acid strength. The results are summarized in Table 2.

Effect of Metal Loading Amount in Fe/H-MFI and Zn/H-MFI Catalysts

The catalytic performances on toluene methylation with methanol of Fe/H-MFI and Zn/H-MFI catalysts containing Fe or Zn within the range of 0-2 wt.% loading are shown in Figs. 4 and 5. These data reveal that H-MFI ion-exchanged with 0.8 wt% of Fe, Fe(0.8)/H-MFI, and H-MFI ion-exchanged with 1.0 wt% of Zn, Zn(1.0)/H-MFI, exhibited the best aromatics and xylene selectivities. On the other hand, Fe(0.2)/H-MFI and Zn(0.2)/H-MFI provided the best *p*-xylene selectivity but exhibited the lowest toluene conversion and xylene selectivities. Of all xylene produced, the amount of *o*-xylene was almost constant while the amount of *p*-xylene was inversely related with that of *m*-xylene and toluene conversion. This can be explained by considering that isomerization of *p*-xylene proceeds as the secondary reaction and plays an important role on xylene selectivities [Yashima et al., 1981, Olson et al., 1984, Kaeding, 1985, Sotelo et al., 1993].

Effect of Metal Loading by Incorporation and Ion-exchange

For comparison, H-MFI incorporated with Fe or Zn, H-Fe,Al-silicate or H-Zn,Al-silicate were prepared. The comparative results are shown in Table 3. The thermodynamic compositions of xylene isomers at reaction temperature are given in parentheses.

From Table 3, both H-Fe,Al-silicate (Si/Fe=150) and H-Zn,Al-silicate (Si/Zn=150) exhibited catalyst activity and xylene selectivities approximately equivalent to Fe(0.8)/H-MFI and Zn(1.0)/H-MFI containing nearly the same amount of Fe or Zn. However, *p*-xylene selectivities obtained from toluene methylation with methanol on Fe(0.8)/H-MFI and Zn(1.0)/H-MFI were close to those expected from the thermal equilibrium. A further comparison of *p*-xylene to *m*-xylene and *p*-xylene to *o*-xylene ratios between Fe(0.8)/H-MFI and H-Fe,Al-silicate (Si/Fe=150); Zn(1.0)/H-MFI and H-Zn,Al-silicate (Si/Zn=150) at various reaction temperatures is given in Fig. 6.

The higher *p*-xylene selectivity was achieved with H-Fe,Al-silicate (Si/Fe=150) and H-Zn,Al-silicate (Si/Zn=150) at any reaction temperatures and hence less *p*-xylene isomerization than did Fe/H-MFI and Zn/H-MFI. Moreover, H-Fe,Al-silicate and H-Zn,Al-silicate can be prepared in only one-step crystallization and need no post-synthesis treatment by ion-exchange. This suggests that the modification of the catalytic properties of MFI-type zeolite by loading Fe or Zn as an active component by incorporation method is rather suitable for toluene methylation with methanol than ion-exchanged method because of the high selectivity of *p*-xylene obtained and the convenience of one-step preparation. In addition, it should be noted that the *p*-xylene selectivity decreased while *m*-xylene and *o*-xylene selectivities increased with the increasing reaction temperature.

Regarding the results in Table 2 it has been found that the increasing order of Brönsted acid strength in Fe-containing MFI was Fe(0.2)/H-MFI < H-Fe,Al-silicate (Si/Fe=150) < Fe(0.8)/H-MFI, and that in Zn-containing MFI was Zn(0.2)/H-MFI < H-Zn,Al-silicate (Si/Zn=150) < Zn(1.0)/H-MFI. The order of Brönsted acid strength was inversely related to *p*-xylene selectivity obtained from toluene methylation reaction. This suggests that the Brönsted acid strength plays a more important role to *p*-xylene selectivity than amount of Brönsted acid sites. Either Fe, Zn ion-exchanged or incorporated in H-MFI caused the decrease in amount and strength of Brönsted acid sites and the increase in amount of Lewis acid sites. It has been found that Zn-containing MFI catalysts especially the high amount loading samples exhibited the higher strength of Lewis acid sites than H-MFI which was consistent with the study of Berndt et al. [Berndt et al., 1996].

CONCLUSION

The different metal loading methods, i.e. incorporation and ion-exchanged ones, affect the structural properties and catalytic activity of the modified H-MFI zeolites. The variation in acidic properties between the incorporated catalysts and the ion-exchanged ones reflects the different location of metal in H-MFI zeolites. According to the results obtained, it is worthy to note that the strength of Brönsted acid sites plays a more important role to *p*-xylene selectivity than the amount of Brönsted acid sites. The higher *p*-xylene selectivity obtained on H-MFI zeolites containing Fe or Zn via incorporation method was attributed to the moderate Brönsted acid strength by which the isomerization of *p*-isomer was considerably suppressed.

ACKNOWLEDGEMENT

The authors would like to express their appreciation to the Thailand Research Fund (TRF) which partly supports this work.

REFERENCES

Berndt, H., Lietz, G. and Volter, "Zinc Promoted HZSM-5 Catalysts for Conversion of Propane to Aromatics", *J. Appl. Catal. A.*, **146**, 351 (1996).

Campbell, M., Bibby, M., Coddington, M., Howe, F. and Meinhold, H., "Dealumination of HZSM-5 Zeolites", *J. Catal.*, **161**, 358 (1996).

Connerton, J., Joyner, R. and Padley, M., "Characterisation of the Acidity of Well Defined Cu-ZSM-5 Catalysts Using Pyridine as a Probe Molecule", *J. Chem. Soc. Faraday Trans.*, **91**, 1841 (1995).

Inui, T., "Mechanism of Rapid Zeolite Crystallizations and Its Applications to Catalyst Synthesis", *ACS. Symp.*, 480 (1989).

Inui, T., Nagata, H., Okazumi, F., and Matsuda, H., "Catalytic Properties of Metallosilicates Containing Iron Group Metals in Light-Olefin Conversions", *Catal. Lett.*, 13, 297 (1992).

Kaeding, W.W., "Shape-Selective Reactions with Zeolite Catalyst V. Alkylation or Disproportionation of Ethylbenzene to Produce p-Diethylbenzene", *J. Catal.*, 95, 512 (1985).

Kaeding, W.W., Chu, C., Young, L.B., Weistein and Butter, S.A., "Selective Alkylation of Toluene with Methanol to Produce *p*-Xylene", *J. Catal.*, 67, 159 (1981).

Kaeding, W.W., Chu, C. and Young, L.B., "Shape-Selective Reactions with Zeolite Catalysts IV. Alkylation of Toluene with Ehylene to Produce p-Ethyltoluene", *J. Catal.*, 89, 267 (1984).

Karge, H.G., "Characterization by Infrared Spectroscopy", *Microporous Materials*, 22, 547 (1998).

Olson, D.H. and Haag, W.O., "Catalytic Materials Relationship Between Structure and Reactivity", *ACS. Symp.*, 248, 275 (1984).

Paparatto, G., de Alberti, G., Leofanti, G. and Padovan, M., "Toluene Ethylation on ZSM-5 Zeolites", *Stud. Surf. Sci. Catal.*, 41, 225 (1989).

Parikh, P.A., Subamanyum, N., Bhat, Y.S., and Halgeri, A.B., "Toluene Ethylation over Metallosilicates of MFI Structure", *Catal. Lett.*, 14, 107 (1992).

Sotelo, J.L., Uguina, M.A., Valverde, J.L. and Serrano, D.P., "Kinetics of Toluene Alkylation with Methanol over Mg-Modified ZSM-5", *J. Ind. Eng. Chem. Prod. Res.*, 32, 2548 (1993).

Venuto, P.B., Hamilton, L.A. and Landis, P.S., "Organic Reactions Catalyzed by Crystalline Aluminosilicates II. Alkylation Reactions", *J. Catal.*, 5, 484 (1966).

Weitkamp, "Isomerization of Long-Chain n-Alkanes on a Pt/CaY Zeolite Catalyst", *J. Ind. Eng. Chem. Prod. Res.*, 21, 550 (1982).

Yashima, T., Sakaguchi, Y. and Namba, S., "Selective Formation of *p*-Xylene by Alkylation of Toluene with Methanol on ZSM-5 Type Zeolites", *Stud. Surf. Sci. Catal.*, 7, 739 (1981).

Table 1. BET surface area of MFI catalysts prepared here

Catalyst	Ext. surf. area (m^2/g)	Micropore area (m^2/g)	BET surf. area (m^2/g)	Avg. pore dia. (^oA)
H-MFI	160.07	215.65	375.72	17.49
Fe(0.2)/H-MFI	138.93	247.55	386.48	19.82
Fe(0.8)/H-MFI	190.66	189.83	380.48	17.97
H-Fe,Al-silicate (Si/Fe=150)	156.74	221.38	378.11	17.76
Zn(0.2)/H-MFI	130.04	238.63	368.67	19.93
Zn(1.0)/H-MFI	225.39	160.38	385.76	17.63
H-Zn,Al-silicate (Si/Zn=150)	161.16	217.62	378.78	19.53

* All the prepared catalysts have bulk Si/Al ratio in the range of 31-35.

Table 2. Brönsted and Lewis acidities on catalysts

Catalyst	A_B	A_L	$T_{B/2}$ (°C)	$T_{L/2}$ (°C)
H-MFI	82.8	39.2	366	242
Fe(0.2)/H-MFI	36.8	90.1	320	241
Fe(0.8)/H-MFI	60.1	63.5	354	200
H-Fe,Al-silicate (Si/Fe=150)	79.6	61.9	348	208
Zn(0.2)/H-MFI	36.7	73.1	255	234
Zn(1.0)/H-MFI	54.9	66.0	320	262
H-Zn,Al-silicate (Si/Zn=150)	46.0	93.6	298	260

* A_B and A_L refer to areas by weight of band at 1540 cm^{-1} due to Brönsted acid sites and at 1450 cm^{-1} due to Lewis acid sites, respectively. $T_{B/2}$ and $T_{L/2}$ refer to temperature required for reduce a half of pyridine adsorbed on Brönsted and Lewis acid sites, respectively.

Table 3. Comparison of catalytic performances of different catalysts

(450 °C, GHSV 6000 h^{-1}, 1.5 h on stream, Methanol/Toluene feed ratio 2.5-3.5:1 by wt.)

Catalyst	H-MFI	Fe-containing MFI			Zn-containing MFI		
		(0.2)	(0.8)	(150)	(0.2)	(1.0)	(150)
Fe or Zn Observed (wt %)	0.00	0.25	0.46	0.50	0.19	0.74	0.76
Conversion (%)							
Methanol	90.7	73.1	93.5	94.0	77.7	93.3	93.9
Toluene	66.0	55.1	71.7	70.6	55.5	70.2	72.0
Products Distribution (wt %)							
C1-C4	40.1	49.4	31.7	31.8	46.7	29.9	27.4
C5-C8	2.0	2.1	2.5	4.0	7.7	3.6	1.8
Benzene	2.2	0.2	1.0	0.5	0.2	1.1	1.0
Toluene	14.6	17.2	12.4	13.3	17.4	14.3	12.2
Ethylbenzene	0.2	0.2	0.3	0.3	0.2	0.3	0.4
Xylene	30.3	20.7	33.6	31.6	22.5	33.9	37.0
Ethyltoluene	8.4	6.8	14.3	13.5	7.5	13.2	16.3
Others	2.2	3.5	4.1	5.2	3.9	3.6	4.0
Xylene Composition (%)							
p-xylene (21.56)	30.5	44.7	26.3	34.4	45.1	26.7	29.0
m-xylene (53.33)	46.8	32.0	51.2	45.3	32.5	51.7	49.3
o-xylene (25.11)	22.6	23.3	22.5	20.3	22.4	21.6	21.7

* Fe(0.2), Fe(0.8), Fe(150), Zn(0.2), Zn(1.0) and Zn(150) refer to Fe(0.2)/H-MFI, Fe (0.8)/H-MFI, H-Fe,Al-silicate(Si/Fe=150), Zn(0.2)/H-MFI, Zn(1.0)/H-MFI and H-Zn,Al-silicate(Si/Zn=150), respectively.

Fig. 1 XRD patterns of the prepared catalysts

Fig. 2 FTIR spectra of the prepared catalysts

(a) H-MFI, (b) Fe(0.8)/H-MFI, (c) H-Fe,Al-silicate (Si/Fe=150), (d) Zn(1.0)/H-MFI, and (e) H-Zn,Al-silicate (Si/Zn=150)

Fig. 3 FTIR spectra of pyridine adsorbed on the prepared catalysts

(a) H-MFI, (b) Fe(0.2)/H-MFI, (c) Fe(0.8)/H-MFI, (d) H-Fe,Al-silicate (Si/Fe=150), (e) Zn(0.2)/H-MFI, (f) Zn(1.0)/H-MFI, and (g) H-Zn,Al-silicate (Si/Zn=150)

Fig. 4 Catalytic performances of Fe/H-MFI with different amounts of Fe on toluene methylation with methanol

(a) Toluene conversion, Product selectivities; (b) Xylene selectivities

Reaction conditions: 450 °C, 6000 h^{-1} GHSV, 1.5 h on stream, methanol/toluene feed ratio 2.5-3.5:1 by wt.

Fig. 5 Catalytic performances of Zn/H-MFI with the different amounts of Zn on toluene methylation with methanol

(a) Toluene conversion, Product selectivities; (b) Xylene selectivities

Reaction conditions: 450 °C, 6000 h^{-1} GHSV, 1.5 h on stream, methanol/toluene feed ratio 2.5-3.5:1 by wt.

Fig. 6 (a) Xylene selectivities on

(i) Fe(0.8)/H-MFI and (ii) H-Fe,Al-silicate (Si/Fe=150)

(b) Xylene selectivities on

(i) Zn(1.0)/H-MFI and (ii) H-Zn,Al-silicate (Si/Zn=150)

Reaction conditions: 350-550 °C, 6000 h^{-1} GHSV, 1.5 h on stream, methanol/toluene feed ratio 2.5-3.5:1 by wt.

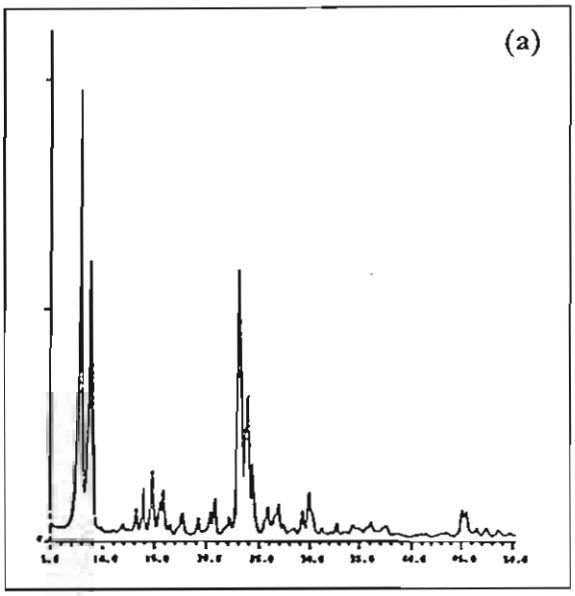
(a)

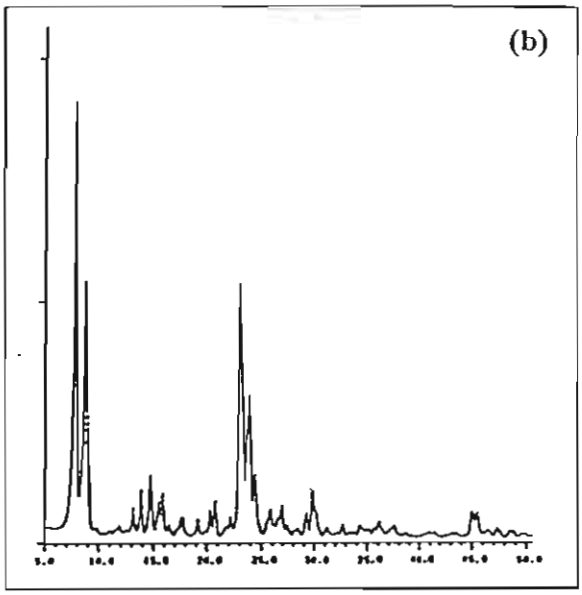
(b)

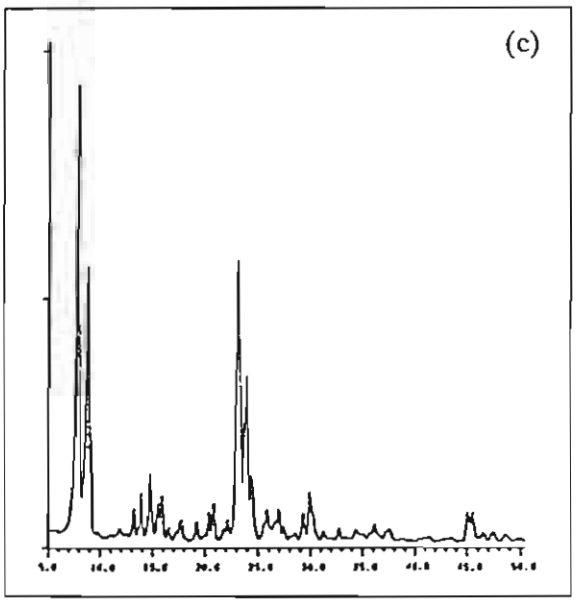
(c)

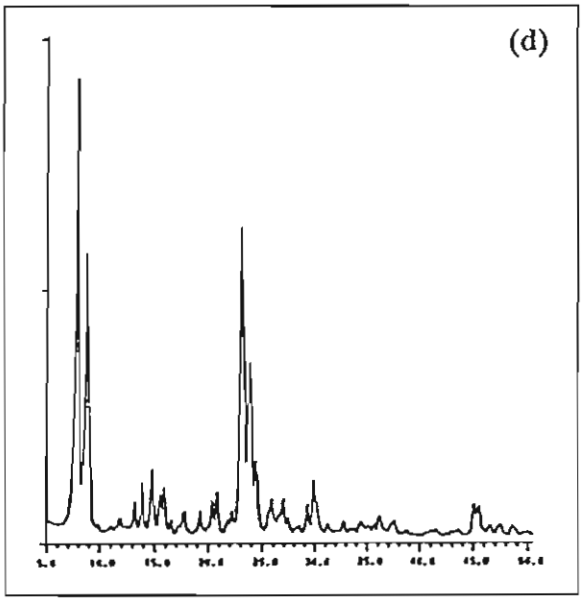
(d)

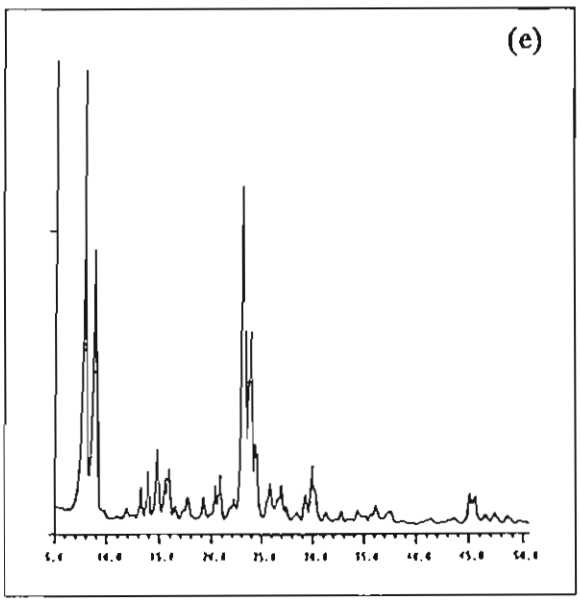
(e)

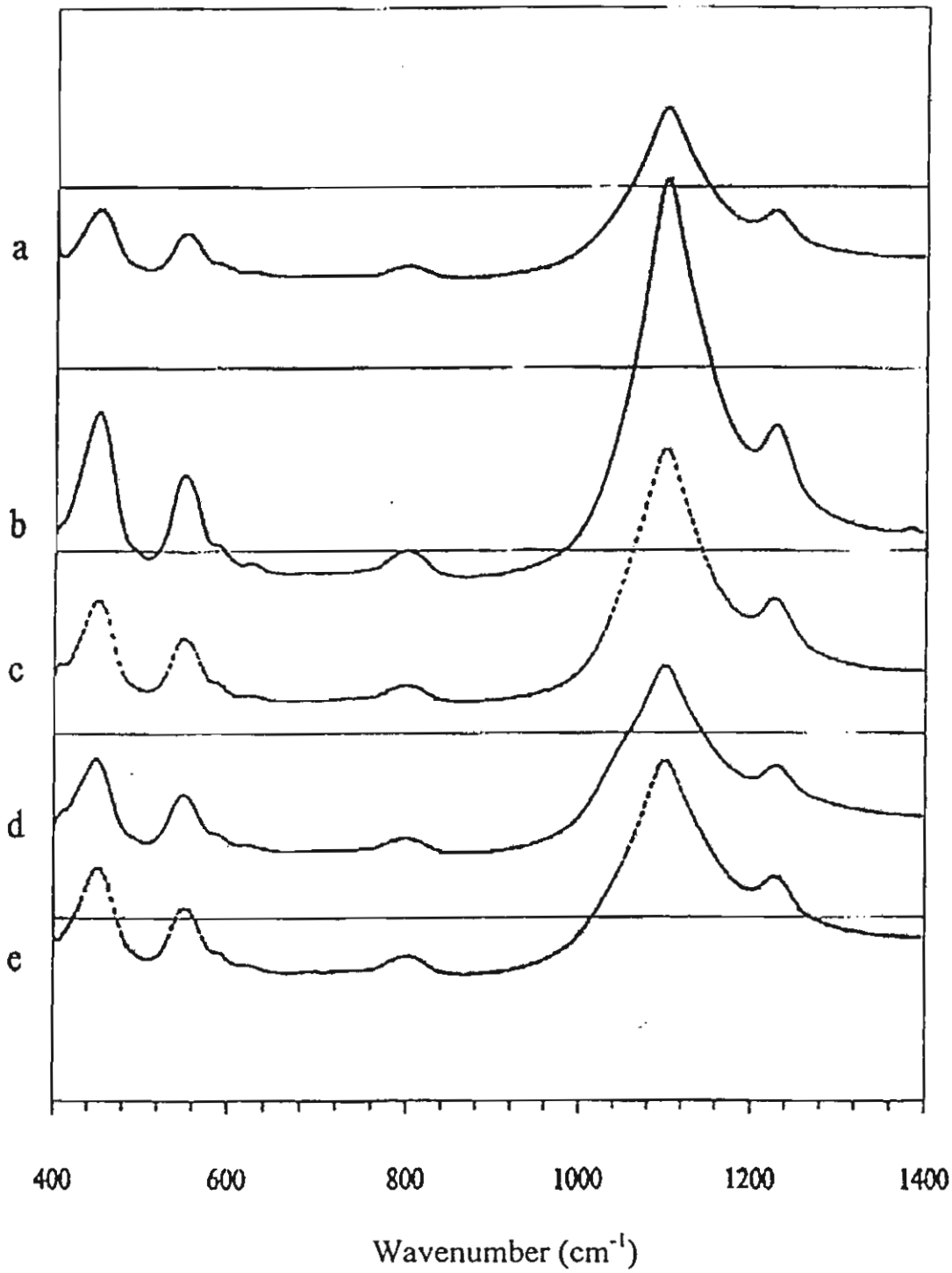
a
b
c
d
e
400
600
800
1000
1200
1400
Wavenumber (cm-1)

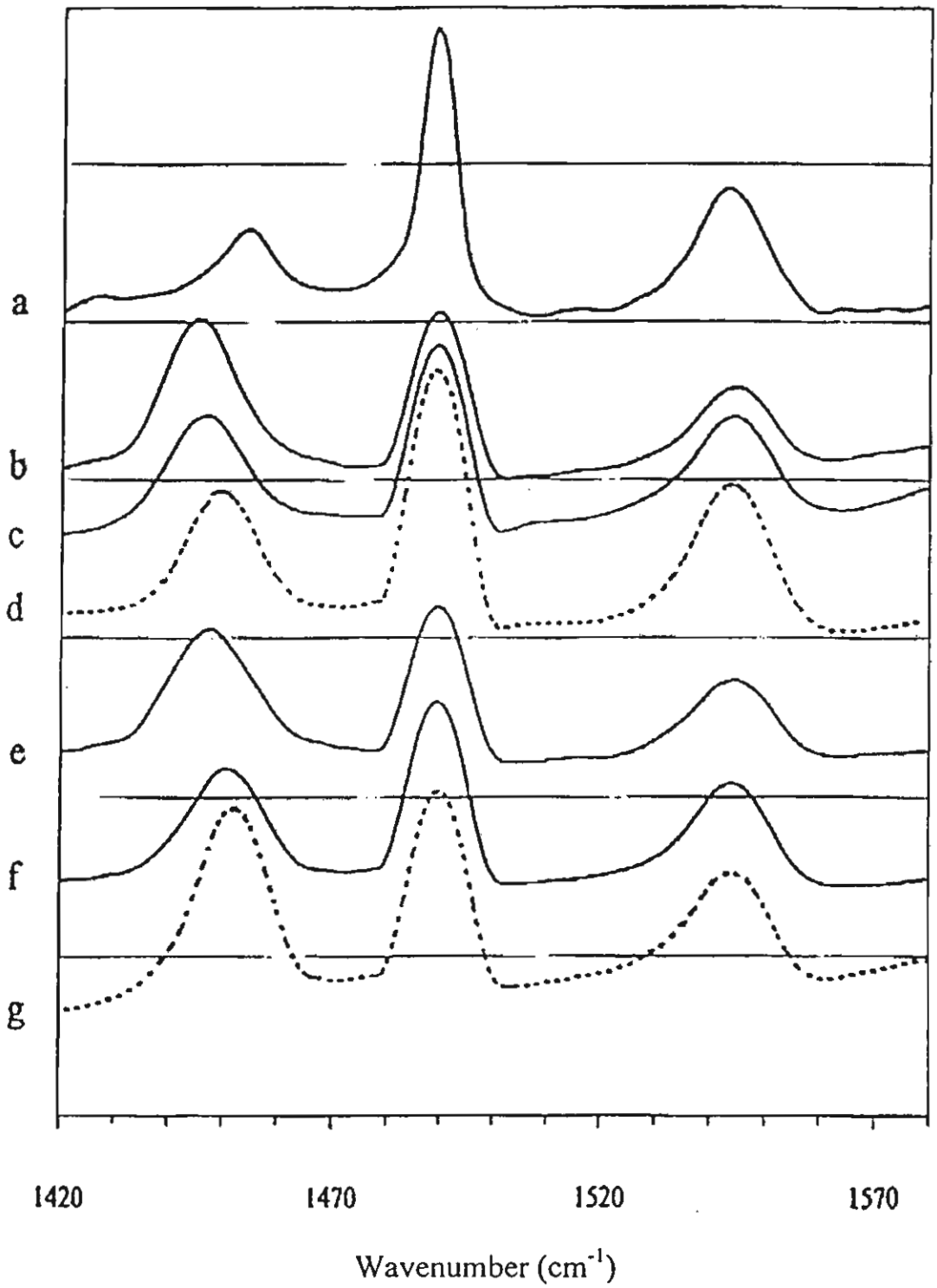
a
b
c
d
e
f
g
1420
1470
1520
1570
Wavenumber (cm-1)

4(a)

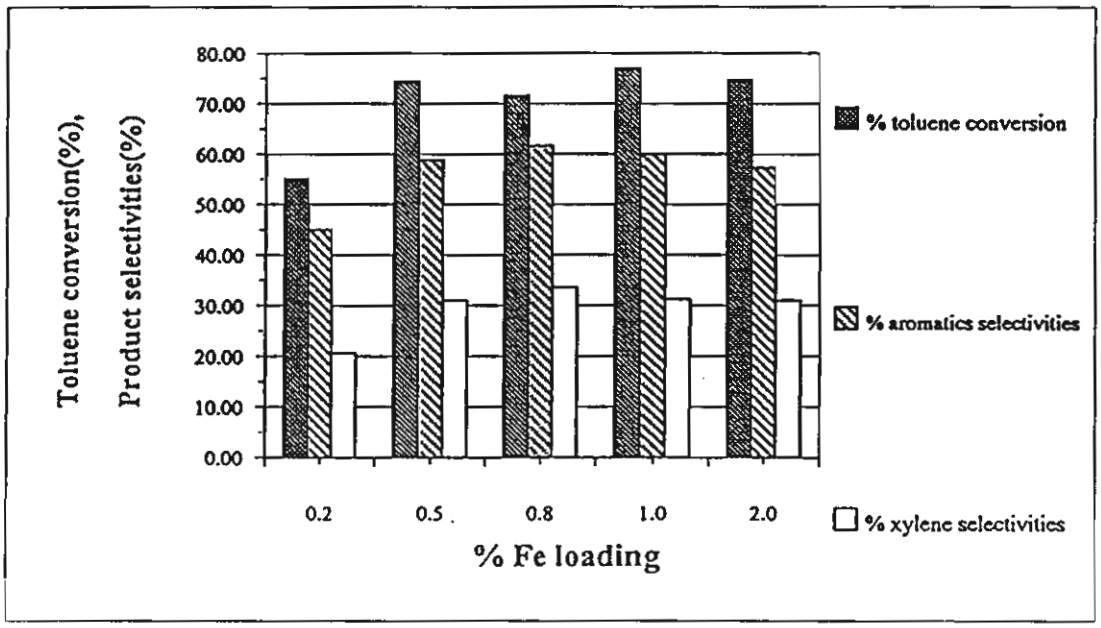
Toluene conversion(%), Product selectivities(%)
80.00
70.00
60.00
50.00
40.00
30.00
20.00
10.00
0.00
0.2
0.5
0.8
1.0
2.0
% Fe loading
% toluene conversion
% aromatics selectivities
% xylene selectivities

4(b)

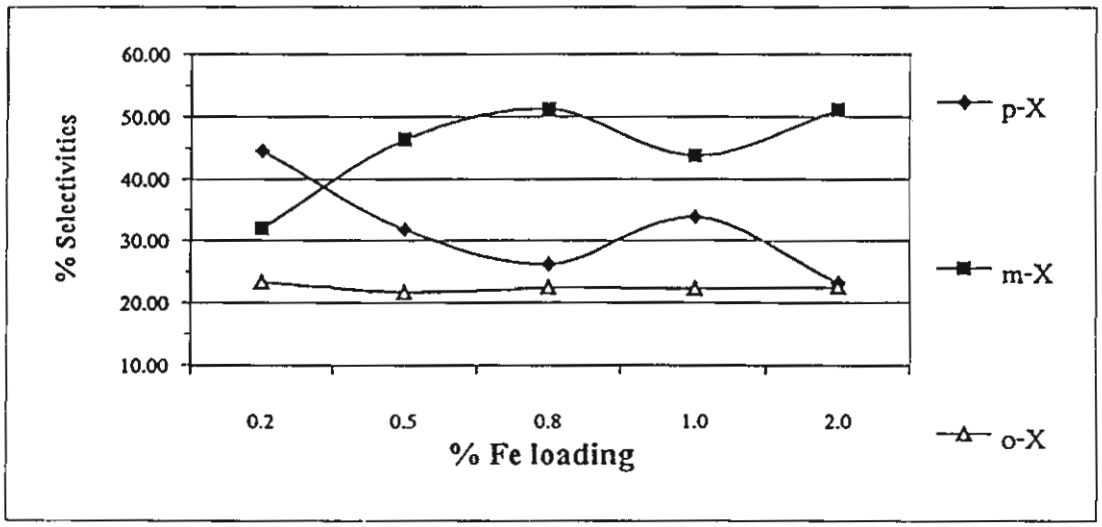
% Selectivities
60.00
50.00
40.00
30.00
20.00
10.00
0.2
0.5
0.8
1.0
2.0
% Fe loading
p-X
m-X
o-X

5(a)

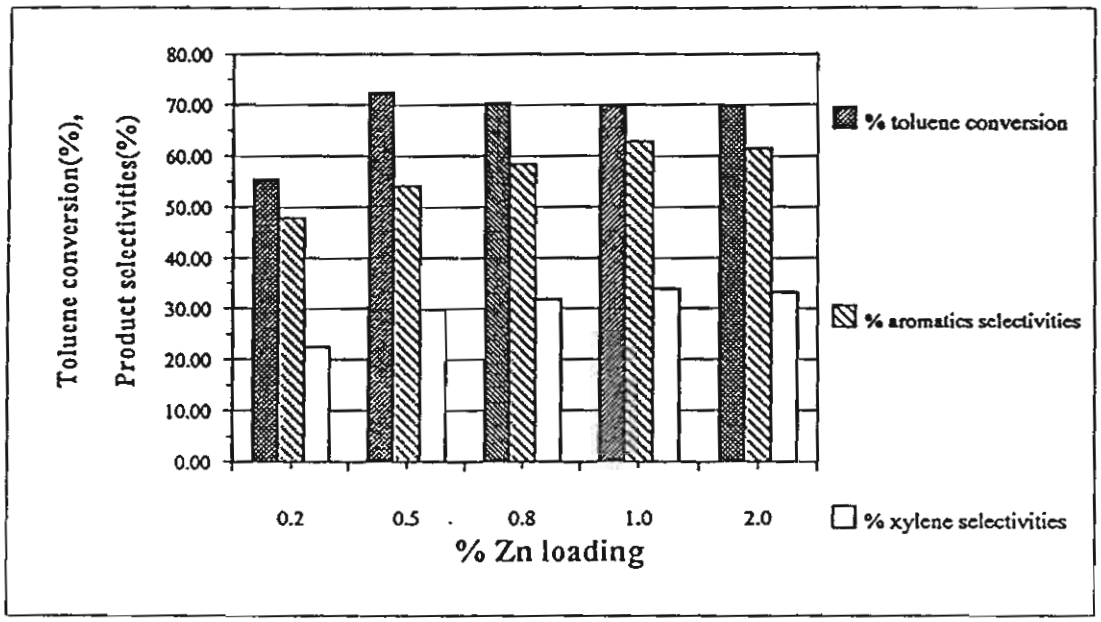
80.00
70.00
60.00
50.00
40.00
30.00
20.00
10.00
0.00
Toluene conversion(%), Product selectivities(%)
0.2
0.5
0.8
1.0
2.0
% Zn loading
% toluene conversion
% aromatics selectivities
% xylene selectivities

5(b)

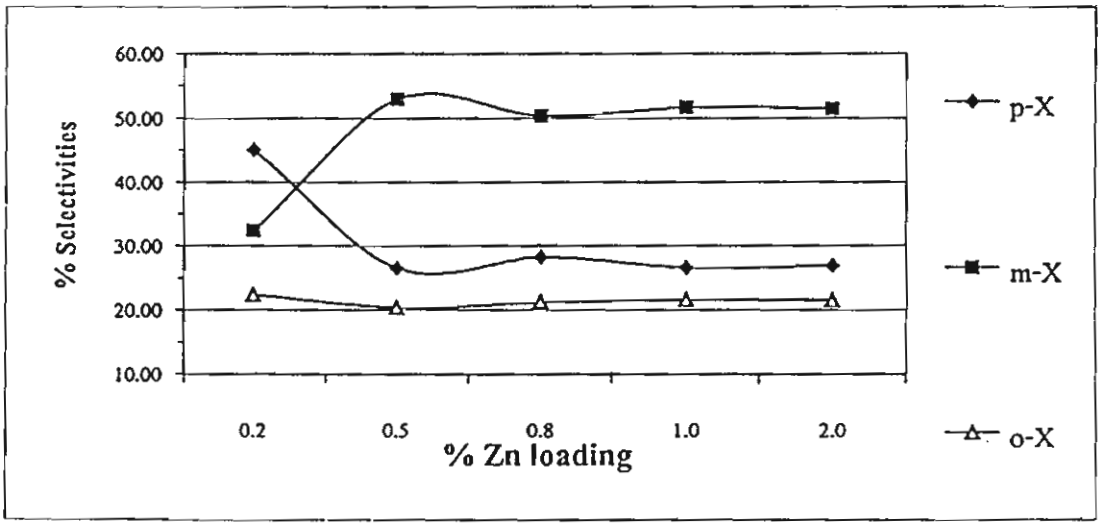
60.00
50.00
40.00
30.00
20.00
10.00
% Selectivities
0.2
0.5
0.8
1.0
2.0
% Zn loading
p-X
m-X
o-X

6(a)

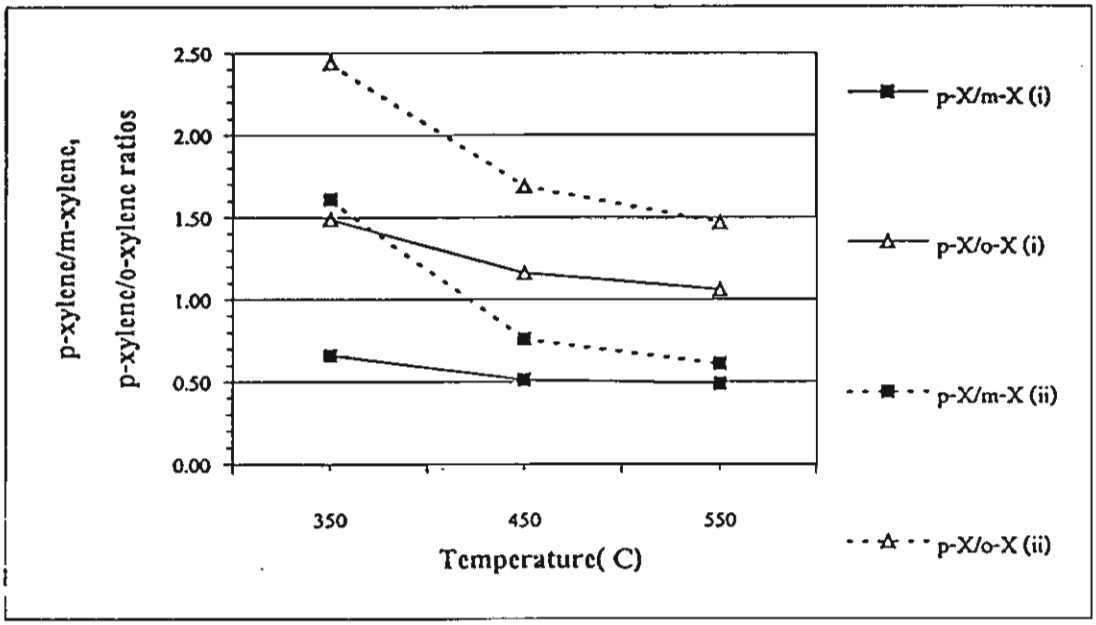
p-xylene/m-xylene,
p-xylene/o-xylene ratios
2.50
2.00
1.50
1.00
0.50
0.00
350
450
550
Temperature(C)
p-X/m-X (i)
p-X/o-X (i)
p-X/m-X (ii)
p-X/o-X (ii)

6(b)

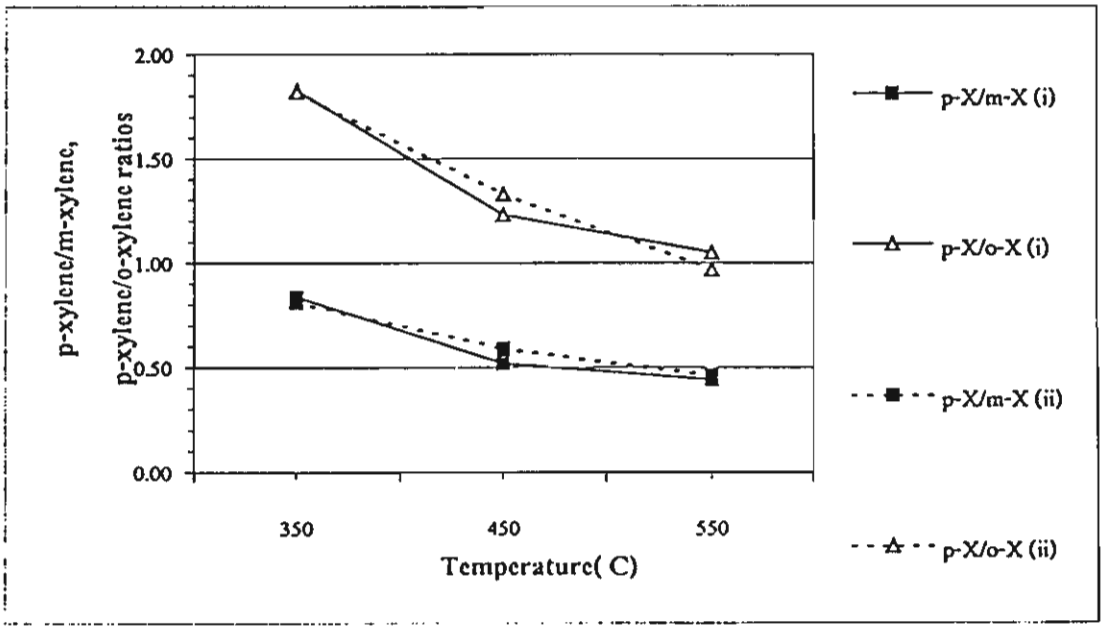
p-xylene/m-xylene,
p-xylene/o-xylene ratios
2.00
1.50
1.00
0.50
0.00
350
450
550
Temperature(C)
p-X/m-X (i)
p-X/o-X (i)
p-X/m-X (ii)
p-X/o-X (ii)

ACTIVATION OF Pd-Ag CATALYST FOR SELECTIVE HYDROGENATION OF ACETYLENE VIA NITROUS OXIDE ADDITION

*Piyasan Praserthdam, Suphot Phatanasri, Jumpod Meksikarin

Petrochemical Engineering Research Laboratory, Department of Chemical Engineering, Chulalongkorn University, Bangkok 10330, Thailand

Abstract

Hydrogenation of acetylene in the presence of a large excess of ethylene has been investigated on the Pd-Ag catalyst under 60°C and a space velocity of 2,000 h^{-1}. It was found that an enhancement in the performance of Pd-Ag catalyst can be obtained by pretreatment with N_2O. It is suggested that added N_2O on the catalyst before use not only augments the sites associated with ethylene production from acetylene but also depletes the sites responsible for direct ethane formation.

Keywords: Selective hydrogenation, Acetylene, Silver promoted palladium catalyst, N_2O pretreatment

INTRODUCTION

The selective hydrogenation of acetylene over supported palladium catalysts is a process widely used to purify the ethylene produced by steam cracking of hydrocarbons. The ethylene to acetylene ratio in the stream to be treated is generally higher than seventy [1]. At present all such catalysts are based on palladium supported on alumina carrier. Palladium-based catalysts promoted by a second metal are now available [2]. The promoter improves selectivity or stability of the catalyst. A. Sarkany et al. [3] have clearly demonstrated that the addition of copper to palladium causes a significant decrease in the overall rate of ethane

* Corresponding author. E-mail : Piyasan.p@chula.ac.th

formation and at the same time there is a decrease in the catalyst activity as well as a marginal decrease in oligomer selectivity. Recently, it has been discovered that the catalyst comprising elements of group IB and transition metals could be activated with N_2O before use [4]. Thus it is an objective of the study to pretreat the Pd-Ag catalyst before being used on the selective hydrogenation of acetylene.

EXPERIMENTAL

A 0.04 wt% Pd-Ag/γAl_2O_3 (Ag:Pd = 4:1) was prepared by the serial impregnation method. The order of catalyst impregnation was the deposition of palladium followed by silver, respectively. Alumina support was Al_2O_3 (CS-303) supplied by United Catalyst Incorporation (UCI), USA. Palladium nitrate and silver nitrate were used as sources for Pd and Ag, respectively. The calcination temperatures for palladium and silver were 300°C and 370°C, respectively.

0.2 g of the catalyst was packed into the 0.6 cm-ID quartz reactor and heated from room temperature to 100°C in Ar, then replaced Ar with H_2 and maintained at this temperature for 2 h. After reduction, the reactor was cooled down to 60°C under argon flow and held for 10 minutes. Then a gas mixture of 0.3% C_2H_2, 0.8%H_2 and C_2H_4 balanced was switched to replace Ar with the flow rate of 30 ml/min. Consequently, the gas mixture was reacted under catalytic hydrogenation, i.e., C_2H_2 was selectively hydrogenated to C_2H_4. However, in the case of N_2O treatment, the reactor was cooled down from 100°C to 90°C under Ar flow and held for 10 minutes before N_2O injection. Then the temperature was reduced to 60°C and the reaction was started. The products were analysed by SHIMADZU FID GC 14B equipped with Carbosieve column s-2.

The active sites of the catalysts were determined by CO adsorption technique and the BET surface areas by a Micromeritic Surface Area Analyser (model ASAP 2000).

The following terms used herein are defined as:

$$\text{Acetylene conversion (\%)} = \frac{\text{acetylene in feed - acetylene in product}}{\text{acetylene in feed}} \times 100$$

$$\text{Ethylene selectivity (\%)} = \frac{\text{ethylene in product - ethylene in feed}}{\text{acetylene converted}} \times 100$$

RESULTS AND DISCUSSION

From several previous investigations (Al-Ammar et al. [5-7], Margitfalvi et al. [8,9], Moses et al. [10], and Weiss et al. [11]), it has

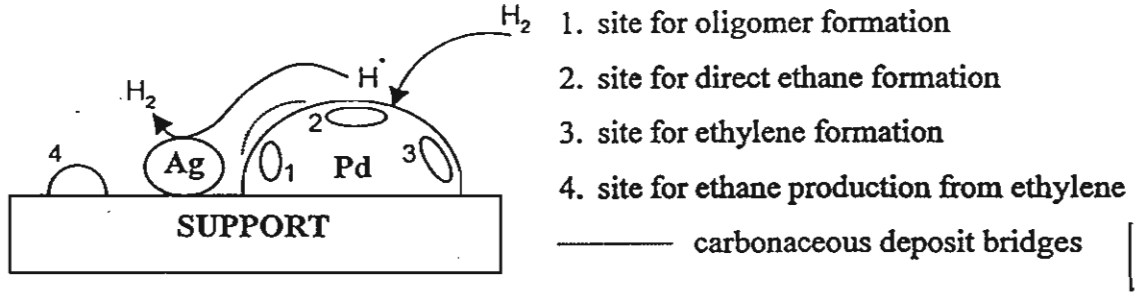

Figure 1 Conceptual model demonstrating four main types of surface sites on Al_2O_3-supported Pd catalyst and the role of Ag promoter as desorption site for transferred H_2

been generally accepted that four main types of surface sites are involved in the alumina-supported Pd catalyst. Three types of which, locating on the Pd metal surface, are responsible for selective conversion of acetylene to ethylene, direct ethane production from acetylene, and oligomer formation from acetylene as shown in Fig. 1. Another site accounting for the hydrogenation of ethylene to ethane is on the surface of alumina

support. It has been reported from some researchers [3,12] that the decrease in ethylene selectivity (i.e. increase in ethylene hydrogenation) during aging has been related to the amount of carbonaceous adsorbate on the catalyst surface. In other words, the carbonaceous deposit acts as hydrogen bridge for the hydrogen spillover from Pd to support. To prove this, the experiment was designed to obtain the set of data at an early period (5 min on stream), or set A, during which the negligible amount of coke was formed. Another one was the set of data at 44 h on stream, or set B, during which the considerable amount of coke was presumably formed though the exact amount of coke deposit was not determined.

As shown in Table 1, the substantial amount of ethane obtained for 0.04% Pd/Al_2O_3 of set A should be produced directly from acetylene, and the ethylene hydrogenation to ethane should be negligible with the

Table 1

Product distribution in C wt% of three kinds of catalysts.

Reaction conditions: 60°C, GHSV 2000h^{-1}

Set	Catalyst	TOS	Feed					
			0.2099	99.7708	0.0121	0.0072		
			Product					
			C_2H_2	C_2H_4	C_2H_6	CH_4	C_2H_2 Conv.(%)	C_2H_4 Selectivity(%)
A	Base[a]	5 min	0.0037	99.8568	0.1321	0.0074	98.23	41.71
	Untreated[b]		0.0065	99.8566	0.1294	0.0074	96.90	42.18
	Treated[c]		0.0015	99.8784	0.1126	0.0073	99.28	51.63
B	Base[a]	44 h	0.0192	99.8338	0.1396	0.0074	90.85	33.04
	Untreated[b]		0.0156	99.8465	0.1305	0.0073	92.56	38.96
	Treated[c]		0.0059	99.8731	0.1134	0.0075	97.18	50.15

[a] 0.04% Pd/Al_2O_3

[b] 0.04% $Pd\text{-}Ag/Al_2O_3$

[c] 0.04% $Pd\text{-}Ag/Al_2O_3$ treated with 0.1 cc of N_2O

assumption that no carbonaceous deposit bridge was formed. When the base catalyst was promoted with Ag, the amount of ethane significantly decreased and so did the acetylene conversion while the amount of

ethylene was almost constant. This implies that the alumina-supported Pd catalyst promoted by Ag may reduce the sites responsible for direct ethane formation from acetylene which is consistent with the previous investigation [12]. In case of the N_2O treatment for set A, both acetylene conversion and ethylene selectivity markedly increased and the amount of ethane was further decreased. This means that the addition of nitrous oxide augments the sites responsible for ethylene formation from acetylene as described above, and advantageously reduces the sites accounting for direct ethane formation as well. As for set B, the amount of ethylene obtained for 0.04% Pd/Al_2O_3 was considerably less than that of the corresponding catalyst for set A, and so did the acetylene conversion. The carbonaceous deposit on the catalyst surface should be responsible for the decrease in acetylene conversion. It is interesting to note that the amount of ethane formed on the base catalyst for set B was higher than that for set A even with less acetylene conversion. This means the substantial amount of ethane was formed via the ethylene hydrogenation on the support sites, with aid of carbonaceous deposit acting as H_2 bridge, rather than the direct ethane formation from acetylene on Pd sites. Sarkany [13,14] has found that the hydrocarbonaceous deposit on Pd/Al_2O_3 catalyst may enhance the over-hydrogenation of 1,3-butadiene and permits the hydrogenation of propene in the presence of 1,3-butadiene due to transport hindrance of 1,3-butadiene. Thus, the over-hydrogenation of acetylene and hydrogenation of ethylene in the presence of acetylene can also be interpreted by transfer limitation of acetylene caused by the presence of carbonaceous deposits. With the Ag-promoted catalyst, the increase in amount of ethylene and acetylene conversion was obtained while the amount of ethane declined. This also implies that the ethylene hydrogenation was reduced by Ag promotion, and the direct ethane formation from acetylene on Pd sites

covered with carbonaceous deposit was negligible. Thus it has been suggested that Ag may hinder the hydrogen spillover from the metal surface to alumina support probably by providing the desorption sites for transferred hydrogen as illustrated in Fig. 1. With the N_2O treatment, both acetylene conversion and ethylene selectivity significantly increased while the amount of ethane was further decreased as similar to those obtained for set A. The improved results achieved on N_2O-treated Pd-Ag/Al_2O_3 catalyst for both sets of data essentially contend that the addition of N_2O increases the sites responsible for ethylene formation from acetylene and decreases the sites involving direct ethane formation as mentioned above. Table 2 shows the results of BET surface area of the catalysts. It has been found that the BET surface area of the N_2O-treated catalyst was slightly higher than that of the untreated one. This reflects that two silver atoms may move closely to one oxygen atom to form Ag_2O. This phenomenon can expose the active palladium sites which normally locate under the surface of metal cluster as modeled in Fig. 2. Table 3 shows the metal active sites of catalysts measured by co adsorption. It has been found that the Ag-Promoted Pd catalyst exhibited less amount of active sites than that of the unpromoted one. This may be due to the alloy formation between both metals. The addition of N_2O to

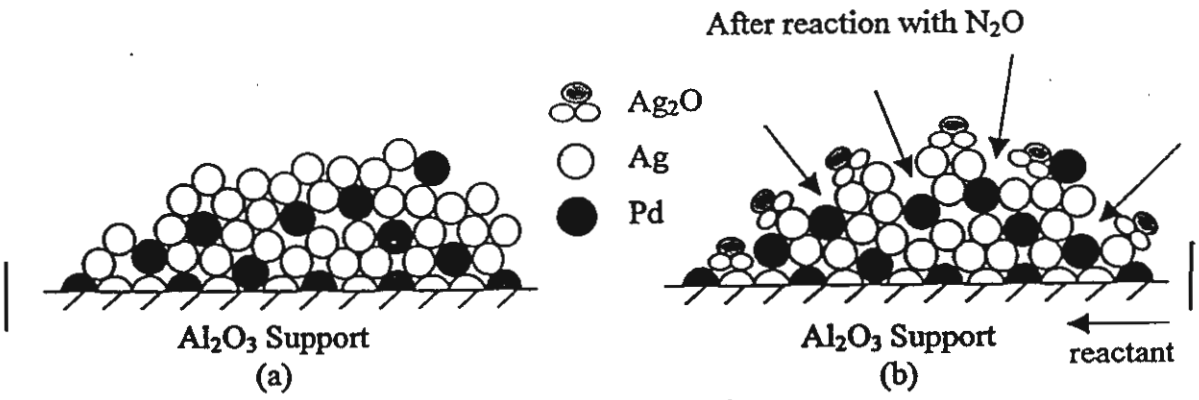

Figure 2 Proposed model illustrating the effect of N_2O addition on enhancing the accessible sites of active Pd responsible for acetylene hydrogenation to ethylene.

Table 2

BET surface area of three catalysts

Catalyst	BET (m^2/g)
0.04% Pd/Al_2O_3	4.74
0.04% $Pd-Ag/Al_2O_3$ (untreated)	4.36
0.04% $Pd-Ag/Al_2O_3$ (treated)	4.98

Table 3

The metal active sites of catalysts measured by CO adsorption

Catalyst	Metal active sites (sites/gram of catalyst)
0.04% Pd/Al_2O_3	3.30×10^{17}
0.04% $Pd-Ag/Al_2O_3$	2.52×10^{17}
0.04% $Pd-Ag/Al_2O_3$ (0.02 cc of N_2O)	3.14×10^{17}
0.04% $Pd-Ag/Al_2O_3$ (0.035 cc of N_2O)	3.22×10^{17}
0.04% $Pd-Ag/Al_2O_3$ (0.05 cc of N_2O)	3.70×10^{17}
0.04% $Pd-Ag/Al_2O_3$ (0.10 cc of N_2O)	4.04×10^{17}
0.04% $Pd-Ag/Al_2O_3$ (0.15 cc of N_2O)	3.37×10^{17}
0.04% $Pd-Ag/Al_2O_3$ (0.33 cc of N_2O)	3.18×10^{17}

the silver-promoted catalyst was found to enhance the amount of active sites, and the highest amount of which was achieved with the injection of 0.1 cc of N_2O. Though N_2O addition may cause the formation of both silver oxide and palladium oxide on the surface of Al_2O_3 support corresponding to the reproduction and destruction of active sites, respectively, the highest amount of active sites obtained with 0.1 cc injection of N_2O may be attributed to the predominant reproduction of Pd active sites.

CONCLUSION

It might be concluded that N_2O treatment could improve the catalytic performance of the silver-promoted palladium catalyst by enhancing the accessible sites of active Pd responsible for ethylene production from

acetylene, and meanwhile decreasing the sites involving the direct ethane formation from acetylene.

ACKNOWLEDGEMENTS

The financial support of this research by The Thailand Research Fund (TRF) is gratefully acknowledged.

REFERENCES

1. G.C. Battiston, L. Dallord, G.R. Tauszik: *Appl. Catal.*, 2, 1 (1982).
2. J.P. Boitianx, J. Cosyn, M. Derrien, and G. Leger: *Hydrocarbon Processing*, March, 51 (1985).
3. A. Sarkany, and L. Guczi: *Appl. Catal.*, **10**, 369 (1984).
4. P. Praserthdam, U.S. Patent 5,849,662, Dec. 15, 1998.
5. Al-Ammar A.S., and G. Webb: *J.C.S. Faraday*, **174**, 195 (1978).
6. Al-Ammar A.S., and G. Webb: *J.C.S. Faraday*, **174**, 657 (1978).
7. Al-Ammar A.S., and G. Webb: *J.C.S. Faraday*, **175**, 1900 (1978).
8. J. Margitfalvi, L. Guczi, and A.H. Weiss, *J. Catal.*, **72**, 185 (1981).
9. J. Margitfalvi, L. Guczi: *React. Kinet. Catal. Lett.*, **15**, 475 (1980).
10. J.M. Moses, A.H. Weiss, K. Matsusek, and L. Guczi: *J. Catal.*, **86**, 417 (1984).
11. A.H. Weiss, S. Leviness, V. Nau, L. Guczi, A. Sarkany, and Z. Schay: *Proc. 8th Int. Congr. Catal.*, **5**, 591 (1984).
12. S. Leviness, V. Nau, A.H. Wiess, Z. Schay, and L. Guczi: *J. Mol. Catal.*, **25**, 131 (1984).
13. A. Sarkany: *J. Catal.*, **180**, 149 (1998).
14. A. Sarkany: *Appl. Catal.*, **175**, 245 (1998).

Reprinted from

THE CHEMICAL ENGINEERING JOURNAL

An International Journal of Research and Development

Chemical Engineering Journal 77 (2000) 215–219

Short communication

Coke formation over Pt–Sn–K/Al_2O_3 in C_3, C_5–C_8 alkane dehydrogenation

P. Praserthdam [a,*], N. Grisdanurak [b], W. Yuangsawatdikul [a]

[a] *Petrochemical Engineering Laboratory, Department of Chemical Engineering, Chulalongkorn University, Bangkok 10330, Thailand*

[b] *Department of Chemical Engineering, Khon Kaen University, Khon Kaen 40002, Thailand*

Received 9 October 1998; received in revised form 20 February 1999; accepted 1 September 1999

ELSEVIER

CHEMICAL ENGINEERING JOURNAL

An International Journal of Research and Development

Aims and Scope

The *Chemical Engineering Journal* provides an international forum for the presentation of original research, interpretative reviews and discussion of new development in chemical and biochemical engineering. Papers which describe novel theory and its application to practice are welcome, as are those which illustrate the transfer of techniques from other disciplines. Reports of carefully executed experimental work which is soundly interpreted are also welcome.

Publication information: Chemical Engineering Journal (ISSN 1385-8947). For 2000, volume(s) 78–80 are scheduled for publication. Subscription prices are available upon request from the Publisher or from the Regional Sales Office nearest you or from this journal's website (http://www.elsevier.nl/locate/cej). Further information is available on this journal and other Elsevier Science products through Elsevier's website: (http://www.elsevier.nl). Subscriptions are accepted on a prepaid basis only and are entered on a calendar year basis. Issues are sent by standard mail (surface within Europe, air delivery outside Europe). Priority rates are available upon request. Claims for missing issues should be made within six months of the date of dispatch.

USA mailing notice: – *Chemical Engineering Journal* (ISSN 1385-8947) is published *monthly* by Elsevier Science S.A. (P.O. Box 211, 1000 AE Amsterdam, The Netherlands). Annual subscription price in the USA US$ 1731.00 (valid in North, Central and South America), including air speed delivery. Application to mail at periodical postage rate is pending at Jamaica, NY 11431.

USA POSTMASTER: Send address changes to Chemical Engineering Journal, Publications Expediting, Inc., 200 Meacham Avenue, Elmont, NY 11003.

AIRFREIGHT AND MAILING in the USA by Publication Expediting Inc., 200 Meacham Avenue, Elmont, NY 11003..

Orders, claims and product enquiries: please contact the Customer Support Department at the Regional Sales Office nearest you:

New York: Elsevier Science, P.O. Box 945, New York, NY 10159-0945, USA. Tel.: (+1) 212-633-3730 [Toll free number of North American customers: 1-888-4ES-INFO (437-4636)], Fax: (+1) 212-633-3680, E-mail: usinfo-f@elsevier.com

Amsterdam: Elsevier Science, P.O. Box 211, 1000 AE Amsterdam, The Netherlands. Tel.: (+31) 20-485-3757, Fax: (+31) 20-485-3432, E-mail: nlinfo-f@elsevier.nl

Tokyo: Elsevier Science, 9-15 Higashi-Azabu 1-Chome, Minato-ku, Tokyo 106-0044, Japan. Tel.: (+81) 3-5561-5033, Fax: (+81) 3-5561-5047, E-mail: info@elsevier.co.jp

Singapore: Elsevier Science, No. 1 Temasek Avenue, #17-01 Millenia Tower, Singapore 039192. Tel.: (+65) 434-3727, Fax: (+65) 337-2230, E-mail: asiainfo@elsevier.com.sg

Rio de Janeiro: Elsevier Science, Rua Sete de Setembro 111/16 Andar, 20050-002 Centro, Rio de Janeiro-RJ, Brazil; Tel.: (+55) (21) 509 5340; fax.: (+55) (21) 507 1991; e-mail: elsevier@campus.com.br [Note (Latin America): for orders, claims and help desk information, please contact the Regional Sales Office in New York as listed above]

Advertising Information

The paper used in this publications meets the requirements of ANSI/NISO Z39.48-1992 (Permanence of Paper).

Printed in The Netherlands

Chemical Engineering Journal 77 (2000) 215–219

Chemical Engineering Journal

www.elsevier.com/locate/cej

Short communication

Coke formation over Pt–Sn–K/Al_2O_3 in C_3, C_5–C_8 alkane dehydrogenation

P. Praserthdam [a,*], N. Grisdanurak [b], W. Yuangsawatdikul [a]

[a] *hemical Engineering Laboratory, Department of Chemical Engineering, Chulalongkorn University, Bangkok 10330, Thailand*

[b] *Department of Chemical Engineering, Khon Kaen University, Khon Kaen 40002, Thailand*

Received 9 October 1998; received in revised form 20 February 1999; accepted 1 September 1999

actants on coke formation during dehydrogenation (DH) over 0.3 wt.%Pt–0.3 wt.%Sn–0.6 wt.%K/Al_2O_3 was investigated. e carried out in the temperature range 200–600°C at 1 atm with pairs of alkanes and alkenes (C_3, C_5–C_8). The carbonaceous during the process were analyzed using the temperature-programmed oxidation (TPO) technique. With the same amount profiles of the short alkane and alkene (C_3) did not match completely, while those of the larger chain alkanes and alkenes tually identical. From these results, a simple model of coke formation has been proposed. Short alkane DH provides coke er alkane DH generates coke in series and consecutive modes.

dehydrogenation; TPO; Coking

n

of catalysts by carbonaceous deposits is a equently encountered in the petrochemical has far-reaching applications and consent years, it has received increasing attention, the rapidly growing number of publications is topic.

ition (DH) of alkanes is one of the most tions in increasing chemical feedstocks. onditions needed for this process, high temw pressure, result in the formation of coke t, which leads to a short catalyst lifetime. s have been conducted to improve the catalyst . Lin et al. [1] showed that Pt–Sn/Al_2O_3 can gth of chemisorption of the hydrocarbon on nd the carbon precursor can then migrate to ily. This process reduced coke accumulation s. Recent work reported that the addition of –Sn/Al_2O_3 for propane DH can extend the e by decreasing the amount of coke on the

author. Fax: +43-362240.

iyasan@pioneer.netserv.chula.ac.th (P. Praserthdam).

Several research groups have published mechanisms and kinetic models of coke formation [3–5]. A recent mechanism was proposed by Hughes [6], which explained the formation of coke by using a series and parallel model. However, the model did not explain the effect of different reactants with respect to coke formation. Since feedstocks contain mixtures of a variety of paraffins, it is important to know the effects of different paraffin components upon the activity, selectivity and stability of the catalyst. The outcomes could help to decide possible uses of a cut with a certain hydrocarbon composition.

Several techniques have been used to study carbonaceous residues, e.g. Fourier transform infrared (FTIR) [7], transmission electron microscopy (TEM) [8], nuclear magnetic resonance (NMR) [9], Auger electron spectroscopy (AES) [10], temperature-programmed oxidation (TPO) [11–13] etc. All of these techniques give different types of information on coke deposition. A technique widely used to characterize coke deposits is the temperature-programmed technique. This technique supplies information about the location and general structure of coke accumulation over the catalyst surface.

This paper presents the results obtained when a Pt–Sn–K/Al_2O_3 catalyst was used to dehydrogenate pure paraffins. This includes the analysis of the coke and a proposed coke formation model.

7(99)00169-2

2. Experimental details

2.1. Materials

High-purity alumina type NKH-3 (Sumitomo Aluminium Smelting, Japan) was used as the support. Chloroplatinic acid (Wako Pure Chemical I, Japan), stannous chloride dihydrate (Fluka Chemie AG, Switzerland) and potassium nitrate (KNO_3) (E. Merck, USA) were used to prepare the 0.3%Pt–0.3%Sn–0.6%K/Al_2O_3 catalyst. A gas mixture (TIG, Thailand) containing propane, pentane, hexane or octane was used as reaction feed. Diluted oxygen (1 vol%) in helium (TIG, Thailand) was used as an oxidant in the TPO process.

2.2. Catalyst

Alumina support was ground to a mesh size of 60/80, followed by washing with distilled water and then dried at 100°C overnight. The support was then calcined in air at 300°C for 3 h. The impregnation method was used to prepare a catalyst with a calcination step for each addition of the three active chemicals, Pt, Sn and K. Our full report describes this in more detail [14].

2.3. Apparatus and methodology

The apparatus used was an ordinary atmospheric flow system consisting of a quartz reactor. The reactor temperature was controlled by an electric furnace. A schematic diagram of the apparatus is shown in Fig. 1. A variety of gases, shown in Table 1, were used as feed. C_3 was fed directly into the reactor, while C_5–C_8 were vaporized in a saturator at a particular temperature. Nitrogen gas was carried along with the vapour in order to maintain the same concentration of carbon before being introduced into the reactor.

Table 1
Concentration and control temperature of reactants

Reactant	vol% in N_2	Control temperature in the saturator (°C)
Propane	20	–
Propene	20	–
n-Pentane	12	−14.2
1-Pentene	12	−19.5
n-Hexane	10	10.2
1-Hexene	10	5.6
n-Heptane	8.6	32.4
1-Heptene	8.6	28.1
n-Octane	7.5	52.9
1-Octene	7.5	48.8

In each run, 0.1 g of fresh catalyst was placed in the isothermal zone inside the reactor. It was then reduced by hydrogen for 1 h at a flow rate of 30 $cm^3\,min^{-1}$ at 500°C, and then cooled to the required temperature before the reaction. Afterwards, reactant gas was fed into the reactor with a GHSV of 20 000 h^{-1}. The reaction products were analyzed between 5 min and 2 h during the process with a Shimadzu GC-14B flame ionization detector (FID) gas chromatograph (GC). Two kinds of GC columns were used for analysis. The first type was a capillary column. The temperature was initially programmed at 35°C and then followed by a 10°C min^{-1} ramp up to 140°C. The second GC column was a VZ-10 column with an initial temperature set at 65°C followed by an increase of 10°C min^{-1} to 80°C.

The coke formation over each spent catalyst was characterized by a TPO process. The carrier gas containing oxygen in helium was fed into the sample cell at a constant flow rate of 30 $cm^3\,min^{-1}$ under ambient conditions. The temperature was increased linearly from 50 to 700°C at a heating rate of 5°C min^{-1}. At the end of the TPO process, the coke deposits were completely removed. The reaction products were analyzed by an on-line TCD GC with a packed column (Porapack QS). The column temperature was maintained isothermal at 90°C for the entire analysis.

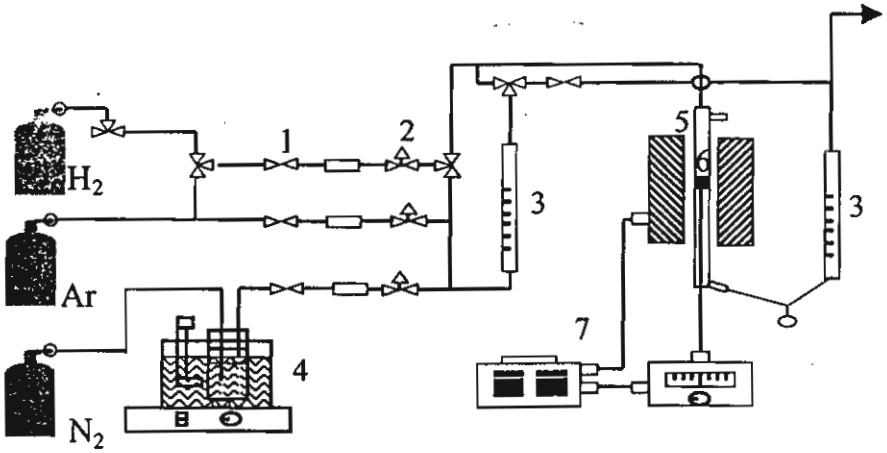

Fig. 1. Schematic diagram of the flow reactor: (1) on–off valve; (2) needle valve; (3) flow meter; (4) saturator; (5) reactor; (6) catalyst bed; (7) temperature control set.

ne reaction selectivity of coke formation was defined as ows:

$$\text{Selectivity of coke formation} = \frac{\text{Atoms of carbon deposited on catalyst} \times 100}{\text{Atoms of carbon feed converted averaged with time}}$$

Results and discussion

was apparent that the products of straight chain alkane would be the parent alkane, the corresponding alkene hydrogen. To better understand the mechanism of coke ation, the corresponding alkenes needed to be investi- d for DH as well. Therefore, normal paraffins and olefins C_3 and C_5–C_8 were used as feeds.

he process for each feed in the absence of a catalyst was ed out to evaluate whether thermal cracking affected It was found that thermal cracking occurred at 500°C; side-reaction was quite significant, especially for high cular weight hydrocarbons, accounting for 5–30% con- ion for C_5–C_8 and almost none for C_3.

reduce the effect of thermal cracking for higher molec- weight hydrocarbons, it was necessary to decrease the ating temperature. The experiments using C_5, C_6, C_7 C_8 alkanes and alkenes showed insignificant thermal cing at 350, 300, 250 and 200°C, respectively, and so experiments were performed at these temperatures. The ity and the selectivity are presented below.

Activity and coke selectivity

propane and propene DH, as shown in Fig. 2, the ac- of propane DH is higher than that of propene DH. The ts corresponded with those of the thermodynamic calcu- ns. However, the activity declined markedly for propane The major products from propane DH were propene, gen and a moderate amount of propadiene. When propene as a feed, more propadiene was produced. idering the percentage of coke produced in the same

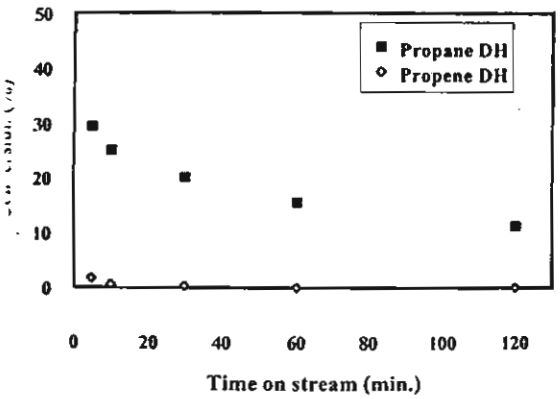

ig. 2. Conversion as a function of time for C_3 DH at 500°C.

Table 2
Coke content and coke selectivity for 2 h time on stream over 0.3 wt.%Pt–0.3 wt.%Sn–0.6 wt.%K/Al_2O_3 operated with a variety of reactants

Reactant	Reaction temperature (°C)	Coke (%)	Selectivity of coke formation (%)
Propane	500	0.80	0.002
Propene	500	2.30	0.185
n-Pentane	350	2.35	0.922
1-Pentene	350	1.93	0.006
n-Hexane	300	1.61	0.393
1-Hexene	300	1.64	0.010
n-Heptane	250	0.22	0.080
1-Heptene	250	0.31	0.016
n-Octane	200	0.16	0.020
1-Octene	200	0.12	0.002

reaction period, it was found that propene DH produced more coke than did propane DH. Therefore, coke selectivity via propene DH was higher than via propane DH, as shown in Table 2. Since propadiene by nature is extremely reactive towards other chemicals, it was reasonable to assume that propadiene would be one of the important precursors for coke formation in low molecular weight alkane DH.

For higher molecular weight hydrocarbons, the activity results are reversed from those of C_3 DH. As shown in Figs. 3–6, the activities of alkene DH are higher than those

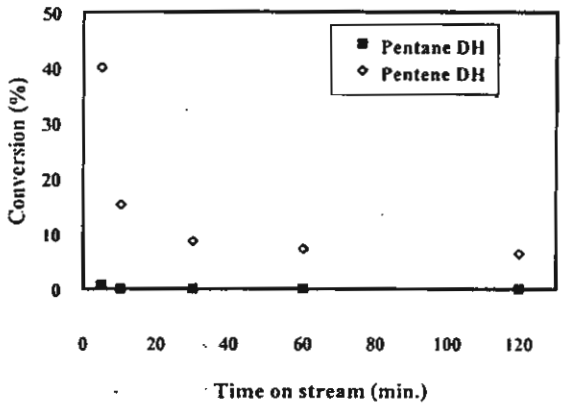

Fig. 3. Conversion as a function of time for C_5 DH at 350°C.

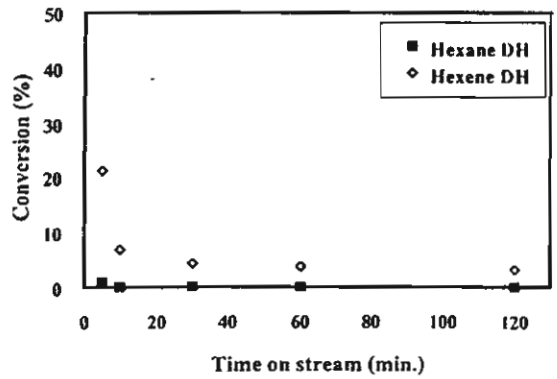

Fig. 4. Conversion as a function of time for C_6 DH at 300°C.

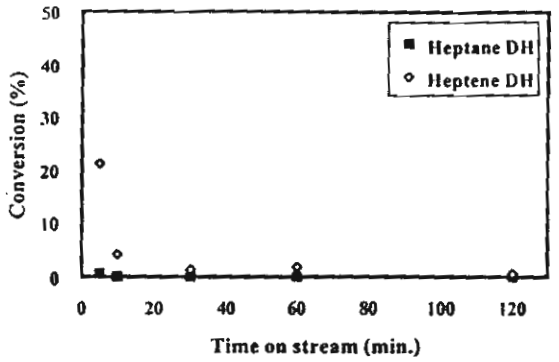

Fig. 5. Conversion as a function of time for C_7 DH at 250°C.

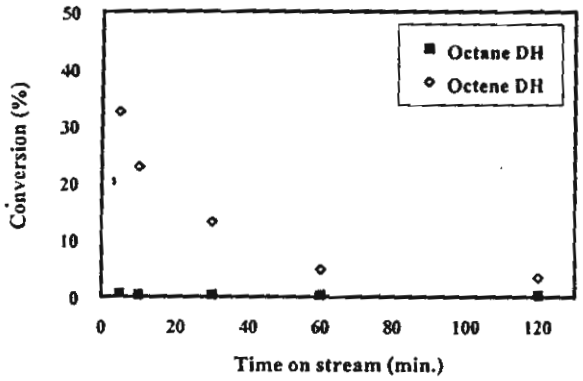

Fig. 6. Conversion as a function of time for C_8 DH at 200°C.

of the corresponding alkane DH. In the early stages, the chromatogram of alkene DH showed a variety of products, including dienes and cycloalkane, while these products were not observed from alkane DH. When the reaction time was increased, 120 min time on stream, both alkane and alkene DH provided similar products. This implied that higher alkane DH over Pt–Sn–K/Al_2O_3 would perform not only DH but also polymerization, cyclization and catalytic cracking. Coke analysis indicated that the percentage of coke was similar for each pair of alkane–alkene DH. The percentage of coke selectivity of the catalyst for alkane DH was higher than that for alkene DH as shown in Table 2. From a thermodynamic viewpoint, reaction through a cyclopentane pathway is one of the most favourable pathways. The experimental results also supported this, as the chromatograms for each feed (C_5–C_8) showed a peak for C_5. Moreover, this indicates that C_5 should be considered as an important coke precursor for high molecular weight hydrocarbons. This result is similar to the study of Beltramini et al. [15]. As shown in Table 2 for the results of pentane through octane, it was found that the higher molecular weight hydrocarbons produced a lower percentage of coke. This confirms that intermediate C_5 is the coke precursor.

Considering the percentage of coke for every reaction studied, it was found that propene DH gave a higher percentage of coke than propane DH, while in the case of large

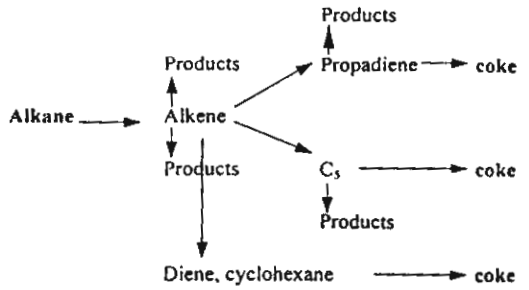

Fig. 7. Schematic representation of coke formation in C_3–C_8 alkane DH.

hydrocarbons, both alkane and alkene DH created an equal percentage of coke. The results suggest that coke formation from different kinds of alkanes occurs via different mechanisms. A schematic diagram of the coke formation mechanism is shown in Fig. 7. This shows that alkanes with a low molecular weight deposit coke via a series mode, while for high molecular weight hydrocarbons, coke formation over catalysts occurs via both consecutive and parallel modes. This also suggests that the coke amount and formation are not directly related to the molecular weight of the hydrocarbon, but related to the structure of the reactants and products, which is similar to the results of Beltramini's work [15].

3.2. Coke analysis

It is accepted that the low temperature peak of the TPO spectrum (280–370°C) corresponds to coke deposited on or in contact with metal sites. The intermediate temperature peak at 445°C is associated with the coke on acid sites close to the metal. The 570°C peak is produced by coke on acid sites far away from any metal sites, called high temperature coke. The aim of this section is to understand the development of coke deposition [16,17].

Fig. 8 shows the TPO patterns of spent catalysts from propane and propene DH, which operated at 500°C after 2 h time on stream. The propene DH spectrum contains two peaks. In contrast, the propene TPO pattern has only one

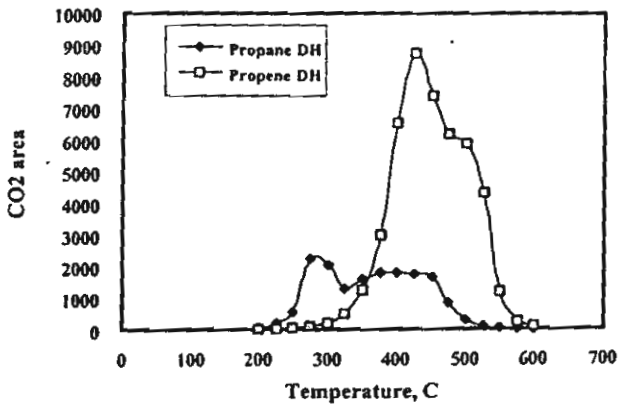

Fig. 8. TPO spectra for C_3 DH operated at 500°C and 2 h time on stream.

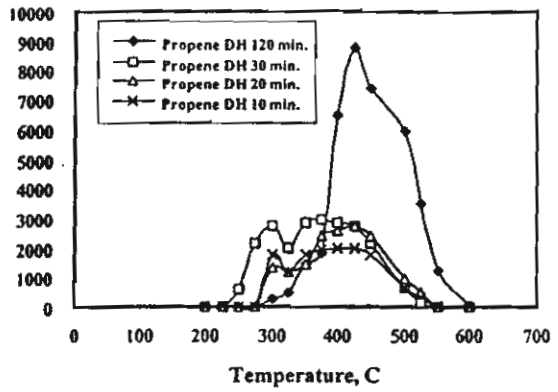

. 9. TPO spectra for propene DH as a function of time on stream.

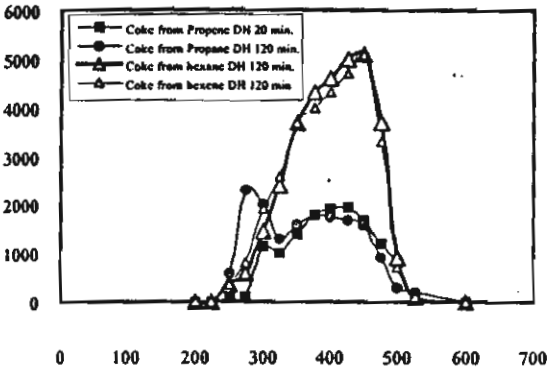

0. TPO spectra for the same amount of coke from C_3 and C_6 DH.

. The coke deposited via propane DH is a low temper- coke and contains a simple structure, while the coke ture obtained from propene DH may be more complex. nderstand the process of development of coke on cat- ; and the content of the coke from propene DH, TPO ra as a function of time were studied, as shown in 9. Two peaks are observed at the initial time interval 30 min). The first peak in the spectrum gradually shifts ime on stream and eventually becomes one peak. This s that coke becomes more complex in structure with ased time on stream. It was therefore theorized that, 120 min, coke was hard to deposit on a small site of . The structure also increased in molecular weight and d to deposit over supports close to metal sites [18].

. 10 presents the TPO patterns obtained from spent st from propane–propene DH at 500°C. The results that both propane and propene DH produce the same nt of coke at 120 min for propane DH and at 20 min opene DH. It was found that both patterns did not etely match. In contrast, TPO patterns of coke by hexane–hexene DH at 300°C were perfectly matched. There was only one peak in the TPO pattern at 445°C and no peak was observed at 280°C. Comparing the amount of coke between C_3 and C_5 (area under the TPO pattern) at 120 min time on stream, C_5 DH had a higher coking rate than C_3 DH.

4. Conclusions

The effect of reactants on coke formation in hydrocarbon DH was investigated over 0.3 wt.%Pt–0.3 wt.%Sn–0.6 wt.% K/Al_2O_3 using the TPO technique. A reactant having three carbon atoms produced coke in a series pathway, while reactants with five to eight carbon atoms produced coke in series and parallel pathways. Propadiene is a coke precursor for C_3 DH and C_5 is a coke precursor for C_5 or higher hydrocarbon DH. Coke increases in molecular weight and prefers to cover the supports rather than the metal sites.

Acknowledgements

Funding provided by the Thailand Research Fund for this study is gratefully acknowledged.

References

[1] L. Lin, Z. Tao, Z. Jingling, X. Zhusheng, Appl. Catal. 67 (1990) 11–23.
[2] N. Lim, Effect of promoters on coke formation on metal site of propane DH catalysts, M.Eng. Thesis, Chulalongkorn University, Thailand, 1996.
[3] N. Daisuke, S. Tomoya, Ind. Eng. Chem. Res. 31 (1992) 14–19.
[4] C.A. Querini, S.C. Fung, Appl. Catal. A: Gen. 117 (1994) 53–74.
[5] K. Liu, S.C. Fung, T.C. Ho, D.S. Rumschitzki, Catalyst Deactivation (1997) 625–638.
[6] R. Hughes, Deactivation of Catalyst, ACS Series, 1984.
[7] C.L. Pieck, E. Jablonsky, E. Parera, J.M. Parera, R. Frety, F. Lefebre, Ind. Eng. Chem. Res. 31 (1992) 1017.
[8] R.A. Cabrol, A. Oberlin, J. Catal. 89 (1984) 256.
[9] F. Diez, B.C. Gates, J.T. Miller, F.J. Sajkowski, S.G. Kukes, Ind. Eng. Chem. Res. 31 (1992) 1017.
[10] J. Niemantsverdiert, A.D. Langeveld, Fuel 65 (1986) 1396.
[11] P. Praserthdam, C. Chaisuk, P. Kanchanawanichkun, Res. Chem. Intermed. 24 (1998) 605–612.
[12] N.S. Figoli, J.N. Beltramini, E.E. Martinelli, J.M. Parer, Appl. Catal. 5 (1983) 19.
[13] C.A. Querini, S.C. Fung, J. Catal. 141 (1993) 389.
[14] W. Yuangsawatdikul, Effect of reactants on coke formation in dehydrogenation, M. Eng. Thesis, Chulalongkorn University, Thailand, 1996.
[15] J.N. Beltramini, E.E. Martinelli, E.J. Churin, N.S. Fogoli, J.M. Parera, Pt–Sn–Cl/Al_2O_3 in pure hydrocarbon reforming, Appl. Catal. 5 (1983) 43–55.
[16] J. Barbier, Catalyst Deactivation (1987) 1–17.
[17] S.C. Fung, C.A. Querini, J. Catal. 138 (1992) 240–254.
[18] J. Barbier, Appl. Catal. 23 (1986) 225–243.

Guide for Authors

Submission of Papers

Papers for *Chemical Engineering Journal* should be submitted to the Editor, Dr R.C. Darton or the Reviews Editor or to one of the Associate Editors.

Addresses of the Editors may be found on the inside cover of the journal.

Submission of a manuscript implies it is not being simultaneously considered for publication elsewhere and that the authors have obtained the necessary authority for publication.

All paper will be independently refereed.

Types of Contribution

Original papers–these should be complete and authoritative accounts of work which has a special significance and must be presented clearly and concisely.

Review articles – these will normally be commissioned by the Editor or the Reviews Editor. Prospective authors of a review article should consult with either Editor to check the suitability of their topic and material before submitting their review.

Short communications – will be accepted for the early communication of important and original advances. Such accounts may be of a preliminary nature but should always be complete and should not exceed the equivalent of 3000 words, including figures and tables.

Letters to the Editor – Letters commenting on work published in the journal shold be sent to the Editor.

The journal will also publish *Book reviews.*

Language

The principle language of the Journal is English, but papes in French are also published.

Authors in Japan please note: upon request, Elsevier Science Japan will Provide authors with a list of people who can check and improve the English of their paper (*before submission*). Please contact our Tokyo office: Elsevier Science Japan, 1-9-15 Higashi-Azabu, Minato-ku, Tokyo 106-0044, Japan. Tel: (03) 5561 5032; Fax: (03) 5561 5045.

Manuscript Preparation

Three copies should be provided in double-space typing on numbered pages of uniform size with a wide margin to the left.

Correspondence address

The name, complete postal address, telephone number, fax number and e-mail address of the corresponding author should be given on the first page of the manuscript.

Abstract

A brief summary (50-200 words) of the contents and conclusions of the paper and an indication of the relevance of new material should be included at the beginning of the paper. Authors of papers in French should provide a translation of the Abstract in English.

References

These should be indicated by numerals in square brackets, introduced consecutively in the text and must be listed at the end of the paper in numerical order. Journal titles should be abbreviated according to the Chemical Abstracts Service Source Index, 1970 edition, and supplements. The abbreviated title should be followed by the volume number, year (in parentheses) and page numbers.

Equations

These should be numbered (1), (2) etc.

Illustrations

It is imperative that authors supply the original and two copies of each illustration. Artwork should be supplied as black ink tracings or as high contrast black and white glossy photographs. High quality computer graphics are also acceptable. Because artwork will generally be reduced in size before printing, any lettering must be sufficiently large (3–5 mm) to be ligible after reduction. All illustrations should preferably require the same degree of reduction and must be clear numbered. Legends to illustrations must be submitted on a separa list. Illustrations can be printed in colour when they are judged t the Editor to be essential to the presentation. Further informatk concerning colour illustrations and the costs to the authors can b obtained from the publisher.

Units

The use of SI units is preferred.

Referees

When submitting a paper authors many suggest up to 3 referee supplying the full name and address in each case. However, the fin choice of referees will remain entirely with the Editor.

Accepted articles on disk

The final and accepted text should be submitted on a 3.5 in diskette (addition to a hard copy with original figures). Double density (D or high density (HD) diskettes formatted for MS-DOS or Apple Ma intosh compatibility are acceptable, but must be formatted to the capacity before the files are copied on to them. The files should b saved in the native format of the word processing program used. Mo popular wordprocessor file formats are acceptable. It is essential th the name and version of the word processing program, type of cor puter on which the text was prepared, and format of the text files a clearly indicated.

Copyright Transfer

All authors must sign the 'Transfer of Copyright' agreement before a article can be published. This transfer agreement enables Elsevi Science to protect the copyrighted material for the authors, but doe not relinquish the author's proprietary rights. The copyright transf covers the exclusive rights to reproduce and distribute the articl including reprints, photographic reproductions, microform or a other reproductions of similar nature and translations, and include the right to adapt the article for use in conjunction with computer sy tems and programs, including reproduction or publication machine-readable form and incorporation in retrieval system Authors are responsible for obtaining from the copyright hold permission to reproduce any figures for which copyright exists.

Proofs

Corresponding authors will receive proofs of their paper. (Authors w not receive proofs of Letters, in order to achieve rapid publicatio They are requested to return corrected proofs as soon as possibl No new material may be inserted in the text at the time of proof rea ing. A "note added in proof" will be accepted only if permission ha been obtained from the Editor.

Offprints

Twenty-five offprints are provided free of charge. Further copies ca be ordered at prices shown on the offprint order form which accon pany the proofs.

Page charges

There are no page charges.

Further Information

All questions arising after the acceptance of manuscripts, especiall those relating to proofs, should be directed to: Elsevier Science Irelan Ltd, Elsevier House, Brookvale Plaza, East Park, Shannon, Co. Clar Ireland. Tel.: +353(61) 709600, Fax: +353(61) 709113. The full and com plete Instructions to Authors can be found on the World Wide Wel access under http://www.elsevier.nl or http://www.elsevier.com.

J. Chin. Inst. Chem. Engrs., Vol. 31, No. 1, 19-25, 2000

Oxidative Coupling of Methane in a Ceramic Membrane Reactor: Uniform Oxygen permeation Pattern

Suttichai Assabumrungrat[1] **and Piyasan Praserthdam**
Petrochemical Research Laboratory, Department of Chemical Engineering, Faculty of Engineering, Chulalongkorn University
Bangkok 10330, Thailand

Shigeo Goto
Department of Chemical Engineering, Nagoya University
Chikusa, Nagoya 464-8603, Japan

Abstract — This paper models the oxidative coupling of methane in a porous ceramic membrane reactor. The catalyst is packed in the tube side of a membrane reactor where the reaction takes place. Methane and oxygen are fed to the tube side and shell side of the membrane, respectively. The membrane controls the distribution of oxygen from the shell side to the tube side and, hence, improves the yield to C_2 hydrocarbon products. The side products such as carbon dioxide and water are suppressed because a low concentration of oxygen in the tube side is maintained. The performance of the membrane reactor is compared with a plug flow reactor where both reactants are fed together to the catalyst bed. It is found that the membrane reactor provides much higher selectivity to C_2 hydrocarbons than the plug flow reactor. Moreover, the membrane reactor is superior to the plug flow reactor in yield when the CH_4/O_2 ratio and the oxygen feed side pressure are high. There is a minimum membrane thickness in which complete permeation occurs for each operating condition. In addition, there is an optimum membrane thickness in which the yield is maximized.

Key Words: Oxidative Coupling of Methane, Membrane Reactor, Optimization and Ceramic Membran

INTRODUCTION

Membrane reactor is one of the fastest expanding subjects of researches in chemical reaction engineering. The concept can be traced back for a few decades. Various types of inorganic membranes have been used in the high-temperature applications. Most of the earlier studies on membrane reactors have focused on overcoming equilibrium by selective removal of one of reaction products from a reaction zone through a membrane. As a result, it can drive equilibrium-limited reactions continuously towards the product side and results in higher than equilibrium conversions, thus limiting the need for high temperature and reducing recycle and downstream separation requirements. This process has often been applied to dehydrogenation reactions (Zeika et al., 1993, Collin et al., 1996; Szegner et al., 1997). Another main field of applications of the membrane reactors is to use the membrane to introduce a reactant in a controlled manner. The membrane is not necessary to be selective but acts as a barrier to separate two streams of reactants. Its applications are, for example, for a reaction which is so highly exothermic that reactants should not be mixed in the same feed inlet, and for a selective oxidation of hydrocarbons where excessive oxygen in the reaction zone should be avoided due to the favorable complete oxidation to carbon dioxide and water. Oxidative coupling of methane to C_2 hydrocarbons, with which this work is concerned, is an example of this case.

The oxidative coupling of methane to C_2 hydrocarbons has become the topic of interest after the pioneering work of Keller and Bhasin (1982). This reaction is important as it represents one of the most effective way to convert methane, the most abundant component of natural gas, to more useful products. Now most of the effort has focused on catalyst characterization, reaction mechanism, catalyst screening and reactor configurations. From the kinetics study it was found that high ratio of methane to oxygen throughout the reactor should favour the desired C_2 formation reaction (Lane and Wolf, 1988). The operation under high oxygen atmosphere enhances the formation of side products, CO_2 and water, leading to a low selectivity to the C_2 hydrocarbons. Taking into account this feature, a series of reactor configurations such as plug flow reactor with discrete feed points of

[1] * To whom all correspondence should be addressed

oxygen (Choudhary et al., 1989), counter-current moving bed chromatographic reactor (Tonkovich and Carr 1995), fluidized-bed reactor (Edwards et al., 1992), riser simulator reactor (Pekediz and de Lasa, 1994) and membrane reactor has been developed. The first and the last reactor configurations are based on the concept of distributing oxygen to the reaction zone discretely and continuously, respectively, along the reactor length. Choudhary et al. (1989) compared a fixed bed reactor with co-feeding of oxygen and methane and a reactor with discrete oxygen feed points along the reactor length. They found that with a fixed overall ratio of methane to oxygen, the C_2 yield increased as the number of oxygen feed points increased in the tubular reactors. However, some researchers found that by splitting the feed of oxygen at various discrete feed points along the reactor length did not significantly improve the C_2 yield (Schweer et al., 1994; Campbell and Ekstrom, 1993). They concluded that the effectiveness of the distributed feed of oxygen depended mainly on the applied catalysts.

Various types of membranes have been used in membrane reactors for the oxidative coupling of methane. Most of them are solid oxides such as yttria-stabilized zirconia (YSZ), PbO or Ag. These membranes are capable of conducting either ionic oxygen or protons and, hence, they are very selective to oxygen. However, because the flux of oxygen obtained is generally low due to its low permeability, the hydrocarbon yield is usually small (Lafarga et al., 1994) and a conversion per pass is low (Omata et al. 1989). Recently membranes with much higher permeability such as modified alumina membrane and porous Vycor glass have been studied. The transport mechanisms include laminar flow and Knudsen diffusion, rather than solid state ionic diffusion. Since the oxygen flows to the reaction side at rates controlled by the applied pressure difference, it results in significantly higher hydrocarbon yield. Lu et al. (1997) compared the oxidative coupling of methane in membrane reactors with various reactor configurations. The overall methane to oxygen feed ratio was optimized such that the C_2 yield at the reactor outlet was maximized. They found that distributed feed oxygen could give rise to much higher C_2 yields than the co-feeding reactor. They also considered the case of a two-membrane reactor where one membrane was used for oxygen feed and the other for C_2 product removal. It was found that the selectivity of the second membrane played an important role on the performance of the reactor. Alternative way to improve the C_2 yield of the oxidative coupling process is to separate C_2 either by a cryogenic method or by adsorption and recycle the unconverted methane (Sofranko and Jubin, 1989).

In this paper the modelling of the oxidative coupling of methane in a ceramic membrane reactor was investigated. Kinetics data of 34 wt% lead oxide catalyst impregnated on γ-alumina (Hinsen et al., 1985) and data on permeation rate of gases through a commercial "Membralox" membrane with 4 nm pore size (Assabumrungrat and White, 1996) were used in the modelling. The performance of the membrane reactor was compared with a plug flow reactor. Particular interest was to investigate the optimum thickness of the membrane in which maximum yield to C_2 hydrocarbons was obtained.

MODELLING OF A MEMBRANE REACTOR

The membrane reactor in this study is a double tubular reactor; the inner tube is made of an alumina membrane, and the outer shell of an impermeable wall. The catalyst is packed in the tube side where a feed of methane is introduced. Oxygen is fed to the shell side. The membrane is exploited to distribute oxygen to the reaction chamber. The model can be simplified by the following assumptions.

(1) The flow in the system is at steady state.
(2) The reaction is operated at isothermal conditions.
(3) The ideal gas law can be used to determine gas properties.
(4) There is a constant pressure in both the shell and the tube side.
(5) The interfacial mass transfer resistance between the gas and the surface of membrane is small compared with the internal mass transfer resistance in the membrane.
(6) Axial diffusion is negligible and all species are ideally mixed in the radial direction.
(7) The membrane is not catalytically active.

Figure 1 illustrates the membrane configuration used in this study. It is operated under cocurrent flow pattern. By performing the material balance across a small distance dz, the following differential equations can be obtained.

For tube side:

$$\frac{d}{dz}N_i = \frac{\pi}{4}D_t^2 r_i + \pi D_t q_i \tag{1}$$

For shell side:

$$\frac{d}{dz}Q_i = -\pi D_t q_i \tag{2}$$

The transport of gas phase through a porous membrane can be taken place by many mechanisms, namely, viscous bulk flow, Knudsen diffusion, surface diffusion, capillary condensation and molecular sieving. Viscous flow (or Poiseuille flow) takes place when the membrane pores are larger than the mean free path of the permeating gas molecules. This mechanism is non-separative and undesired for gas separation process. The transport rate can be described by the Hagen-Poiseuille equation. Knudsen

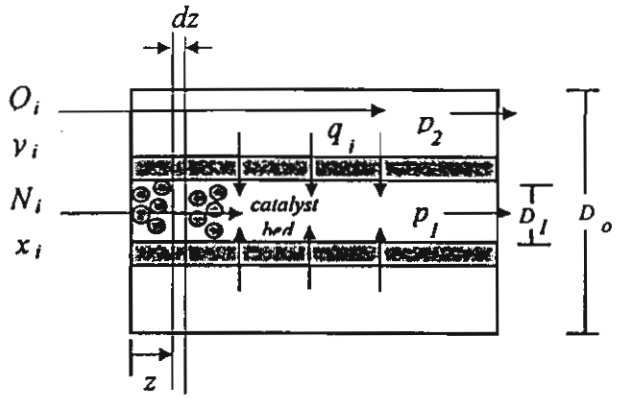

Fig. 1. The membrane reactor configuration.

flow regime predominates when the pore diameter is smaller than the mean free path of gases to be separated. The permeation flux is inversely proportional to the square root of molecular weight. The permeation data used in this study is based on the permeation data of gases through a commercial "Membralox" membrane. The membrane consists of a porous α-alumina support and a separative layer of γ-alumina with pore size of 4 nm and thickness of 5 μm. It was found that both Knudsen and viscous flow mechanisms are important for the permeation of gas through the membrane and the permeation flux of specie i can be expressed as follows (Assabumrungrat and White, 1996).

$$q_i = \frac{a}{t_m\sqrt{M_i}}(p_2 y_i - p_1 x_i) + \frac{b y_i}{t_m \mu}(p_2^2 - p_1^2) \qquad (3)$$

where

$$a = \frac{\epsilon d_p}{3RT\tau}\sqrt{\frac{8RT}{\pi}} \qquad (4)$$

$$b = \frac{\epsilon d_p^2}{64\tau RT} \qquad (5)$$

$$x_i = \frac{N_i}{\Sigma N_i} \qquad (6)$$

and

$$y_i = \frac{Q_i}{\Sigma Q_i} \qquad (7)$$

It should be noted that surface diffusion is unlikely in this study because the reaction is carried out at high temperatures and that the permeation flux is inversely proportional to the thickness.

In the model, the kinetics data of 34 wt% lead oxide catalyst impregnated on γ-alumina was used (Hinsen et al., 1985). The chemical reactions and the rate expressions are given as follows:

$$CH_4 + 2\,O_2 \rightarrow CO_2 + 2\,H_2O \qquad -r_{CH_4} = 15.0 \exp(-6134/T)\, C_{CH_4}^{0.4} \cdot C_{O_2}^{0.5} \qquad (8)$$

$$CH_4 + 1/4\,O_2 \rightarrow 1/2\,C_2H_6 + 1/2\,H_2O \qquad -r_{CH_4} = 1.2 \times 10^3 \exp(-11908/T)\, C_{CH_4}^{0.8} \cdot C_{O_2}^{1} \qquad (9)$$

$$C_2H_6 + 1/2\,O_2 \rightarrow C_2H_4 + H_2O \qquad -r_{C_2H_6} = 1.0 \times 10^{-1} \exp(-722/T)\, C_{C_2H_6}^{0.8} \cdot C_{O_2}^{0} \qquad (10)$$

$$C_2H_4 + 3\,O_2 \rightarrow 2\,CO_2 + 2\,H_2O \qquad -r_{C_2H_4} = 1.0 \times 10^{-13} \exp(26461/T)\, C_{C_2H_4}^{0.8} \cdot C_{O_2}^{6} \qquad (11)$$

It should be noted that the C_2 formation reaction has a lower reaction order in O_2 and a higher reaction order in methane than CO_2 formation. Hence, the selectivity to the C_2 production can be maximized by operating the reactor using high methane concentration and low oxygen concentrations.

Since the obtained system of ordinary differential equations from the cocurrent operation leads to an initial value problem, the Runge-Kutta method is used to integrate the initial value case with the following initial conditions

$$\text{at} \quad z = 0 \qquad N_i = N_i^0$$

and

$$\text{at} \quad z = 0 \qquad Q_i = Q_i^0$$

RESULTS AND DISCUSSION

In this study, the effect of oxygen feed pressure and CH_4/O_2 ratio (defined as the inlet flow rate of CH_4 divided by that of O_2) were investigated. In addition, the membrane thickness was optimized to maximize the yield. The numerical values of the parameters used in the simulations are summarized in Table 1.

Partial pressure profiles at the standard condition

Figures 2 and 3 show partial pressure profiles of all species in the tube and shell sides, respectively, under the standard condition with shell side pressure of 607.8 kPa and CH_4/O_2 ratio of 2. It can be seen that using the membrane reactor the partial pressure of oxygen in the tube size is kept at small value and that there is only a small amount of methane and the reaction products permeating through the membrane because of the high pressure in the shell side.

Figures 4, 5 and 6 compare the conversion, selectivity and yield of the membrane reactors at different values of oxygen feed pressure and CH_4/O_2 ratios with those of the plug flow reactor. It should be noted that the pressure in the reaction side of both plug flow and membrane reactors is the same at 101.3 kPa.

The conversion, selectivity and yield are defined as follows:

$$\text{Conversion} = (N_{CH_4}^0 - N_{CH_4} - Q_{CH_4})/N_{CH_4}^0$$

Table 1. Summary of the values of parameters at standard condition.

Parameters	value	unit
Temperature	1,023	K
Tube side pressure	101.3	kPa
Catalyst bed density	1,500	kg/m^3
Mole fraction of methane in tube side	1	-
Mole fraction of oxygen in shell side	1	-
Membrane inner diameter	0.006	m
Reactor length	0.05	m
Membrane thickness	5×10^{-6}	m
Catalyst weight/molar flow rate of methane (W/F)	50	kg-cat.s/mol
Knudsen parameter (a)	1.26×10^{-12}	$s.(mol/kg)^{1/2}$
Viscous flow parameter (b)	1.30×10^{-22}	$s^2.mol/kg$
Viscosity of pure oxygen	4.55×10^{-5}	kg/(m.s)

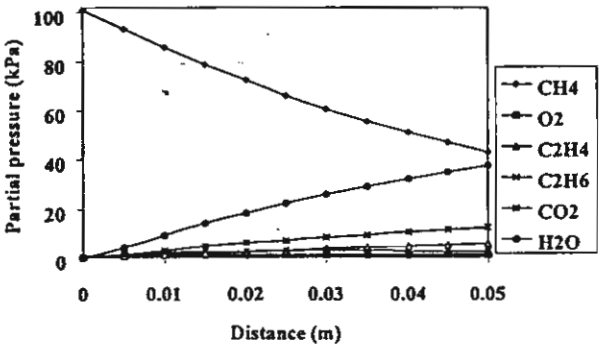

Fig. 2. Partial pressure of all species in the tube side.

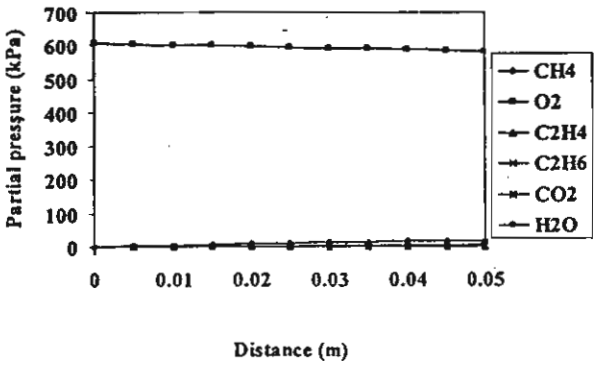

Fig. 3. Partial pressure of all species in the shell side.

$$\text{Selectivity} = 2\,(N_{C_2\text{hydrocarbons}} + Q_{C_2\text{hydrocarbons}})/(N_{CH_4}{}^0 - N_{CH_4} - Q_{CH_4})$$

$$\text{Yield} = (\text{conversion}) \times (\text{selectivity})$$

where $N_{CH_4}{}^0$ and N_{CH_4} are molar flow rates of methane in the tube side at the feed and the exit, respectively. Q_{CH_4} is the molar flow rates of methane in the shell side at the exit. $N_{C_2\text{hydrocarbon}}$ and $Q_{C_2\text{hydrocarbon}}$ are molar flow rates of C_2 hydrocarbons at the exit of the tube side and the shell side, respectively. For the

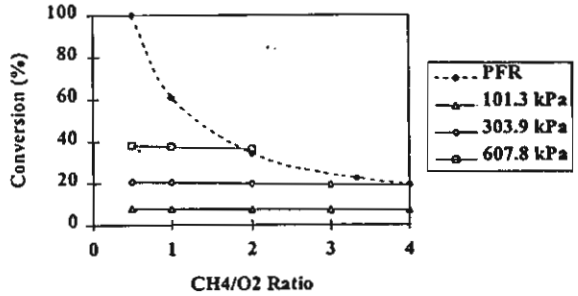

Fig. 4. Conversion versus CH_4/O_2 ratio at different oxygen feed pressures.

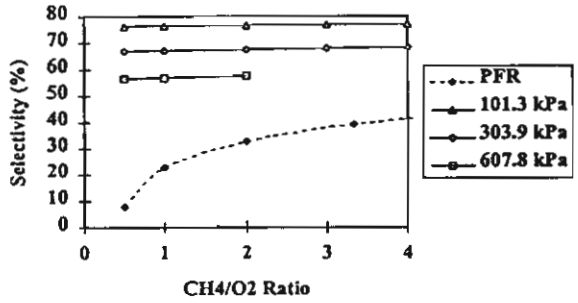

Fig. 5. Selectivity versus CH_4/O_2 ratio at different oxygen feed pressures.

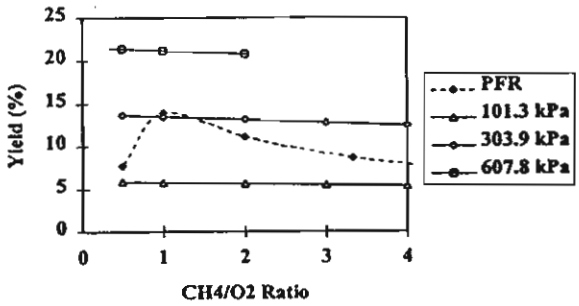

Fig. 6. Yield versus CH_4/O_2 ratio at different oxygen feed pressures.

plug flow reactor $Q_{C_2 hydrocarbon}$ is equal to zero.

The plug flow reactor without the shell side was simulated by the feed mixture of CH_4 and O_2 at 101.3 kPa of total pressure in the tube side. Considering only the effect of CH_4/O_2 ratio, it is obvious that the conversion, selectivity and yield of the plug flow reactor are highly dependent on the CH_4/O_2 ratio while that of the membrane reactors are not. The decrease in the CH_4/O_2 ratio of the plug flow reactor results in the increase in conversion and the decrease in selectivity. This is because at high oxygen partial pressures the undesired complete oxidation to CO_2 and H_2O is favorable (Lane and Wolf, 1988). From Fig. 6, it should be noted that there is an optimum CH_4/O_2 ratio for the plug flow reactor in which the yield to C_2 hydrocarbons is maximized. However, at that optimum ratio the selectivity is only around 22%. For membrane reactor, it was found that selectivity is much higher than that of the plug flow reactor and that the CH_4/O_2 ratio does not significantly affect the conversion, selectivity and yield of the reactor. It is because the membrane controls the supply of oxygen from the shell side to the tube side and, hence, the oxygen partial pressure is maintained at low values throughout the reactor length.

One way to control the supply of oxygen to the tube side is to adjust the oxygen feed pressure in the shell side. From the same figure, it can be found that the oxygen feed pressure in the shell side of the membrane reactor significantly affects the performance of the reactors. When the oxygen feed pressure in the shell side increases, the conversion is higher but the selectivity is lower. This is because more oxygen passes through the membrane and reacts with methane. Even though the selectivity is lower, the selectivity of the membrane reactor is still much higher than that of the plug flow reactor. From Fig. 6, it can be seen that the yield of the membrane reactor is higher than that of the plug flow reactor when the oxygen feed pressure is higher than 303.9 kPa.

Optimizing the maximum yield

Another way to control the oxygen permeation rate is to control the membrane thickness because the permeation flux is inversely proportional to the membrane thickness. Consequently, in order to obtain the maximum yield an optimum membrane thickness should be chosen. Figures 7 and 8 show the selectivity and yield of the membrane reactor at different values of oxygen feed pressure. The CH_4/O_2 ratio is fixed at 2. The dotted lines show the corresponding values of the plug flow reactor. It should be noted that the left end of each curve (different oxygen feed pressures) represents its minimum membrane thickness at which the complete permeation of gases from the shell side to the tube side occurs . It can be seen

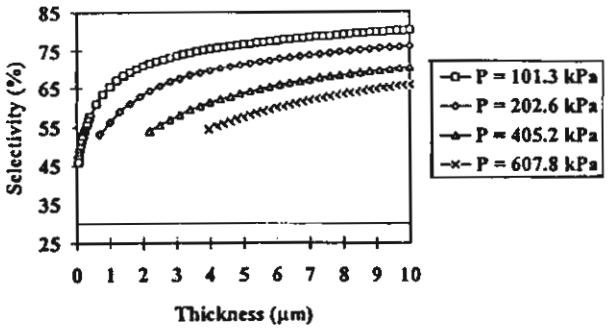

Fig. 7. Selectivity versus membrane thickness at different oxygen feed pressures.

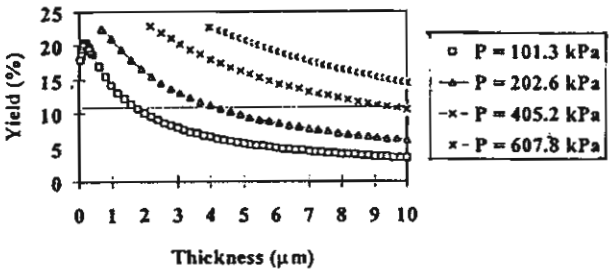

Fig. 8. Yield versus membrane thickness at different oxygen feed pressures.

from the figures that as the membrane thickness is thinner, the selectivity decreases while the yield increases. The increase of the yield means that the increase of the reaction conversion is more significant than the decrease of the selectivity. However, with the oxygen feed pressure of 101.3 kPa when the membrane thickness is thinner, the yield increases until reaching its maximum value and then starts decreasing. The decrease of the yield means that the decrease of the selectivity is more pronounced than the increase of the reaction conversion. This behaviour is similar to the plug flow reactor presented earlier in that there is an optimum CH_4/O_2 in which the yield is maximized. It is obvious from Figs. 7 and 8 that the optimum membrane thickness varies with the oxygen feed pressure; however, the maximum yields obtained from the membrane reactor for the membrane reactor are the same (around 22%) and higher than that of the plug flow reactor (only 11%). In addition, the selectivity of the membrane reactor at the maximum yield is 52% compared to only 30% from the plug flow reactor. It should be noted that the yield of the membrane reactor can be maximized by either adjusting the oxygen feed pressure or choosing an appropriate membrane thickness or by considering both of them together.

Figures 9 and 10 show the selectivity and yield of the membrane reactor at different CH_4/O_2 ratios. The oxygen feed pressure was fixed at 607.8 kPa. Dotted lines in the figures are used to indicate the location of minimum membrane thickness where com-

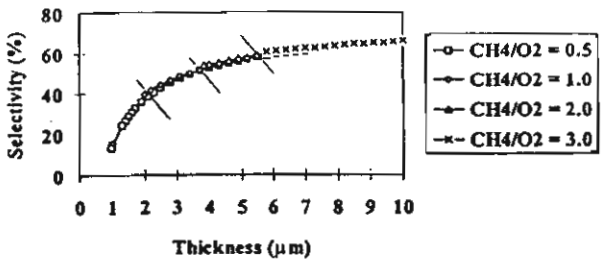

Fig. 9. Selectivity versus membrane thickness at different feed ratios.

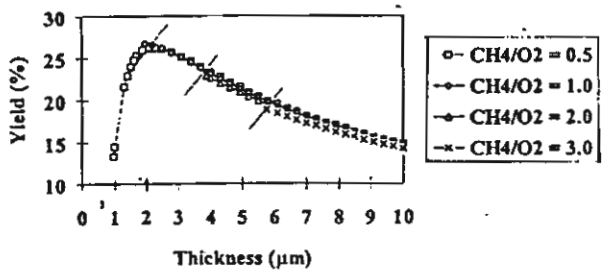

Fig. 10. Yield versus membrane thickness at different feed ratios.

plete permeation of gases in the shell side takes place for different CH_4/O_2 ratios. It can be seen from the figures that the trends of the selectivity and yield of the membrane reactor with the membrane thickness for different values of CH_4/O_2 ratio are similar to those for different values of oxygen feed pressure. However, the minimum membrane thickness and the obtained maximum yield are different for the different CH_4/O_2 ratios. When the CH_4/O_2 ratio is smaller, the more oxygen can be supplied to the reaction system and, hence, thinner membrane thickness can be used. It should be noted that even though the yield increases with the decrease of CH_4/O_2 ratio, the selectivity becomes worsen. From Figs. 7, 8, 9 and 10 it can be concluded that the optimum membrane thickness which gives the maximum yield depends on the operating pressure and the CH_4/O_2 ratio.

It should be noted that in this paper the effects of pressure drop, non-isothermal condition and radial dispersion are not considered. The results from the simulations may slightly deviate from the real values; however, they are still able to represent the benefits of applying the membrane to distribute the oxygen to the reactor for the oxidative coupling of methane.

CONCLUSION

Oxidative coupling of methane in a membrane reactor was modelled using the kinetics and permeation data from the literatures. It was found that the membrane reactor shows much higher selectivity and yield than the plug flow reactor. In addition, for the plug flow reactor there is an optimum CH_4/O_2 ratio that gives the maximum yield while for the membrane reactor there is an optimum membrane thickness that gives the maximum yield. The optimum membrane thickness depends on the operating pressure and the CH_4/O_2 ratio. In addition, for the membrane reactor there is also a minimum membrane thickness in which the complete permeation of gases from the shell side to the tube side occurs for each operating condition.

ACKNOWLEDGMENT

This research was supported by the Thailand Research Fund.

NOMENCLATURE

a	Knudsen parameter defined as Eq. (4), s. $(mol/kg)^{1/2}$
b	viscous flow parameter defined as Eq. (5), $s^2.mol/kg$
C_i	gas concentration of species i, mol/m^3
D_I	inner diameter of membrane reactor, m
D_o	outer diameter of membrane reactor, m
d_p	membrane pore diameter, m
L	length of the reactor, m
M_i	molecular weight, kg/mol
N_i	molar flow rate of species i in the tube side, mol/s
p	pressure at any distance in membrane, Pa
p_i	partial pressure of species i, Pa
p_1	pressure in the tube side, Pa
p_2	pressure in the shell side, Pa
Q_i	molar flow rate of species i in the shell side, mol/s
q_i	molar flow flux of specie i across the membrane, $mol/s.m^2$
r_i	rate of formation of component i, mol/kg-catalyst.s
R	universal gas constant (= 8.314J/(mol.K))
T	temperature, K
t_m	thickness of the separative membrane layer, m
x_i	composition of species i in the tube side
y_i	composition of species i in the shell side
z	axial distance, m

Greek Letters

ε	porosity of membrane, –
μ	viscosity of gas mixture, kg/(m.s)
ρ	density of the catalyst bed, kg/m^3

τ toutorsity factor of membrane, –

REFERENCES

Assabumrungrat, S. and D. A. White, "Permeation of Ethanol and Methanol Vapours through a Porous Alumina Membrane," *Chem. Eng. Sci.*, **51**, 5241, (1996).

Cambell, I. and A. Ekstrom, "Methane Oxidative Coupling in a Pressurized Distributed Feed Reactor," *Symposium on Methane Activation, Conversion and Utilization*, Australia, (1993).

Choudhary, V.R., S.T. Chaudhari, A.M. Rajput and V. H. Rane, "Beneficial Effect of Oxygen Distribution on Methane Conversion and C_2 Selectivity in Oxidative Coupling of Methane to C_2 Hydrocarbon Over Lanthanum-promoted Magnesium Oxide," *J. Chem. Soc., Chem. Commun.*, **20**, 1526, (1989).

Collins, J.P., R.W. Schwartz, R. Sehgal, T. L. Ward, C.J. Brinker, G. P. Hagen and C. A. Udovich, "Catalytic Dehydrogenation of Propane in Hydrogenation Permselective Membrane Reactors," *Ind. Eng. Chem. Res.*, **35**, 4398, (1996).

Edwards, J.H., K.T. Do and R.J. Tyler, "The Catalytic Oxidative Coupling of Methane: I. Comparison of Experimental Performance Data from Various Types of Reactor," *Methane Conversion by Oxidative Process: Fundamental and Engineering Aspects: Wolf, E.E., Ed.; Catalyst Series;* Van Nostrand Reinhold: New York, 429, (1992).

Hinsen, W., W. Bytyn and M. Baerns, "Oxidative Dehydrogenation and Coupling of Methane," *Proceedings of the 8th International Congress on Catalysis, Verlag Chemie: Weinheim, Germany*, 3, 581, (1985).

Keller, G.E. and M.M. Bhasin, "Synthesis of Ethylene via Oxidative Coupling of Methane I. Determination of Active Catalyst," *J. Catal.*, **73**, 9, (1982).

Lane, G.S. and E.E. Wolf, "Methane Utilization by Oxidative Coupling: I. A Study of Reaction in the Gas Phase during the Cofeeding of Methane and Oxygen," *J. Catal.*, **113**, 144, (1988).

Larfarga, D., J. Santamaria and M. Menendez, "Methane Oxidative Coupling using Porous Membrane Reactor I. Reactor Development," *Chem. Eng. Sci.*, **49**, 2005, (1994).

Lu, Y., A.G. Diixon, W.R. Moser and Y.H. Ma, "Analysis and Opitmization of Cross-Flow Reactors for Oxidative Coupling of Methane," *Ind. Eng. Chem. Res.*, **36**, 559, (1997).

Omata, K.S., S. Hashimoto, H. Tominaga and K. Fujimoto, "Oxidative Coupling of Methane Using a Membrane Reactor," *Appl. Catal.*, **52**, L1, (1989).

Pekediz, A. and H.L. de Lasa, "Methane Oxidative Coupling in a Novel Riser Simulator Reactor," *Chem. Eng. Sci.*, **49**, 4759, (1994).

Sofranko, J.A. and J.C. Jubin, Natural Gas to Gasoline: the ARCO GTG Process. Paper 165. Preprints, *Pacifichem* 89, Honolulu, HI, 152, (1989).

Schweer, D., L. Mleczko and M. Bauerns, M. "Oxidative Coupling of Methane in a Fixed-Bed Reactor: Limits and Perspectives," *Catal. Today*, **21**, 357, (1994).

Szegner, J., K. L. Yeung and A. Varma, "Effect of Catalyst Distribution in a Membrane Reactor: Experiments and Model," *AIChE*, **43**, 2059, (1997).

Tonkovich, A. L. Y. and R. W. Carr, "Modeling of the Simulated Counter-Current Moving-Bed Chromatographic Reactor Used for the Oxidative Coupling of Methane," *Chem. Eng. Sci.*, **49**, 4657, (1995).

Ziaka, Z.D., R.G. Minet and T.T. Tsotsis, "A High Temperature Catalytic Membrane Reactor for Propane Dehydrogenation," *J. Mem. Sci.*, **77**, 221, (1993).

(Manuscript Received March 4, 1999)

Kinetics for Dehydrogenation of Propane on Pt-Sn-K/γ-Al_2O_3 Catalyst

SUTTICHAI ASSABUMRUNGRAT[1],
WIROJ JHORALEECHARNCHAI[1],
PIYASAN PRASERTHDAM[1] AND SHIGEO GOTO[2]
[1]*Petrochemical Engineering Laboratory, Department of Chemical Engineering, Chulalongkorn University, Bangkok 10330, Thailand*
[2]*Department of Chemical Engineering, Nagoya University, Nagoya 464-8603, Japan*

Reprinted from
JOURNAL OF
CHEMICAL ENGINEERING
OF
JAPAN
Vol. 33, No. 3 (2000)
Pages 529–532

ırnal of Chemical Engineering of Japan, Vol. 33, No. 3, pp. 529–532, 2000

:inetics for Dehydrogenation of Propane on Pt-Sn-K/γ-Al_2O_3 Catalyst

SUTTICHAI ASSABUMRUNGRAT[1],
WIROJ JHORALEECHARNCHAI[1],
PIYASAN PRASERTHDAM[1] AND SHIGEO GOTO[2]
[1]*Petrochemical Engineering Laboratory, Department of Chemical Engineering, Chulalongkorn University, Bangkok 10330, Thailand*
[2]*Department of Chemical Engineering, Nagoya University, Nagoya 464-8603, Japan*

:ywords: Dehydrogenation, Propane, Propene, Kinetics, Platinum-Based Catalyst

The performance of three catalysts, namely Pt/γ-Al_2O_3, Pt-Sn/γ-Al_2O_3 and Pt-Sn-K/γ-Al_2O_3 for dehy-ogenation of propane is discussed. All catalysts are found to be highly selective towards propene. Pt-ı-K/γ-Al_2O_3 appears to be the most stable and suitable catalyst for the dehydrogenation of propane. Pt-n/γ-Al_2O_3 is also found to be superior to Pt/γ-Al_2O_3. In the kinetic study, the reaction rate constants ısed on the number of active sites are calculated from the apparent reaction rate constants and the ımber of metal active sites. The reaction rate constants for Pt/γ-Al_2O_3, Pt-Sn/γ-Al_2O_3 and Pt-Sn-K/γ-l_2O_3 catalysts at 773 K are 0.48×10^{-25}, 0.67×10^{-25} and 2.98×10^{-25} mol/(site·s·Pa), respectively. In ddition, for Pt-Sn-K/γ-Al_2O_3, the frequency factor and the activation energy are 6.14×10^{-24} mol/(site·s·Pa) nd 62.7 kJ/mol, respectively.

ntroduction

The concept of membrane reactor has shown high ɔotential for applications in the fields of biological and hemical reaction engineering during the past several ecades. One of the major applications of membrane eactors is overcoming an equilibrium conversion by ombining reaction and separation in a single unit operation. The dehydrogenation of propane to propene is ɔne of the reactions of interest in this type of application. A number of researchers have studied this reaction using various types of membrane materials and atalysts. Sheintuch and Dessau (1996) used a Pd/Ru or Pd/Ag) membrane reactor packed with a supported t catalyst. They found that the yield was limited by eactivation of the catalyst due to the low partial pressure of hydrogen in the reaction side. Weyten *et al.* (1997) investigated the system using H_2-selective silica nembrane with a chromia/alumina catalyst, and found hat the propene yield was at least twice as high as the value obtained at thermodynamic equilibrium in a conentional reactor. Yildirim *et al.* (1997) evaluated the elative performance of three composite membranes; namely Pd/Ag, silica, and Pd-dispersed porous membranes. They found that the dense Pd-Ag composite ystem possessed higher performance levels. However, metal-dispersed porous systems had advantages due to their significantly higher contact surface-to-volume atio.

Received on September 9, 1999. Correspondence concerning this article should be addressed to S. Assabumrungrat.

Although significant research has been carried out in this area, there is little effort to investigate the reaction rate constants of propane dehydrogenation. This study is focused on kinetic determination for the dehydrogenation of propane. Three catalysts, namely Pt/γ-Al_2O_3, Pt-Sn/γ-Al_2O_3, and Pt-Sn-K/γ-Al_2O_3 were tested to find out the catalytic performance and the reaction rate constants were determined. These data are useful in the modeling of the dehydrogenation of propane in the membrane reactor.

1. Experiment

1.1 Catalyst preparation

0.3%Pt/γ-Al_2O_3 catalyst was prepared by impregnation of a γ-alumina support. γ-Alumina (produced by Sumitomo Alumina Smelting Co., Ltd., Japan) was ground to the desired mesh size, and then impregnated in a solution of chloroplatinic acid dissolved in de-ionized water. The catalyst was heated at the rate of 10 K per minute, and calcined at 773 K for 3 h. 0.3%Pt-0.3%Sn/γ-Al_2O_3 catalyst was prepared by using an impregnation solution with mixtures of chloroplatinic acid and $SnCl_2$ dissolved in de-ionized water. 0.3%Pt-0.3%Sn-0.6%K/γ-Al_2O_3 could be made by re-impregnation of the calcined 0.3%Pt-0.3%Sn/γ-Al_2O_3 catalyst with potassium nitrate solution.

1.2 Carbon monoxide chemisorption technique

The metal active sites of fresh and used catalyst were measured using a carbon monoxide chemisorption technique whose concept is based on the assumption that one molecule of carbon monoxide adsorbs onto

Table 1 Values of $N_{site,fresh}$, $N_{site,3min}$, $N_{site,120min}$ and conversions at 3 and 120 min for three catalysts

Time	0 min	3 min		120 min		
Catalyst	$N_{site,fresh} \times 10^{-21}$ [site/kg]	Conversion [%]	$N_{site,3min} \times 10^{-21}$ [site/kg]	Conversion [%]	$N_{site,120min} \times 10^{-21}$ [site/kg]	$N_{site,120min}/N_{site,fresh}$
$Pt/\gamma\text{-}Al_2O_3$	29.0	17.0	12.5	1.5	1.33	0.046
$Pt\text{-}Sn/\gamma\text{-}Al_2O_3$	18.2	17.1	8.2	1.8	0.82	0.045
$Pt\text{-}Sn\text{-}K/\gamma\text{-}Al_2O_3$	5.24	29.8	3.6	6.7	0.67	0.128

one metal active site (Burch *et al.*, 1994). Measurements were made using a pulse method. This technique involved pulsing a known volume of carbon monoxide over a catalyst sample at room temperature. The carbon monoxide that was not adsorbed was measured using a gas chromatography with a thermal conductivity detector. Pulses were continued until no further carbon monoxide adsorption was observed. The quantity of carbon monoxide adsorbed by the catalyst sample could then be calculated and hence the amount of metal active sites obtained.

1.3 Experiment

Dehydrogenation of propane was carried out in a micro reactor installed in a furnace with a temperature controller. The reactor was a quartz tube reactor whose inner diameter was 6.35 mm. The catalyst was packed in the middle of the quartz tube. Hydrogen gas was used to reduce the catalyst for 1 h, and then argon was used for purging hydrogen. The feed gas supplied by Thai Industrial Gases Limited was mainly a mixture of 3% propane in nitrogen. The experiment was performed at 773 K unless otherwise specified.

2. Kinetics

The rate equation for the dehydrogenation reaction can be expressed in the following simple form

$$-r_A = k_{app}\left(p_A - \frac{p_B p_C}{K}\right) = k_{app}\left(\frac{p_{Ao}(1-X_A)}{(1+y_{Ao}X_A)} - \frac{(p_{Bo}+p_{Ao}X_A)(p_{Co}+p_{Ao}X_A)}{(1+y_{Ao}X_A)^2 K}\right) \quad (1)$$

$$k_{app} = \frac{F_{Ao}}{W}\int_0^{X_A} \frac{dX_A}{\left(\frac{p_{Ao}(1-X_A)}{(1+y_{Ao}X_A)} - \frac{(p_{Bo}+p_{Ao}X_A)(p_{Co}+p_{Ao}X_A)}{(1+y_{Ao}X_A)^2 K}\right)} \quad (2)$$

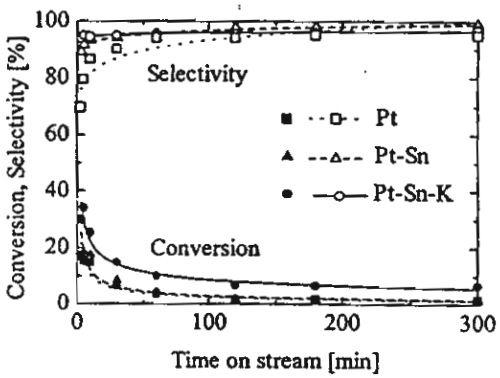

Fig. 1 Conversion and selectivity with time on stream: $F_{Ao} = 6.24 \times 10^{-7}$ mol/s, $T = 773$ K, $W = 0.1$ g, $y_{Ao} = 0.03$, $p_{Ao} = 3039$ Pa, $p_{Bo} = p_{Co} = 0$ Pa

By assuming a plug flow reactor, the apparent rate constant k_{app} can be determined as

The equilibrium constant, K can be calculated from Gibb's free energy data at different temperatures and correlated as the following expression.

$$K = 1.76 \times 10^{12} \exp(-15{,}521/T) \quad (3)$$

3. Results and Discussion

3.1 Comparison between catalysts

A set of experiment was carried out to compare the performance of $Pt/\gamma\text{-}Al_2O_3$, $Pt\text{-}Sn/\gamma\text{-}Al_2O_3$, and $Pt\text{-}Sn\text{-}K/\gamma\text{-}Al_2O_3$ catalysts. The conversion and selectivity to propene were measured as shown in **Fig. 1**. The propane molar flow rate was fixed at 6.24×10^{-7} mol/s, and the catalyst weight was 0.1 g.

All catalysts are highly selective towards propene, and the selectivities are higher than 95%. In addition, the conversions of all the catalysts decrease with time on stream, and reach the asymptotes after 120 min. Deactivation may be due to coke formation on the catalyst. The addition of Sn on $Pt/\gamma\text{-}Al_2O_3$ catalyst improves the conversion of $Pt/\gamma\text{-}Al_2O_3$ catalyst. This can be explained by the ensemble effect in which the addition of Sn results in an increase in Pt dispersion and, hence, the stability of the catalytic activity is improved from

Table 2 Values of k_{app} and k_{site} for three catalysts

Time	3 min		120 min		
Catalyst	$k_{app,3min} \times 10^7$ [mol/(kg·s·Pa)]	$k_{site,3min} \times 10^{28}$ [mol/(site·s·Pa)]	$k_{app,120min} \times 10^7$ [mol/(kg·s·Pa)]	$k_{site,120min} \times 10^{28}$ [mol/(site·s·Pa)]	$k_{site,average} \times 10^{28}$ [mol/(site·s·Pa)]
Pt/γ-Al_2O_3	5.3	0.42	0.59	0.44	0.43
Pt-Sn/γ-Al_2O_3	5.7	0.70	0.54	0.64	0.67
Pt-Sn-K/γ-Al_2O_3	11.0	3.09	1.9	2.86	2.98

the reduced amount of coke depositing on the metal active sites (Barias *et al.*, 1996; Krishnamurthy, 1998). Moreover, the addition of Sn can improve the selectivity to propene due to blocking or poisoning of acid sites on the support (Barias *et al.*, 1995). Figure 1 also shows that Pt-Sn-K/γ-Al_2O_3 catalyst gives the highest conversion. This may be explained by three reasons, i.e.; (1) alkali metals such as potassium enhance hydrogen spillover on the catalyst surface; (2) alkali metals reduce the amount of coke depositing on the active sites (Praserthdam *et al.*, 1997); and (3) alkali metals neutralize the acid sites of the alumina support (Demiguel *et al.*, 1995).

3.2 Kinetic studies

As preliminary experiments, operating conditions where the resistances of external mass transfer and internal mass transfer are negligible were searched to obtain intrinsic kinetics. In this study, only Pt-Sn-K/γ-Al_2O_3 catalyst with the highest activity was tested. To investigate the effect of external mass transfer on the conversions, the experiment was carried out by using the same value of time factor, W/F_{A0} = 160 s·kg/mol and the catalyst mesh size of 60–80 mesh. The feed flow rate was varied between 2.5–10.0 × 10^{-7} m^3(STP)/s. The resistance of external mass transfer could be neglected when the feed flow rate was higher than 7.5 × 10^{-7} m^3(STP)/s. Another set of experiment was carried out to investigate the effect of internal mass transfer on conversion. Three ranges of catalyst sizes, 60–80, 200–250 and 250–325 meshes, were tested under the same operating conditions such as the catalyst weight of 0.1 g, operating temperature of 773 K, and propane molar flow rate of 9.63 × 10^{-7} mol/s. The resistance of internal mass transfer was negligible for the catalyst size smaller than 60–80 mesh.

In order to determine the reaction rate constants, it was assumed that the decrease of catalyst activity was due to the formation of coke on metal active sites, and that the dehydrogenation of propane reached steady state within seconds (Larrson *et al.*, 1997, 1998). The experiment was carried out using 0.1 g of catalyst. The operating temperature was 773 K and the propane molar flow rate was 9.63 × 10^{-7} mol/s. **Table 1** summarizes the number of metal active sites of fresh catalysts and those of used catalysts after 3 and 120 min together with their corresponding conversions. The apparent reaction rate constants, k_{app} (calculated from Eq. (2)) at 3 and 120 min reaction times on stream are also presented in **Table 2**. It should be noted that the last column in Table 1 also provides some insight into the superior stability of the Pt-Sn-K/γ-Al_2O_3 catalyst by comparing the ratio of the metal active site of spent catalyst at 120 min (the values at the asymptotes) and of fresh catalysts, $N_{site,120min}/N_{site,fresh}$. It is clearly seen that the value of Pt-Sn-K/γ-Al_2O_3 catalyst is higher than the others. In other words, deactivation of the Pt-Sn-K/γ-Al_2O_3 catalyst is less than the other catalysts.

The reaction rate constants based on the number of active sites, k_{site}, is defined as follows.

$$k_{site} = k_{app}/N_{site} \tag{4}$$

The values of the reaction rate constants, k_{site}, can be determined from the number of available active sites, N_{site} in Table 1 and are also presented in Table 2. The average reaction rate constant of Pt-Sn-K/γ-Al_2O_3 ($k_{site,average}$ = 2.98 × 10^{-28} mol/(site·s·Pa)) is higher than those of Pt-Sn/γ-Al_2O_3 (0.67 × 10^{-28} mol/(site·s·Pa)) and Pt/γ-Al_2O_3 (0.43 × 10^{-28} mol/(site·s·Pa)). This implies that the presence of Sn does not significantly alter the strength of the metal active site while the presence of potassium increases the strength. This phenomena was also addressed previously by Demiguel *et al.* (1995), where it was found that the addition of alkali metals produced a modification of the characteristics of the metallic phase which involved an electronic modification of the metallic phase.

To confirm the value of reaction rate constant of Pt-Sn-K/γ-Al_2O_3, one experiment was carried out using the same conditions except for a 20% mixture of propane in nitrogen. The obtained reaction rate constant of 3.08 × 10^{-28} mol/(site·s·Pa)) agrees well with that of 3% propane (2.98 × 10^{-28} mol/(site·s·Pa)).

To complete the kinetics for Pt-Sn-K/γ-Al_2O_3 the reaction rate constants were determined at different temperatures from 723 to 873 K. The obtained results fit very well with Arrhenius's equation as shown in **Fig. 2**. The following expression can be determined.

$$k_{site} = 6.14 \times 10^{-24} \exp(-7{,}545/T) \tag{5}$$

The activation energy was 62.7 kJ/mol.

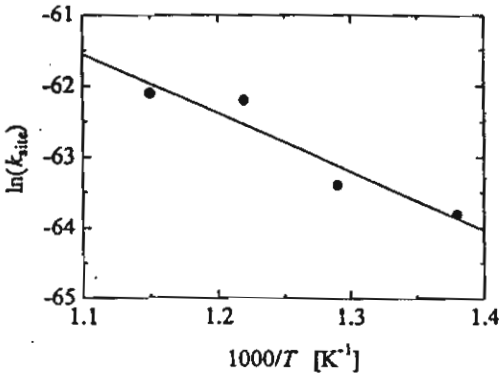

Fig. 2 Arrhenius plot for Pt-Sn-K/γ-Al_2O_3

Conclusion

The performance of Pt/γ-Al_2O_3, Pt-Sn/γ-Al_2O_3 and Pt-Sn-K/γ-Al_2O_3 catalysts were investigated. All catalysts exhibit the selectivity towards propene higher than 95%. Pt-Sn-K/γ-Al_2O_3 appears to be the most suitable catalyst for dehydrogenation of propane. The reaction rate constant based on the number of metal active site for Pt/γ-Al_2O_3, Pt-Sn/γ-Al_2O_3 and Pt-Sn-K/γ-Al_2O_3 catalysts at 773 K are 0.43×10^{-28}, 0.67×10^{-28} and 2.98×10^{-28} mol/(site·s·Pa), respectively. Arrhenius's equation can be determined by changing temperatures.

Acknowledgment

This research was financially supported by the Thailand Research Fund and TJTTP-OECF.

Nomenclature

F_{Ao}	=	feed flow rate of propane	[mol/s]
K	=	equilibrium constant	[Pa]
k_{app}	=	apparent reaction rate constant	[mol/(kg·s·Pa)]
k_{site}	=	reaction rate constant based on active site	[mol/(site·s·Pa)]
N_{site}	=	number of active site	[site/kg]
p_i	=	partial pressure of component i	[Pa]
$-r_A$	=	rate of reaction	[mol/(kg·s)]
W	=	catalyst weight	[kg]
X_A	=	reaction conversion	[—]
y_{io}	=	initial mole fraction of component i in the feed inlet	[—]

<Subscript>

A	=	propane
B	=	propene
C	=	hydrogen
o	=	condition at feed inlet

Literature Cited

Barias, O. A., A. Holmen and E. A. Blekkan; "Propane Dehydrogenation over Supported Platinum Catalysts—Effect of Tin as a Promoter," *Cat. Tod.*, 24, 361–364 (1995)

Barias, O. A., A. Holmen and E. A. Blekkan; "Propane Dehydrogenation over Supported Pt and Pt-Sn Catalysts: Catalyst Preparation, Characterization, and Activity Measurements," *J. Cat.*, 158, 1–12 (1996)

Burch, R., P. J. Millington and A. P. Walker; "Mechanism of the Selective Reduction of Nitrogen Monoxide on Platinum-Based Catalysts in the Presence of Excess Oxygen," *App. Cat. B: Envi.*, 4, 65–94 (1994)

Demiguel, S. R., A. A. Castro, O. A. Scelza and J. Soria; "Effect of the Addition of Alkali-Metals on the Metallic Phase of Pt/Al_2O_3 Catalysts," *Cat. Letts.*, 32, 281–291 (1995)

Krishnamurthy, K. R.; "Modifications in Supported Metal Catalysts: Effect of Promoters," *Recent Advances in Basic and Applied Aspects of Industrial Catalysis*, 113, 139–150 (1998)

Larrson, M., N. Henriksson and B. Andersson; "Estimation of Reversible and Irreversible Coke by Transient Experiments," *Catalyst Deactivation*, 111, 673–680 (1997)

Larrson, M., N. Henriksson and B. Andersson; "Investigation of the Kinetics of a Deactivating System by Transient Experiments," *App. Cat. A*, 166, 9–19 (1998)

Praserthdam, P., T. Mongkhonsi, S. Kunatippapong, B. Jaikaew and N. Lim; "Determination of Coke Deposition on Metal Active Sites of Propane Dehydrogenation Catalysts," *Catalyst Deactivation*, 111, 153–158 (1997)

Sheintuch, M. and R. M. Dessau; "Observations, Modeling and Optimization of Yield, Selectivity and Activity during Dehydrogenation of Isobutane and Propane in a Pd Membrane Reactor," *Chem. Eng. Sci.*, 51, 535–547 (1996)

Weyten, H., K. Keizer, A. Kinoo, J. Luyten and R. Leysen; "Dehydrogenation of Propane Using a Packed-Bed Catalytic Membrane Reactor," *AIChE J.*, 43, 1819–1827 (1997)

Yildirim, Y., E. Gobina and R. Hughes; "An Experimental Evaluation of High-Temperature Composite Membrane Systems for Propane Dehydrogenation," *J. Mem. Sci.*, 135, 107–115 (1997)

Dependence of Hydrogen Pressure on the Permeation Rate through Composite Palladium Membranes

SHIGEO GOTO[1], SUTTICHAI ASSABUMRUNGRAT[2], TOMOHIKO TAGAWA[1] AND PIYASAN PRASERTHDAM[2]

[1]*Department of Chemical Engineering, Nagoya University, Nagoya 464-8603, Japan*

[2]*Department of Chemical Engineering, Faculty of Engineering, Chulalongkorn University, Bangkok 10330, Thailand*

Reprinted from
JOURNAL OF CHEMICAL ENGINEERING OF JAPAN
Vol. 33, No. 2 (2000)
Pages 330–333

Journal of Chemical Engineering of Japan, Vol. 33, No. 2, pp. 330–333, 2000

Dependence of Hydrogen Pressure on the Permeation Rate through Composite Palladium Membranes

SHIGEO GOTO[1], SUTTICHAI ASSABUMRUNGRAT[2], TOMOHIKO TAGAWA[1] AND PIYASAN PRASERTHDAM[2]

[1]*Department of Chemical Engineering, Nagoya University, Nagoya 464-8603, Japan*

[2]*Department of Chemical Engineering, Faculty of Engineering, Chulalongkorn University, Bangkok 10330, Thailand*

Keywords: Membrane Reactor, Composite Palladium Membrane, Order, Permeation Rate Expression

A composite pailadium membrane consists of a thin film of palladium layer coated on a ceramic support. Two kinds of models are formulated for the direction of permeation through the composite membrane (CP mode and PC mode). The apparent order of hydrogen pressure is varied from 0.5 to 1.0 by the relative values between two resistances of palladium film and ceramic support for the hydrogen permeation rate through the composite membrane. The relation between the apparent order and the relative resistance is dependent on the operating conditions. Once the apparent order can be determined from the linearity of experimental data, we can estimate the relative resistance.

Introduction

A composite palladium membrane consists of a thin film of palladium layer coated on a ceramic support. Since the defectless palladium film in the composite membrane can be made much thinner on an asymmetric ceramic support than the normal dense membrane, the resulting permeation rate may be significantly improved. The ceramic support provides the mechanical strength for the membrane; however, the small pore diameter of such ceramic supports may affect the permeation rate. Nowadays, this type of composite membrane has become attractive for applications in the field of membrane reactors due to its superior permeability and permselectivity to hydrogen (Dittmeyer *et al.*, 1999).

There are two directions of hydrogen permeation through the composite palladium membrane, that is, CP mode (at first through the ceramic support and then through the palladium film) and PC mode (opposite manner). The permeation rate for CP mode is higher by 20% than that for PC mode in some cases (Goto *et al.*, to be submitted).

It is well-known through Sievert's law that the pressure dependence of hydrogen is half order through the palladium film. On the other hand, the pressure dependence of hydrogen is first order through the ceramic support due to Knudsen and molecular diffusions. In the composite membrane, the apparent order may be in the range between 0.5 and 1. For example, the values of 0.552–0.622 (Collins and Way, 1993), 0.68 (Hurlbert and Konecny, 1961), 0.76 (Umemiya *et al.*, 1991) and 0.80 (DeRosset, 1960) were reported as the apparent order. Umemiya *et al.* (1991) explained the reason for this discrepancy from Sievert's law in that hydrogen diffusivity might vary with the concentration of hydrogen.

In this work, the deviation of the apparent order from Sievert's law for the permeation of hydrogen through the composite membrane is illustrated by relating the apparent order with the relative resistances of the palladium film and the ceramic support.

Received on October 14, 1999. Correspondence concerning this article should be addressed to S. Goto (E-mail address: goto@park.nuce.nagoya-u.ac.jp).

1. Mathematical Model

The permeation rate of hydrogen through a composite membrane may be expressed by an apparent order, n as follows:

$$Q_H = \alpha_{H,app}\left\{\left(p_{H,R} / p_0\right)^n - \left(p_{H,S} / p_0\right)^n\right\} \quad (1)$$

1.1 CP mode

Performing the material balance of hydrogen, a set of equations can be obtained. Let $p_{H,M}$ be the pressure of hydrogen at the membrane interface between the palladium film and ceramic support. Since transport through the support may mainly be governed by the first order of pressure of hydrogen, the permeation rate, Q_H can be expressed as

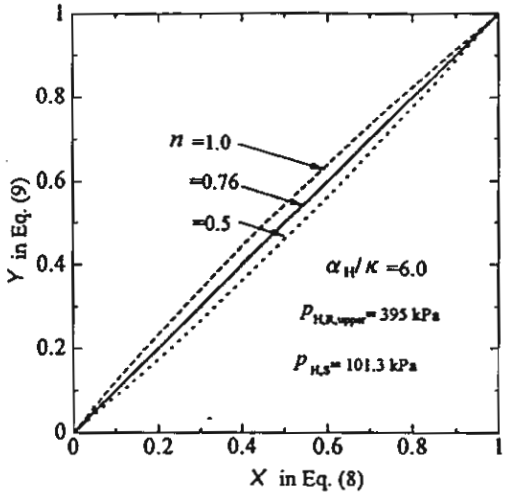

Fig. 1 Linearity of order for PC mode

$$Q_H = \kappa\left\{\left(p_{H,R}/p_0\right)-\left(p_{H,M}/p_0\right)\right\} = \alpha_H\left\{\left(p_{H,M}/p_0\right)^{1/2}-\left(p_{H,S}/p_0\right)^{1/2}\right\} \quad (2)$$

where α_H is the permeability coefficient of hydrogen through the palladium film and κ is the diffusion coefficient of hydrogen through the ceramic support.

From Eq. (2), the pressure of hydrogen at the interface between the palladium film and the membrane support can be solved as

$$\frac{p_{H,M}}{p_0} = \frac{1}{4}\left(\sqrt{\left(\frac{\alpha_H}{\kappa}\right)^2+4\left(\frac{p_{H,R}}{p_0}+\frac{\alpha_H}{\kappa}\left(\frac{p_{H,S}}{p_0}\right)^{1/2}\right)}-\frac{\alpha_H}{\kappa}\right)^2 \quad (3)$$

Hence

$$Q_H\left(p_{H,R},p_{H,S}\right) = \alpha_H\left(\frac{1}{2}\left(\sqrt{\left(\frac{\alpha_H}{\kappa}\right)^2+4\left(\frac{p_{H,R}}{p_0}+\frac{\alpha_H}{\kappa}\left(\frac{p_{H,S}}{p_0}\right)^{1/2}\right)}-\frac{\alpha_H}{\kappa}\right)-\left(\frac{p_{H,S}}{p_0}\right)^{1/2}\right) \quad (4)$$

1.2 PC mode

The material balance for PC mode can be carried out using the same manner as that of CP mode. The hydrogen permeation rate can be expressed as

$$Q_H = \alpha_H\left\{\left(p_{H,R}/p_0\right)^{1/2}-\left(p_{H,M}/p_0\right)^{1/2}\right\} = \kappa\left\{\left(p_{H,M}/p_0\right)-\left(p_{H,S}/p_0\right)\right\} \quad (5)$$

From Eq. (5), the pressure of hydrogen at the interface between the palladium film and the membrane support can be solved as

$$\frac{p_{H,M}}{p_0} = \frac{1}{4}\left(\sqrt{\left(\frac{\alpha_H}{\kappa}\right)^2+4\left(\frac{p_{H,S}}{p_0}+\frac{\alpha_H}{\kappa}\left(\frac{p_{H,R}}{p_0}\right)^{1/2}\right)}-\frac{\alpha_H}{\kappa}\right)^2 \quad (6)$$

Hence

$$Q_H\left(p_{H,R},p_{H,S}\right) = \alpha_H\left(\left(\frac{p_{H,S}}{p_0}\right)^{1/2}-\frac{1}{2}\left(\sqrt{\left(\frac{\alpha_H}{\kappa}\right)^2+4\left(\frac{p_{H,S}}{p_0}+\frac{\alpha_H}{\kappa}\left(\frac{p_{H,R}}{p_0}\right)^{1/2}\right)}-\frac{\alpha_H}{\kappa}\right)\right) \quad (7)$$

2. Results and Discussions

Figure 1 shows one typical result for the PC mode. The parameters were derived from a set of data in the conditions of Umemiya *et al.* (1991). In their study, the pressure of hydrogen in the reaction side was varied from 145 to 395 kPa while the pressure of hydrogen in the sweep side was fixed at 101.3 kPa.

X-axis and Y-axis represent as follows:

$$X = \frac{\left(\frac{p_{H,R}}{p_0}\right)^n-\left(\frac{p_{H,S}}{p_0}\right)^n}{\left(\frac{p_{H,R,upper}}{p_0}\right)^n-\left(\frac{p_{H,S}}{p_0}\right)^n} \quad (8)$$

$$Y = \frac{Q_H\left(p_{H,R},p_{H,S}\right)}{Q_H\left(p_{H,R,upper},p_{H,S}\right)} \quad (9)$$

where $p_{H,R,upper}$ is the upper limit of the pressure of hydrogen in the reaction side (=395 kPa) and $p_{H,S}$ is fixed at 101.3 kPa. $Q_H(p_{H,R}, p_{H,S})$ in the Y-axis can be calculated from Eq. (7) for PC mode.

Three lines in Fig. 1 are drawn by changing the pressure of hydrogen in the reaction side, $p_{H,R}$ from 101.3 to 395 kPa for the order, $n = 0.5$, 0.76 and 1.0, at the relative resistance, $\alpha_H/\kappa = 6.0$. It is seen from Fig. 1 that when the resistance through the ceramic support is six times higher than the resistance through the palladium film, the linearity can hold at $n = 0.76$, which was the value reported by Umemiya *et al.* (1991) who used a composite membrane consisting of thin palladium film (the thickness, 20 μm) supported on the outer surface of a porous glass cylinder (the thickness, 800

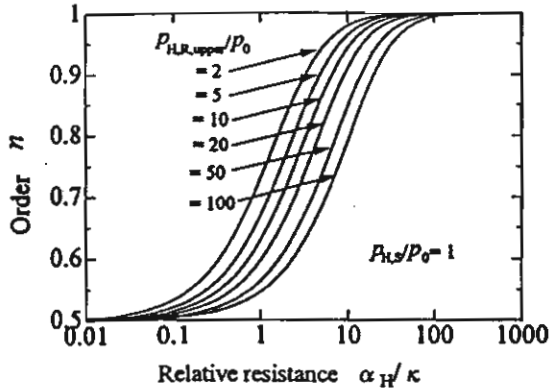

Fig. 2 Relation of order and the relative resistance for CP mode

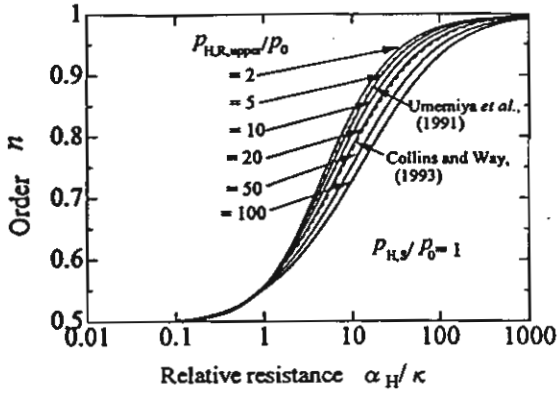

Fig. 3 Relation of order and the relative resistance for PC mode

μm). Here, the presence of resistance from the ceramic support is proposed to be one explanation why the order in some composite membranes may be higher than 0.5. However, measurements of respective resistances may be required to confirm them. Another possibility for the deviation of the apparent order is due to the presence of pinholes on the palladium film or leakage through sealing (Collins and Way, 1993). However, this should be carefully checked by permeation tests with helium gas, and its contribution should be excluded from the experimental results. Therefore, it will not be considered in this paper.

It should be noted that the dependency of pressure of hydrogen on the permeation of hydrogen through the composite membrane can be expressed in Eqs. (4) and (7) for CP and PC modes, respectively. However, the expressions are rather complicated, and it is usually approximated by correlating the experimental results with Eq. (1). The apparent order, n, only shows the best fit parameter for a certain range of experimental results.

The square deviation, Δ, is introduced to determine the linearity.

$$\Delta = \int_{p_{H,S}}^{p_{H,R,upper}} (Y - X)^2 \, dp_{H,R} \qquad (10)$$

where Y and X can be calculated from Eqs. (8) and (9).

The apparent order, n, can be obtained by minimizing the square deviation, Δ, at the specified value of the relative resistance, α_H/κ, within the specified range of pressure of hydrogen. The all-purpose equation solver, EQUATRAN-G (Omega Simulation Co. Ltd) is useful to solve these equations.

Figures 2 and 3 show the relation between n and α_H/κ for CP and PC modes, respectively, for the ranges of interest from $p_{H,S}/p_0$ of 1 to $p_{H,R,upper}/p_0$ at various values of 2, 5, 10, 20, 50 and 100. Two dotted lines in Fig. 3 show the results for experimental conditions of Umemiya *et al.* (1991) and Collins and Way (1993).

In the palladium film controlling region ($\alpha_H/\kappa < 0.01$), the order is naturally 0.5. On the other hand, in the ceramic support controlling region ($\alpha_H/\kappa > 1000$), the order becomes 1.0.

In the transition region ($0.01 < \alpha_H/\kappa < 1000$), the order varies between 0.5 and 1.0. In this region, the pressure of hydrogen at the interface, $p_{H,M}$ in Eq. (3) for CP mode is higher than that in Eq. (6) for PC mode as indicated in Goto *et al.* (to be submitted). This makes the contribution of permeation in ceramic membrane (first order) for CP mode greater than that for PC mode. Therefore, the order n for CP mode is higher than that for PC mode at the same value of α_H/κ.

The relation between n and α_H/κ is dependent on the upper limit of the pressure of hydrogen in the reaction side, $p_{H,R,upper}$.

Once the order can be determined from the linearity of the experimental data at the known range pressure of hydrogen, we can estimate the relative resistance by using Figs. 2 or 3. For example, the relative resistance, α_H/κ may be within 0.95 and 2.5 in the case of Collins and Way (1993), who obtained the apparent order in PC mode, n, in the range of 0.526 and 0.622 for the $p_{H,R,upper}$ of 2445 kPa.

Conclusion

The apparent order of hydrogen pressure on the hydrogen permeation rate through the composite membrane is related to the relative resistance of palladium film and ceramic support. Once the apparent order can be determined from the linearity of experimental data, we can estimate the relative resistance. However, the relation is dependent on the operating conditions.

Acknowledgment

The authors would like to thank NGK INSULATOR LTD, TJTTP-OECF and the Thailand Research Fund.

Nomenclature

$p_{H,M}$	=	pressure of hydrogen at interface between palladium film and ceramic support	[Pa]
$p_{H,R}$	=	pressure of hydrogen in reaction side	[Pa]
$p_{H,S}$	=	pressure of hydrogen in sweep side	[Pa]
p_0	=	standard pressure (=101.3 kPa)	[Pa]
Q_H	=	permeation rate of hydrogen	[mol/s]
α_H	=	permeation rate constant through palladium film	[mol/s]
κ	=	diffusion rate constant through ceramic support	[mol/s]

Literature Cited

Collins, J. P. and J. D. Way; "Preparation and Characterization of a Composite Palladium-Ceramic Membrane," *Ind. Eng. Chem. Res.*, 32, 3006–3013 (1993)

DeRosset, A. J.; "Diffusion of Hydrogen through Palladium Membranes," *Ind. Eng. Chem.*, 52, 525–528 (1960)

Dittmeyer, R., V. Hollein, P. Quicker, G. Emig, G. Hausinger and F. Schmidt; "Factors Controlling the Performance of Catalytic Dehydrogenation of Ethylbenzene in Palladium Composite Membrane Reactors," *Chem. Eng. Sci.*, 54, 1431–1440 (1999)

Goto, S., S. Assabumrungrat, T. Tagawa and P. Praserthdam; "Permeation of Hydrogen through a Composite Palladium Membrane," *J. Membr. Sci.* (to be submitted)

Hurlbert, R. C. and J. O. Konecny; "Diffusion of Hydrogen through Palladium," *J. Chem. Phys.*, 34, 655–658 (1961)

Umemiya, S., N. Sato, H. Ando and E. Kikuchi; "The Water Gas Shift Reaction Assisted by a Palladium Membrane Reactor," *Ind. Eng. Chem. Res.*, 30, 585–589 (1991)

Journal of Chemical Engineering of Japan, Vol. 33, No. 2, pp. 333–336, 2000 **Short Communication**

Application of a Zeolite A Membrane to Reverse Osmosis Process

IZUMI KUMAKIRI, TAKEO YAMAGUCHI AND SHIN-ICHI NAKAO

Department of Chemical System Engineering, The University of Tokyo, Tokyo 113-8656, Japan

Keywords: Zeolite Membrane, Reverse Osmosis (RO), Pervaporation (PV), Liquid Separation

The reverse osmosis process needs no phase transformation during separation, and thus it has a potential in saving energy for liquid mixture separations. Application of reverse osmosis to organic liquid is limited, owing to the lower stability of polymer membranes against organic liquid. Zeolites are inorganic materials having durability against organic liquid and heat, and they show good separation ability in pervaporation. In this study, zeolite membrane was firstly applied to the reverse osmosis process. Zeolite A membrane, having thickness around 5 μm, showed 0.44 rejection from 10wt% ethanol water mixture. The membrane was stable to applied pressures up to 50 kgf cm^{-2}.

Introduction

For liquid mixture separation, much attention has been paid to membrane separation technology because of energy saving. For this purpose, reverse osmosis (RO) and pervaporation (PV) processes can be used. In the RO process, a membrane is placed between liquid feed and liquid permeate. Since the driving force is mainly pressure gradient, high applied pressure should be used to cancel the osmotic pressure effect. In the PV process, on the other hand, liquid feed is vaporized while passing through the membrane and the process thus includes a phase change. This means that the PV process needs additional energy for vaporization. Nakao (1994) showed the advantages of the RO system in energy saving compared with PV and distillation systems in ethanol/water separation.

However, the application of RO to organic mixture separation has been limited because of two problems. One issue is that most RO membranes are made of organic materials, and most of them do not have much resistance to organic liquid. The application of RO is, thus, limited to the separation of aqueous solutions (Ohya *et al.*, 1981). The other is the durability at high pressures. If an inorganic membrane could be applied to RO processes, it will significantly improve the application range of RO separation.

Zeolites are inorganic materials having good stability against organic liquids. The application of zeolite membranes in PV processes has been reported this

Received on October 22, 1999. Correspondence concerning this article should be addressed to I. Kumakiri (E-mail address: izumi@nakao1.t.u-tokyo.ac.jp).

ELSEVIER

Journal of Membrane Science 175 (2000) 19–24

journal of MEMBRANE SCIENCE

www.elsevier.nl/locate/memsci

The effect of direction of hydrogen permeation on the rate through a composite palladium membrane

Shigeo Goto[a,*], Suttichai Assabumrungrat[b], Tomohiko Tagawa[a], Piyasan Praserthdam[b]

[a] *Department of Chemical Engineering, Nagoya University, Chikusa, Nagoya 464-8603, Japan*

[b] *Department of Chemical Engineering, Faculty of Engineering, Chulalongkorn University, Bangkok 10330, Thailand*

Received 1 June 1999; accepted 15 March 2000

Abstract

This paper reports the effect of direction of hydrogen permeation on the rate through a composite palladium membrane. Palladium film is coated on the outer surface of a tubular ceramic support. Permeation rates of hydrogen through the palladium membrane were measured at 573, 673 and 773 K under two modes. The first one is called 'CP mode' in which hydrogen permeates at first through the ceramic support and then through the palladium film. The other mode is called 'PC mode' in which hydrogen permeates in the opposite manner. It was found from the measurements that the permeation rate of hydrogen increased with the increase of temperature and that the permeation rate under CP mode was higher than that under PC mode.

Mathematical models taking into account the combined resistances of both palladium film and ceramic support were developed to describe the hydrogen permeation rate through the composite palladium membrane tube under both modes of permeation. In addition, the mathematical models were used to predict the relative contributions of two resistances for both CP mode and PC mode.

Keywords: Composite palladium membrane; Permeation rate; Hydrogen permeation; Membrane reactor; Resistance model

1. Introduction

Palladium-based membranes have been studied extensively due to their extremely high hydrogen permselectivity and the applications to many reactions [1]. Although the palladium-based membrane reactors have shown the promising improvement of reaction selectivity and yield, the process is still not economically attractive because of high cost, low hydrogen permeation and low chemical stability. Recent studies [2,3] have focused on the use of composite palladium membrane in which a thin film of palladium layer is coated on a porous support such as vycor glass, alumina and stainless steel. The support provides the mechanical strength for the membrane. Since the palladium film in the composite membrane is much thinner than the normal dense membrane, the resulting permeation rate may be significantly improved. An extensive review on the development of composite metal membranes, especially for hydrogen separation was presented by Uemiya [4].

There are two directions of hydrogen permeation through the composite palladium membrane, that is, CP mode (at first through the ceramic support and then

* Corresponding author. Tel.: +81-52-789-3261; fax: +81-52-789-3261.
E-mail address: goto@park.nuce.nagoya-u.ac.jp (S. Goto)

0376-7388/00/$ – see front matter
PII: S0376-7388(00)00405-1

through the palladium film) and PC mode (opposite manner). However, according to our knowledge, no publications have been found on these topics.

In this study, a composite palladium membrane prepared by NGK Insulators Ltd. in Japan was used to investigate the hydrogen permeation rate at 573, 673 and 773 K under these two modes.

Mathematical models taking into account the combined resistances of both palladium film and ceramic support were developed to describe the hydrogen permeation rate through the composite membrane.

2. Experiment

The membrane employed in this study was a tubular configuration. The outer part of ceramic membrane was coated with palladium film. Fig. 1 shows the schematic composition of the membrane supplied by NGK Insulators Ltd. The inner and outer diameters are 6 and 10.6 mm, respectively. The total length of the membrane is 156 mm. The supporting tube made of alumina with 2 mm thickness and 5.0 μm pore size was coated with two alumina layers with pore sizes of 1.0 and 0.5 μm with 0.3 and 0.02 mm thickness, respectively. At the outer surface of the support, palladium film of 0.02 mm thickness was plated. The district interfaces were observed from SEM photographs. The porosity in ceramic layers was about 0.3 independently of pore sizes.

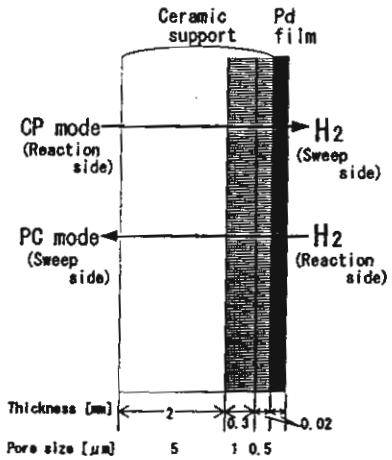

Fig. 1. Schematics of a composite Pd/ceramic membrane.

A needle valve was used to control the inlet gas flow, which was monitored by an orifice meter. The membrane tube was placed in an electric furnace to control the operation temperature. Quartz sand (13.0 g) was packed inside the membrane tube. The outlet flow rate was measured using a soap film meter. There are two modes of operation as shown in Fig. 1. The first one is named 'CP mode' where hydrogen flows inside the membrane tube packed with quartz sand while the pressure in the shell side is reduced by using an aspirator. Therefore, hydrogen can permeate at first through the ceramic support and then through the palladium film. The other is named 'PC mode' where hydrogen is fed into the shell side while the pressure inside the membrane tube is reduced.

The inlet molar flow rate of pure hydrogen in the feed side (reaction side) is $F_{H,R,0}$ and the pressure in the sweep side is $p_{H,S}$. The outlet molar flow rate of hydrogen in the reaction side is $F_{H,R}$. Then, the molar flow rate of permeated hydrogen, Q_H is equal to $F_{H,R,0}-F_{H,R}$.

3. Permeation rate expressions

The mathematical expressions of hydrogen permeation through a composite palladium membrane can be developed using the resistance model taking into account of the combined resistances through both the ceramic support and the palladium film. The expressions for two modes of hydrogen permeation are different and can be formulated as follows.

3.1. CP mode

Let $p_{H,M}$ be the pressure of hydrogen at the membrane interface between the palladium film and ceramic support. Since the transport through the support is mainly governed by the first order with respect to the pressure of hydrogen according to Knudsen diffusion and that through the palladium film is governed by the half order with respect to the pressure of hydrogen, the permeation rate ($Q_{H,CP}$) can be expressed as

$$Q_{H,CP} = \kappa_{CP}\left\{\left(\frac{p_{H,R}}{p_0}\right) - \left(\frac{p_{H,M}}{p_0}\right)\right\} = \alpha_H\left\{\left(\frac{p_{H,M}}{p_0}\right)^{1/2} - \left(\frac{p_{H,S}}{p_0}\right)^{1/2}\right\} \quad (1)$$

where α_H is the permeability coefficient of hydrogen though the palladium film and κ_{CP} is the diffusion coefficient of hydrogen through the ceramic support.

From Eq. (1), the pressure of hydrogen at the interface between the palladium film and the membrane support can be solved as

$$\frac{p_{H,M}}{p_0} = \frac{1}{4}\left(\sqrt{\left(\frac{\alpha_H}{\kappa_{CP}}\right)^2 + 4\left(\left(\frac{p_{H,R}}{p_0}\right) + \frac{\alpha_H}{\kappa_{CP}}\left(\frac{p_{H,S}}{p_0}\right)^{1/2}\right)} - \frac{\alpha_H}{\kappa_{CP}}\right)^2 \quad (2)$$

hence

$$Q_{H,CP} = \alpha_H\left(\frac{1}{2}\left(\sqrt{\left(\frac{\alpha_H}{\kappa_{CP}}\right)^2 + 4\left(\left(\frac{p_{H,R}}{p_0}\right) + \frac{\alpha_H}{\kappa_{CP}}\left(\frac{p_{H,S}}{p_0}\right)^{1/2}\right)} - \frac{\alpha_H}{\kappa_{CP}}\right) - \left(\frac{p_{H,S}}{p_0}\right)^{1/2}\right). \quad (3)$$

3.2. PC mode

The expression for PC mode can be carried out using the same manner as that of CP mode. The hydrogen permeation rate can be expressed as

$$Q_{H,PC} = \alpha_H\left\{\left(\frac{p_{H,R}}{p_0}\right)^{1/2} - \left(\frac{p_{H,M}}{p_0}\right)^{1/2}\right\} = \kappa_{PC}\left\{\left(\frac{p_{H,M}}{p_0}\right) - \left(\frac{p_{H,S}}{p_0}\right)\right\}. \quad (4)$$

From Eq. (4), the pressure of hydrogen at the interface between the palladium film and the membrane support can be solved as

$$\frac{p_{H,M}}{p_0} = \frac{1}{4}\left(\sqrt{\left(\frac{\alpha_H}{\kappa_{PC}}\right)^2 + 4\left(\left(\frac{p_{H,S}}{p_0}\right) + \frac{\alpha_H}{\kappa_{PC}}\left(\frac{p_{H,R}}{p_0}\right)^{1/2}\right)} - \frac{\alpha_H}{\kappa_{PC}}\right)^2 \quad (5)$$

hence

$$Q_{H,PC} = \alpha_H\left(\left(\frac{p_{H,R}}{p_0}\right)^{1/2} - \frac{1}{2}\left(\sqrt{\left(\frac{\alpha_H}{\kappa_{PC}}\right)^2 + 4\left(\left(\frac{p_{H,S}}{p_0}\right) + \frac{\alpha_H}{\kappa_{PC}}\left(\frac{p_{H,R}}{p_0}\right)^{1/2}\right)} - \frac{\alpha_H}{\kappa_{PC}}\right)\right). \quad (6)$$

3.3. Comparison between CP and PC modes

Fig. 2 shows one typical result with $p_{H,R}/p_0=1$, $p_{H,S}/p_0=0.2$ and $\alpha_H=\kappa_{CP}=\kappa_{PC}$. The relative pressure of hydrogen at the interface between the palladium film and the ceramic support, $p_{H,M}/p_0$ can be calculated as 0.64 and 0.50 by using Eqs. (2) and (5) for CP and PC modes, respectively. The ratio of permeation rate for CP mode to PC mode, $Q_{H,CP}/Q_{H,PC}$, can be calculated as 1.20 by using Eqs. (3) and (6). Therefore, the permeation rate for CP mode is higher by 20% than that for PC mode in this case. This is due to the difference in the pressure dependence of the permeation rates between the palladium film (half order) and the ceramic support (first order).

4. Results and discussion

4.1. Permeation rate of hydrogen

Fig. 3 shows experimental data of permeation rate on various relative pressures in the sweep side, $p_{H,S}/p_0$ at three different temperatures, T=573, 673 and 773 K.

As the pressure in the sweep side decreases and the temperature increases, the permeation rate of hydrogen increases. The permeation rate for CP mode is always higher than that for PC mode as expected from Fig. 2.

Solid and broken lines are the results calculated by using Eqs. (3) and (6), respectively, and the values of parameters determined in the next section for CP and PC modes, respectively. Although no replications of

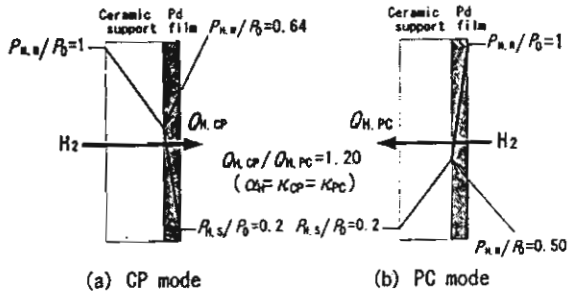

Fig. 2. Comparison between CP and PC modes.

experimental data have been made, these are almost on lines of calculated results.

4.2. Determination of parameters

The permeability coefficient of hydrogen through the palladium film, α_H is given as

$$\alpha_H = D_H C_0 \frac{\pi dz_t}{t_m} \quad (\mathrm{mol/s}) \tag{7}$$

The diffusivity of hydrogen, D_H and the concentration of dissolved hydrogen, C_0 are adopted from Adballa and Elnashaie [5] and Hermann et al. [3].

$$D_H = 2.30 \times 10^{-7} \exp\left(\frac{-21700}{R_g T}\right) \quad (\mathrm{m^2/s}) \tag{8}$$

$$C_0 = 3.03 \times 10^5 T^{1.0358} \quad (\mathrm{mol/m^3}) \tag{9}$$

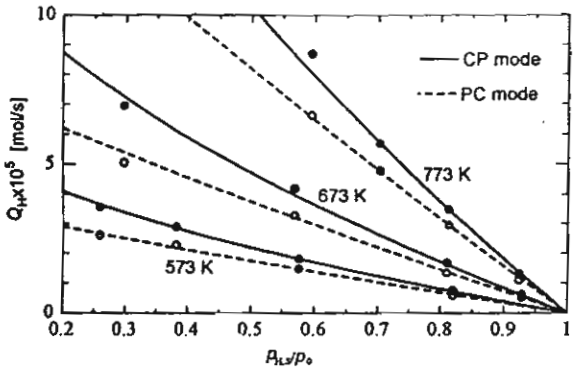

Fig. 3. Permeation rate of hydrogen for CP and PC modes.

Table 1
Determined values of parameters

T (K)	$\alpha_H \times 10^4$ (mol/s)	$\kappa_{CP} \times 10^4$ (mol/s)	$\kappa_{PC} \times 10^4$ (mol/s)	α_H/κ_{PC}	κ_{CP}/κ_{PC}
573	2.63	0.623	0.498	5.28	1.25
673	4.38	1.45	1.08	4.06	1.34
773	6.10	5.36	3.56	1.71	1.51

The diffusion of hydrogen through the ceramic support may include both Knudsen diffusion and viscous bulk flow. Since the structure of the ceramic support is complicated as shown in Fig. 1, the estimation of diffusion coefficient may be difficult. Therefore, the diffusion coefficients of hydrogen through the ceramic support for CP and PC modes, κ_{CP} and κ_{PC} are adjusted by curve fittings of Fig. 3 with Eqs. (3) and (6) for CP and PC modes, respectively.

Table 1 summarizes the determined values of parameters. The ratio, α_H/κ_{PC} is greater than unity. This means that the diffusion resistance through the ceramic support is higher than that through the palladium film. The ratio, κ_{CP}/κ_{PC} is also greater than unity. The difference between κ_{CP} and κ_{PC} may be explained by the asymmetric configuration of the ceramic support as shown in Fig. 1. The direction of permeation should affect the permeation rate through the asymmetric ceramic support. It is suggested from our preliminary estimation that the direction from coarse to fine pores has higher permeation rates than the opposite direction when both Knudsen diffusion and viscous bulk flow dominate.

4.3. The effect of the relative resistance on the relative permeation rate

Fig. 4 shows the effect of the ratio of rate constants, α_H/κ_{PC} on the ratio of permeation rates, $Q_{H,CP}/Q_{H,PC}$ for the values of κ_{CP}/κ_{PC}=1.0 and 1.2. The relative pressure in the sweep side, $p_{H,S}/p_0$ is changed from 0 to 0.8. The lower pressure in the sweep side enhances the effect of the direction of permeation.

When both resistances through the palladium film and the ceramic support are comparative ($0.1 < \alpha_H/\kappa_{PC} < 10$), the effect of the relative pressure in the sweep side, $p_{H,S}/p_0$ on the ratio of $Q_{H,CP}/Q_{H,PC}$

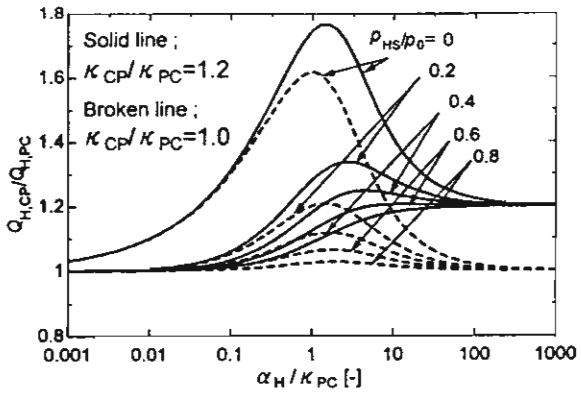

Fig. 4. The effect of the relative resistance on the relative permeation rate at κ_{CP}/κ_{PC}=1.0 and 1.2.

is significant. CP mode is always superior to PC mode.

When the resistance through the palladium film is much greater than that through the ceramic support ($\alpha_H/\kappa_{PC}<0.01$), the permeation through palladium membrane dominates and $Q_{H,CP}/Q_{H,PC}$ value reached to unity. In this case, the direction of permeation is not important.

On the other hand, when the resistance through the ceramic support is much greater than that through the palladium film ($\alpha_H/\kappa_{PC}>100$), the permeation rate of hydrogen is controlled by the resistance through the ceramic support. Therefore, the $Q_{H,CP}/Q_{H,PC}$ value reached to the value of κ_{CP}/κ_{PC}.

5. Conclusions

The permeation rate through a composite palladium membrane was affected by the direction of hydrogen permeation. The first one is 'CP mode'. The other mode is 'PC mode'. It was found from the experimental results that the permeation rate of hydrogen increased with the increase of temperature and that the permeation rate under the CP mode in which hydrogen permeates at first through the ceramic support and then through palladium film was higher than the permeation rate under the PC mode in which hydrogen permeates in the opposite manner. The difference in the permeation rate between two modes indicated the effect of resistance of the support on the hydrogen permeation through the asymmetric composite palladium membrane.

The mathematical model was used to predict the relative resistances of palladium film and ceramic support for both CP mode and PC mode.

6. Nomenclature

C_0	concentration of dissolved hydrogen (mol/m^3)
D_H	diffusivity of hydrogen (m^2/s)
d	outer diameter of membrane tube (m)
$F_{H.R.0}$	molar flow rate of hydrogen in the feed (mol/s)
$F_{H.R}$	molar flow rate of hydrogen in the exit (mol/s)
$p_{H.M}$	pressure at the interface between palladium film and ceramic support (Pa)
$p_{H.R}$	pressure in the reaction side (Pa)
$p_{H.S}$	pressure in the sweep side (Pa)
p_0	standard pressure (=1.013×10^5 Pa) (Pa)
$Q_{H.CP}$	permeation rate of hydrogen for CP mode (mol/s)
$Q_{H.PC}$	permeation rate of hydrogen for PC mode (mol/s)
R_g	gas constant (=8.314 J/(mol K)) (J/(mol K))
T	temperature (K)
t_m	thickness of palladium film (m)
z_t	total length of membrane tube (m)

Greek symbols

α_H	permeation rate constant through palladium film (mol/s)
κ_{CP}	diffusion rate constant through ceramic support for CP mode (mol/s)
κ_{PC}	diffusion rate constant through ceramic support for PC mode (mol/s)

Acknowledgements

The authors would like to thank NGK Insulator Ltd., JSPS, TJTTP-OECF and the Thailand Research Fund for the support and Mr. Isao Takakuwa and Mr. Hajime Itoh for their experimental help.

References

[1] J. Hu, B.P.A. Grandjean, A. Van Neste, S. Kaliaguine, Catalytic palladium-based membrane reactors: a review, Can. J. Chem. Eng. 69 (1991) 1036.

[2] J.P. Collins, J.D. Way, Preparation and characterization of a composite palladium-ceramic membrane, Ind. Eng. Chem. Res. 32 (1993) 3006.

[3] C. Hermann, P. Quicker, R. Dittmer, Mathematical simulation of catalytic dehydrogenation of ethylbenzene to styrene in a composite palladium membrane reactor, J. Membr. Sci. 136 (1997) 161.

[4] S. Uemeya, State of the art of supported metal membranes for gas separation, Sep. Purif. Method 28 (1999) 51.

[5] B.K. Adballa, S.S.H. Elnashaie, Catalytic dehydrogenation of ethylbenzene in membrane reactor, AIChE J. 40 (1994) 2055.

Submission of papers: Papers may be submitted in quadruplicate to the following Editors on the basis of geographic location or area of expertise:

W.J. Koros – gas separation, membrane formation, vapor and reverse osmosis
K.W. Böddeker – liquid separation, bioseparations, dialysis, pervaporation
A.G. Fane – micro-, ultra- and nanofiltration, fouling, porous membranes, engineering
S. Nakao – inorganic membranes, micro- and ultrafiltration, fouling

Electronic manuscripts: Electronic manuscripts have the advantage that there is no need for the rekeying of text, thereby avoiding the possibility of introducing errors and resulting in reliable and fast delivery of proofs.

For the initial submission of manuscripts for consideration, hardcopies are sufficient. For the processing of *accepted papers*, electronic versions are preferred. After *final acceptance*, your disk plus one final and exactly matching printed version should be submitted together. Double density (DD) or high density (HD) diskettes (3.5 or 5.25 inch) are acceptable. It is important that the file saved is in the native format of the wordprocessor program used. Label the disk with the name of the computer and wordprocessing package used, your name, and the name of the file on the disk.

For detailed instructions to authors (including submission of manuscripts on floppy disks) contact one of the editors or the publisher. The instructions can be found in *Journal of Membrane Science*, Vol. 163, pp. 155–157, and also on the World Wide Web: access under http://www.elsevier.nl or http://www.elsevier.com.

Proofs and reprints: Authors will receive **proofs,** which they are requested to correct and return as soon as possible. No new material may be inserted in the text at the time of proofreading. A total of **50 reprints** of each paper will be supplied free of charge to the author(s). Additional copies can be ordered at prices shown on the reprint order form.

All questions arising after acceptance of the manuscript, especially those relating to proofs, should be directed to *Journal of Membrane Science*, Elsevier Science Ireland Ltd., Elsevier House, Brookvale Plaza, East Park, Shannon, Co.Clare, Ireland, Tel. (+353-61) 709600, Fax (+353-61) 709100/709101, E-mail: r.sweeney@elsevier.ie

Journal of Membrane Science **has no page charges.**

Publication information: *Journal of Membrane Science* (ISSN 0376-7388). For 2000, volumes 163–177 are scheduled for publication. Subscription prices are available upon request from the Publisher or from the Regional Sales Office nearest you or from this journal's website (http://www.elsevier.nl/locate/memsci). Further information is available on this journal and other Elsevier Science products through Elsevier's website: (http://www.elsevier.nl). Subscriptions are accepted on a prepaid basis only and are entered on a calendar year basis. Issues are sent by standard mail (surface within Europe, air delivery outside Europe). Priority rates are available upon request. Claims for missing issues should be made within six months of the date of dispatch.

Orders, claims, and product enquiries: please contact the Customer Support Department at the Regional Sales Office nearest you:
New York: Elsevier Science, PO Box 945, New York, NY 10159-0945. USA; phone: (+1) (212) 633 3730 [toll free number for North American customers: 1-888-4ES-INFO (437-4636)]; fax: (+1) (212) 633 3680; e-mail: usinfo-f@elsevier.com
Amsterdam: Elsevier Science, PO Box 211, 1000 AE Amsterdam, The Netherlands; phone: (+31) 20 4853757; fax: (+31) 20 4853432; e-mail: nlinfo-f@elsevier.nl
Tokyo: Elsevier Science, 9-15, Higashi-Azabu 1-chome, Minato-ku, Tokyo 106-0044, Japan; phone: (+81) (3) 5561 5033; fax: (+81) (3) 5561 5047; e-mail: info@elsevier.co.jp
Singapore: Elsevier Science, No. 1 Temasek Avenue, #17-01 Millenia Tower, Singapore 039192; phone: (+65) 434 3727; fax: (+65) 337 2230; e-mail: asiainfo@elsevier.com.sg
Rio de Janeiro: Elsevier Science, Rua Sete de Setembro 111/16 Andar, 20050-002 Centro, Rio de Janeiro - RJ, Brazil; phone: (+55) (21) 509 5340; fax: (+55) (21) 507 1991; e-mail: elsevier@campus.com.br [Note (Latin America): for orders, claims and help desk information, please contact the Regional Sales Office in New York as listed above]

Advertising Information: Advertising orders and enquiries can be sent to: **USA, Canada and South America:** Mr Tino DeCarlo, The Advertising Department, Elsevier Science Inc., 655 Avenue of the Americas, New York, NY 10010-5107, USA; phone: (+1) (212) 633 3815; fax: (+1) (212) 633 3820; e-mail: t.decarlo@elsevier.com. **Japan:** The Advertising Department, Elsevier Science K.K., 9-15 Higashi-Azabu 1-chome, Minato-ku, Tokyo 106-0044, Japan; phone: (+81) (3) 5561 5033; fax: (+81) (3) 5561 5047. **Europe and ROW:** Rachel Leveson-Gower, The Advertising Department, Elsevier Science Ltd., The Boulevard, Langford Lane, Kidlington, Oxford OX5 1GB, UK; phone: (+44) (1865) 843565; fax: (+44) (1865) 843976; e-mail: r.leveson-gower@elsevier.co.uk.

USA mailing notice: *Journal of Membrane Science* (ISSN 0376-7388) is published semi-monthly with additional issues in January, April, July and October by Elsevier Science B.V. (P.O. Box 211, 1000 AE Amsterdam, The Netherlands). Annual subscription price in the USA US$ 4574.00 (valid in North, Central and South America), including air speed delivery. Application to mail at periodical postage rate is pending at Jamaica, NY 11431.
USA POSTMASTER: Send address changes to *Journal of Membrane Science*, Publications Expediting Inc., 200 Meacham Avenue, Elmont, NY 11003.
AIRFREIGHT AND MAILING in the USA by Publications Expediting Inc., 200 Meacham Avenue, Elmont, NY 11003.

♾ The paper used in this publication meets the requirements of ANSI/NISO Z39.48-1992 (Permanence of Paper).

PRINTED IN THE NETHERLANDS

JOURNAL OF MATERIALS SCIENCE LETTERS 19, 2000, 1439–1443

Synthesis of large-surface area silica-modified titania ultrafine particles by the glycothermal method

S. IWAMOTO
Department of Energy and Hydrocarbon Chemistry, Graduate School of Engineering, Kyoto University, Sakyo-ku, Kyoto 606-8501, Japan

W. TANAKULRUNGSANK
Department of Chemical Technology, Rajamangala Institute of Technology, 2 Nanglinchee RD, Yannawa Bangkok 10120, Thailand

M. INOUE
Department of Energy and Hydrocarbon Chemistry, Graduate School of Engineering, Kyoto University, Sakyo-ku, Kyoto 606-8501, Japan

K. KAGAWA
The Kansai Electric Power Company, INC., 3-11-20 Nyakuoji, Amagasaki 661, Japan

P. PRASERTHDAM
Department of Chemical Engineering, Faculty of Engineering, Chulalongkorn University, Phayathai RD, Bangkok 10330, Thailand

The preparation of titania is the subject of considerable interest because this material is widely used as catalyst supports for the selective catalytic reduction (SCR) of NOx with ammonia [1] and the selective oxidation of hydrocarbons [2], and as photocatalysts for various reactions [3]. Besides catalytic applications, it also has many uses such as pigment, filler, more recently, membrane and anti-reflection coating. Surface area is one of the important factors for the use of titania as catalyst materials. However, large-surface area materials have high tendency for sintering because of their surface energies. Amorphous titania having extremely large surface area has been prepared by sol-gel methods [4–6]; however, it crystallizes into anatase at around 500 °C, which is accompanied by a marked decrease in surface area [6–8]. Since thermal stability seriously affects the catalyst life, titania having large surface area with reasonable thermal stability has been sought. Thus, many studies have been devoted to improve the thermal stability of titania using additives such as Al [8, 9], Si [10, 11], La [12, 13] and others [14–16]. The effects of these additives are quite different by the procedures of the doping and the amounts of the additives, and the mechanisms for the stabilization effects of these dopants are not yet fully elucidated. One possible method for the preparation of thermally stable titania seems to be direct synthesis of well-crystallized materials. One of the authors has examined the thermal reaction of metal alkoxides in glycols (glycothermal reaction) or other organic media and demonstrated that a number of novel or characteristic crystalline products can be obtained directly without bothersome procedures such as purification of the reactants or handling in inert atmosphere to exclude the effect of moisture [17–21]. By applying this method, nanocrystalline anatases having large surface areas (>50 m^2/g after calcination at 550 °C) were obtained by the reaction of $TiO(acac)_2$ in toluene [22, 23]. Further optimization of the reaction conditions and careful choice of the titanium source and organic solvent provided anatase nanocrystals having an extremely large surface area (>100 m^2/g after calcination at 550 °C) [24]. However, transformation of anatase into rutile took place in the temperature range of 600–1000 °C resulting in drastic decrease in surface area. To improve the thermal stability of titania, we prepared the silica-modified titanias by the glycothermal method and found that these materials had quite large surface areas and exhibited high thermal stabilities.

Titanium tetraisopropoxide (TIP; 25 g) and an appropriate amount of tetraethyl orthosilicate (TEOS, Si/Ti atomic ratio of 0–0.50) were added to 100 ml of 1,4-butanediol, and this mixture was placed in a 300 ml autoclave. After the atmosphere inside the autoclave was replaced with nitrogen, the mixture was heated at a rate of 2.3 °C/min to a desired temperature (200–300 °C) and kept at that temperature for 2 h. After the assembly was cooled, the resulting powders were collected by centrifugation, washed with methanol or ammoniacal methanol and air-dried. The calcination of the thus-obtained product was carried out in a box furnace in air: the product was heated at a rate of 10 °C/min to a desired temperature and kept at that temperature for 30 min. Powder X-ray diffraction (XRD) patterns were recorded on a Shimadzu XD-D1 diffractometer using CuK_α radiation and a carbon-monochrometer. The crystallite size was calculated by the Scherrer equation from the half-height width of the (101) diffraction peak of anatase after correction for the instrumental broadening. Simultaneous thermogravimetric and differential thermal analyses (TGA and DTA) were performed on a Shimadzu DTG-50 thermal analyzer at a heating rate

0261–8028

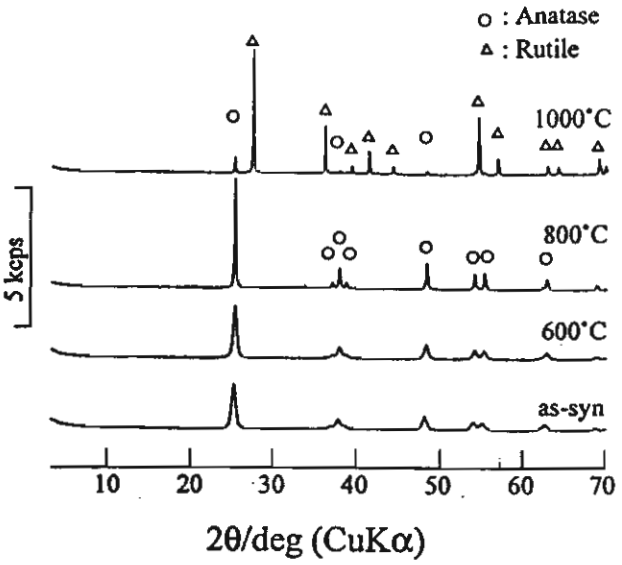

Figure 1 XRD patterns of the product obtained by the reaction of titanium tetraisopropoxide in 1,4-butanediol at 300 °C and the samples obtained by calcination thereof at the temperatures specified in the figure.

of 10 °C/min in a 40 ml/min flow of dried air. The specific surface area was calculated using the BET single-point method on the basis of the nitrogen uptake measured at 77 K using a Micromeritics Flowsorb II 2300. X-ray photoelectron spectroscopy (XPS) measurement was performed on an ULVAC-PHI Model 5500 spectrometer with 15 kV–400 W MgK_α emission as the X-ray source. NH_3 temperature-programmed desorption (NH_3-TPD) profiles were obtained on a Bel Japan TPD-1-AT with a Q-MASS detector.

The XRD pattern of the product obtained by the reaction of TIP alone at 300 °C (Fig. 1) showed that anatase was directly crystallized by the reaction. The crystallite size calculated by the XRD broadening was 17 nm. The average particle size determined from the transmission electron micrograph of the product (Fig. 2) was 17 nm, which is in good agreement with the crystallite size, indicating that each primary particle observed by TEM is a single crystal of anatase. BET surface area of the product was 91.5 m^2/g. When one assumes that each particle is truly spherical, the surface area calculated from the particle size is 90.5 m^2/g, suggesting that each particle of the product exposes its outer surface to the adsorbate, nitrogen. The product preserved relatively large surface area even after calcination at high temperatures. The anatase-rutile transformation began at around 1000 °C. This transformation temperature is much higher than that of the titania prepared by the hydrazine method [25], and as high as that of the titania prepared by the non-hydrous sol-gel method [26], suggesting that the product prepared by the glycothermal method has high crystallinity.

The XRD patterns of the products obtained with addition of TEOS revealed that all the products had the anatase structure (Fig. 3) and that the peak intensities were not affected by the TEOS content in the reaction mixture. This result shows a sharp contrast against the titanias synthesized by other methods, where the peak intensities of anatase decreased with the increase in the silica content due to formation of amorphous phases [25, 27]. The surface areas and crystallite sizes of the products are summarized in Table I. With the increase of the amounts of TEOS added, the surface area increased and the crystallite size decreased.

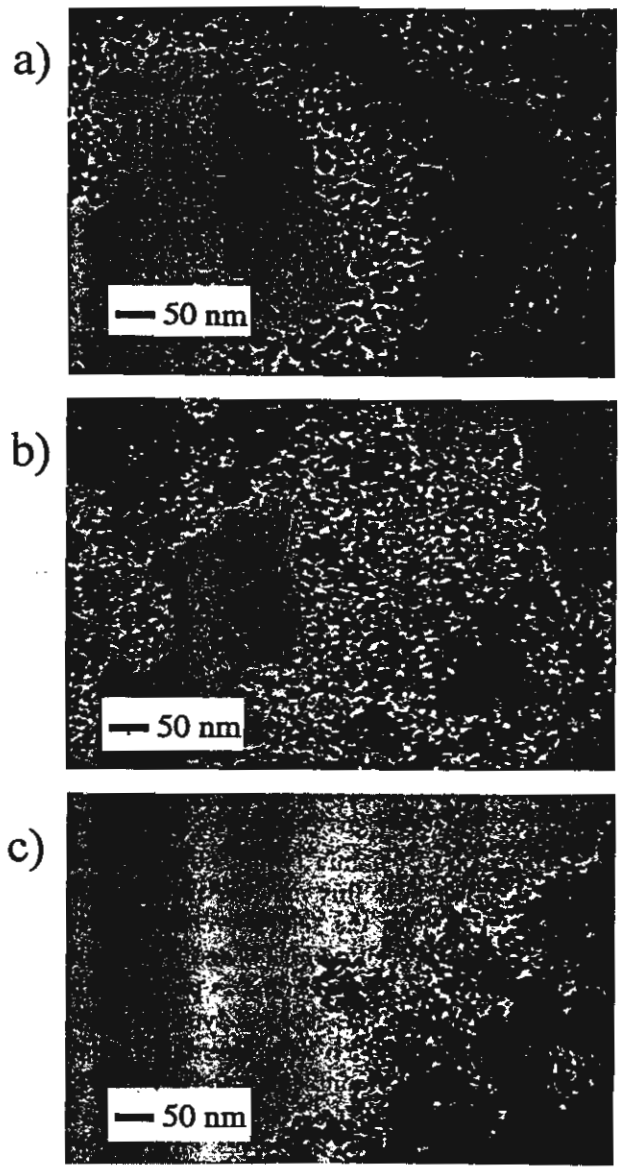

Figure 2 TEM images of products synthesized by the glycothermal reaction of titanium tetraisopropoxide and tetraethyl orthosilicate with the charged ratio of: a) Si/Ti = 0, b) Si/Ti = 0.01, c) Si/Ti = 0.10.

The effect of the reaction temperature was examined by fixing the Si/Ti ratio at 0.10. The reaction at 230–250 °C also afforded products having the anatase structure. The products had larger surface areas as well as smaller crystallite sizes than the product obtained by the 300 °C reaction. When these products were calcined, however, surface areas decreased drastically as compared with the 300 °C product. When the reaction was carried out at 200 °C, a transparent viscous solution was obtained without formation of any solid product. On addition of drops of water into the solution, white precipitates immediately formed. Therefore, this solution contained titanium and silicon in the form of alkoxides or more probably glycoxides.

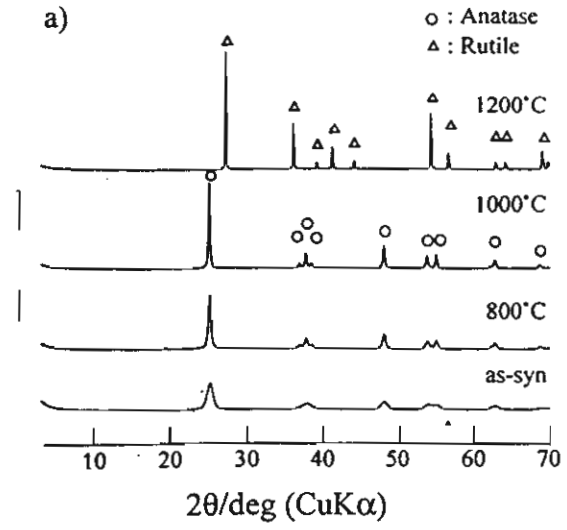

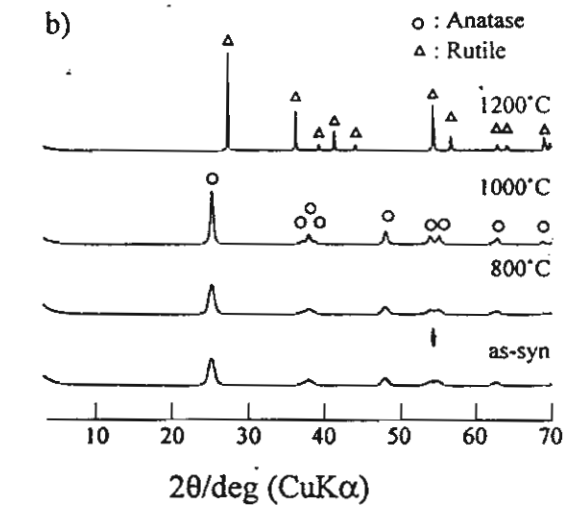

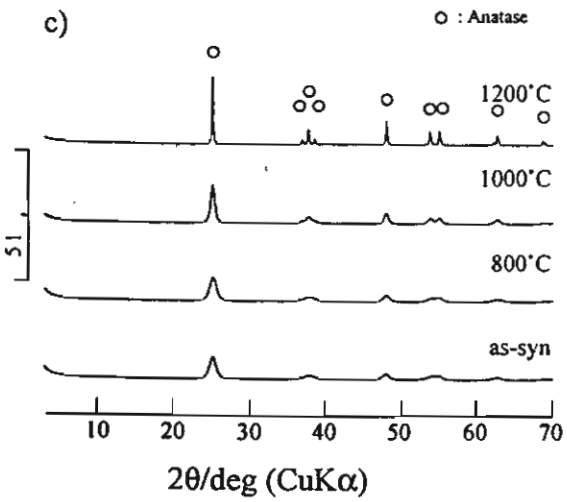

3 XRD patterns of the products by the reaction of titanium isopropoxide and tetraethyl orthosilicate with the charged ratio of: i/Ti = 0.02; b) Si/Ti = 0.10; c) Si/Ti = 0.20; in 1,4-butanediol at and the samples obtained by calcination thereof at the temperaecified in the figure.

; 4 shows the relation between surface area and stallite size of all the samples prepared in this work. surface area was inversely proportional to the allite size. Because the datum for the titania sample

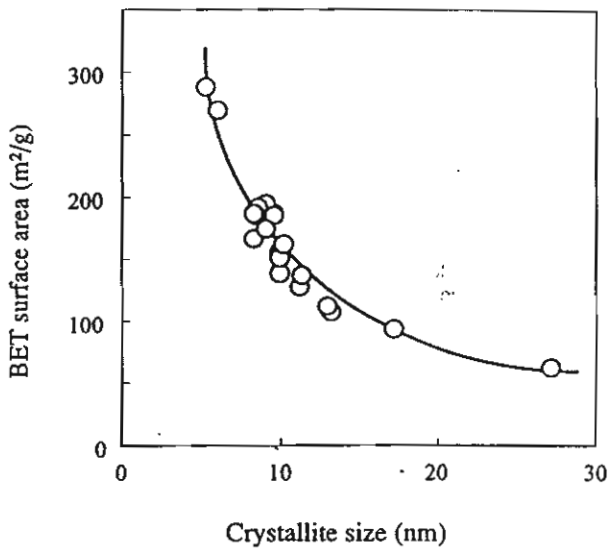

Figure 4 Relation between surface area and crystallite size of the samples obtained by the glycothermal method.

prepared without the addition of TEOS is also included in the plot, the relation indicates that all the crystallites of the products are well dispersed.

The XRD patterns of the products after calcination are shown in Fig. 3. A small amount of TEOS added to the reaction mixture caused the anatase-rutile phase transformation to shift markedly toward higher temperatures, and the samples with the silica content higher than 0.20 preserved the anatase structure even after calcination at 1200 °C for 30 min. Changes in BET surface area and crystallite size by calcination are also shown in Table I. Apparently, the grain growth of anatase was retarded with increasing the amount of TEOS added. Even after calcination at 1000 °C, the products with the Si/Ti >0.20 maintained BET surface areas of >70 m^2/g and crystallite size of <20 nm. To the best of our knowledge, the present product maintained the highest surface area at higher temperatures of the titania-based materials reported so far.

Thermal analysis of the product obtained without the TEOS addition showed 1.5% weight loss from 200 to 600 °C which is associated with an exothermic peak in DTA. This peak is attributed to the combustion of the organic species on the surface of the product. The TG-DTA profiles of the products with the Si/Ti ratio of 0.01–0.06 were similar to that of the product obtained without the TEOS addition. However, this exothermic peak was not observed for the products with Si/Ti of >0.10. This result indicates the decrease of the amount of the surface organic species and suggests the change of surface property. The XPS analysis revealed that the surface compositions of the samples calcined at 600 °C were rich in Si as compared with the charged Si/Ti ratios. With increasing the calcination temperature, the surface composition became more Si-rich. This indicates that Si ions in the products migrate towards the surface of the particles by calcination at high temperatures.

Fig. 5 shows NH_3-TPD profiles of the products. With the increase of Si content, the total amount of adsorbed ammonia increased, but acid-site population based on

TABLE I BET surface area and crystallite size of product synthesized by the glycothermal method and the sample calcined at various temperatures

Charged Si/Ti ratio	Reaction temperature (°C)	S_{BET}[a] (m^2/g)				d_{101}[b] (nm)			
		300 °C	600 °C	800 °C	1000 °C	300 °C	600 °C	800 °C	1000 °C
0	300	91.5	62.1	12.3	2.3	17	22	95	320
0.01	300	138	102	44.6	13.8	10	13	37	120
0.02	300	154	128		16.8	10	11	28	85
0.04	300	150	145	96.0	29.5	10	10	16	48
0.06	300	174	169	112	36.4	9.1	9.1	12	37
0.10	300	161	157	124	49.5	10		11	26
0.15	300	186		111	54.5	9.7		10	21
0.20	300	194	189	168	71.9	9.1		9.2	17
0.30	300	191	185	168	83.8	8.7		8.8	14
0.50	300	166	168	151	79.3	8.4		8.6	16
0.10	270	185			39.0	9.6		11	33
0.10	250	288	240	117	34.4	5.4		10	33
0.10	230	268	200	95.9	14.7	6.1		11	44
0.10	200	—				—			

[a]BET surface area.
[b]Crystallite size of anatase calculated from the 101 diffraction peak.

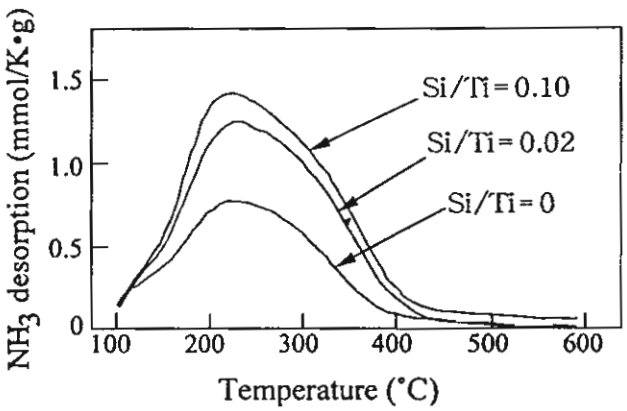

Figure 5 NH_3-TPD profiles of the silica-modified titanias synthesized by the glycothermal method.

a unit surface area rather decreased. Silica modification did not alter the acid strength. These results show a sharp contrast against the acid properties of amorphous TiO_2-SiO_2. Tanabe *et al.* reported that amorphous TiO_2-SiO_2 samples prepared by a coprecipitation method had higher acid strength and much larger number of acid sites than TiO_2. Therefore, the results of Figure 5 suggest the absence of amorphous TiO_2-SiO_2 layer in the present sample. TEM images (Fig. 2b, c) of the silica-modified titania samples as well did not show any indication of the amorphous phase. The presence of Si in the titania lattice seems to contribute to the deceleration of the grain growth of anatase and the suppression of anatase-rutile transformation. Further experiments are in progress to elucidate the mechanism of the surface stabilization of titania by the silica modification.

In conclusion, silica-modified titanias with various silica contents were directly synthesized by the reaction of TIP and TEOS in 1,4-butanediol. The products possessed significantly large surface areas with small crystallite sizes, and exhibited remarkable thermal stabilities.

Acknowledgment

This work was funded in part by The Thailand Research Fund.

References

1. H. BOSCH and F. JANSSEN, *Catal. Today* **2** (1988) 369.
2. I. E. WACHS, R. Y. SALEH, S. S. CHAN and C. CHERSICH, *Chemtech* (1985) 756.
3. M. R. HOFFMANN, S. T. MARTIN, W. CHOI and D. W. BAHNEMANN, *Chem. Rev.* **95** (1995) 69.
4. M. ZAHARESCU and M. CRISAN, *J. Sol-Gel Sci. Technol.* **8** (1997) 249.
5. G. DAGAN and M. TOMKIEWICZ, *J. Non-Crystl. Solids* **175** (1994) 294.
6. I. A. MONTOYA, T. VIVEROS, J. M. DOMÍNGUEZ, L. A. CANALES and I. SCHIFTER, *Catal. Lett.* **15** (1992) 207.
7. A. HESS and E. KEMNITZ, *Appl. Catal. A: General* **149** (1997) 373.
8. X. DING, L. LIU, X. MA, Z. QI and Y. HE, *J. Mater. Sci. Lett.* **13** (1994) 462.
9. K. P. KUMAR, *Appl. Catal. A: General* **119** (1994) 163.
10. B. M. REDDY, S. MEHDI and E. P. REDDY, *Catal. Lett.* **20** (1993) 317.
11. J. E. SWAIN, M. V. JUSKELIS, J. P. SLANGA, J. G. MILLER, M. UBEROI and N. D. SPENCER, *Appl. Catal. A: General* **139** (1996) 175.
12. R. GOPALAN and Y. S. LIN, *Ind. Eng. Chem. Res.* **34** (1995) 1189.
13. C. A. LEDUC, J. M. CAMPBELL and J. A. ROSSIN, *ibid.* **35** (1996) 2473.
14. G. OLIVERI, G. RAMIS, G. BUSCA and V. S. ESCRIBANO, *J. Mater. Chem.* **3** (1993) 1239.
15. M. K. AKHTAR and S. E. PRATSINIS, *J. Am. Ceram. Soc.* **75** (1992) 3408.
16. A. KUROSAKI and S. OKAZAKI, *Nippon Kagaku Kaishi* (1976) 1821.
17. M. INOUE, H. TANINO, Y. KONDO and T. INUI, *J. Am. Ceram. Soc.* **72** (1989) 352.
18. M. INOUE, H. OTSU, H. KOMINAMI and T. INUI, *J. Mater. Sci. Lett.* **11** (1992) 269.
19. M. INOUE, T. NAKAMURA, H. OTSU, H. KOMINAMI and T. INUI, *Nippon Kagaku Kaishi* (1993) 612.
20. M. INOUE, H. OTSU, H. KOMINAMI and T. INUI, *J. Alloys Comp.* **226** (1995) 146.
21. M. INOUE, T. NISHIKAWA, T. NAKAMURA and T. INUI, *J. Am. Ceram. Soc.* **80** (1997) 2157.

22. M. INOUE, H. KOMIMAMI, H. OTSU and T. INUI, *Nippon Kagaku Kaishi* (1991) 1364.
23. H. KOMINAMI, Y. TAKADA, H. YAMAGIWA, Y. KERA, M. INOUE and T. INUI, *J. Mater. Sci. Lett.* 15 (1996) 197.
24. H. KOMINAMI, J. KATO, Y. TAKADA, Y. DOUSHI, B. OHTANI, S. NISHIMOTO, M. INOUE, T. INUI and Y. KERA, *Catal. Lett.* 46 (1997) 235.
25. M. YOSHINAKA, K. HIROTA and O. YAMAGUCHI, *J. Am. Ceram. Soc.* 80 (1997) 2749.
26. P. ARNAL, R. J. P. CORRIU, D. LECLERCQ, P. H. MUTIN and A. VIOUX, *J. Mater. Chem.* 6 (1996) 1925.
27. M. ITOH, H. HATTORI and K. TANABE, *J. Catal.* 35 (1974) 225.

Received 13 October 1999
and accepted 26 January 2000

Selective Oxidation of Ethanol and 1-Propanol over V-Mg-O/TiO_2 catalyst

Tharathon Mongkhonsi*, Purida Pimanmas, and Piyasan Praserthdam
Department of Chemical Engineering, Faculty of Engineering, Chulalongkorn University, Bangkok 10330 THAILAND.

Ethanol and 1-propanol can be selectively oxidized to ethanal and propanal, respectively, by V-Mg-O catalyst supported on TiO_2 (anatase). Aldehyde yields up to 73% and 66% for ethanal and propanal, respectively, were achieved in the temperature range 573-623 K. The catalyst was rather inactive for the further oxidation of aldehyde products to carboxylic acids.

In the last decade, much attention has been devoted to produce olefins and oxygenates by direct oxidation of light paraffins. There are three main motivations behind these researches. The first one is paraffins are less toxic than aromatics. The second one is paraffins are cheaper than olefins. And the last one is the oxidation reaction is thermodynamically more favorable at lower reaction temperature than dehydrogenation reaction which requires high temperature. Only few, however, could achieve industrial application. An example is the replacement of benzene by butane in maleic anhydride production. The future of the oxidative dehydrogenation of paraffins to olefins is still in doubt since a suitable catalyst has yet to be found. The main problem is the fact that paraffin is rather in active than its respective olefin. A catalyst capable to oxidize paraffin is usually very reactive for the olefin product formed.[1]

Using an alcohol as reactant is another alternative. C_1-C_4 alcohols can be produced by fermentation of agricultural products. Although the alcohol obtained from fermetation process has low concentration, the possibility to convert this low concentration feed to a more expansive product exists. In this study the gas phase oxidation process is selected since this process operates at low reactant concentration to avoid explosive mixture.

V-Mg-O catalyst system has found some limited success in the oxidative dehydrogenation reaction.[2-6] To the best of our knowledge, there is no published information about supported V-Mg-O catalyst. V_2O_5 has been known to have strong interaction with MgO and TiO_2(anatase). Therefore, in our research we experimentally supported V-Mg-O on TiO_2 (anatase) and applied this new catalyst system to the gas phase oxidation of alcohols.

The catalyst studied 9V2MgTi (8.7 wt% V_2O_5, 2 wt% Mg, surface area, BET method, 9.27 m^2g^{-1}) was prepared by wet impregnation method. TiO_2 was added to an aqueous solution of NH_4VO_3 and dried at 353 K until achieving a thick paste. The obtained paste was calcined in air at 823 K for 6 hours to convert the paste into V_2O_5/TiO_2. Then, Mg was introduced into V_2O_5/TiO_2 by impregnation from $Mg(NO_3)_2$ solution. The suspension was dried and calcined again at the conditions mentioned above. The XRD pattern of the obtained V-Mg-O catalyst showed only the peaks of TiO_2(anatase).

The catalytic performance test was performed in a quartz fixed-bed reactor (6 mm ID) packed with 0.3 gram of catalyst

(100-150 mesh). Alcohols (ethanol and 1-propanol) were fed via a saturator. Pure dry air was used as oxygen source and nitrogen was used as balancing gas. The feed contained 8 vol% alcohol and 5 vol% oxygen, total flow rate 100 ml min^{-1}. The reaction was studied in the temperature range 473-773 K. Combustion products (CO, CO_2, and H_2O) were analyzed using a gas chromatograph Shimadzu GC 8A equipped with a TCD and a MS-5A Porapak-Q column. Hydrocarbons were analyzed using a gas chromatograph Shimadzu GC 14A equipped with a FID and a VZ-10 column. Oxygenate compounds were analyzed using a gas chromatograph Shimadzu GC 14B equipped with a FID and a capillary column. Total carbon balance in product stream was with in the range 100±5% The selectivity towards products was calculated from the following expression:

$$\%S = \frac{\text{mole product formed}}{\text{mole alcohol converted}} \times \frac{\text{no of C atom of product}}{\text{no of C atom of alcohol}} \times 100$$

The result obtained from ethanol oxidation is shown in Figure 1. Between 473-623 K, ethanol conversion rapidly increased up to a maximum about 86% while selectivity to ethanal was still higher than 80%. The other observed products were mainly CO_2, with traces of CH_4, C_2H_4, and C_3H_6. No CO appeared in the product stream. The maximum ethanal yield, 73%, occurred at 623 K. Beyond 623 K, both ethanol conversion and ethanal selectivity slightly decreased.

1-Propanol conversion and product selectivities are shown in Figure 2. The conversion of 1-propanol increased rapidly between 473-573 K, reaching a maximum conversion about 85%. Beyond 573 K, the conversion was quite constant. The main products observed were propanal and CO_2. Methanal, CH_4, C_2H_4, and C_3H_6 also appeared in the product stream. No CO was detected in the product stream. The maximum propanal yield (about 66%) was achieved at 573 K.

The mass balance of O_2 showed that O_2 was nearly completely consumed at 623 K for ethanol and 573 K for 1-propanol. This is the reason why beyond these temperatures, ethanol and 1-propanol conversions were quite constant. For ethanol oxidation, the slight decrease of ethanol conversion when the reaction temperature was higher than 623 K was the result of the competitive reaction between ethanol/ethanal with O_2. At high temperature, part of oxygen reacted with ethanal rather than ethanol. This reaction caused the decrease in ethanal selectivity as well as ethanol conversion.

It is known that on MgO support, vanadium ion can form bridging oxygen structure, V-O-V, apart from V=O species. This V-O-V species plays role as selective oxidation site. For the oxidation of ethanol, the reaction mechanism shown in Figure 3 is purposed.

The mechanism shown in figure 3 was based on the studies on the selective oxidation and combustion of light hydrocarbons at metal oxide surfaces.[7,8] Ethanol is adsorbed on V-O-V sites to

produce an adsorbed alkoxide species (step 1). H-atom of the alcohol hydroxyl group is eliminated in the form of hydroxyl group by an O anion on the catalyst surface. The surface hydroxyl group further subtracts a H atom of the C atom attaches to the O atom to form water and ethanal (step 2). Desorption of water causes a vacant oxygen site, V-□-V, on the catalyst surface. Finally, the V-□-V site is reoxidized by an oxygen molecule from the gas phase to form V-O-V again (step 3). 1-Propanol is believed to react in the same way as ethanol.

This work was supported by Thai Research Fund (TRF).

References

1. F. Cavani, F. Trifiró, *Catal. Today*, **36**, 431 (1997).
2. M.A. Charr, D. Patel, M.C. Kung, and H.H. Kung, *J. Catal.*, **105**, 483 (1987).
3. M.A. Charr, D. Patel, and H.H. Kung, *J. Catal.*, **109**, 463 (1988).
4. O.S. Owen, M.C. Kung, and H.H. Kung, *Catal. Lett.*, **12**, 45 (1992).
5. X. Gao, P. Ruiz, Q. xin, X. Guo, and B. Delmon, *Catal. Lett.*, **23**, 321 (1994).
6. F. Cavani, F. Trifiró, *Catal. Today*, **24**, 307 (1995).
7. M.M. Bettahar, G. Costentin, L. Savary, and J.C. Lavalley, *Appl. Catal. A*, **145**, 1 (1996).
8. E. Finocchio, R.J. Willey, G. Busca, and V. Lorenzelli, *J. Chem. Soc. Faraday Trans.*, **93**, 175 (1997).

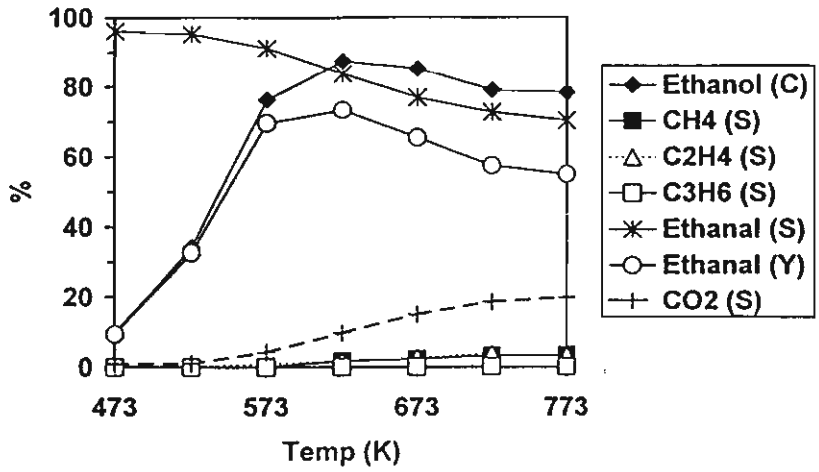

Figure 1 Ethanol oxidation : C - conversion, S - selectivity, Y - Yield

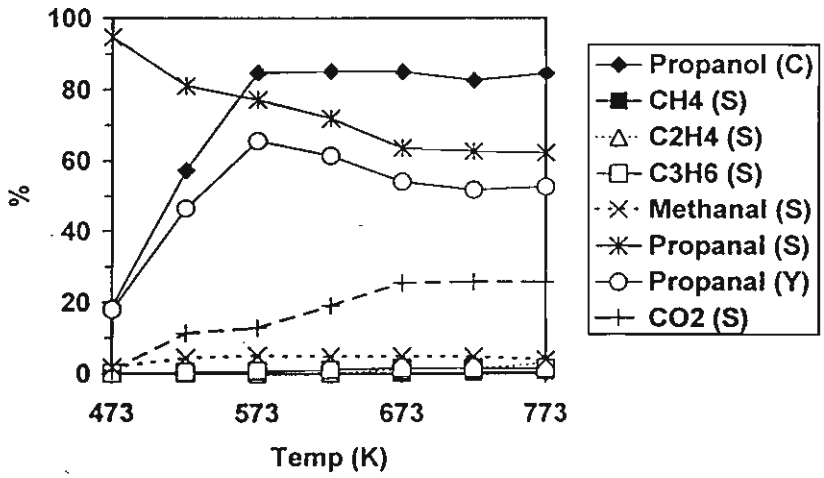

Figure 2 1-Propanol oxidation : C - conversion, S - selectivity, Y - Yield

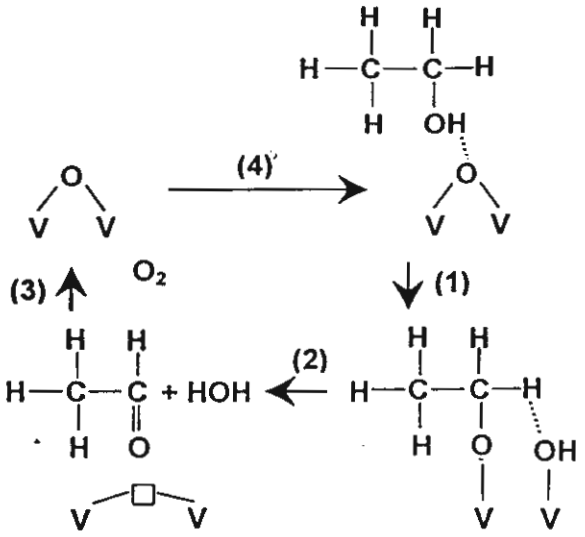

Figure 3 Proposed scheme for ethanol oxidation to ethanal

Inbox

From: gseo <gseo@chonnam.chonnam.ac.kr> Save Address - Block Sender
To: sunee srihiranpullop <sunee11@hotmail.com> Save Address
Subject: Acceptance
Date: Fri, 07 Jul 2000 14:04:14 +0900

Ms Sunee Srihiranpullop
Petrochemical Laboratory
Department of Chemical Engineering
Chulalongkorn University,Bangkok 10330
Thailand
Fax: (662)-218-6769

July 7, 2000

RE:" Deactivation of The Metal and Acidic Functions for Pt, Pt-Sn and Pt-Sn-K using Physically Mixed Catalysts" (ARTICLE NO: 00-05CCE)

Dear Ms Srihiranpullop,

I am pleased to inform the acceptance of your paper to the Korean Journal of Chemical Engineering. I sent your paper to the Office. Your will receive a formal acceptance letter from Chief-of-Editor. I appreciate your contribution.

Sincerely yours,

Gon Seo
Editor of The Korean Journal of Chemical Engineering
Chonnam National University
300, Yongbong-dong, Buk-gu
Kwangju 500-757
Korea

DEACTIVATION OF THE METAL AND ACIDIC FUNCTIONS FOR Pt, Pt-Sn AND Pt-Sn-K USING PHYSICALLY MIXED CATALYSTS

Sunee Srihiranpullop*, Piyasan Praserthdam and Tharathon Mongkhonsi

Department of Chemical Engineering, Chulalongkorn University, 10330 Thailand

Abstract- The effect of K addition on the amount and dispersion of carbon deposition on the metal sites and the support sites was investigated on a physical mixture for hexane dehydrogenation. TPO, BET and ESR experiments were used for characterization. The K addition significantly decreases catalyst deactivation involving the amount of coke deposits and the density of carbon radicals on the metal and support sites because of the ensemble and electronic effects, especially on the metal sites. Coke on the metal sites associated with carbonaceous species rich in hydrogen is less polymerized than coke on the support sites corresponded to a more graphitic-like carbon.

Running title: Deactivation of the Physically Mixed Catalysts

Keywords: deactivation, Pt-based catalyst, Pt-based catalyst modified with Sn and/or K, physically mixed catalyst

***To whom correspondence should be addressed**

TEL: +662-218-6710

FAX: +662-218-6769

E-mail: sunee11@hotmail.com

INTRODUCTION

Catalytic processing of many industrial feedstocks is frequently accompanied by the deposition of carbonaceous deposits. For metal catalysts, the supported mono- and multi-metal Pt containing catalysts are widely used for dehydrogenation in the petroleum and other industries. The addition of the modifiers such as K and/or Sn into Pt-containing catalysts may change the selectivity of catalysts and can increase the resistance of carbon deposition [1-3]. It has been reported that coking on the catalyst surface is a dynamic process [4-7]. Carbon deposition takes place on both the active metal sites and the support surface for supported metal catalysts. Numerous species of carbon are observed to be deposited or formed on the surface of coked catalysts, ranging from carbides or microcrystalline and amorphous species to highly aromatic/ graphitic carbons apparently through polymerization reaction and rearrangement for the polymer formed to be stabilized [3,5,8]. Additionally, analysis by temperature programmed oxidation (TPO) generally indicates two types of coke; the first one burns at low temperatures (polymeric carbon), which is associated with the metal phase and the second type burns at high temperatures (amorphous/graphitized carbon), associated with the support [9,10]. Although catalyst deactivation has been studied for many years, coke growth completely separated between coke on the metal and coke on the support sites has not been investigated sufficiently so far. In order to shed some light on this matter, the physically mixed Pt/SiO_2 and Al_2O_3 was used in this work as a representative catalyst of Pt/Al_2O_3. Since the SiO_2 support in Pt/SiO_2 has a very low acidity, its contribution to the acidic function is, therefore, negligible. The mesh sizes of Al_2O_3 and SiO_2 selected for the physically mixed catalyst are based on ones that give approximately

the conversion of hexane similar to that obtained from the conventional Pt/Al_2O_3 catalyst [7,11,12]. With this simulated catalyst associated with the presence of K and /or Sn, much debate about how the additive metal brings about the enhancement in catalytic properties should be better conceived.

Thus, this work involved a detailed study of coke deposition on Pt, Pt-Sn and Pt-Sn-K catalysts employed in a physically mixed system where silica-supported platinum, Pt/SiO_2, represents the metal sites and acidic alumina, Al_2O_3, represents the support sites. The dehydrogenation of n-hexane was adopted to cause coked catalysts with the carefully selected reaction conditions so that the thermal cracking effect may be negligible. The main goal was to determine the effect of K and/or Sn on coke distribution over the metal sites and support sites in order to better understand the deactivation process of the catalysts.

EXPERIMENTAL

Catalyst preparation

The alumina used in this study was obtained from Sumitomo Alumina Smelting (type NKH-3) and the silica was manufactured by Merck. They were ground and then sieved to retain particles with sizes between 60-80 mesh and 100-120 mesh, respectively. Three types of catalyst, namely, 0.3wt% Pt/SiO_2, 0.3wt%Pt-0.3wt%Sn/SiO_2 and 0.3wt%Pt-0.3wt%Sn-0.6wt%K/SiO_2 were employed in this work. The catalysts were prepared by impregnation method using H_2PtCl_6, $SnCl_2$ and KNO_3 as salt precursors. All chemicals used were normally analytical grade. After drying at 110°C overnight, the catalysts were calcined in an air flow at 500°C for 3 h.

RESULTS AND DISCUSSION

Carbon deposition on the metal sites and the acidic sites of the Pt, Pt-Sn and Pt-Sn-K catalysts

Carbon depositions on Pt-based catalysts were investigated by temperature programmed oxidation (TPO). On the active metal sites of various catalysts, Fig. 1A shows TPO profiles of Pt, Pt-Sn and Pt-Sn-K catalysts, respectively. It is observed that two peaks appear at 300°C and 425°C in every TPO profile. This indicates that carbon depositions on these catalysts can be divided into two types: (i) coke deposited directly on metal and (ii) coke in the vicinity of metal centers, which correspond to the report somewhere else [4,13]. In addition, it is obvious that coke is depositing on different sites on the different catalysts and affecting deactivation to deferring extents. From Fig. 1A, the difference of the modified catalysts is that, for Pt and Pt-Sn catalysts, the area of the first peak at lower temperature is less than that of the second peak at higher temperature. For the Pt-Sn-K catalyst, the situation is just opposite. Interestingly, the peak of the K-doped catalyst decreased more than any other catalysts, especially in the position at 425°C. In previous studies [4-10], it was speculated that the active metal site was linked with the originally generated coke precursors. Consequently, K addition dramatically inhibits the production of coke intermediates resulting in the lower area of carbonaceous compounds. It is seen that the order of their TPO areas is as follows: Pt > Pt-Sn > Pt-Sn-K. Furthermore, the total carbon accumulate on the metal sites of different catalysts listed in Table 1 was determined from the areas under the TPO profiles. The order of decreasing amount of carbon per gram is Pt > Pt-Sn > Pt-Sn-K. It has been found that the areas of the TPO peaks increase with the amount of carbon deposition for the Pt-based catalysts.

On the other hand, Fig. 1B exhibits spectra of TPO on the acidic sites of Pt, Pt-Sn and Pt-Sn-K catalysts. It is observed that a single peak appears on the spectra of TPO for the modified catalysts. Coke burns off at higher temperature, about 525°C, compared with coke on the metal sites. This implies that the peak shifts to a higher temperature because of a larger degree of polymerization of coke [14]. Moreover, the TPO area of the Pt catalyst is diminished by the addition of Sn and especially in combination with K. As presented above, it is relevant to note that the surface coverage has different compositions, which is summarized in Table 1. The amount of coke on both the metal sites and support sites decreased significantly by the addition of Sn and/or K.

As mentioned above, carbonaceous materials deposit either on the active metal sites or on the acidic alumina support surface. The migration of coke precursor from one type of sites to another may possibly occur. Hence, a model of coking is proposed in Fig. 2. Hydrocarbons first undergoes dehydrogenation and cracking on the active metal surface to form precursors of coke deposits. In general, unsaturated reaction intermediates such as monocyclic diolefins are formed and then reversibly adsorbed to form coke on the metal and in its direct vicinity. However, they can migrate to acid sites and become polymerized to the more graphite-like material. Additionally, when comparing the amount of coke on the metal sites and the support sites as shown in Table1, it is obvious that a small part of coke is located on the metal sites whereas the major fraction is accumulated on the acidic sites. These results imply that coke deposits on the metal sites is less dehydrogenated and corresponds to species rich in hydrogen in accordance with the literature reviews [15,16]. Accordingly, the H/C ratio of coke deposits on metal sites is higher than that of the coke deposits on acidic support sites. It displays the different nature of coke between

the metal sites and alumina. Finally, the modifications of Pt catalyst by addition of Sn and K are able to reduce the amount of coke on both sites.

Carbon radicals of coke on the metal sites and the acidic sites of the Pt, Pt-Sn and Pt-Sn-K catalysts

In order to examine the effect of Sn and K addition on coke formation with both sites in more detail, Electron Spin Resonance (ESR) has long been an effective technique to estimate the radical density of coke. ESR spectra are obtained by measuring the intensity vs. wavelength (or frequency) of a beam of electromagnetic radiation as it passes through a sample of matter, which is presented in a derivative trace of absorption curve. Then, the radical density can be computed from the integrated area of the spectra obtained [17,18]. Further coke radicals are representative of the overall coke, for both its nature and its amount because the amount of olefin or allylic radicals are characteristic of carbonaceous matter as introduced elsewhere [19-23]. In an earlier study, H.G. Karge *et al.* [19,20] investigated low temperature coke (below about 500 K) and high temperature coke radicals (above about 500 K). They found that olefinic or allylic oligomeric species were low-temperature coke radicals while highly unsaturated species were high-temperature coke radicals. Consequently, the formation of radicals enable us to discriminate between individual coke of various catalysts including coke on the metal sites and the support surface. In this study, Fig. 3A shows the ESR spectra of coke radicals for various catalysts on the metal sites. The carbon radicals density computed form the total peak area is given in Table 2. The g value of coke radicals is estimated to be 2.003 in agreement with earlier literature [22,24]. It is found that the modification of catalysts displays a dominant role in reducing the intensity of

carbonaceous radicals as well as reducing the amount of coke precursors. Interestingly, the K-doped sample has a sharply lower amount of radicals of coke, by 27 times, compared with the Pt catalyst resulting in the lowest amount of coke shown in Table 1. Another modification of the Pt catalyst diminishes carbonaceous radicals about 1.7 times. A comparison between ESR results and TPO results, which are described above, exhibits a good correlation between the number of radicals and the amount of coke.

For the acidic alumina, the ESR spectra of radicals are illustrated in Fig. 3B with the Pt-based catalysts. Table 2 also lists the intensity of them on these sites. This characteristic of carbon radicals is similar to that already reported above. However, the density of coke radicals is greater on the alumina sites than on the active metal sites. It is clear that the amount of radicals compared with the carbonaceous radicals intensity of Pt catalyst is reduced by 1.45 times for Sn modification and 1.65 times for K addition. As mentioned above, it is introduced that the metal sites is relevant to generate coke intermediates, which adsorbed to form coke on this site and can migrate to the acidic support sites. Thus, if the modification of catalysts inhibits the production of coke precursors on the metal sites, then the amount of carbonaceous compounds is consequently decreased. From the result shown in Table 2, it is obvious that the K-doped sample dramatically reduces coke radicals concerned with coke species on the active metal sites. Accordingly, a lower amount of coke deposits is produced as shown by the TPO results.

The changes of textural properties and the dispersion factors of coke on the metal sites and the acidic sites of the Pt, Pt-Sn and Pt-Sn-K catalysts

Coking is claimed to be responsible for a decrease in the specific surface, pore surface and pore volume depending on a limitation of diffusion (dispersion) and nature of coke deposits. As a result, an investigation of texture changes in surface area before and after coke deposition of Pt-based catalysts was carried out. Jovanovic and Putanov [13] introduced the dispersion factor to consider catalyst degradation of Pt/Al_2O_3 and $Pt\text{-}Re/Al_2O_3$. The dispersion factor is the ratio of change of surface area to the quantity of carbon deposits. Higher values of dispersion factor proved that carbon deposited on this catalyst is better dispersed with the fine small grain structure. In this work, the dispersion factor of carbonaceous deposit defined as the ratio of change of surface area to the amount of coke was investigated on Pt, Pt-Sn and Pt-Sn-K catalysts. Table 3 summarizes the textural properties of catalyst samples before and after coking and the dispersion factor, which is separated into the metal sites and the acidic alumina in each catalyst. The change of surface area may be attributed to the blockage of catalysts by coke, though thermal sintering and the other factor except coking should not be ruled out. It has been found that the modified catalyst lost their surface area after the reaction more than the unmodified one containing only platinum. This might be due to the fine structure of coke readily occurred in case of Pt catalysts with the presence of Sn and/or K, which easily block the existing porous area of the catalyst. The obtained results were consistent with the report of fine small grain structure of coke deposits for the modification catalysts suggested in literature reviews [21,25,26]. Moreover, noticeably higher values of dispersion factors are obtained from the Pt-Sn and particularly Pt-Sn-K catalysts as illustrated in Table 3. Comparing with the Pt catalyst, the dispersion factor of the Pt-Sn catalyst is about 1.7

times on the metal sites and about 1.8 times on the acidic sites. In the case of K addition, dispersion factors on the metal sites and on the support sites are about 2.4 times and 4.5 times compared with Pt catalyst, respectively.

The influence of Sn and K addition on coke formation

The main theories put forward to account for the improved properties of multi-metallic catalysts tend to involve either geometric or electronic effects. Coke formation is known to require relatively large clusters or ensembles of adjacent metal atoms. For the Sn addition, the presence of Sn improves the diluting of the active metal surface into smaller ensembles, which enhance the catalysts' resistance to deactivation. The addition of Sn to Pt catalyst forms substitutional surface alloys and it has been shown that Sn interacts with platinum on silica to form a Pt/Sn alloy [1,2,3,27,28]. Thus, carbon intermediates cannot readily form multiple carbon-metal bonds. Furthermore, it inhibits the formation of highly dehydrogenated surface species that are intermediates for coking. According to Padro *et al.* and Larsson *et al.* [14,29], one reason is that coke deposits bind more strongly to the Pt catalyst than to the Pt-Sn catalyst.

From TPO profiles and ESR spectra of the metal sites, that the adsorbed species are attached less strongly to the metal surface would be explained by the significant minimizing of these sites and promotion of the migration of coke precursors to the carrier. These effects are evident by the change in the heights of peaks in the TPO profiles and ESR spectra.

The addition of K into bimetallic Pt-Sn catalyst produces a significant decrease in the catalyst deactivation as shown in Fig. 4 illustrating the conversion of hexane as a function of time. The decline in conversion is slower for catalysts

containing tin and potassium than for catalysts containing platinum only due to less amount of coke was formed on the modified catalysts. In Fig. 4 and Table 1, it is obvious that Pt catalyst deactivates quickly and a considerable amount of coke was formed. It may be related to the incorporation of tin into the surface of platinum through the formation of a substituted alloy, while potassium may be present on top of the platinum surface. As described elsewhere [14,27], it was found that K- doped catalyst significantly decreases the activation energy of CH dehydrogenation which would suggest that K effect diminishes the interaction between Pt and Sn. This modification in the interaction between both metal components could be due either to a direct addition of K on the metal phase or to an indirect effect of the alkali metal addition to support, which could change the metal-support and the metal-metal interactions, as suggested in the literature [27,29,30]. This results in a weakening of Pt-C bond strength to make the catalyst less susceptible to deactivation by deposition of carbonaceous species on both sites as illustrated in Fig. 1, Table 1, Fig. 3 and Table 2. This is known as an electronic effect [1,2,3,30].

CONCLUSION

The addition of Sn and K resists coke formation both on the metal sites and on the support sites. It seems due to the ensemble and electronic effects. They also reduce the density of carbon radicals and affect the nature of coke. For textural properties, noticeably higher values of dispersion factor were obtained on Pt-Sn and Pt-Sn-K catalysts than on Pt catalysts. It can indicate that coke on the Pt-Sn and Pt-Sn-K catalysts has a softer coke nature. Specifically, K addition significantly inhibits coking. Comparing coke on the metal sites and on the support sites, it can be

concluded that coke on the metal is soft in nature, rich in hydrogen and has a lower degree of polymerization.

ACKNOWLEDGEMENTS

The authors would like to thank Thailand Research Fund (TRF) and National Science and Technology Development Agency (NSTDA) for financial support of this project.

REFERENCES

[1] Rostrup-Nielsen, J.R., "Industrial relevance of coking", Catal.Today , 37, 225. (1997).

[2] Trimm, D.L., "Catalysts for the control of coking during steam reforming", Catal. Today, 49,3 (1999).

[3] Trimm, D.L., "Catalyst design for reduced coking", Appl. Catal., 5, 263 (1983).

[4] Lietz, G., and Volter, J., "Initial changes of the catalytic properties of platinum containing catalysts: I. Transformations of mono- and bimetallic Pt/Al_2O_3 catalysts by carbonaceous deposits", Appl. Catal., 13, 77 (1984).

[5] Biswas, J., Bickle, G.M., Gray, P.G., Do, D.D., and Barbier, J., "The role of deposited poisons and crystallite surface structure in the activity and selectivity of reforming catalysts", Catal. Rev.-Sci. Eng., 30 (2), 161 (1988).

[6] Liwu, L., Tao, Z., Jingling, Z., and Zhusheng, X., "Dynamic process of carbon deposition on Pt and Pt-Sn catalysts for alkane dehydrogenation", Appl. Catal., 67, 11 (1990).

[7] Bond, G.C., "Heterogeneous Catalysis: Principles and Application", Clarendon

Press: Oxford (1987).

[8] Afonso, J.C., Schmal, M., and Frety, R., "The chemistry of coke deposits formed on a Pt-Sn catalyst during dehydrogenation of n-alkanes to mono-olefins", Fuel Pro. Tech., 41, 13 (1994).

[9] Barbier, J., "Coking of reforming catalysts", Catalyst Deactivation, 1 (1987).

[10] Biswas, J., Gray, P.G., and Do, D.D., "The reformer lineout phenomenon and its fundamental importance to catalyst deactivation" Appl. Catal., 32, 249 (1987).

[11] Shum, V.K., Butt, J.B., and Sachtler, W.M.H., "The dehydrocyclization-controlling site in bifunctional reforming catalysts", Appl. Catal., 11, 151 (1984)

[12] Inaba, M., Kintaichi,Y., and Hamada, H., "Cooperative effect of platinum and alumina for the selective reduction of nitrogen monoxide with propane", Catal. Lett., 36, 223 (1996).

[13] Jovanovic, M.R., and Putanov, P.S., "Nature and distribution of coke formed on mono-metallic platinum and bimetallic platinum-rhenium catalysts", Appl. Catal., 159,1 (1997).

[14] Padro, C.L., de Miguel, S.R., Castro, A.A., and Scelza, O.A., "Stability and regeneration of supported PtSn catalysts for propane dehydrogenation", Catalyst Deactivation, 191 (1997).

[15] Tao, Z., Jingling, Z., and Liwu, L., "Relation between surface structure and carbon deposition on Pt/Al_2O_3 and $Pt\text{-}Sn/Al_2O_3$ catalysts", Catalyst Deactivation, 143 (1991).

[16] Beltramini, J., and Trimm, D.L., "Activity, selectivity and coking over mono-and bi-metallic reforming catalysts", Appl. Catal., 32, 71 (1987).

[17] Werlz, J.E., and Bolton, J.R., " Electron Spin Resonance: Elementary Theory and Practical Applications", Chapman and Hall Ltd.: New York(1972).

[18] Lunsford, J.H., " Electron Spin Resonance in Catalysis", Advances in Catalysis, 22, 265 (1972).

[19] Butt, J.B., and Peterson, E.E., "Activation Deactivation and Poisioning of Catalysts", Academic Press Inc (1988).

[20] Guisnet, M., and Magnoux, P., "Coking and Deactivation of zeolites: Influence of the pore structure", Appl. Catal., 54, 1 (1989).

[21] Lange, J.P., and Gutsze, A., "Coke formation through the reaction of ethene over hydrogen mordenite: III. IR and 13C-NMR studies", Appl. Catal., 45, 345 (1988).

[22] Lange, J.P., Gutsze, A., and Karge, H.G., "Coke formation through the reaction of olefins over hydrogen mordenite: I. EPR measurements under static conditions", J. Catal., 114, 136 (1988).

[23] Lange, J.P., Gutsze, A., and Karge, H.G., "Coke formation through the reaction of olefins over hydrogen mordenite: II. Insitu EPR measurements under on-stream conditions", J. Catal., 114, 144 (1988).

[24] Gutsze, A., Roland, U., and Karge, H.G., "Evidence for a charge transfer from spilt-over hydrogen to platinum by means of ESR spectroscopy", Spillover and Migration of Surface Species on Catalysts, 417 (1997).

[25] Kirszensztejn, P., Foltynowicz, Z., and Wachowski, L., "Peculiar pore structure of the coke coating formed on Pt-Sn/γ-Al_2O_3 catalysts", Ind. Eng. Chem. Res., 30, 2276 (1991).

[26] Mann, R., "Catalyst deactivation by coke deposition: approaches based on interactions of coke laydown with pore structure", Catal. Today , 37, 331 (1997).

[27] Hill, J.M., Cortright, R.D., and Dumesic, J.A., "Silica- and L-zeolite-supported Pt, Pt/Sn and Pt/Sn/K catalysts for isobutane dehydrogenation", Appl. Catal.,

168, 9 (1998).

[28] Macleod, N., Fryer, J.R., Stirling, D., and Webb, G., "Catal. Deactivation of bi- and multimetall reforming catalysts: Influence of alloy formation on catalyst activity", Catal. Today , 46, 37 (1998).

[29] Larsson, M., Hulten, M., Blekkan, E.A., and Andersson, B., "The effect of reaction conditions and time on stream on the coke formed during propane dehydrogenation", J. Catal., 164, 44 (1996).

[30] Cortright, R.D., and Dumesic, J.A., "Effects of potassium on silica-supported Pt and Pt/Sn catalysts for isobutane dehydrogenation", J. Catal., 157, 576 (1995).

Figure 1A. Temperature Programmed Oxidation of carbonaceous deposits produced on the metal sites with different catalysts

Symbols: ● the Pt catalyst, ▲ the Pt-Sn catalyst and ■ the Pt-Sn-K catalyst

Figure 1B. Temperature Programmed Oxidation of carbonaceous deposits produced on the support sites with different catalysts

Symbols: ● the Pt catalyst, ▲ the Pt-Sn catalyst and ■ the Pt-Sn-K catalyst

Figure 2. Coking mechanism on both sites of catalyst.

Figure 3A. ESR spectra of coke on the metal sites ; (a) reference spectrum before coking reaction (b) coke on Pt-Sn-K catalyst (c) coke on Pt-Sn catalyst and (d) coke on Pt catalyst.

Figure 3B. ESR spectra of coke on the support sites; (a) reference spectrum before coking reaction (b) coke on Pt-Sn-K catalyst (c) coke on Pt-Sn catalyst and (d) coke on Pt catalyst.

Figure 4. %conversion of hexane dehydrogenation for physically mixed catalysts;

Symbols: ● the Pt catalyst, ▲ the Pt-Sn catalyst and ■ the Pt-Sn-K catalyst

Table 1. The amount of carbon deposited on the catalysts

Table 2. The density of carbon radicals of coke per gram catalyst

Table 3. The textural properties of catalysts samples before and after testing and factor of SA change

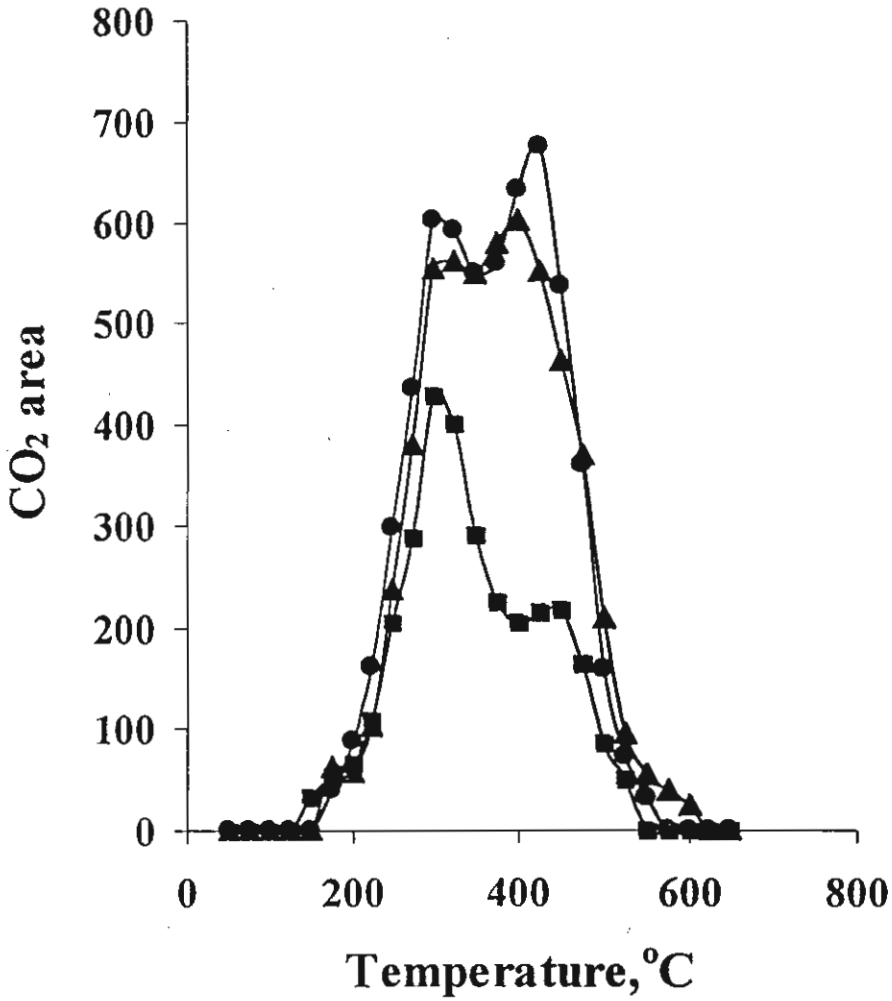

Figure 1A. Temperature Programmed Oxidation of carbonaceous deposits produced on the metal sites with different catalysts

Symbols: ● the Pt catalyst, ▲ the Pt-Sn catalyst and ■ the Pt-Sn-K catalyst.

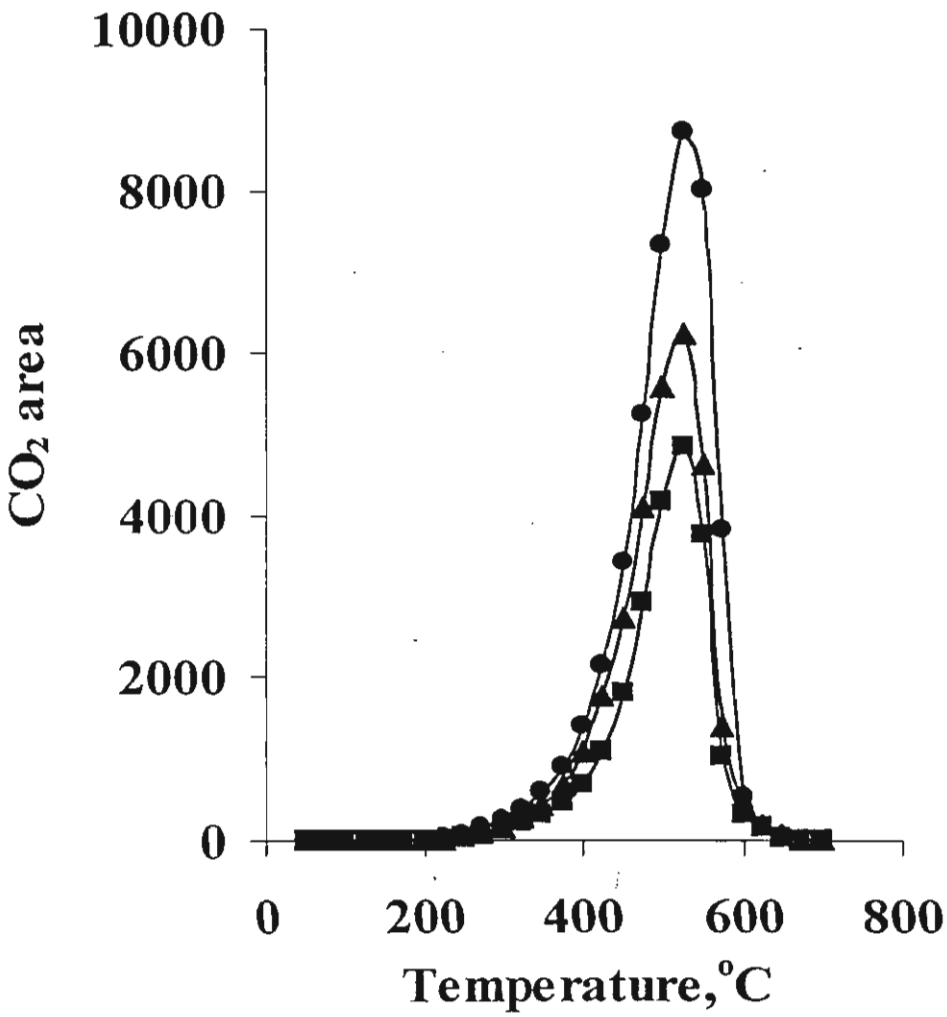

Figure 1B. Temperature Programmed Oxidation of carbonaceous deposits produced on the support sites with different catalysts

Symbols: ● the Pt catalyst, ▲ the Pt-Sn catalyst and ■ the Pt-Sn-K catalyst.

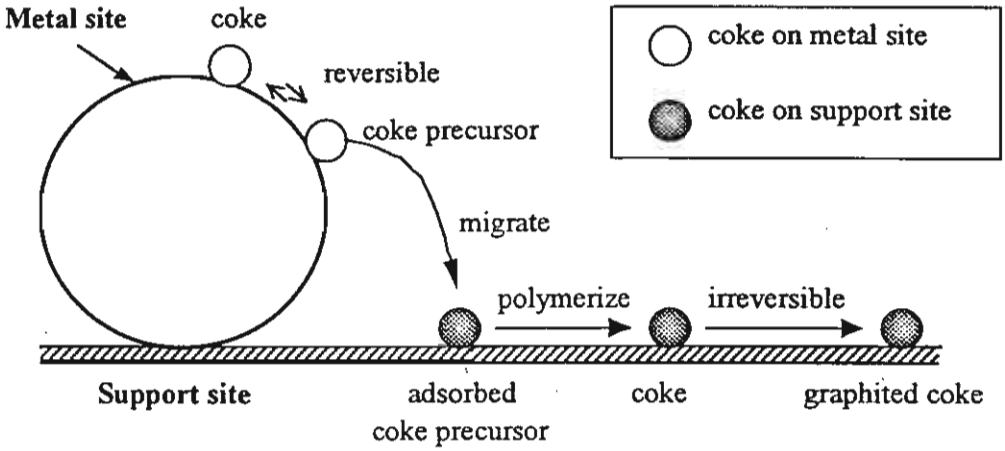

Figure 2. Coking mechanism on both sites of catalyst.

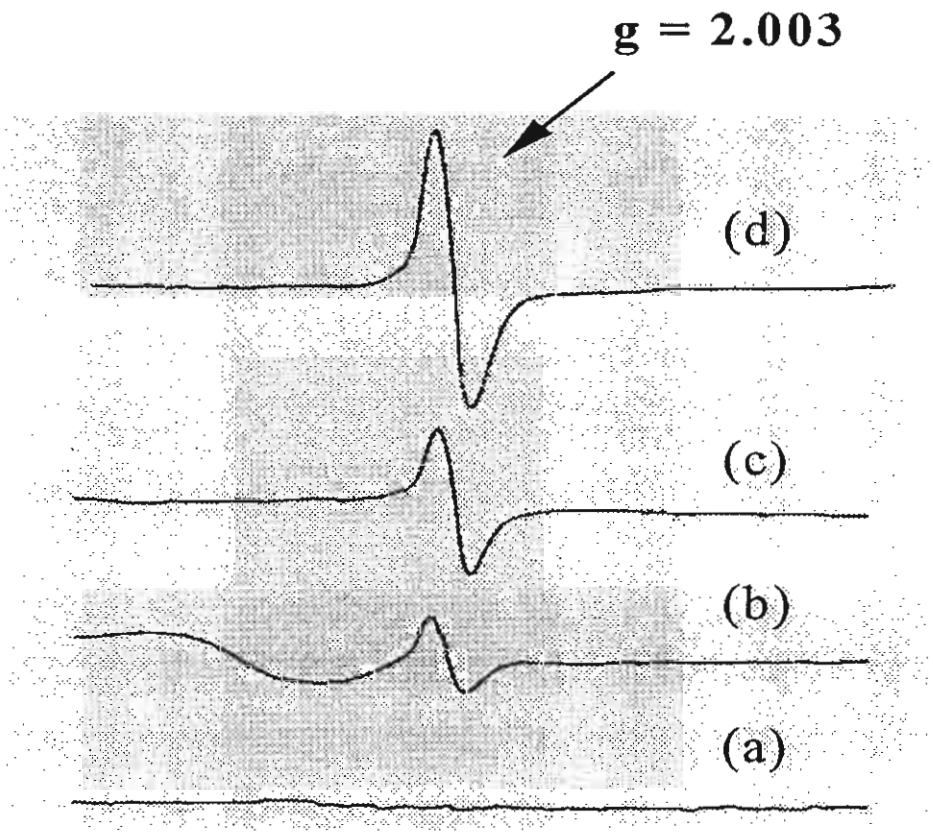

(A)

Figure 3A. ESR spectra of coke on the metal sites ; (a) reference spectrum before coking reaction (b) coke on Pt-Sn-K catalyst (c) coke on Pt-Sn catalyst and (d) coke on Pt catalyst.

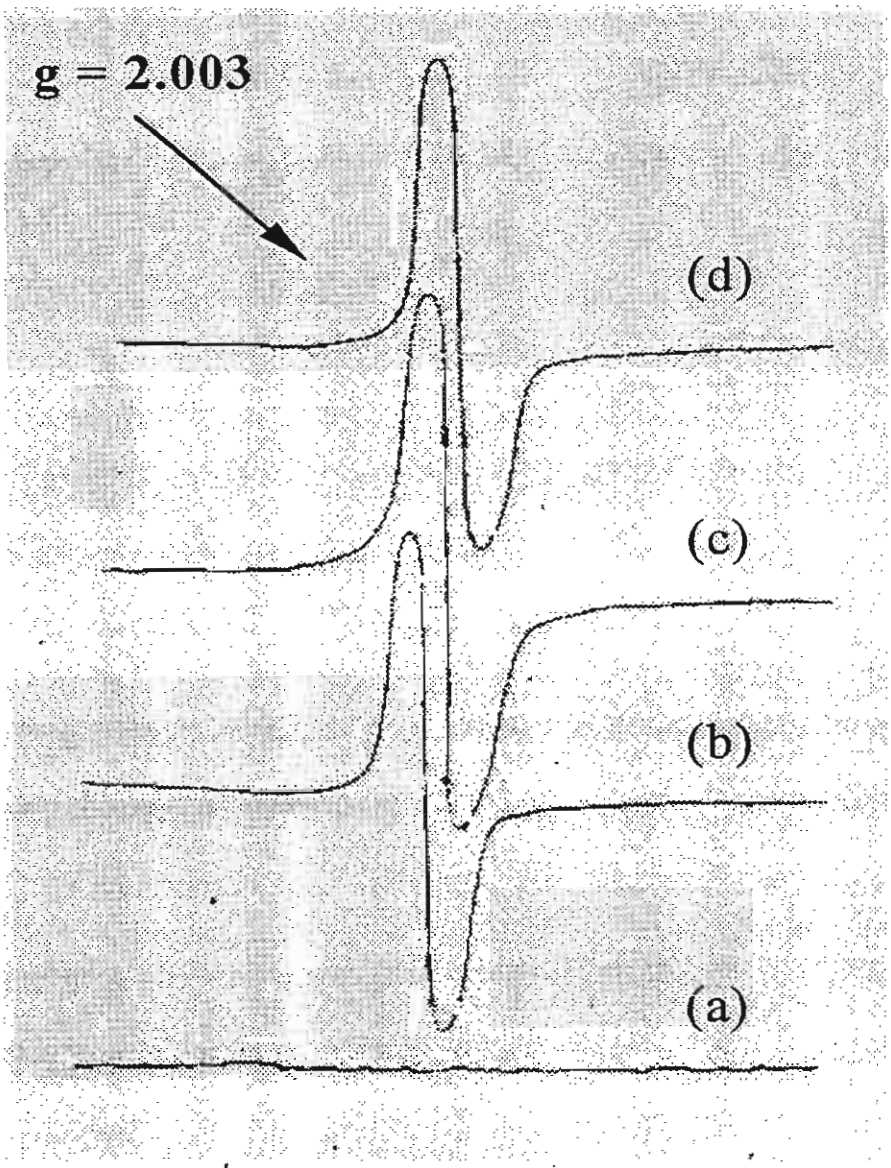

Figure 3B. ESR spectra of coke on the support sites; (a) reference spectrum before coking reaction (b) coke on Pt-Sn-K catalyst (c) coke on Pt-Sn catalyst and (d) coke on Pt catalyst.

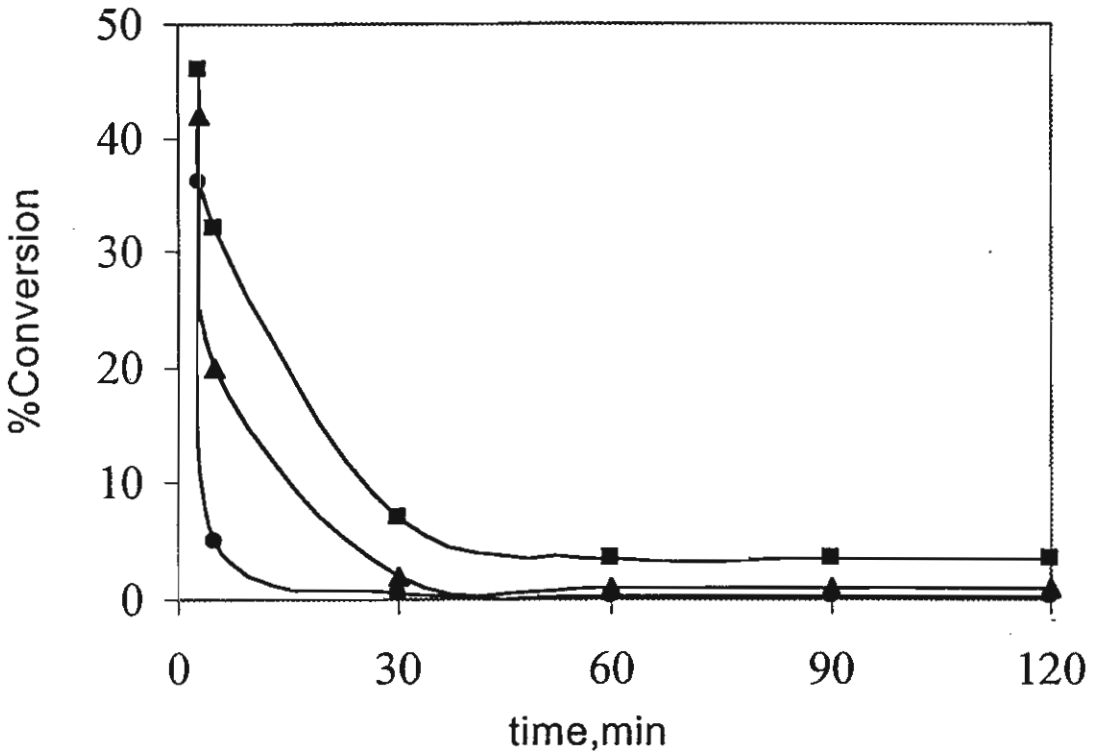

Figure 4 % conversion of hexane dehydrogenation for physically mixed catalysts; Symbols: ● the Pt catalyst, ▲ the Pt-Sn catalyst and ■ the Pt-Sn-K catalyst.

Table 1. The amount of carbon deposited on the catalysts

Catalysts	Coke on the metal sites %C	Coke on the support sites %C
Pt catalyst	0.36	2.50
Pt-Sn catalyst	0.32	1.73
Pt-Sn-K catalyst	0.21	1.26

Table 2. The density of carbon radicals of coke per gram catalyst

catalysts	The metal sites	The support sites
Pt catalyst	8.55×10^5	3.02×10^6
Pt-Sn catalyst	5.18×10^5	2.07×10^6
Pt-Sn-K catalyst	3.17×10^4	1.83×10^6

Table 3. The textural properties of catalysts samples before and after testing and dispersion factor

Catalysts	The metal sites			The support sites		
	SA (m2/g) Fresh	Used	dispersion factor	SA (m2/g) Fresh	Used	dispersion factor
Pt catalyst	447	386	171	390	343	19
Pt-Sn catalyst	417	325	291	390	330	35
Pt-Sn-K catalyst	380	283	462	390	283	85

Activation of Acetylene Selective Hydrogenation Catalysts Using Oxygen Containing Compounds

*Piyasan Praserthdam, Suphot Phatanasri, Jumpod Meksikarin

Petrochemical Engineering Research Laboratory, Department of Chemical Engineering, Chulalongkorn University, Bangkok 10330, Thailand

Abstract

Hydrogenation of acetylene in the presence of a large excess of ethylene has been investigated on the Pd-Ag catalyst at 60°C with a space velocity of 2,000 h^{-1}. It was found that an enhancement in the performance of Pd-Ag catalyst can be obtained by pretreatment with N_2O. It is suggested that a certain amount of N_2O added to the catalyst before use not only augments the sites associated with ethylene production from acetylene but also depletes the sites responsible for direct ethane formation. Upon aging, the pretreated catalyst exhibited good stability.

Keywords: Selective Hydrogenation, acetylene, silver promoted palladium catalyst, N_2O pretreatment

INTRODUCTION

The selective hydrogenation of acetylene over supported palladium catalysts is a process widely used to purify the ethylene produced by steam cracking of hydrocarbons. The ethylene to acetylene ratio in the stream to be treated is generally higher than 70 [1]. Typically the acetylene concentration can be reduced from an initial value in the region of 5,000 to below 5 ppm with hydrogenation of no more than 1% of the ethylene, operating at temperatures in the range of about 60-70°C [2]. At present all such catalysts are based on palladium using alumina as

* Corresponding author. E-mail : Piyasan.p@chula.ac.th

support, and palladium-based catalysts promoted by a second metal are now available [3]. The promoter improves selectivity or stability of the catalyst. A. Sarkany et al. [4] have clearly demonstrated that the addition of copper to palladium causes a significant decrease in the overall rate of ethane formation and at the same time there is a decrease in the catalyst activity as well as a marginal decrease in oligomer selectivity. Recently, it has been discovered that the catalyst comprising elements of group IB and transition metals could be activated with N_2O before use [5]. Thus it is an objective of the study to pretreat the Pd-Ag catalyst before being used for the selective hydrogenation of acetylene.

EXPERIMENTAL

A 0.04 wt% Pd-Ag/γAl_2O_3 (Ag:Pd = 4:1) was prepared via the serial impregnation method. Alumina support was impregnated with palladium first followed by silver. Alumina support was Al_2O_3 (CS-303) supplied by United Catalyst Incorporation (UCI), USA. Palladium nitrate and silver nitrate were used as sources for Pd and Ag, respectively. The calcination temperatures for palladium and silver were 300°C and 370°C, respectively.

A portion of 0.2 g of the catalyst was packed into a 0.6 cm-ID quartz reactor and heated from room temperature to 100°C in Ar. When the temperature reached 100°C, the reduction was made by switching Ar to H_2 and maintained at that temperature for 2 h. After reduction, H_2 was purged with a flow of Ar while the reactor was cooled down to 60°C and held at that temperature for 10 min. Then a gas mixture of 0.3% C_2H_2, 0.8%H_2 and C_2H_4 balanced was switched to replace Ar with a flow rate of 30 ml/min. Consequently, the gas mixture was reacted under catalytic hydrogenation, i.e., C_2H_2 was selectively hydrogenated to C_2H_4.

However, in the case of N_2O treatment, the reactor was cooled down from 100°C to 90°C under Ar flow and held for 10 minutes before N_2O injection. Then the temperature was reduced to 60°C and the reaction was started. The products were analysed by SHIMADZU FID GC 14B equipped with Carbosieve column s-2.

To investigate the effect of carbonaceous deposit on the catalysts, the following experiment was designed: set A was obtained at an early period (5 min on stream) during which the negligible amount of coke was formed, while set B was obtained at 44 h on stream during which the considerable amount of coke was presumably formed though the exact amount of coke deposit was not determined.

The active sites of the catalysts were determined by CO adsorption technique and the BET surface areas by a Micromeritic Surface Area Analyser (model ASAP 2000).

The following terms used herein are defined as:

$$\text{Acetylene conversion (\%)} = \frac{\text{acetylene in feed - acetylene in product}}{\text{acetylene in feed}} \times 100$$

$$\text{Ethylene selectivity (\%)} = \frac{\text{ethylene in product - ethylene in feed}}{\text{acetylene converted}} \times 100$$

Yield per pass (YPP) = (% acetylene conversion)×(%ethylene selectivity)

RESULTS AND DISCUSSION

Figure 1 shows the effect of N_2O addition on the performance of 0.04 wt% Pd-Ag/Al_2O_3 (Ag:Pd = 4:1). Addition of 0.02 to 0.1 cc of N_2O markedly increased the yield per pass (YPP) of ethylene. The best result was obtained with 0.1 cc injection of N_2O while the YPP declined with the amount of N_2O higher than 0.1 cc. It has been suggested that N_2O addition may cause the formation of both silver oxide and palladium

oxide on the surface of Al_2O_3 support [5]. The formation of silver oxide should increase the number of accessible Pd active sites, as shown in Fig. 2, thus promoting the hydrogenation of acetylene to ethylene. The oxidation of active Pd to palladium oxide, however, may possibly cause the loss of active sites also. The maximum YPP of ethylene obtained with 0.1 cc injection of N_2O may be attributed to the simultaneous reproduction and destruction of active sites in which the former is more predominant, particularly the sites responsible for ethylene production from acetylene.

Figures 3 and 4 show the effect of catalyst aging on acetylene conversion and ethylene selectivity, respectively for 0.04 wt% Pd-Ag/Al_2O_3 with and without N_2O treatment. It has been found that both catalysts exhibited similar results in decreasing ethylene selectivity with time on stream, while acetylene conversion was only slightly changed. After 60 h of operation, both catalysts attained an apparent steady state of ethylene selectivity. It has been clearly observed that the N_2O-treated catalyst exerted higher activity and selectivity than the untreated one.

From several previous investigations (Al-Ammar et al. [6-8], Margitfalvi et al. [9,10], Moses et al. [11], and Weiss et al. [12]), it has been generally accepted that four main types of surface sites are involved in the alumina-supported Pd catalyst. Figure 5 illustrates four main types of surface sites; three types of which, located on the Pd metal surface, are responsible for selective conversion of acetylene to ethylene, direct ethane production from acetylene, and oligomer formation from acetylene. Another site located on the alumina support surface involves the hydrogenation of ethylene to ethane. It has been reported from some researchers [3,13] that the decrease in ethylene selectivity (i.e. increase in ethylene hydrogenation) during aging has been related to the amount of carbonaceous adsorbate on the catalyst surface. In other words, the

carbonaceous deposit acts as a hydrogen bridge for the hydrogen spillover from Pd to support.

As shown in Table 1, the substantial amount of ethane obtained for 0.04% Pd/Al_2O_3 of set A should be produced directly frcm acetylene, and the ethylene hydrogenation to ethane should be negligible with the that no carbonaceous deposit bridge was formed. When the base catalyst was promoted with Ag, the amount of ethane significantly decreased and so did the acetylene conversion while the amount of ethylene was almost constant. This implies that the alumina-supported Pd catalyst promoted by Ag may reduce the sites responsible for direct ethane formation from acetylene which is consistent with the previous investigation [13]. In case of the N_2O treatment for set A, both acetylene conversion and ethylene selectivity markedly increased and the amount of ethane was further decreased. This means that the addition of nitrous oxide augments the sites responsible for ethylene formation from acetylene as described above, and advantageously reduces the sites accounting for direct ethane formation as well. As for set B, the amount of ethylene obtained for 0.04% Pd/Al_2O_3 was considerably less than that of the corresponding catalyst for set A, and so did the acetylene conversion. The carbonaceous deposit on the catalyst surface should be responsible for the decrease in acetylene conversion. It is interesting to note that the amount of ethane formed on the base catalyst for set B was higher than that for set A even with less acetylene conversion. This means the substantial amount of ethane was formed via the ethylene hydrogenation on the support sites, with aid of carbonaceous deposit acting as H_2 bridge, rather than the direct ethane formation from acetylene on Pd sites. Sarkany [14,15] has found that the hydrocarbonaceous deposit on Pd/Al_2O_3 catalyst may enhance the over-hydrogenation of 1,3-butadiene and permits the hydrogenation of propene in the presence of 1,3-butadiene due to

transport hindrance of 1,3-butadiene. Thus, the over-hydrogenation of acetylene and hydrogenation of ethylene in the presence of acetylene can also be interpreted by transfer limitation of acetylene caused by the presence of carbonaceous deposits. With the Ag-promoted catalyst, the increase in amount of ethylene and acetylene conversion was obtained while the amount of ethane declined. This also implies that the ethylene hydrogenation was reduced by Ag promotion, and the direct ethane formation from acetylene on Pd sites covered with carbonaceous deposit was negligible. Thus it has been suggested that Ag may hinder the hydrogen spillover from the metal surface to alumina support probably by providing the desorption sites for transferred hydrogen as illustrated in Fig. 5. With the N_2O treatment, both acetylene conversion and ethylene selectivity significantly increased while the amount of ethane was further decreased as similar to those obtained for set A. The improved results achieved on N_2O-treated Pd-Ag/Al_2O_3 catalyst for both sets of data essentially contend that the addition of N_2O increases the sites responsible for ethylene formation from acetylene and decreases the sites involving direct ethane formation as mentioned above. Table 2 shows the results of BET surface area of the catalysts. It has been found that the BET surface area of the N_2O-treated catalyst was slightly higher than that of the untreated one. This reflects that two silver atoms may move closely to one oxygen atom to form Ag_2O. This phenomenon can expose the active palladium sites which normally locate under the surface of metal cluster as modelled in Fig. 2.

Table 3 shows the metal active sites of catalysts measured by co adsorption. It has been found that the Ag-Promoted Pd catalyst exhibited less amount of active sites than that of the unpromoted one. This may be due to the alloy formation between both metals. The addition of N_2O to the silver-promoted catalyst was found to enhance the amount of active

sites which also supported the proposed model as described above. The highest amount of active sites was achieved with the injection of 0.1 cc of N_2O.

CONCLUSION

It might be concluded that N_2O treatment could improve the catalytic performance of the silver-promoted palladium catalyst by enhancing the accessible sites of active Pd responsible for ethylene production from acetylene, and meanwhile decreasing the sites involving the direct ethane formation from acetylene. Furthermore, the N_2O-treated catalyst has the same stability as the untreated one during the aging period.

ACKNOWLEDGEMENTS

The financial support of this research by The Thailand Research Fund (TRF) is gratefully acknowledged.

REFERENCES

1. G.C. Battiston, L. Dallord, G.R. Tauszik: *Appl. Catal.*, **2**, 1 (1982).
2. C.N. Satterfield: *Heterogeneous Catalysis in Practice*, McGraw-Hill, New York, 1980.
3. J.P. Boitianx, J. Cosyn, M. Derrien, and G. Leger: *Hydrocarbon Processing*, March, 51 (1985).
4. A. Sarkany, and L. Guczi: *Appl. Catal.*, **10**, 369 (1984).
5. P. Praserthdam, U.S. Patent 5,849,662 Dec. 15, 1998.
6. Al-Ammar A.S., and G. Webb: *J.C.S. Faraday*, **174**, 195 (1978).
7. Al-Ammar A.S., and G. Webb: *J.C.S. Faraday*, **174**, 657 (1978).

8. Al-Ammar A.S., and G. Webb: *J.C.S. Faraday*, **175**, 1900 (1978).
9. J. Margitfalvi, L. Guczi, and A.H. Weiss, *J. Catal.*, **72**, 185 (1981).
10. J. Margitfalvi, L. Guczi: *React. Kinet. Catal. Lett.*, **15**, 475 (1980).
11. J.M. Moses, A.H. Weiss, K. Matsusek, and L. Guczi: *J. Catal.*, **86**, 417 (1984).
12. A.H. Weiss, S. Leviness, V. Nau, L. Guczi, A. Sakany, and Z. Schay: *Proc. 8th Int. Congr. Catal.*, **5**, 591 (1984).
13. S. Leviness, V. Nau, A.H. Wiess, Z. Schay, and L. Guczi: *J. Mol. Catal.*, **25**, 131 (1984).
14. A. Sarkany: *J. Catal.*, **180**, 149 (1998).
15. A. Sarkany: *Appl. Catal.*, **175**, 245 (1998).

Figure 1 Performance of 0.04 wt% Pd-Ag/Al_2O_3 (Ag:Pd = 4:1) versus the amount of nitrous oxide addition ranging from 0.02 to 0.33 cc
Reaction conditions: 60°C, GHSV 2000 h^{-1}, 5 min on stream

Figure 2 Proposed model illustrating the effect of N_2O addition on enhancing the accessible sites of active Pd responsible for acetylene hydrogenation to ethylene

Figure 3 Effect of catalyst aging on acetylene conversion over untreated and N_2O-treated Pd-Ag/Al_2O_3
Reaction conditions: 60°C, GHSV 2000 h^{-1}

Figure 4 Effect of catalyst aging on ethylene selectivity,over untreated and N_2O-treated Pd-Ag/Al_2O_3
Reaction conditions: 60°C, GHSV 2000 h^{-1}

Figure 5 Conceptual model demonstrating four main types of surface sites on Al_2O_3-supported Pd catalyst and the role of Ag promoter as desorption site for transferred H_2

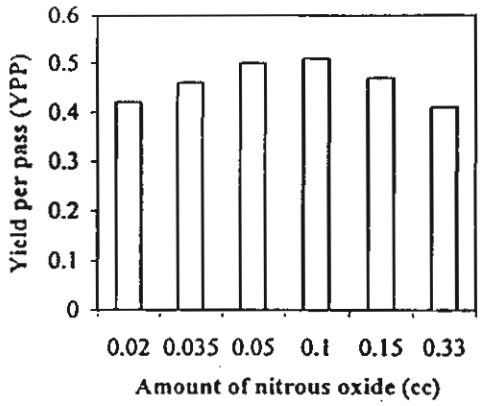
0.6
0.5
0.4
0.3
0.2
0.1
0
Yield per pass (YPP)
0.02 0.035 0.05 0.1 0.15 0.33
Amount of nitrous oxide (cc)

Fig. 1

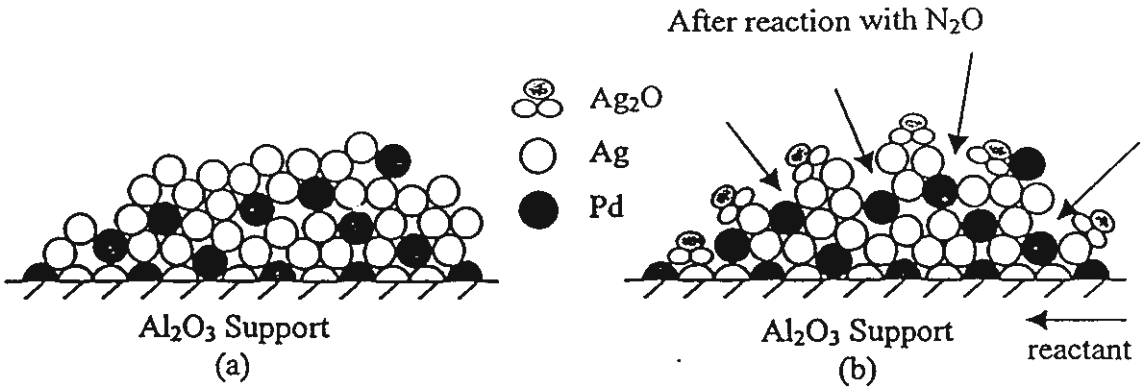
After reaction with N_2O
Ag_2O
Ag
Pd
Al_2O_3 Support
(a)
Al_2O_3 Support
(b)
reactant

Fig. 2

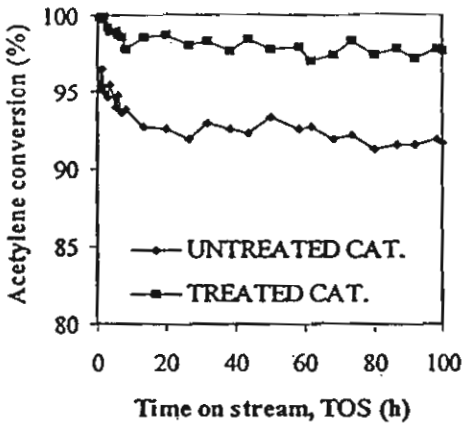
100
95
90
85
80
Acetylene conversion (%)
UNTREATED CAT.
TREATED CAT.
0
20
40
60
80
100
Time on stream, TOS (h)

Fig. 3

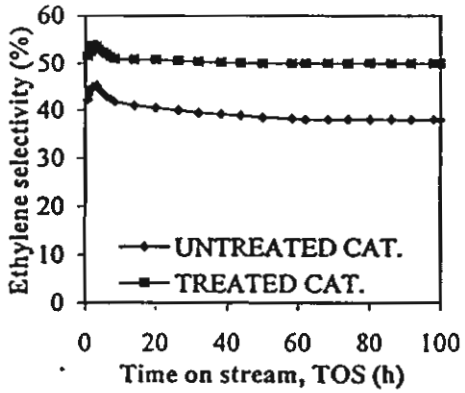
Ethylene selectivity (%)
60
50
40
30
20
10
0
UNTREATED CAT.
TREATED CAT.
0
20
40
60
80
100
Time on stream, TOS (h)

Fig 4

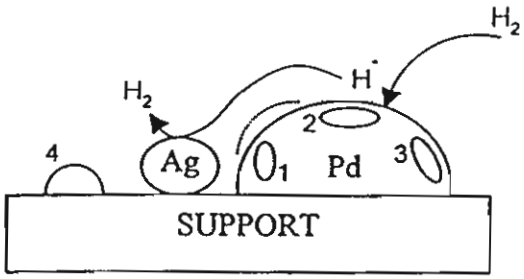

1. site for oligomer formation
2. site for direct ethane formation
3. site for ethylene formation
4. site for ethane production from ethylene

_____ carbonaceous deposit bridges

Fig. 5

Table 1

Product distribution in C wt% of three kinds of catalysts.

Reaction conditions: 60°C, GHSV 2000h^{-1}

Set	Catalyst	TOS	Composition (%)				C_2H_2 Conv.(%)	C_2H_4 Selectivity(%)
			C_2H_2	C_2H_4	C_2H_6	CH_4		
			Feed					
			0.2099	99.7708	0.0121	0.0072		
			Product					
	Base[a]		0.0037	99.8568	0.1321	0.0074	98.23	41.71
A	Untreated[b]	5 min	0.0065	99.8566	0.1294	0.0074	96.90	42.18
	Treated[c]		0.0015	99.8784	0.1126	0.0073	99.28	51.63
	Base[a]		0.0192	99.8338	0.1396	0.0074	90.85	33.04
B	Untreated[b]	44 h	0.0156	99.8465	0.1305	0.0073	92.56	38.96
	Treated[c]		0.0059	99.8731	0.1134	0.0075	97.18	50.15

[a]0.04% Pd/Al_2O_3

[b]0.04% $Pd\text{-}Ag/Al_2O_3$

[c]0.04% $Pd\text{-}Ag/Al_2O_3$ treated with N_2O

Table 2

BET surface area of three catalysts

Catalyst	BET (m^2/g)
0.04% Pd/Al_2O_3	4.74
0.04% $Pd\text{-}Ag/Al_2O_3$ (untreated)	4.36
0.04% $Pd\text{-}Ag/Al_2O_3$ (treated)	4.98

Table 3

The metal active sites of catalysts measured by CO adsorption

Catalyst	Metal active sites (sites/gram of catalyst)
0.04% Pd/Al_2O_3	3.30×10^{17}
0.04% $Pd\text{-}Ag/Al_2O_3$	2.52×10^{17}
0.04% $Pd\text{-}Ag/Al_2O_3$ (0.02 cc of N_2O)	3.14×10^{17}
0.04% $Pd\text{-}Ag/Al_2O_3$ (0.035 cc of N_2O)	3.22×10^{17}
0.04% $Pd\text{-}Ag/Al_2O_3$ (0.05 cc of N_2O)	3.70×10^{17}
0.04% $Pd\text{-}Ag/Al_2O_3$ (0.10 cc of N_2O)	4.04×10^{17}
0.04% $Pd\text{-}Ag/Al_2O_3$ (0.15 cc of N_2O)	3.37×10^{17}
0.04% $Pd\text{-}Ag/Al_2O_3$ (0.33 cc of N_2O)	3.18×10^{17}

Mr. Tharathon Mongkhonsi

Department of Chimical Engineering
Faculty of Engineering
Chulalongkorn University
Bangkok 10330, Thailand

May 25, 2000

Dear Sir:

Re : Manuscript No. CL- 000463

Tharathon Mongkhonsi, Purida Pimanmas, and Piyasan Praserthdam
Selective Oxidation of Ethanol and 1-Propanol over V-Mg-O/TiO_2 Catalyst

As you will see from the enclosed reviews, the referees recommended publication of this paper in Chemistry Letters. However, they made several comments which will merit your consideration. Please send two copies of the revised manuscript, marked REVISED, directly to me, along with a letter indicating what revisions have been made within the next two weeks of receiving this letter. If further delays are necessary, please notify me as soon as possible.

Please keep in mind that the revised manuscript must strictly conform to the format specifications described in Information for Authors, 1998.

Sincerely yours,

PS Please see the FAX version of your manuscript which shows how to modify the format.

朝倉清高

0811
市北区北11条西10丁目
道大学
化学研究センター
委員　朝倉　清高

Kiyotaka Asakura, Associate Editor
Catalysis Research Center
Hokkaido University,
Kita-11-jyo Nishi-10-chome,
Kita-ku, Sapporo 060-0811, Japan

81-11-706-3671　　fax +81-11-706-3671　　email askr@cat.hokudai.ac.jp

Effect of Organic Solvents on the Thermal Stability of Porous Silica-Modified Alumina powders Prepared via One Pot Solvothermal Synthesis

Piyasan Praserthdam[a], Masashi Inoue[b], Okorn Mekasuvandumrong[a], Waraporn Thanakulrangsan[c] and Suphot Phatanasri[a]

[a] Department of Chemical Engineering, Chulalongkorn University, 10330 Thailand E-mail: Okornm@yahoomail.com

[b] Department of Hydrocarbon Chemistry, Faculty of Engineering, Kyoto University, Kyoto 606, Japan

[c] Department of Chemical Engineering, Rajamanggala Institute of Technology, Patumthani 12110 Thailand

Abstract

Mixtures of alumina isopropoxide (AIP) and tetraethyl orthosilicate (TEOS) with weight ratios of AIP/TEOS = 8 in various organic solvents were set in an autoclave and heated at 300 °C for 2 h. The fluid phase was removed at the supercritical temperature. The products were calcined in air to yield silica-modified aluminas. These silica-modified aluminas had different morphology that affected the surface area and thermal stabilities at high temperatures. The reactions of AIP and TEOS in 1-butanol gave substantially the wrinkled sheets morphology having the thermal stability higher than the spherical particles obtained by reaction in toluene.

Introduction

Recently, much attention has been paid to improve the properties of catalyst at high temperatures. Transition aluminas have large surface areas with reasonable mechanical strength and are widely used as catalyst supports in industry. However, because of metastable nature of transition aluminas, they usually transform to α-alumina at around 1100°C which causes a drastic decrease in the surface area. For the purpose of increasing the thermal stability of transition aluminas, the effect of dopants has been investigated and partial success was achieved by incorporation of ThO_2, ZrO_2, SiO_2, etc., in to the alumina matrix.

Iler (1964) found that the addition of silicic acid to fibrillar colloidal boehmite increased the thermal stability of the resultant alumina. Yoldas (1976) examined the thermal stabilities of silica-modified aluminas prepared by a sol-gel method and reported that the alumina doped with 6% silica had the maximum temperature (1380°C) for α-alumina transformation. Murrell and Dispenziere (1988) reported that the alumina doped with 5% silica by reaction with tetraethyl orthosilicate (TEOS) led to marked stabilization against loss of the surface area by vanadium attack at high temperatures. In other papers in this field, Johnson (1990) and Beguin (1991) also prepared silica-modified alumina and confirmed the increase of the thermal stability of the resultant alumina by addition of silica.

For the synthesis of inorganic materials by using organic media, Inoue et al. (1988-1992) found that the glycothermal treatment (the use of glycol instead of water for

hydrothermal treatment) of gibbsite at 250 °C yielded the product having a structure of boehmite with glycol moieties incorporated between the boehmite layers with the covalent bonding. Inoue et al. (1988) also found that treatment of aluminum alkoxide in various glycols at 300 °C yielded the glycol derivatives on boehmite. Inoue et al. (1995) prepared the silica-modified alumina by the reaction of aluminum isopropoxide (AIP) and tetraethyl orthosilicate (TEOS) in 1,4 butanediol at 300°C and found that the product with Al/Si ratio of 8 maintained large surface area even after calcination at high temperatures.

Highly porous solids can be prepared by the removal of solvent from a wet gel at a temperature above the critical temperature of the solvent. In recent years, researchers have built up the strong technical background in such materials. Fanelli and Anthony (1983) found the new polymerization catalyst system comprising an aluminum compound and a transition metal compound on an alumina-based aerogel support. Armor and Carlson (1984) prepared a catalyst composition of a uniform dispersion of individual metallic palladium particles. They (1989) also prepared high pore volume alumina by hydrolysis of AIP followed by supercritical removal of the fluid phase. Aerogel has good properties such as high pore volume, high surface area, and high thermal stability. These properties result from this method that obviates the inherent shrinkage or structural collapse that occurs when precursor gel are conventionally dried to a solid form. Such shrinkage or compaction are brought about by the surface tension of residual liquid trapped within the fragile gel structure.

In the present work, mixtures of AIP and TEOS were treated in 1-butanol, and toluene, and the fluid phase was separated by supercritical drying. In other words, solvothermal synthesis of oxides is combined with the supercritical drying method, which provides a convenient route for the synthesis of powders by using only one reaction vessel. The properties of products are also examined. Then the products are calcined at various temperatures, and thermal stabilities of the resulting silica-modified aluminas are investigated.

EXPERIMENT

In this paper, the products were prepared by three different methods. First, the mixtures of aluminum isopropoxide (AIP, Aldrich) and tetraethyl orthosilicate (TEOS, Aldrich) at weight ratios of 8 were suspended in 100 ml of toluene in a beaker, and then set up in a 300 ml autoclave. In the gap between the beaker and the autoclave wall, 30 ml of toluene was added. After the autoclave was completely purged with nitrogen, the suspension was heated to 300°C at a rate of 2.3°C/min and held at that temperature for 2 h. During the reaction, the autogenous pressure gradually increased to 6-14 MPa. After the reaction, the autoclave valve was opened, and the fluid phase in the autoclave was released at that temperature condensing in a cooling coil. The condensed liquid was collected in another beaker. After the autoclave was cooled, the white powder products were obtained. For the second method, the same procedures as the first one were followed except that 1-butanol was used instead of toluene. In the third preparation, the

same procedures as the first one were followed but a mixture of water and toluene was added instead of toluene in the gap between the beaker and the autoclave wall. Amount of water was varied as 10 and 30 ml.

A part of the product was calcined in a box furnace by heating to the desired temperature (600°C, 1000°C, 1150°C) at a rate of 10 °C/min and holding at that temperature for1 h, and thus silica-modified aluminas were obtained.

The reaction products will be designated by abbreviations T, B and H meaning the solvents that used in the reaction: T means toluene, B means 1-butanol, and H means the mixture of water and toluene in the gap between the beaker and the autoclave wall. The abbreviation was followed by AS, which means the silica-modified alumina. When calcined samples are specified, these abbreviations are followed by calcination temperature in the parentheses. Therefore, TAS(1150) means the silica-modified alumina sample prepared in toluene and calcined at 1150 °C.

Characterization

Powder X-ray diffraction (XRD) was measured on a SIEMENS XRD D5000 using Cu Kα radiation, Infrared (IR) Spectra were recorded on a NICOLET FT-IR Impact 400 spectroscopy using the ex-situ IR technique. Morphologies of the particles were observed by JEOL Transmission Electron Microscope. The BET surface areas were calculated by the BET-single point method on the basis of the nitrogen uptake measured at P/Po = 0.3 using a gas chromatograph. The surface areas calculated by the ordinary

BET method were in good agreement with the surface areas calculated by the single-point method.

Results

The products obtained by one-pot synthesis of mixtures of AIP and TEOS in toluene were colorless powders. The XRD patterns of TAS and TAS calcined at different temperatures are shown in Fig.1a. TAS and TAS(600) exhibited the typical pattern for amorphous product. When the product was calcined at 1000°C and 1150°C, TAS(1000) and TAS(1150) exhibited the characteristic of spinel alumina and some mullite phase was observed from a small peak at $2\theta = 26.5$. When mixtures of AIP and TEOS were allowed to react in 1-butanol, the products were colorless powders. As shown in Fig.1b, BAS exhibited the typical pattern for the mixtures of χ-alumina and pseudoboehmite. BAS (600) exhibited the typical pattern for λ-alumina, while BAS(1000) and BAS(1150) exhibited the typical characteristic for spinel alumina. When the product was prepared by using toluene as the solvent and a mixture of water and toluene was added in the gap between the beaker and the autoclave wall, the XRD patterns of HAS calcined at any temperatures were almost similar to BAS as shown in Fig.1c. This indicates that the water added to toluene according to the third method has the same effect on the reaction as in the case of product preparation in 1-butanol.

IR spectra of the products are shown in Fig.2. Bands characteristics of the boehmite structure were seen at 773, 615 and 478 cm^{-1}, suggesting that BAS had the

layer structure of boehmite and BAS exhibited the small band at 1070 cm^{-1} due to stretching vibration mode of Si-O-Si bond. On the other hand, products obtained in toluene had no adsorption band that indicated the boehmite layer. IR spectra of TAS did not show any band at 1070 cm^{-1}. As for IR spectra of the product prepared via the third preparation, HAS showed the band characteristics of the boehmite structure at 773, 615, 478 cm^{-1} and small band at 1070 cm^{-1}. These adsorption bands were similar to BAS.

Transmission electron micrographs of the calcined silica-modified aluminas at AIP/TEOS ratio of 8 prepared in different solvents are shown in Fig.3. The morphology of BAS(600) seems to be the mixture of wrinkled sheets and spherical particles. When the product was calcined at high temperature, BAS(1150) consists of substantially the wrinkle sheets which are almost the same as BAS(600). However, the wrinkled sheets irregularly twisted in the product became progressively straight as the calcination temperature rose. The morphology of TAS(600) seems to be spherical particles with out any observation of the wrinkled sheets and the particle size increased when the calcination temperature was increased(TAS(1150)). Interestingly enough, when the water was added in the gap between the beaker and autoclave wall (HAS(600)). The wrinkled sheets were observed though these sheets were attached by a number of spherical particles and the morphology of HAS(1150) was not far different from HAS(600).

The BET surface areas of products are summarized in Table1, It has been found that HAS had larger surface area than TAS at each calcination temperature. The results obtained suggest that the mechanism of reaction in toluene was difference from the other

two reactions and comparison of the results between HAS and BAS suggests that these reactions took place by the same reaction mechanism.

Discussion

The reaction in toluene occurred by thermal decomposition of aluminum isopropoxide. In the first step, aluminum isopropoxide was decomposed yielding Al-O$^-$ and $(CH_3)_2CH^+$ and in the second step nucleophilic attack of Al-O$^-$ on tetraethyl orthosilicate or another AIP molecule took place yielding the Al-O-Si or the Al-O-Al bond. The latter finally gave χ-alumina.

When small amounts of water was added in the gap between the beaker and the autoclave wall, the mechanism was changed. When the reaction temperature was raised, water in the gap was evaporated and dissolved in toluene in the beaker. In the second step, aluminum isopropoxide was hydrolyzed yielding Al-O-H and isopropanol. Al-O-H would react with other AIP molecules finally yielding pseudoboehmite. During this polymerization reaction, the aluminum species might react with TEOS remaining the silicon moiety between the boehmite layers.

When 1-butanol was used as the solvent in the reaction, AIP reacts with 1-butanol yielding aluminum butoxide. Thermal decomposition of aluminum butoxide gave the alkyl (butyl) derivative of boehmite. Because the aluminum butoxide is a primary alkoxide, thermal decomposition of this compound proceeds much more slowly than AIP itself. On the other hand, 1-butanol can be dehydrated to give water which then

hydrolyzes aluminum isopropoxide or butoxide yielding Al-O-H^+ and isopropanol or butanol. Al-O-H^+ finally yields pseudoboehmite. Since direct decomposition of aluminum alkoxide proceeds slowly, a part of reaction took place by this reaction sequence. In the presence of TEOS, Al-O-H^+ species or AL-O^- species formed by thermal decomposition of aluminum alkoxide attacks TEOS yielding Al-O-Si bond. It's well known silica-alumina has strong acidity and therefore the product also has strong acidity. Once a small amount of product having Al-O-Si bond is formed, surface acidity of the product dehydrates the solvent, 1-butanol, yielding water, which then hydrolyzes aluminum alkoxide yielding pseudoboehmite. Therefore addition of a small amount of TEOS in the starting mixture completely altered the reaction sequence.

From TEM data, the above mechanism of the reaction in each solvent can be proved. The wrinkled sheets found in the third preparation indicated that the water added in the gap between a beaker and the autoclave wall had the effect on the presence of the wrinkled sheets. This suggests that the hydrolysis of AIP gave the boehmite structure having the morphology of wrinkled sheets. Thus the mechanism of the reaction in 1-butanol occurred through the dehydration of 1-butanol to give water, and then the hydrolysis of AIP eventually yielding pseudoboehmite having the wrinkled sheets structure can be predicted.

From BET surface areas of the products shown in Table1, the products obtained in toluene had lower surface area at high calcination temperature than the products obtained in the presence of water in the gap between the autoclave wall and the beaker. This indicates the effect of water on the reaction. However the surface areas were far

lower than that of the product obtained in 1-butanol, the results suggests that the reaction in toluene having water in the gap proceeds by two routes: water dissolved in toluene hydrolyzes AIP, while thermal decomposition of AIP could occur. High thermal stability of product obtained in 1-butanol suggests that the hydrolysis of AIP substantially occurred.

It is generally accepted that α-alumina transformation starts from the contact between particles. Tucker (1985) found that crystallization of α-alumina started from the contact of polycrystalline spherical particles and single crystal are formed. He explained that mechanical strain caused by the thermal expansion concentrating at the contact point of spherical particle and caused tetragonal closest packing of oxygen atom to hexagonal closet packing, which acted as the nuclei of α-alumina. Taking into account of this explanation, the thermal stability of the present products can be elucidated. From BET surface area, the decreasing order of thermal stability of products prepared in each solvent is 1-butanol>toluene+water in the gap>toluene. From the morphological viewpoint, the thermal stability of the products increased with the increase of the content of wrinkled sheets. Since the wrinkled sheets have the limited number of contact points in the unit volume, the nucleation frequency of α-alumina, and hence the α-alumina transformation is reduced. On the other hand, the spherical particles have a large number of contact points between the primary particles which α-alumina transformation can occur much more easily.

Conclusion

The reaction of AIP and TEOS in toluene gave products having the spherical particles. When water was added in the gap between the beaker and the autoclave wall the product was seem as the mixture of wrinkled sheets and spherical particles which was the same as product synthesized in 1-butanol, however, the content of wrinkled sheets in BAS was higher than HAS. The thermal stability of products also increased with the increasing content of the wrinkled sheets. The wrinkled sheets occurred by the hydrolysis of aluminum alkoxide in the reaction system comprise the as-synthesis structure of boehmite, which had the limited number of contact point in the product morphology. BAS sample possessing substantially the wrinkle sheets had the highest thermal stability. The surface area of which is 169 m^2/g even after calcination at 1150 °C

Acknowledgements

The authors would like to thank the Thailand Research Fund (TRF) for their financial support of this project.

Reference

1. Armor, J. N., Carlson, E. J. US Patent 4469816 (1984)
2. Armor, J. N., Carlson, E. J. Variables in synthesis of unusually high pore volume aluminas, J. Mater. Sci. 22,2549-2556 (1989)
3. Beguin, B., Garbowski, E., Primet, M. Stabilization of alumina toward thermal sintering by silicon edition. . J. Catal. 127,595-604 (1991)
4. Fanelli, A. J., Burlew, J. V. US Patent 4387085 (1983)
5. Fanelli, A. J., Burlew, J. V. Preparation of fine alumina powder in alcohol, J. Mater. Sci. 23,2897-2904 (1989)
6. Gani, M. S. J., Mcpherson, R. Glass formation and phase transformation in plasma prepared Al_2O_3-SiO_2 powders. J. Mater. Sci.12, 999-1009 (1977)
7. Iler, R.K. Effect of Silica on transformations of fibrillar colloidal boehmite and gamma alumina. J. Am. Ceram. Soc. 47, 339-341 (1964)
8. Inoue, M., Kondo, Y. An ethylene glycol derivative of boehmite, Inorganic Chemistry 27, 215-221 (1988)
9. Inoue, M., Tanino, H. Formation of microcrystalline α-alumina by glycothermal treatment of gibbsite, J. Am. Cerm. Soc. 72, 352-353 (1989)
10. Inoue, M., Kominami, H. Thermal transformatiom of χ-alumina formed by thermal decomposition of aluminum alkoxide in organic media, J. Am. Cerm. Soc. 75, 2597-2598 (1992)

11. Inoue, M., Otsu, H. Kominami, H. Synthesis of thermally stable, porous silica-modified alumina via formation of a precursor in an organic solvent, Ind Eng Chem Res 35, 295-306 (1995)

12. Johnson, M. F. L. Surface areas stability of aluminas. J. Catal.123, 245-259 (1990)

13. Murrell, L. L., Dispenziere, N. C. Jr. Silica -stabilized aluminas resistance to vanadium attack under severe high temperature condition. J. Catal. 111, 450-452 (1988)

14. Tucker, D. L. Gamma-to-Alpha transformation in spherical aluminum oxide powders. J. Am. Ceram. Soc. 68, C163-164 (1985)

15. Yoldas, B. E. Thermal stabilization of an active alumina and effect of dopants on the surface area. J. Mater. Sci. 11, 465-470 (1976)

Table 1 : BET surface area of products calcined at various temperatures

AIP/TEOS of 8 in each solvents	BET surface areas (m^2/g)		
	600	1000	1150
TAS	244.2	92.4	74.7
BAS	210.6	190.5	168.4
HAS	208.7	182.7	110.8

Figure 1a: XRD patterns of precursor gel obtained by the reaction of AIP and TEOS in toluene at every calcination temperatures

Figure 1b: XRD patterns of precursor gel obtained by the reaction of AIP and TEOS in 1-butanol at every calcination temperatures

Figure 1c: XRD patterns of precursor gel obtained toluene, which the addition of water in the gap at every calcination temperatures

Figure 2: IR spectra of precursor gels for silica-modified aluminas obtained by the reaction of AIP and TEOS in every preparation

Figure 3: TEM image of precursor gel obtained by the reaction of AIP and TEOS in every preparation

Figure 4a: BET surface area of silica-modified aluminas prepared in toluene and calcination at various temperatures

Figure 4b: BET surface area of silica-modified aluminas prepared in 1-butanol and calcination at various temperatures

Figure 5a : TEM image of BAS(600)(*150,000)

Figure 5b : TEM image of BAS(1150)(*150,000)

Figure 5c : TEM image of TAS(600)(*150,000)

Figure 5d : TEM image of TAS(1150)(*150,000)

Figure 5e : TEM image of HAS(600)(*150,000)

Figure 5f : TEM image of HAS(1150)(*150,000)

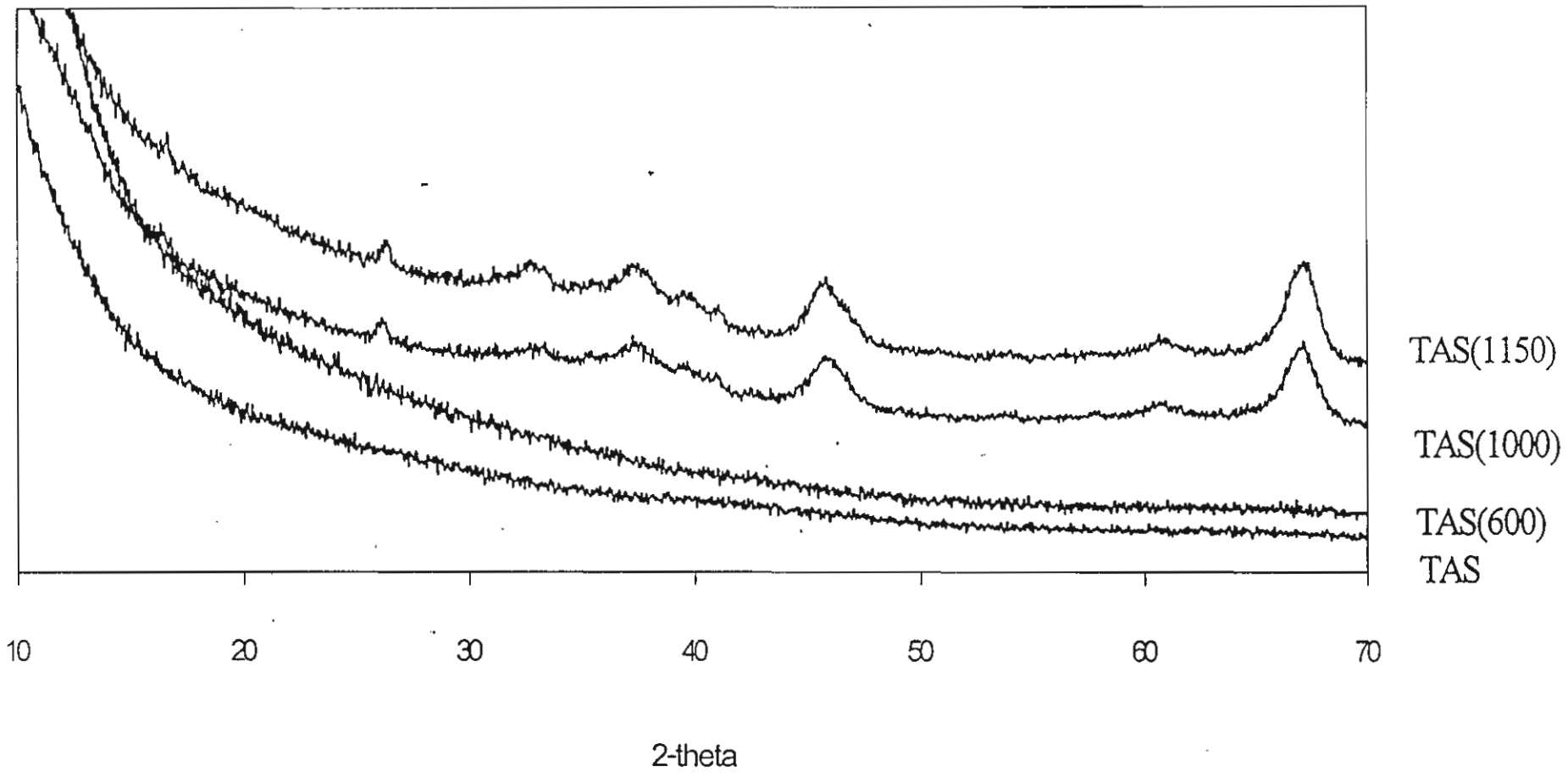
TAS(1150)
TAS(1000)
TAS(600)
TAS
10
20
30
40
50
60
70
2-theta

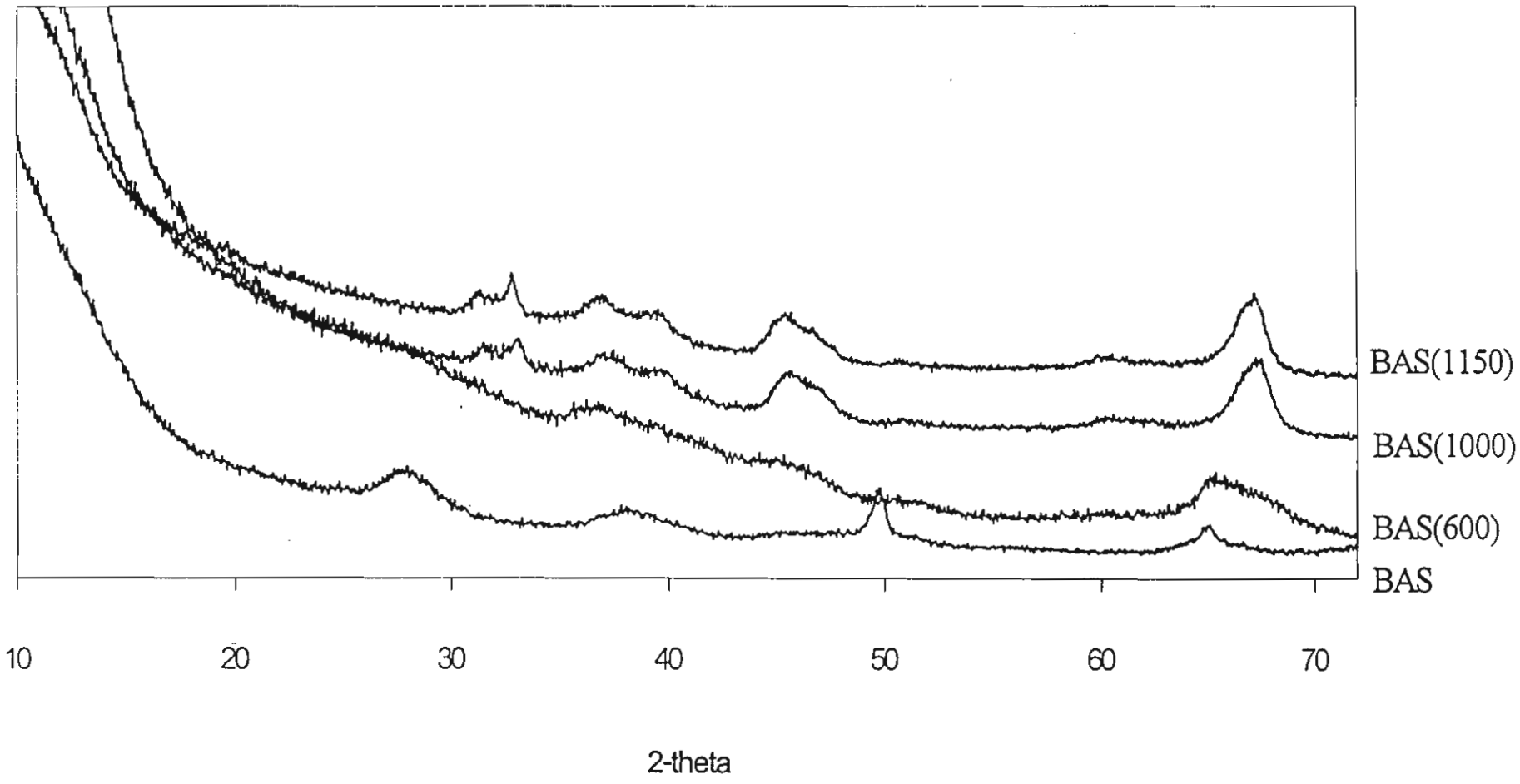
BAS(1150)
BAS(1000)
BAS(600)
BAS
10
20
30
40
50
60
70
2-theta

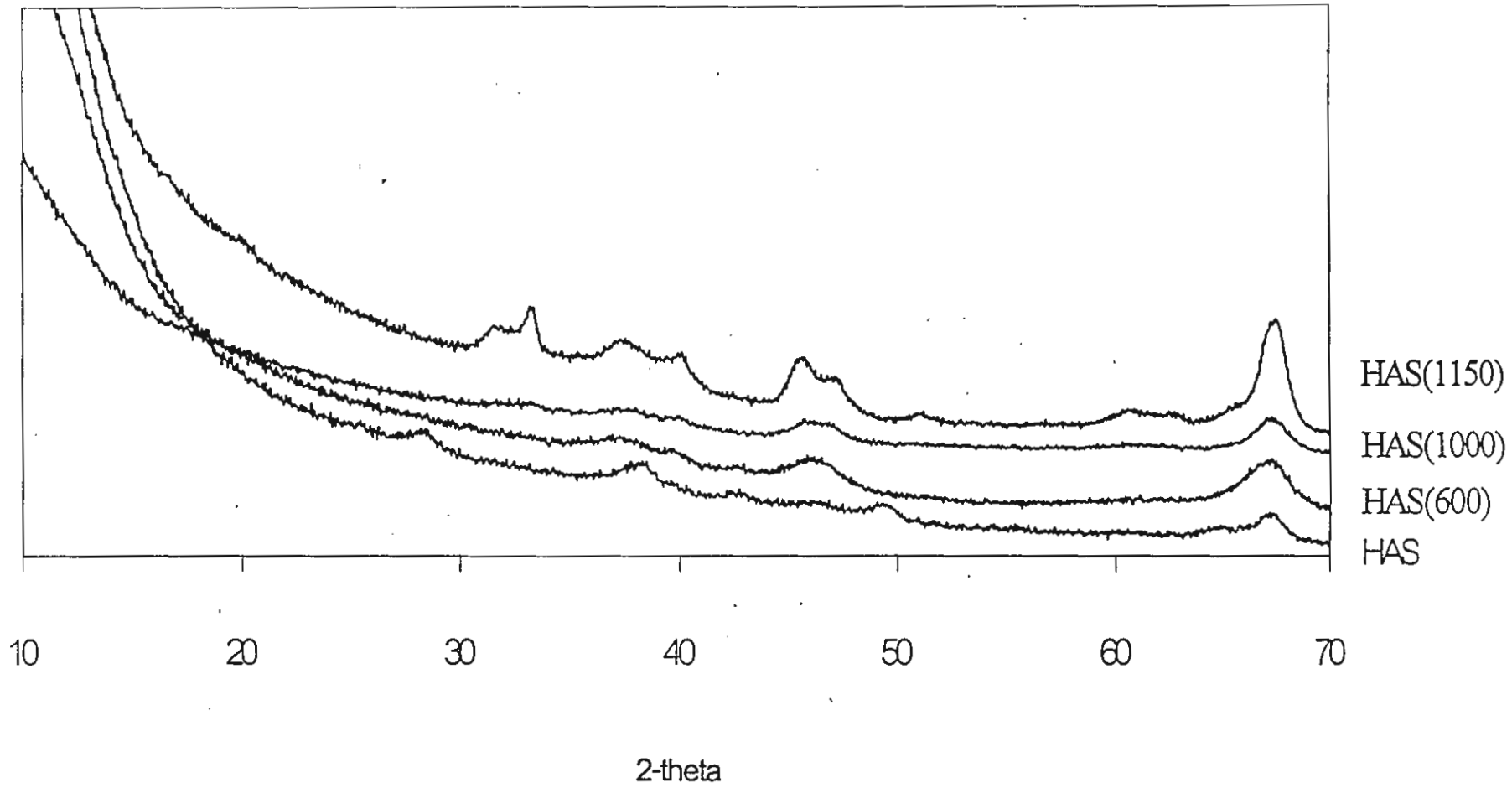
HAS(1150)
HAS(1000)
HAS(600)
HAS
10
20
30
40
50
60
70
2-theta

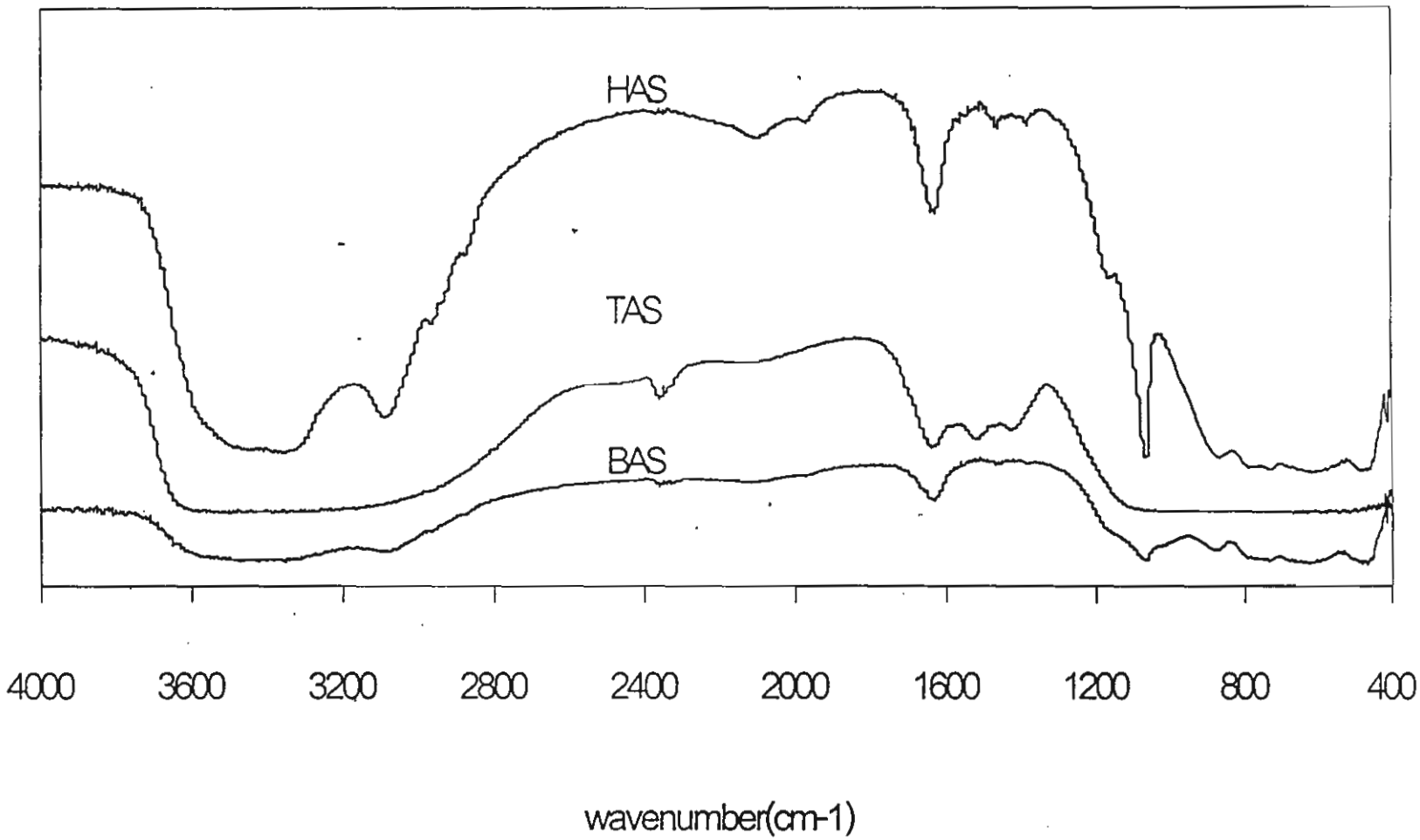
HAS
TAS
BAS
4000
3600
3200
2800
2400
2000
1600
1200
800
400
wavenumber(cm-1)

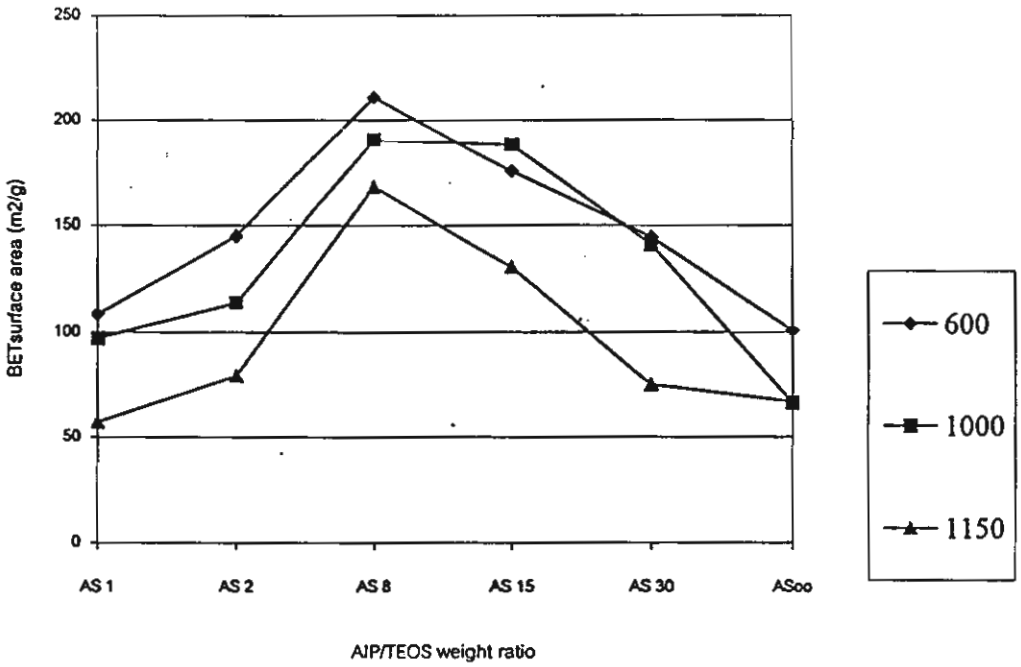
250
200
150
100
50
0
BETsurface area (m2/g)
AS 1
AS 2
AS 8
AS 15
AS 30
ASoo
AIP/TEOS weight ratio
600
1000
1150

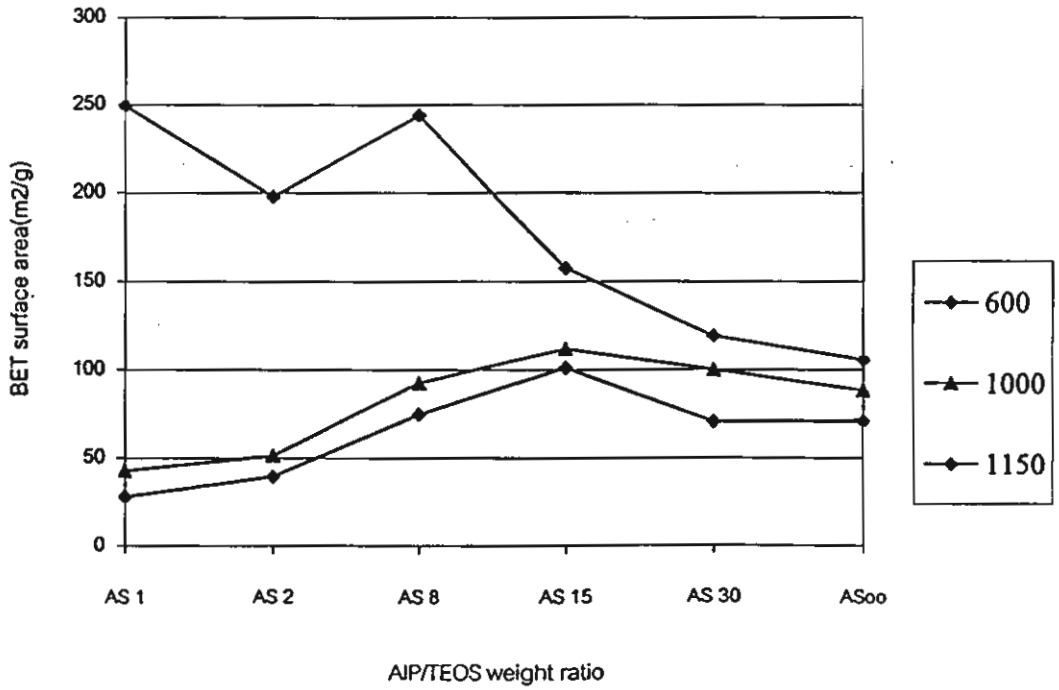
300
250
200
150
100
50
0
BET surface area(m2/g)
AS 1
AS 2
AS 8
AS 15
AS 30
ASoo
AIP/TEOS weight ratio
600
1000
1150

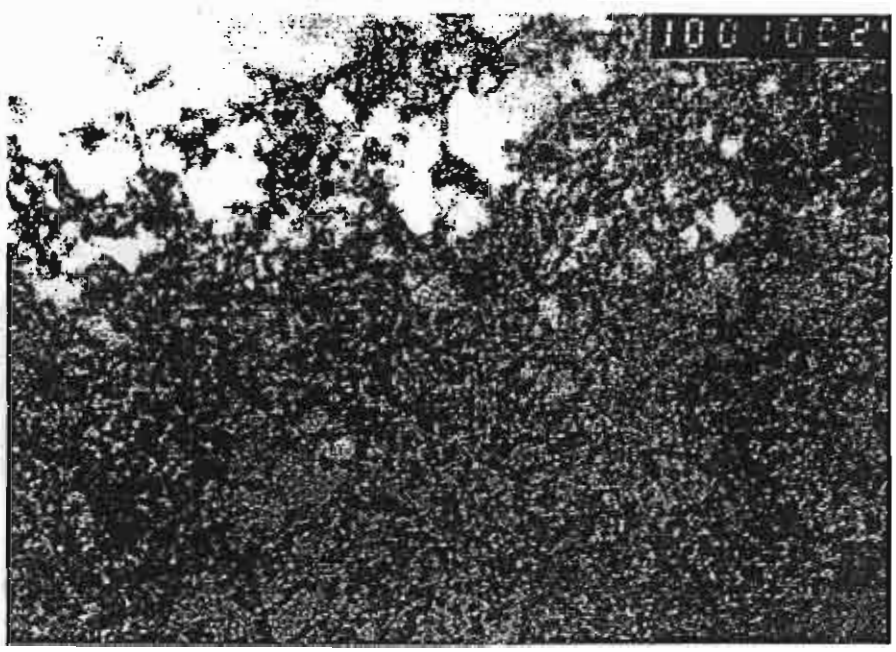

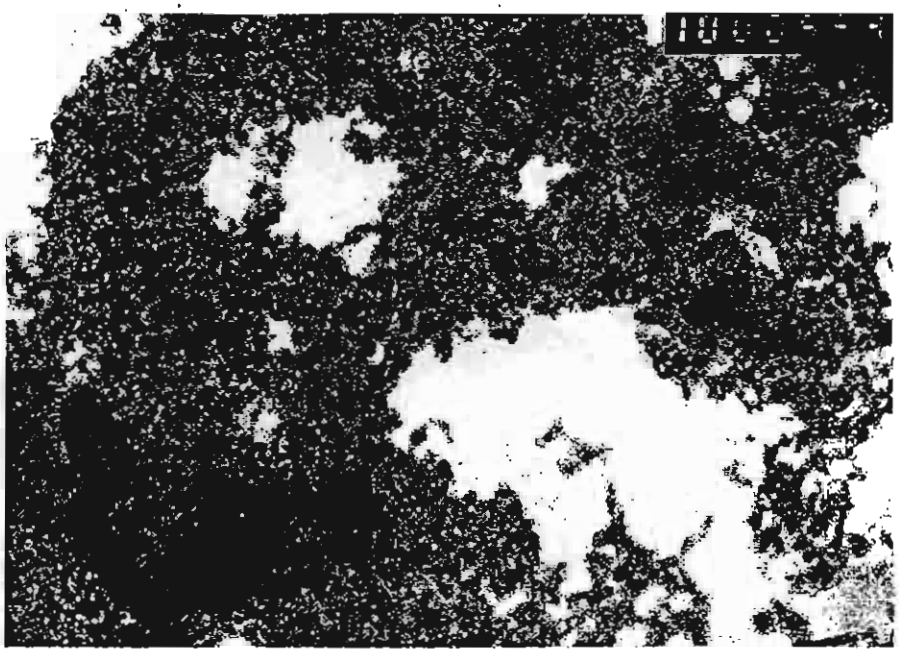

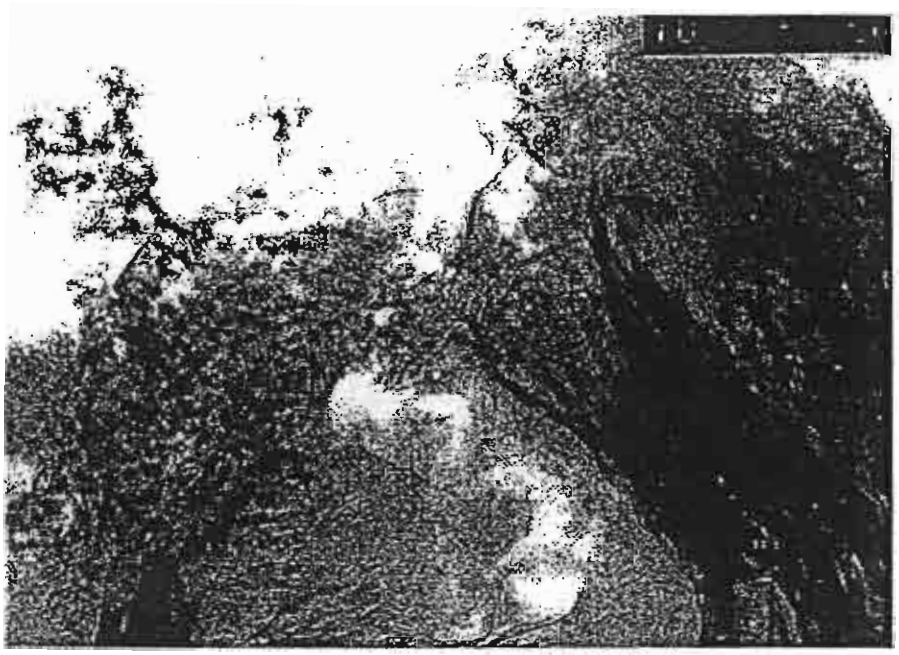

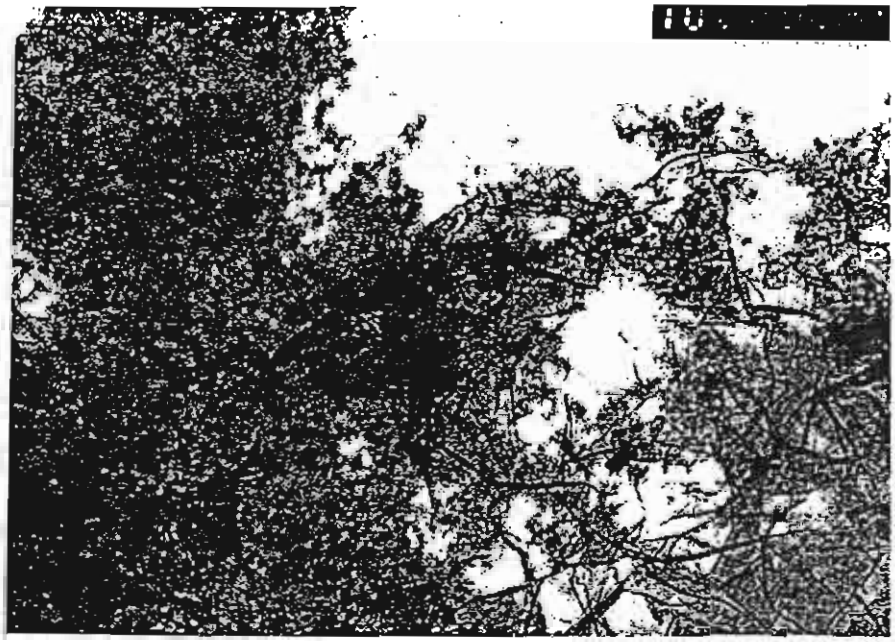

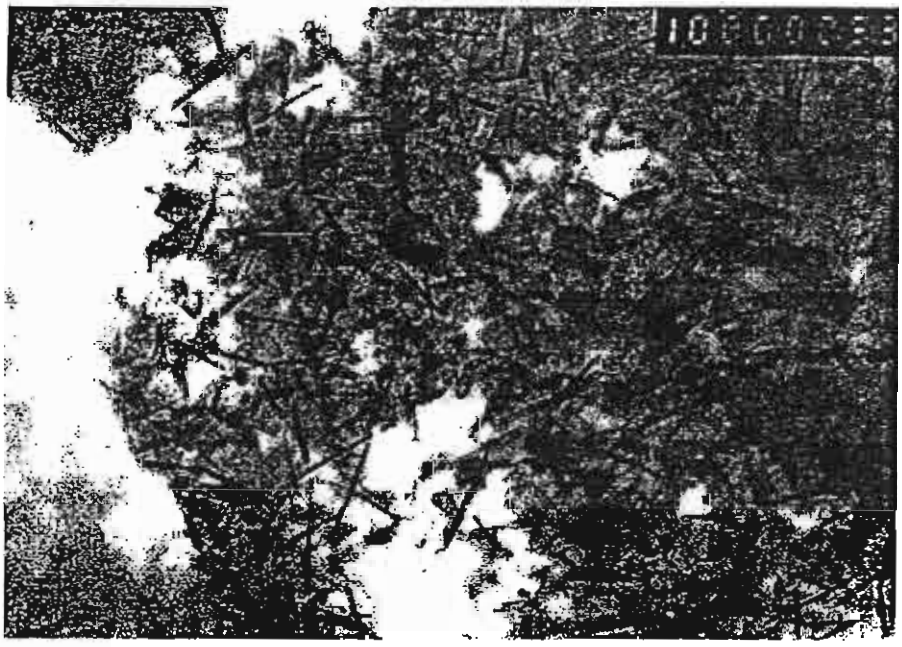

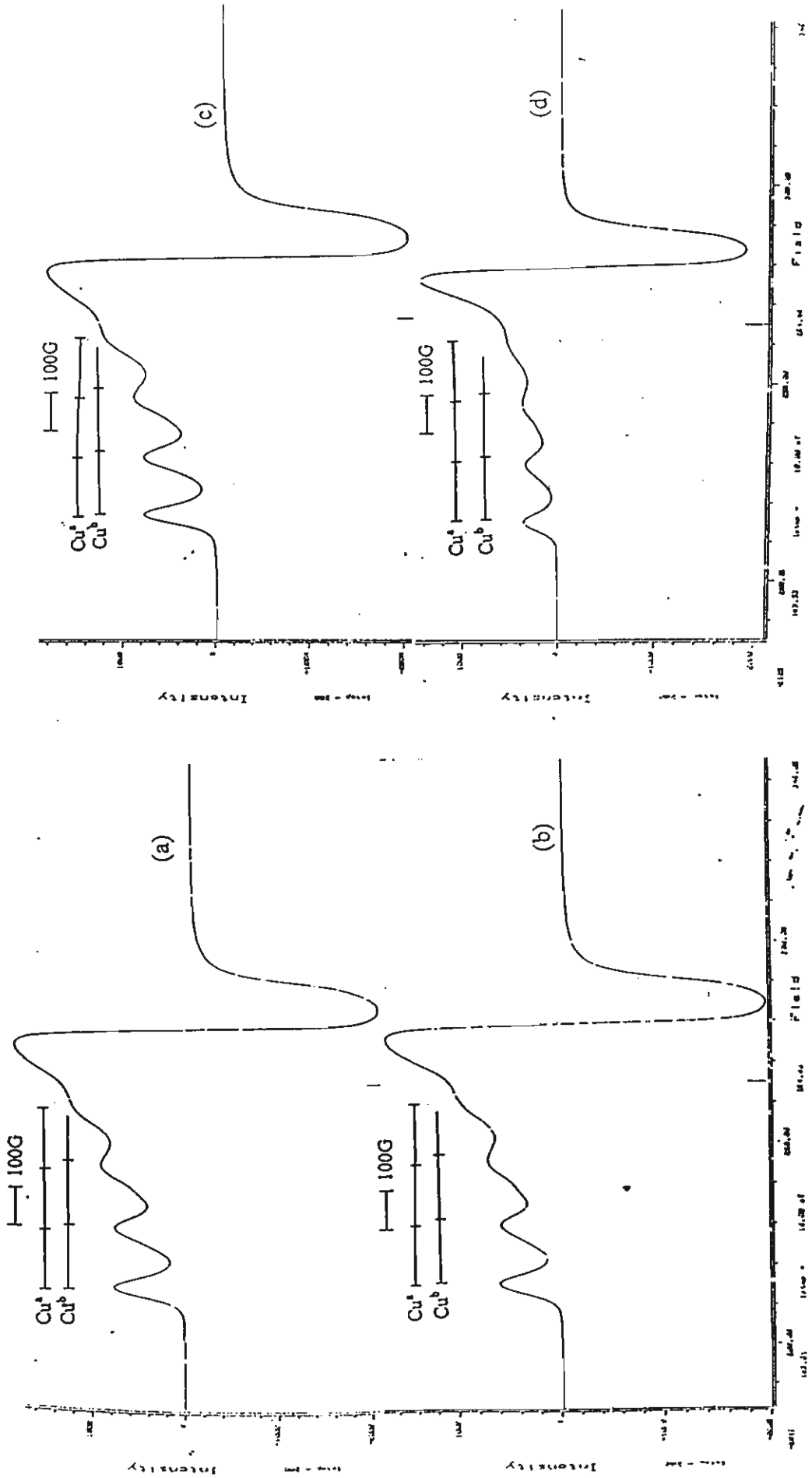

Figure 2.3

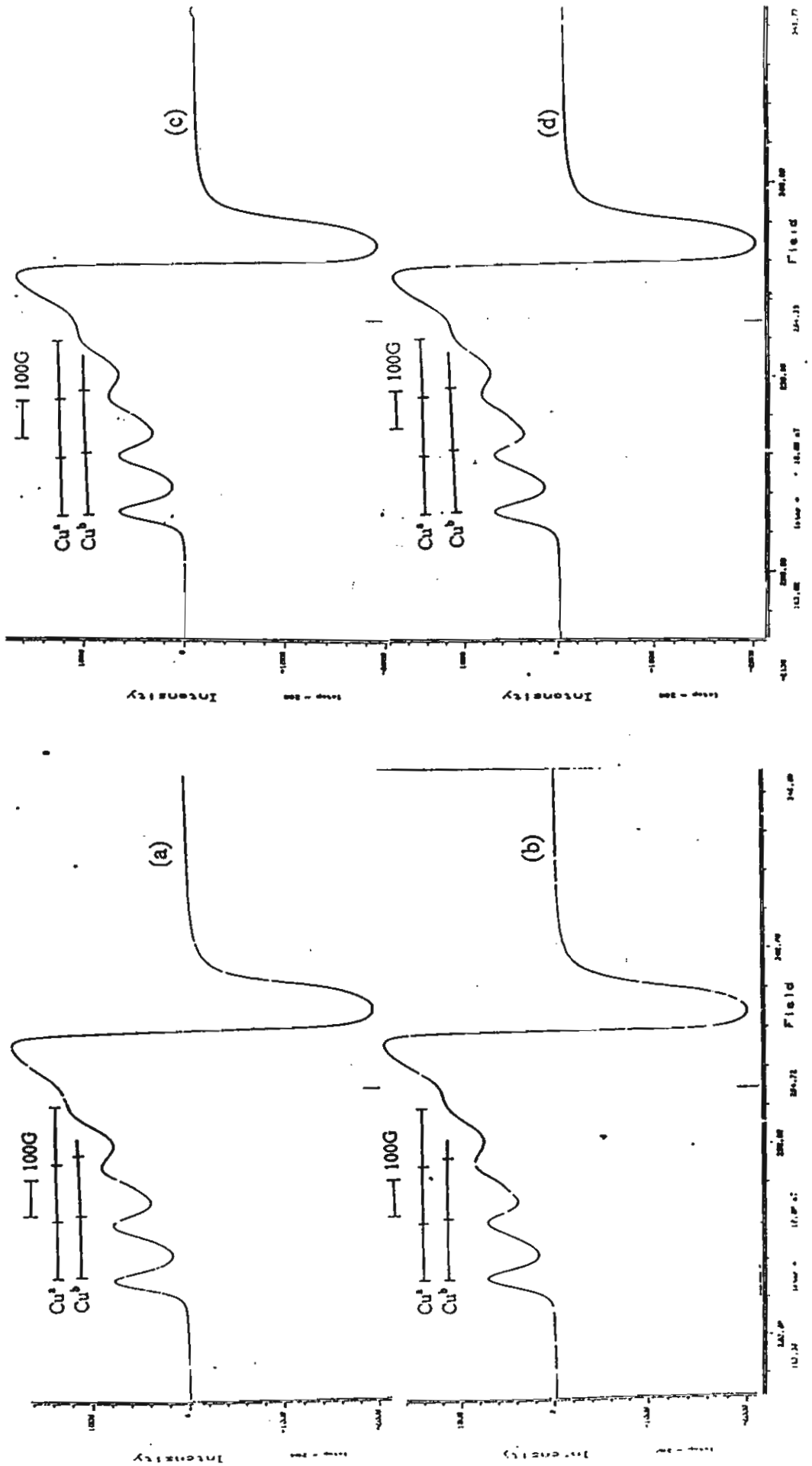

Figure 2.4

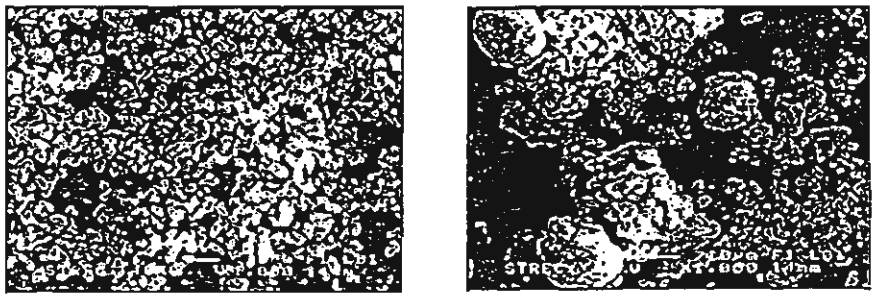

Cu/H-MFI

0.1%Pd/Cu/-MFI

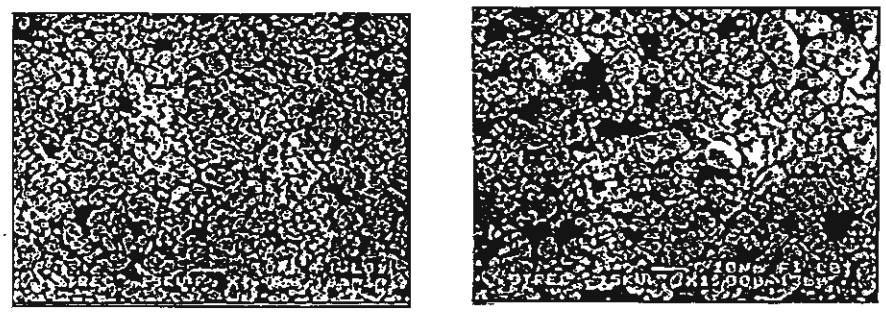

0.2%Pd/Cu/H-MFI

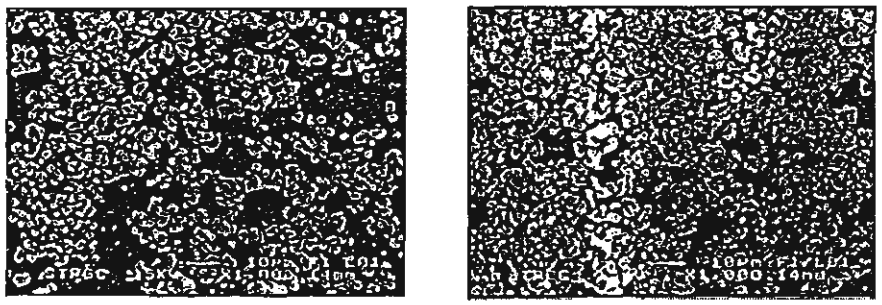

0.3%Pd/Cu/H-MFI

(a) (b)

Figure 3.1

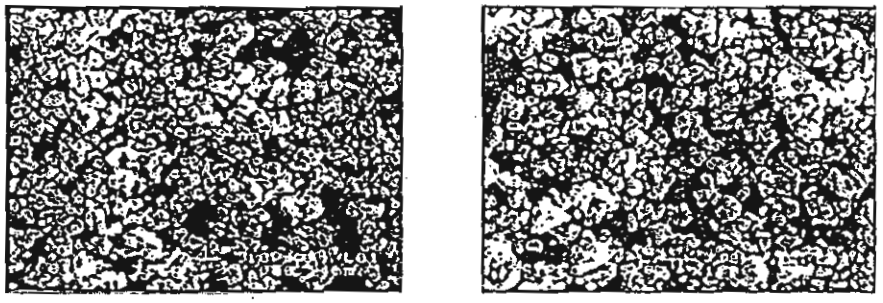

0.4%Pd/Cu/H-MFI

0.6%Pd/Cu/-MFI

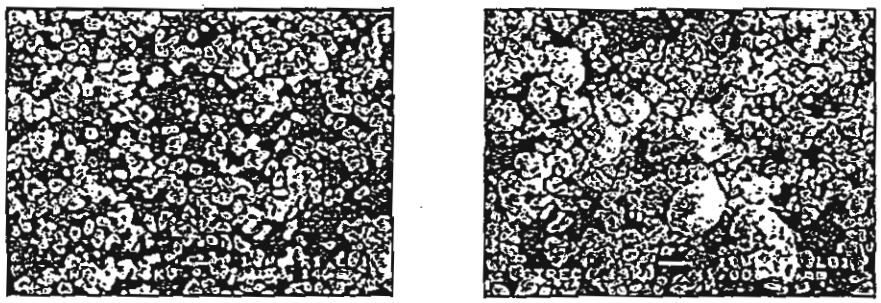

0.8%Pd/Cu/H-MFI

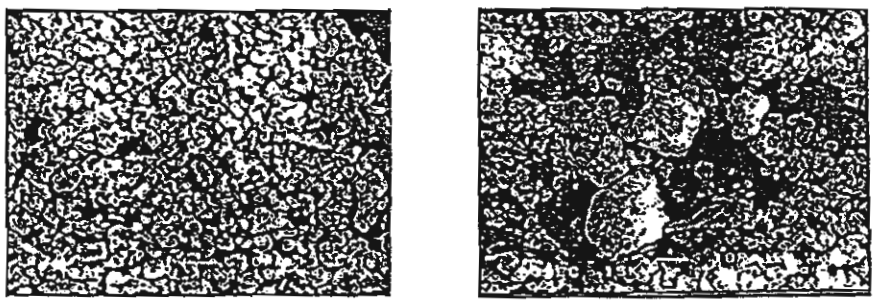

1.0%Pd/Cu/H-MFI

(a) **(b)**

Figure 3.2

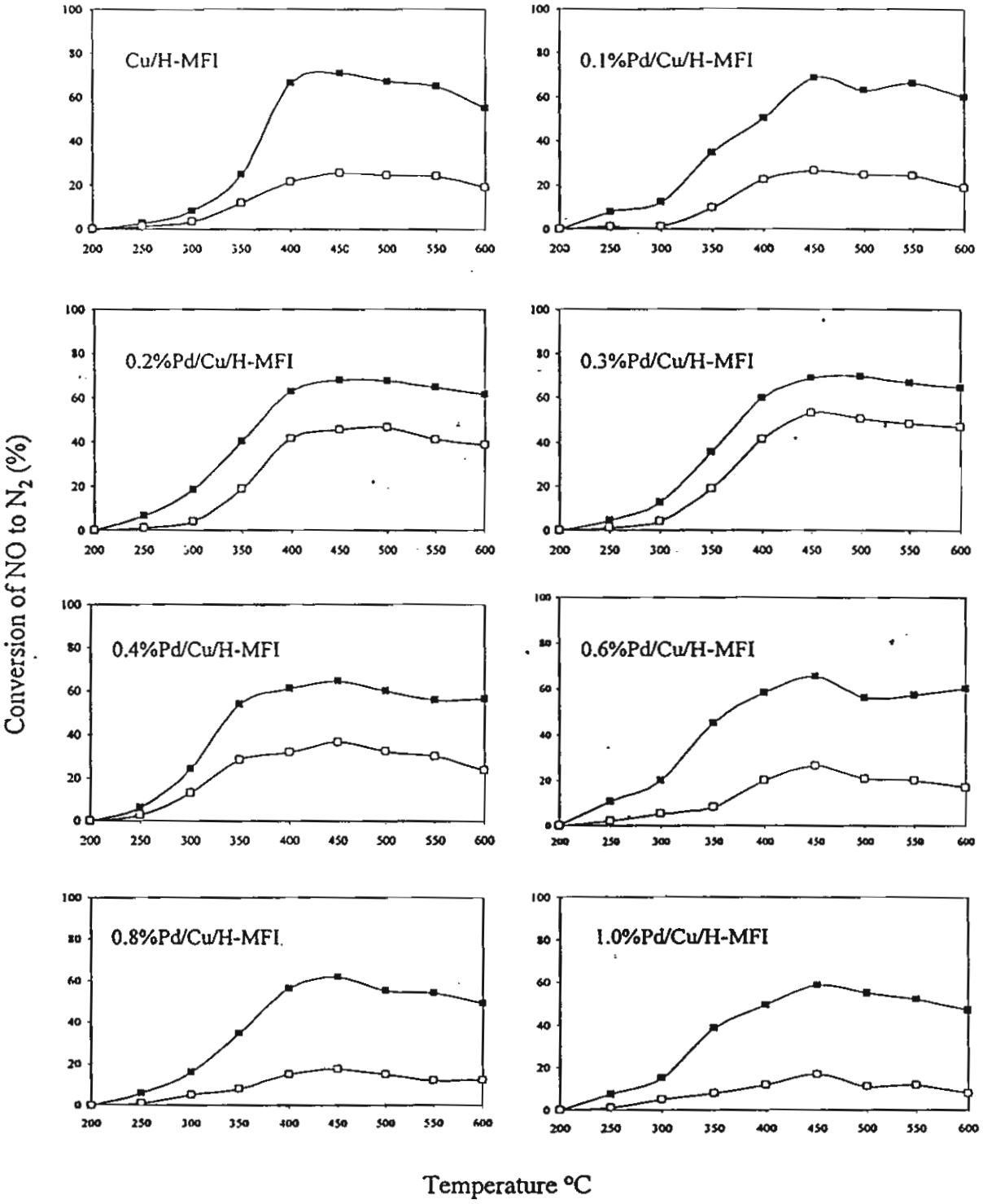
Cu/H-MFI
0.1%Pd/Cu/H-MFI
0.2%Pd/Cu/H-MFI
0.3%Pd/Cu/H-MFI
0.4%Pd/Cu/H-MFI
0.6%Pd/Cu/H-MFI
0.8%Pd/Cu/H-MFI
1.0%Pd/Cu/H-MFI
Conversion of NO to N_2 (%)
Temperature °C

Figure 4

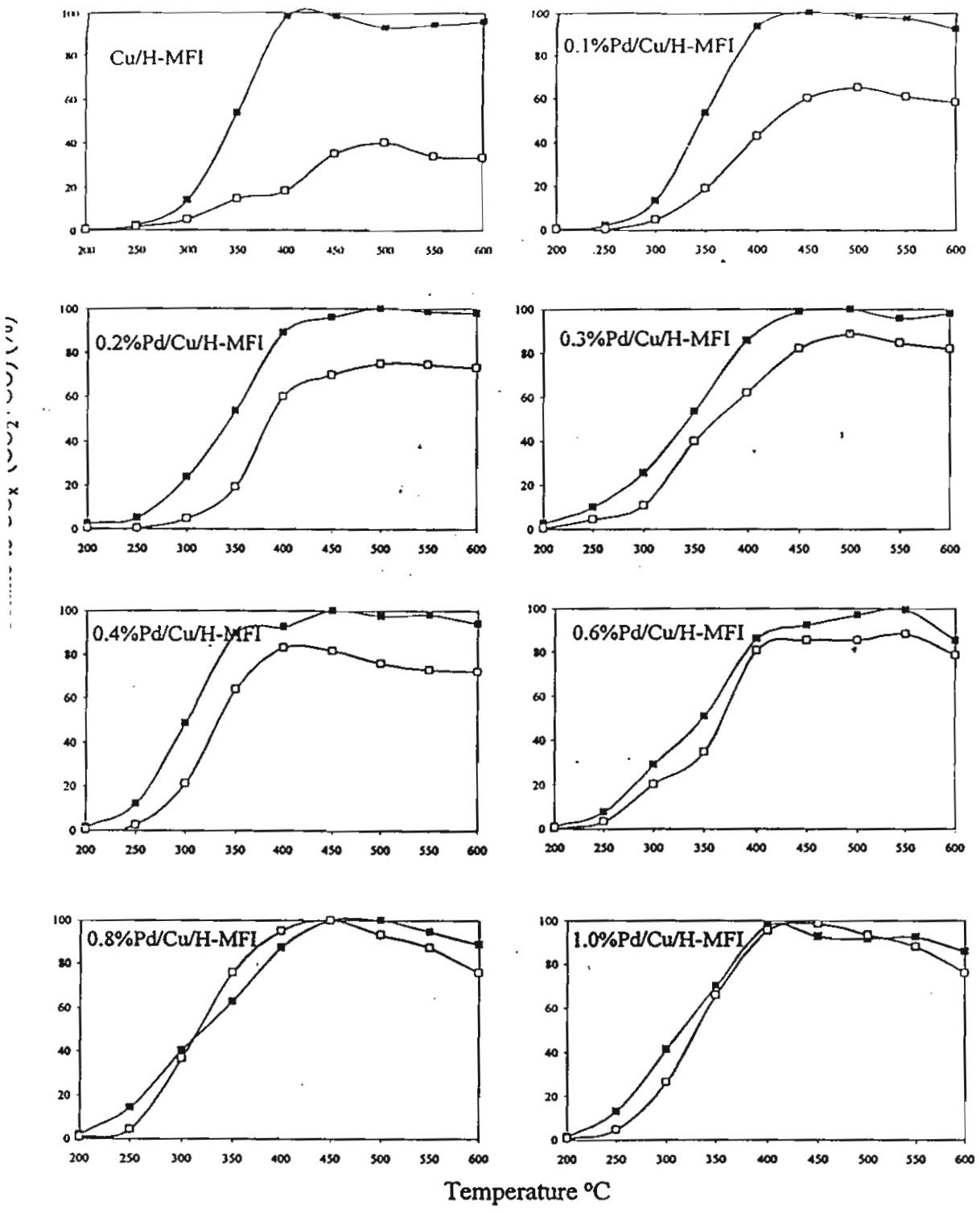
Cu/H-MFI
0.1%Pd/Cu/H-MFI
0.2%Pd/Cu/H-MFI
0.3%Pd/Cu/H-MFI
0.4%Pd/Cu/H-MFI
0.6%Pd/Cu/H-MFI
0.8%Pd/Cu/H-MFI
1.0%Pd/Cu/H-MFI
Temperature °C

Figure 5

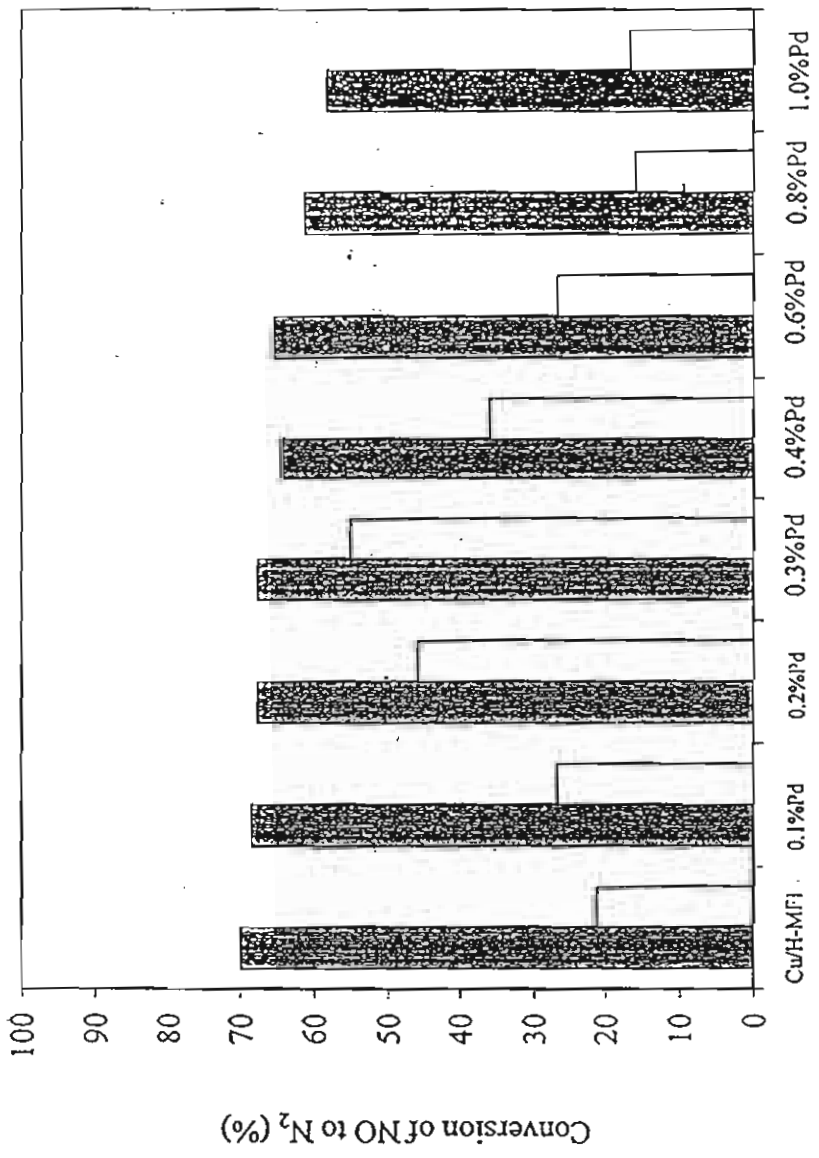
Conversion of NO to N_2 (%)
100
90
80
70
60
50
40
30
20
10
0
Cu/H-MFI
0.1%Pd
0.2%Pd
0.3%Pd
0.4%Pd
0.6%Pd
0.8%Pd
1.0%Pd
fresh catalyst
pretreated catalyst

Figure 6

Table 1. Data for bulk composition, BET surface area and crystallinity of catalysts

Figure 1 ^{27}Al MAS-NMR spectra of fresh (a) and severe steamed (b) catalysts.

Figure 2.1 ESR spectra of high spin Cu^{2+} of Cu/H-MFI and Pd/Cu/H-MFI with and without pretreatment at 800°C 10% H_2O a) fresh Cu/H-MFI, b) severe steamed Cu/H-MFI, c) fresh 0.1%Pd/Cu/H-MFI, d) severe steamed 0.1%Pd/Cu/H-MFI

Figure 2.2 ESR spectra of high spin Cu^{2+} of Cu/H-MFI and Pd/Cu/H-MFI with and without pretreatment at 800°C 10% H_2O a) fresh 0.2%Pd/Cu/H-MFI, b) severe steamed 0.2%Pd/Cu/H-MFI, c) fresh 0.3% Pd/Cu/H-MFI, d) severe steamed 0.3%Pd/Cu/H-MFI

Figure 2.3 ESR spectra of high spin Cu^{2+} of Cu/H-MFI and Pd/Cu/H-MFI with and without pretreatment at 800°C 10% H_2O a) fresh 0.4%Pd/Cu/H-MFI, b) severe steamed 0.4%Pd/Cu/H-MFI, c) fresh 0.6% Pd/Cu/H-MFI, d) severe steamed 0.6%Pd/Cu/H-MFI

Figure 2.4 ESR spectra of high spin Cu^{2+} of Cu/H-MFI and Pd/Cu/H-MFI with and without pretreatment at 800°C 10% H_2O a) fresh 0.8%Pd/Cu/H-MFI, b) severe steamed 0.8%Pd/Cu/H-MFI, c) fresh 1.0% Pd/Cu/H-MFI, d) severe steamed 1.0%Pd/Cu/H-MFI

Figure 3.1 Scanning electron micrograph of catalysts.(a) fresh and (b) severe steamed catalysts

Figure 3.2 Scanning electron micrograph of catalysts.(a) fresh and (b) severe steamed catalysts

Figure 4 The effect of hydrothermal-treatment on the activity of NO conversion of Cu/H-MFI, Pd/Cu/H-MFI. Close symbol: fresh catalysts, Open symbol: pretreated catalysts

Figure 5 The effect of hydrothermal-treatment on the activity of n-Octane conversion of Cu/H-MFI, Pd/Cu/H-MFI. Close symbol: fresh catalysts, Open symbol: pretreated catalysts

Figure 6 Maximum NO conversion of catalysts

Effect of Pd on the Stability Improvement of Cu/H-MFI for NO removal under Hydrothermal Pretreatment Conditions

P.Praserthdram, S.Phatanassri and J.Rungsimanop

Petrochemical Engineering Laboratory, Department of chemical Engineering,

Faculty of Engineering, Chulalongkorn University, Bangkok 10330,Thailand

Tel: +(662) 218-6711, Fax: +(662) 218-6769, E-mail: Piyasan.P@chula.ac.th

Abstract

The effect of Pd-modification of Cu ion-exchanged H-MFI (Pd/Cu/H-MFI) on its performance for removal was studied. The stability of the catalysts subjected to hydrothermal treatment with a He stream containing 10% stream at 800 °C was investigated. The Cu/H-MFI catalyst markedly lost its activity for NO conversion after the hydrothermal pretreatment. The Pd-modification of the Cu/H-MFI resulted in improved stability against the hydrothermal treatment with the presence of Pd loading amount approximately 0.2 to 0.3 wt%. The dealumination of tetrahedral Al in MFI framework was completely prevented with the Pd loading amount of 0.3% or higher. Further loading of Pd higher than 0.3% caused the larger crystallite size upon pretreatment as seen from the Scanning Electron Micrographs (SEM). It has been suggested that there may be some changes in Pd and Cu on H-MFI, such as alloying and/or palladium oxides formation, loading to some lost of Cu^{2+} active species for NO

removal. This results in the limitation of NO conversion improvement for the pretreated Pd/Cu/H-MFI with the loading amount of Pd higher than approximately 0.3%.

Keywords: Copper ion-exchanged MFI, Pd-modification, stability improvement, NO removal, Hydrothermal pretreatment

* To whom correspondence should be directed

1. Introduction

The environmental problems caused by emissions from stationary sources and transportation vehicles are still using despite of the recent advance in catalytic technologies base on NH_3-reduction and the use of three-way catalysts. NO emitted from combustion facilities and diesel engines causes acid rain and photochemical smog [1]. A number of studies concerning various types of catalyst for NO removal have been investigated. Cu ion-exchanged MFI type zeolite (Cu/MFI) proposed by Iwamoto et al. is effective for NO removal under the excess oxygen condition [2,3]. Other kinds of metal ion-exchanged MFI such as gallium [4,5], ion [6,7], cobalt [8-10], cerium [11,12], platinum [13], palladium [14] were also studied for the reaction. In addition, other groups of active catalysts such as transition metal and/or metal oxide (Cu, Co, Mn, Fe, Cr, V, Ag) were also concerned [15-19]. Nevertheless, any types of catalyst referred above suffer from the deactivation under the condition of high temperature and the presence of

stream possibly occurred in practical use [20-22]. On the other hand, platinum group metal catalysts have also been studied for NO conversion [23,24] and it is known that platinum group metal catalysts are highly resistant to large amounts of steam [25]. Based on these reasons, therefore, this work aims to investigate the influence of severe condition on the activity of Cu ion-exchanged MFI. The effect of Pd on the stability improvement of the catalyst for NO removal under such severe condition was also studied.

2. Experimental

2.1 Catalyst Preparation

MFI zeolite with Si/Al ratio of 50 in Na form supplied by ALSI-PENTA ZEOLITE SM-55 was made by ion exchange with ammonium nitrate solution to obtain NH_4-MFI. It was then washed, dried and calcined at 540 °C for 3.5 h in air to convert it the protonated from (H-MFI), Cu ion-exchanged H-MFI and Pd ion -exchanged H-MFI, designated as Cu/H-MFI and Pd/H-MFI were prepared using an ion-exchange procedure at 80 °C and 90 °C, respectively. They were washed, dried and calcined at 540 °C for 3.5 h in air. For Pd/Cu/H-MFI, successive ion-exchange of H-MFI with palladium was made first and then copper was carried out using the method described above. The amount of palladium was varied in the range of 0.1-1 wt% Pd. In order to investigate the stability of the catalyst under severe condition, the catalysts were heated in a He stream while elevating the temperature from room temperature to 600 °C and 600 to 800 °C with

constant heating rate of 10 and 1.67 °C /min, respectively. The catalyst samples were then kept at 800 °C for 12 h while adding 10 mol% of water vapor. The catalysts were then cooled down to room temperature in the He stream. The catalysts thus obtained were in powder form, and were tableted, crushed and sieved to 12-22 mesh to provide the reaction.

2.2 Characterization

The bulk composition and BET surface area of the samples were measured by Inductively Coupled Plasma analysis (ICP JOBIN YVON model JY 2000 S) and surface area analyzer (ASAP 2000, Micromerities) using liquid nitrogen as a probe molecule, respectively. The crystallinity of MFI was estimated by using a SIEMENS D 5000 diffractometer with CuKα radiation. Quantitative analysis of tetrahedral alumina in zeolites was conducted by Al Magnetic Angle Spinning Nuclear Magnetic Resonance (^{27}Al MAS NMR). The ^{27}Al MAS NMR spectra were obtained using a BRUKER DPX-300 spectroscopy operating at 78.2 MHz. The morphology of the catalysts was observed using a Scanning Electron Microscope (JEOL, JSM-35). To determine the state of Cu^{2+} of catalysts, ESR measurements were obtained, an exact weight of catalyst was calcined at 500°C for 2 h. to remove adsorbed species.

2.3 Reaction Method and Analysis

The catalytic reaction test was performed using a tubular flow reactor at atmospheric pressure. A 0.25 g portion of the catalyst was packed into a quartz tube reactor of 6 mm.

inner diameter. It was heated from the ambient temperature to 600°C in a He flow at a constant heating rate of 10°C/min, and maintained at that temperature for 30 min. A feed gas composed of 1000 ppm NO, 1000 ppm n-C_8H_{18}, 2 mol% O_2 and 10 mol% H_2O balanced with He was then introduced into the reactor with a GHSV of 30,000 h^{-1}. Every 30 min, after the catalytic activity was at steady state, the effluent gas composition was analyzed using gas chromatographs (SHIMADZU GC-8ATP with MS-5A column and SHIMADZU GC-8AIT with porapak Q column) equipped with integrators. The reactor temperature was then cooled down from 600 to 200°C with a constant cooling rate of 10 °C/min. After every 50 °C drop in temperature effluent gas was analyzed using the same method. The catalytic activities of NO reduction and n-octane combustion were investigated as the amount of nitrogen and carbon oxides (CO_X: CO + CO_2) produced, respectively.

3. Results and discussion

3.1 Changes in Physical properties upon pretreatment

Table 1. shows the physical properties of the catalysts before and after pretreatment. Crystallinity, as determined by XRD profiles, was calculated using the intensity of diffraction line at 23.5° 2θ, which was compared with that of H-MFI as a reference. As shown in Table 1. H-MFI and Cu/H-MFI considerably lost their crystallinity after pretreatment due to the structural collapse. Such tendency of lost in crystallinity and BET surface area was reduced with the presence of Pd, and no significant lost of

crystallinity was observed on Pd/Cu/H-MFI catalysts with amount of Pd up to 0.2% or more. This suggests the stabilization effect of Pd on MFI framework structure. It should be noted that though some lost of structure occurred after pretreatment particularly the catalysts without Pd, the content of Cu or Pd loaded was not significantly affected by the pretreatment as can be seen from the ICP data. This indicated that there was no significant loss of metal species such as evaporation of metal due to the hydrothermal treatment. The result of ^{27}Al MAS NMR of the catalysts before and after pretreatment is shown in Fig. 1. The fresh catalysts exhibited only one sharp signal at ca. 50 ppm, which is assigned to the tetrahedral aluminum in the zeolite lattice [26-28]. Hydrothermal treatment of H-MFI, Cu/H-MFI and 0.1% Pd/ Cu/ H-MFI at 800 °C caused the appearance of a new ^{27}Al MAS NMR signal at 0 ppm assigned to extra-framework Al atoms in octahedral coordination [26-28]. This is consistent with the report somewhere else of loss in activity and stability after steam pretreatment due to framework dealumination of the zeolite [27]. However, only one signal of ^{27}Al MAS NMR at around 50 ppm was observed on Pd/Cu/H-MFI with the amount of Pd 0.3% or higher even after pretreatment and no peak relating to octahedral aluminum was noticed. This suggests that the presence of a certain amount of Pd, approximately 0.3% loading as observed here, could stabilize the MFI framework structure by preventing the occurrence of dealumination.

Figure 2.1-2.4. shows the ESR spectra of Cu/H-MFI and 0.3% Pd/Cu/H-MFI. The spectra of both fresh catalysts were similar in shape which indicated the presence of two Cu^{2+} species located in two different coordination (i.e. a square pyramidal environment

with $g_{\|} = 2.31\text{-}2.33$, $A_{\|} = 149$ G (Cu^{A}) and a square planar one with $g_{\|} = 2.27\text{-}2.29$, $A_{\|} \sim$ 157 G (Cu^{B})), as is typically found in the literature [29-32]. Shelef [33] proposed that Cu^{2+} in a square planar configuration is very active for NO removal. Since the features of the Cu^{2+} species were the same for fresh Cu/H-MFI and fresh 0.3%Pd/Cu/H-MFI. it can be suggested that Pd does not have an impact on the configuration of Cu. In addition. the 0.3% Pd/Cu/H-MFI after pretreatment exhibited the same ESR features as the fresh one. Nevertheless, the ESR spectra of pretreated Cu/H-MFI and 0.1%Pd/Cu/H-MFI were different from those of the fresh one. The pretreated Cu/H-MFI and 0.1%Pd/Cu/H-MFI not only lost the intensity of the ESR spectra, but the shape of signal also changed. This means that the amount of Cu^{2+} species in both the square pyramidal and square planar coordination was diminished due to pretreatment. Additionally, a new spectrum with $g_{\|} = 2.30$, $A_{\|} = 160$ G (Cu^{C}) appeared indicating a change in the coordination of Cu^{2-} although part of the two old Cu^{2+} species remained. This new signal may be attributed to the migration of Cu ions to the locations near 5-membered oxygen rings as suggested by Iwamoto et al. [34]. On the other hand, the pretreated catalysts with 0.8-1.0 wt.% Pd *loading did not* show any change of coordinated Cu^{2+} species; however some lost of the intensity of ESR has been observed. This means that the amounts of two Cu^{2+} species in both square pyramidal and square planar coordination are diminished due to some change in Pd and Cu on H-MFI such as alloying and/or oxides formation.

The scanning electron micrographs (SEM) of the catalysts before and after hydrothermal treatment are shown in Fig.3.1-3.2. Cu/H-MFI showed an obvious agglomeration after pretreatment. As or Pd/Cu/H-MFI, such agglomeration seems to be

prevented considerably especially for the samples with the Pd loading amount ranging between 0.3 to 0.6%. However, the larger crystallite size was clearly observed on the samples with Pd loading amount 0.8 and 1.0%. This suggests that there should be some change in the Pd and Cu on the H-MFI, such as alloying, due to the hydrothermal treatment provided that the amount of Pd present is higher than a certain level. It is interesting to note that an optimum amount of Pd is necessary to stabilize the crystal morphology of Cu/H-MFI subjected to hydrothermal treatment the temperature as high as 800 °C.

3.2 Catalytic Performance

NO conversion reactions were carried out on the catalysts both with and without pretreatment. The effect of reaction temperature on NO conversion to N_2 for Cu/H-MFI and Pd/Cu/H-MFI with different amount of Pd is shown in Fig.4. The conversion of n-octane to carbon oxides (CO and CO_2) is also demonstrated. It has been found that the conversion of NO markedly decreased at any reaction temperatures after hydrothermal treatment. However, the margin difference in catalyst activity before and after pretreatment was alleviated with the presence of a certain amount of Pd (ca. 0.2-0.3% loading). When the amount of Pd was raised higher than 0.3%, such beneficial effect on the stabilization of Cu/H-MFI was surprisingly lost. As for the conversion of n-octane to carbon oxides shown in Fig. 5, Cu/H-MFI also exhibited a substantial decrease in n-octane conversion upon pretreatment. The presence of Pd improved the n-octane

conversion of the pretreated catalysts similar to NO conversion. Nevertheless, while the improvement of NO conversion for the pretreated catalysts was limited by a certain amount of Pd present, the n-octane conversion was almost continuously improved with the increasing amount of Pd. Pd/Cu/H-MFI catalysts with 0.8 and 1.0% loading of Pd, in particular, exerted more or less conversion of n-octane at the reaction temperatures higher than 400 °C after hydrothermal treatment. This indicates that n-octane would not be effective for use in NO conversion Pd/Cu/H-MFI with the high loading amount of Pd. Therefore, this should be one of the reasons for the limitation of NO conversion improvement on Pd/Cu/H-MFI after hydrothermal treatment by an optimum amount of Pd. In addition, the possibility of any changes in Pd and Cu on H-MFI such as alloying and/or the formation of palladium oxides in case of high loading amount of Pd should not be ruled out.

4. Conclusion

The MFI framework stability of Cu/H-MFI was maintained after pretreatment at 800 °C in a He stream with 10 mol% H_2O by the presence of Pd. The dealumination of tetrahedral Al in MFI framework was completely prevented when the amount of Pd loading was 0.3% or higher. The stabilization effects of Pd are due to the prevention of dealumination and the ability to maintain the active Cu^{2+} species. The optimum amount of Pd, approximately 0.2-0.3% loading, present in Pd/Cu/H-MFI improved the catalysts stability for NO removal under hydrothermal treatment conditions as concluded in Fig. 6.

Further loading of Pd higher than 0.3% may cause some changes in Pd and Cu on H-MFI, such as alloying and/or palladium oxides formation, leading to some lost of Cu^{2-} active species for NO removal. This results in the limitation of NO conversion improvement for the pretreated Pd/Cu/H-MFI with the loading amount of Pd higher than approximately 0.3%.

Acknowledgement

The authors wish to express their deep appreciation to the Thailand Research Fund (TRF) for the financial support to this work.

References

1. Impens, R., Stud. Surf. Sci. Catal., 1987, 30, 11.
2. Iwamoto, M., Yahiro, H., Tanda, K., Mizuno, N., Mine, Y. and Kagawa, S., J. Phys. Chem., 1991, 95, 3727.
3. Iwamoto, M., Yahiro, H., Mizuno, N., Zhang, W., Mine, Y., Furukawa, H. and Kagawa, S., J. Phys. Chem., 1992, 96, 9360.
4. Burch, R., Scire, S., Appl. Catal. B, 1994, 3, 295.
5. Yogo, K., Tanaka, S., Ihara, M., Hishiki, T. and Kikuchi, E., Chem. Lett., 1992, 1025.
6. Tabata, T., Kokitsu, M. and Okada, O., Appl. Catal. B, 1993, 2, L1.
7. Iwamoto, M., Yahiro, H., Shundo, S., Yu, Y. and Mizuno, N., Appl. Catal., 1991,69, L15.

8. Sato, S., Hirabayashi, H., Yahiro, H., Mizuno, N. and Iwamoto, M., Catal. Lett., 1992,12, 193.

9. Li, Y. and Armor, J. N., Appl. Catal. B, 1993,2, 239.

10. Li, Y. and Armor, J. N., Appl. Catal. B, 1993,3, 55.

11. Aylor, A.W., Lobree, L. J., Reimer, J. A. and Bell, A. T., Stud. Surf. Sci. Catal., 1996, 101, 661.

12. Yokoyama, C. and Misuno, M., Catal. Lett., 1994, 29, 1.

13. Kintaichi, Y., Hamada, H., Tabata, M., Sasaki M. and Ito T., Catal. Lett., 1990, 6, 239.

14. Hirabayashi, H., Yahiro, H., Mizuno, N. and Iwamoto, M., Chem. Lett., 1992, 2235.

15. Hamada, H., Kintaichi, Y., Sasaki, M., Ito, T., Appl. Catal., 1990, 64, L1.

16. Tabata, M., Tsuchida, H., Miyamoto, K., Yoshinari, T., Yamazaki, H., Hamada, H., Kintaichi Y., Sasaki, M. and Ito, T., Appl. Catal. B, 1995, 6, 169.

17. Hamada, H., Kintaichi, Y., Sasaki, M., Ito, T. and Tabata, M., Appl. Catal., 1991, 75, L1.

18. Miyadera, T., Appl. Catal. B, 1993, 2, 199.

19. Ukisu, Y., Sato, S., Abe, A. and Yoshida, K., Appl. Catal. B, 1993, 2, 147.

20. Burch, R., Ramli, A., Appl. Catal. B, 1998, 15, 49.

21. Kharas, K.C.C., Robota, H. J. and Liu, D. J., Appl. Catal. B, 1993, 2, 225.

22. Martinez, A., Gomez, S. A. and Fuentes, G. A., Catalyst Deactivation, 1997, 225.

23. Burch, R., Scire, S., Appl. Catal. B, 1994, 3, 295.

24. Burch, R., Ramli, A., Appl. Catal. B, 1998, 15, 49.

25. Hirabayashi, H., Yahiro, H., Mizuno, N. and Iwamoto, M., Chem. Lett., 1992, 2235.

26. Tanabe, T., Iijima, T., Kaiwai, A., Mizuno, J., Yokota, K. and Isogai, A., Appl. Catal. B, 1995, 6, 145.

27. Budi, P., Hyde, E. C. and Howe, R. F., Catal. Lett., 1996, 41, 47.

28. Tanabe, T., Kokitsu, M., Okada, O., Nakayama, T., Yasumatsu, T. and Sakane, H., Stud. Surf. Sci. Catal., 1994, 88, 409.

29. Matsumoto, S., Yokota, K., Doi, H., Kimura, M., Sekizawa, K. and Kasahara, S., Catal. Today, 1994, 22, 127.

30. Grunert, W., Hayes, N. W., Joyner, R. W., Shpiro, E. S., Siddiqui, M. R. H. and Baeva, N., J. Phys. Chem., 1994, 98, 10832.

31. Kucherov, A. V., Shigapov, A. N., Ivanov, A. A. and Shelef, M., J. Catal., 1999, 186, 334.

32. Tapanee, D., Piyasan, P., Kim, J. B., Inui, T., Advances in Environmental Research, 2000, 3, 450.

33. Shelef M., Catal. Lett., 1992, 15, 305.

34. Iwamoto, M., Wang, J., Sperati, K. M., Sajaki, T., and Misono, M., Chem. Lett., 1997, 1281.

Table 1. Data for bulk composition, BET surface and crystallinity of catalysts

Catalyst	BET surface area (m^2 /g. catalyst)		Me/Al atomic ratio		Me/Al atomic ratio		Crystallinity[a] (%)	
			Cu/Al		Pd/Al			
	fresh	severe steamed	fresh	severe steamed	fresh	severe steamed	fresh	severe steamed
H-ZSM-5	350	295	-	-	-	-	100	48
Cu/HZSM-5	326	286	0.911	0.913	-	-	100	85
0.1% Pd/Cu/HZSM-5	310	275	0.890	0.892	0.012	0.012	99	87
0.2% Pd/Cu/HZSM-5	310	289	0.901	0.892	0.023	0.022	99	97
0.3% Pd/Cu/HZSM-5	302	290	0.865	0.863	0.035	0.034	99	98
0.4% Pd/Cu/HZSM-5	300	289	0.864	0.860	0.042	0.048	98	98
0.6% Pd/Cu/HZSM-5	298	280	0.849	0.850	0.072	0.074	97	98
0.8% Pd/Cu/HZSM-5	298	288	0.827	0.824	0.088	0.089	97	97
1.0% Pd/Cu/HZSM-5	298	286	0.821	0.821	0.112	0.110	98	97

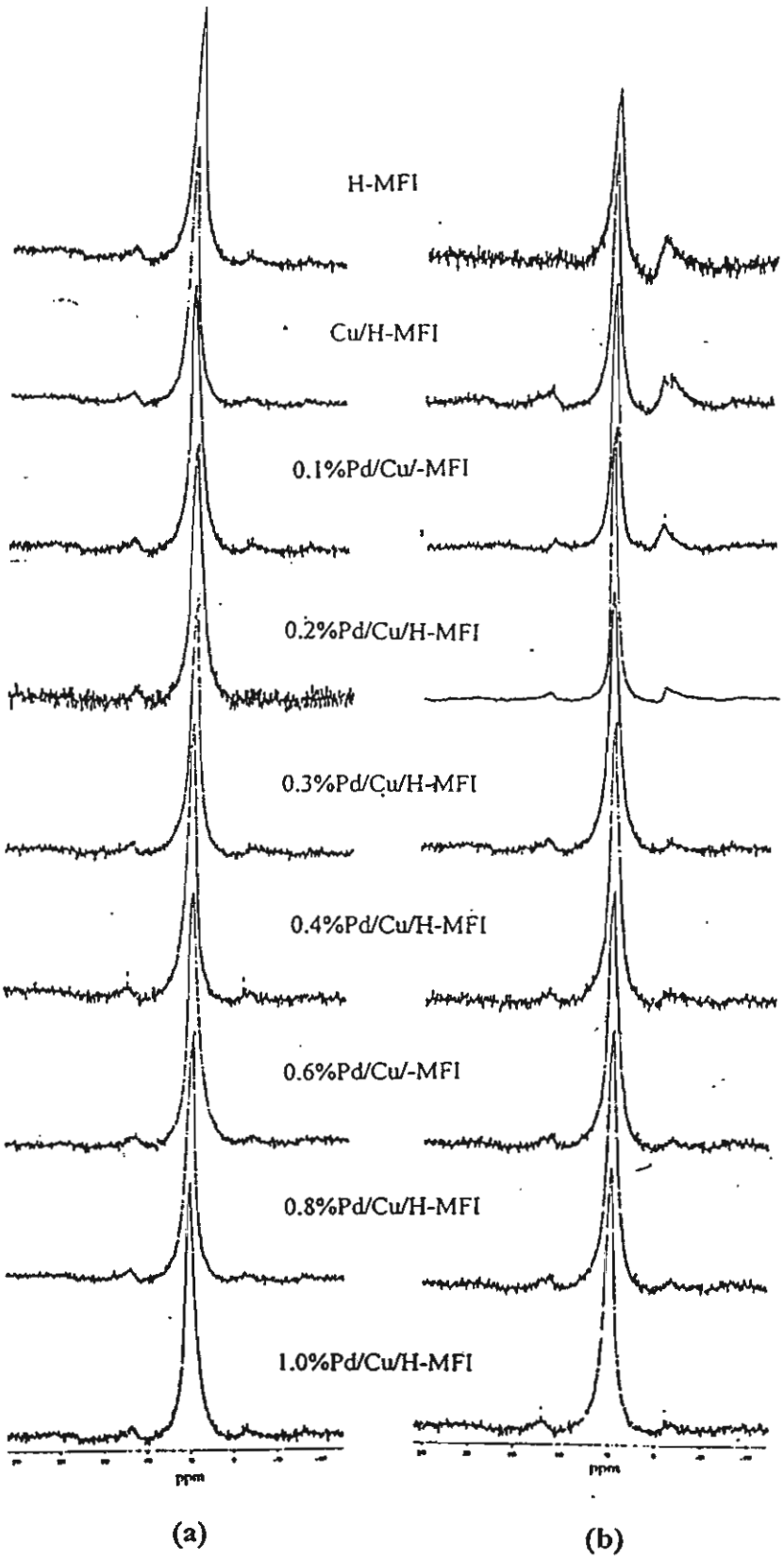
H-MFI
Cu/H-MFI
0.1%Pd/Cu/-MFI
0.2%Pd/Cu/H-MFI
0.3%Pd/Cu/H-MFI
0.4%Pd/Cu/H-MFI
0.6%Pd/Cu/-MFI
0.8%Pd/Cu/H-MFI
1.0%Pd/Cu/H-MFI
ppm
ppm
(a)
(b)

Figure 1.

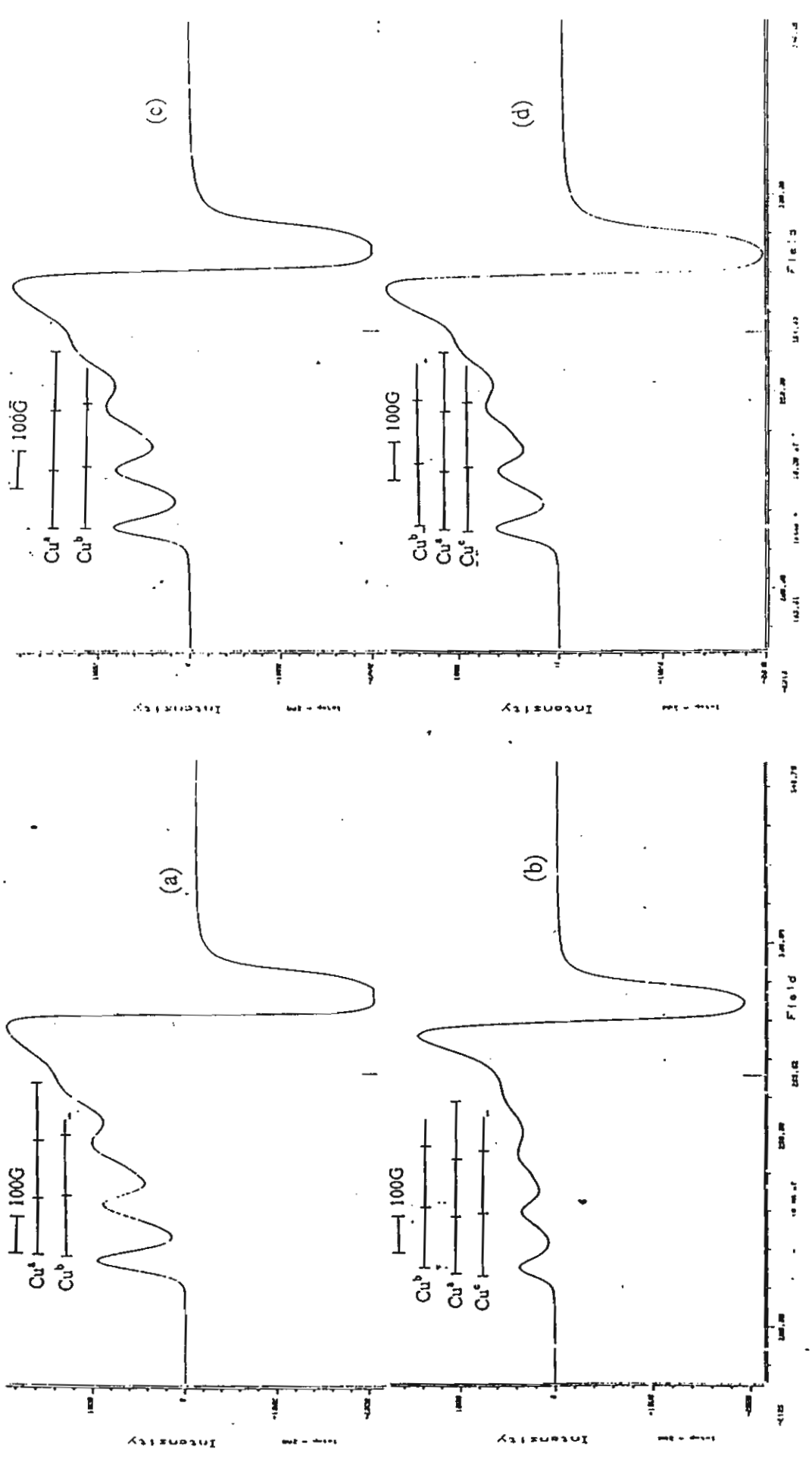

Figure 2.1

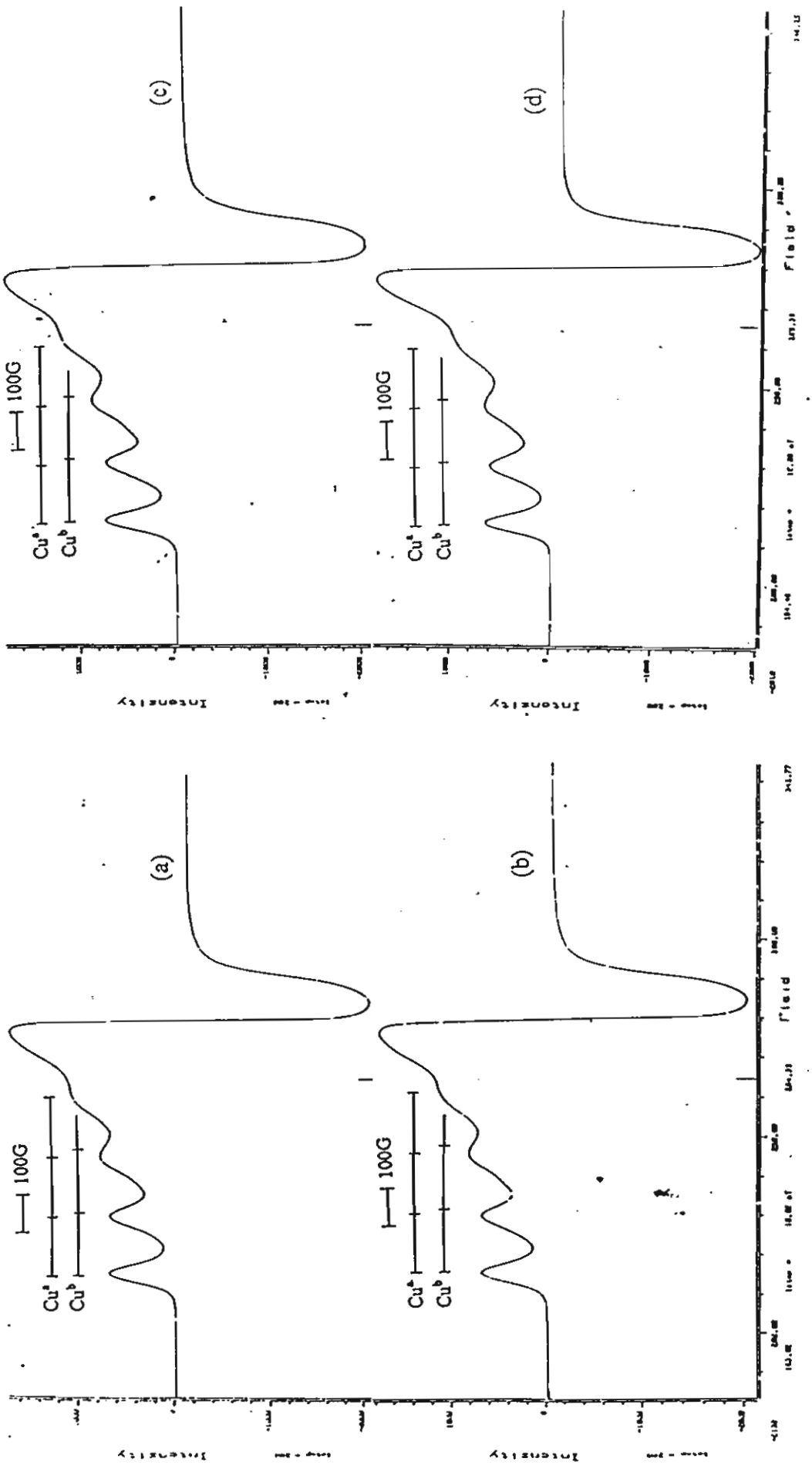

Figure 2.2

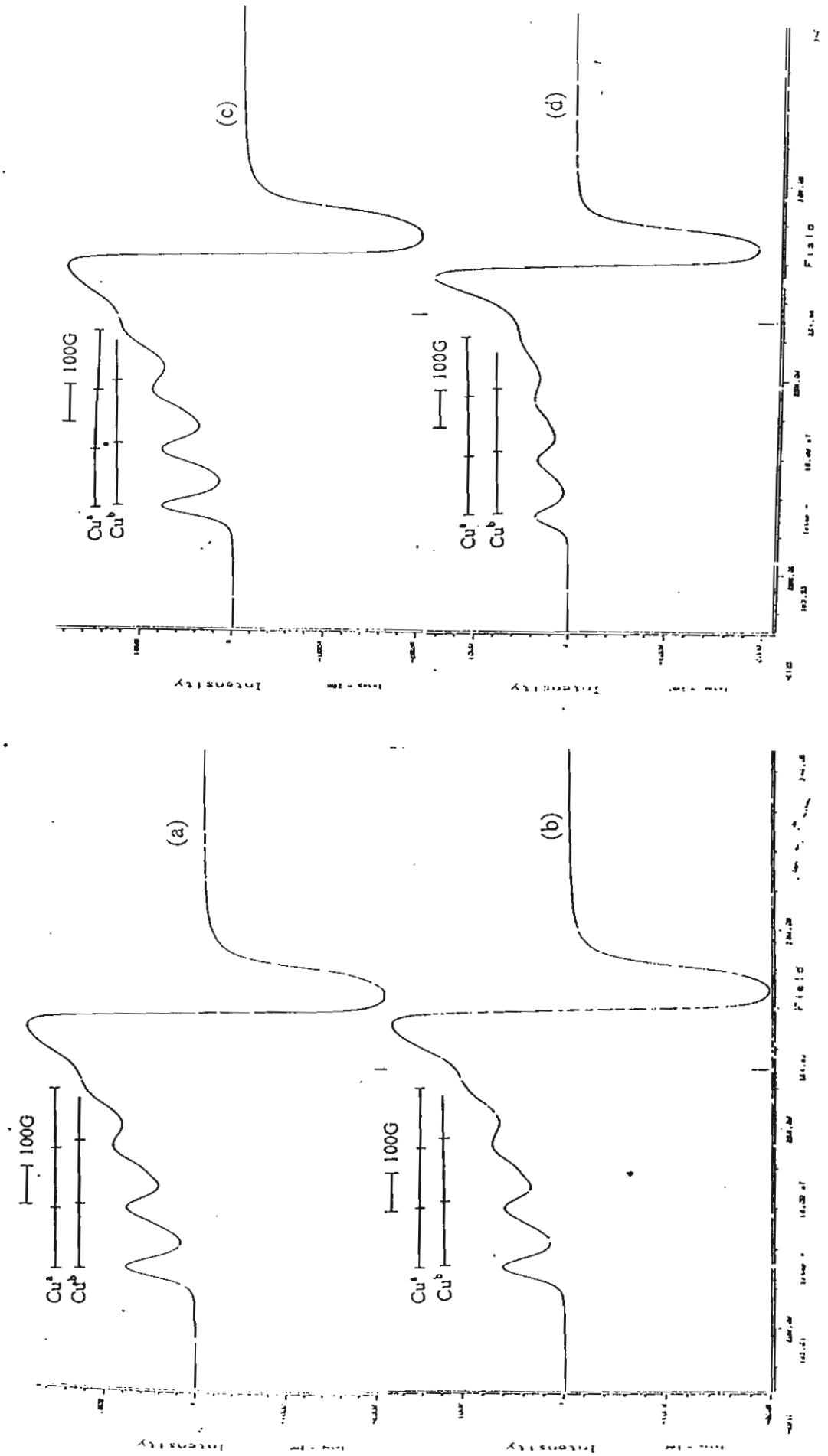

Figure 2.3

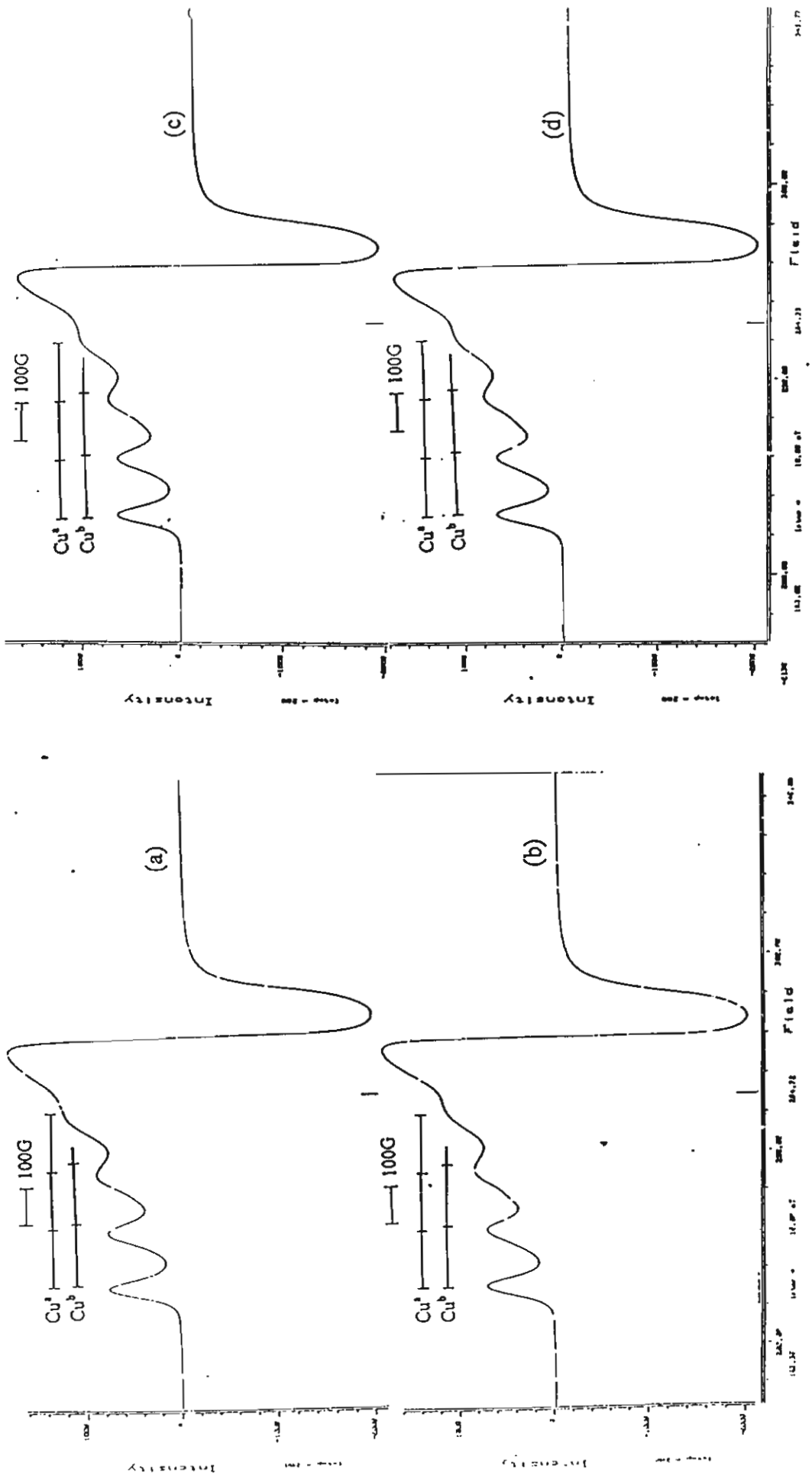

Figure 2.4

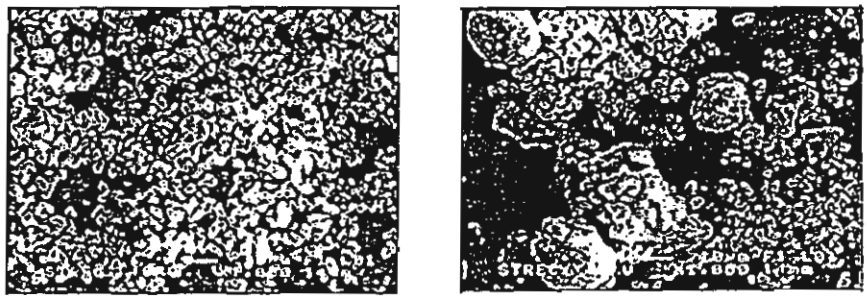

Cu/H-MFI

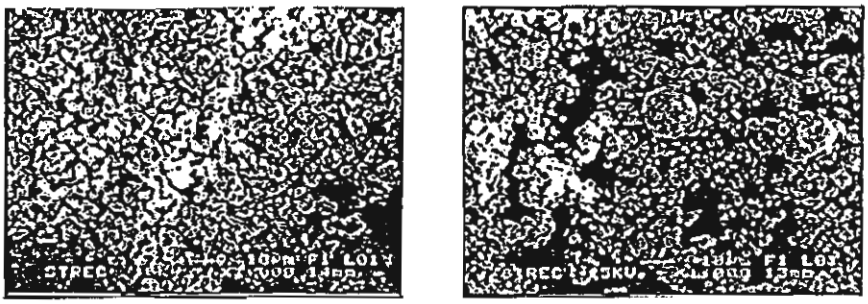

0.1%Pd/Cu/-MFI

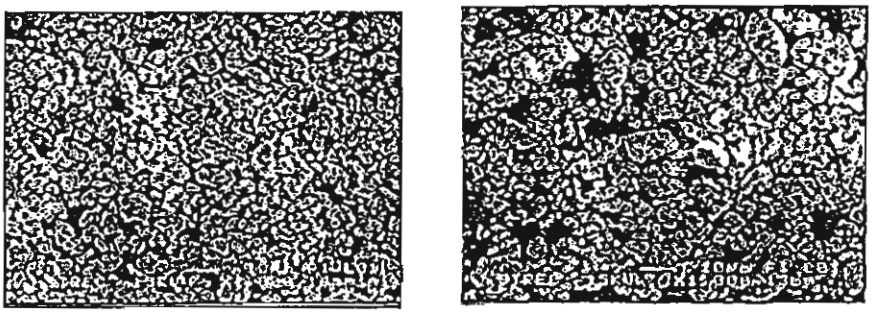

0.2%Pd/Cu/H-MFI

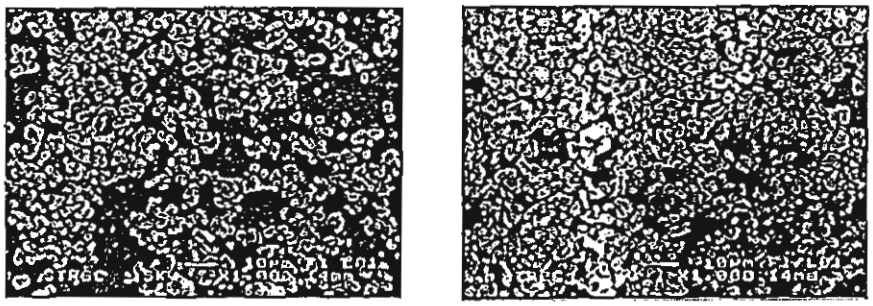

0.3%Pd/Cu/H-MFI

(a) (b)

Figure 3.1

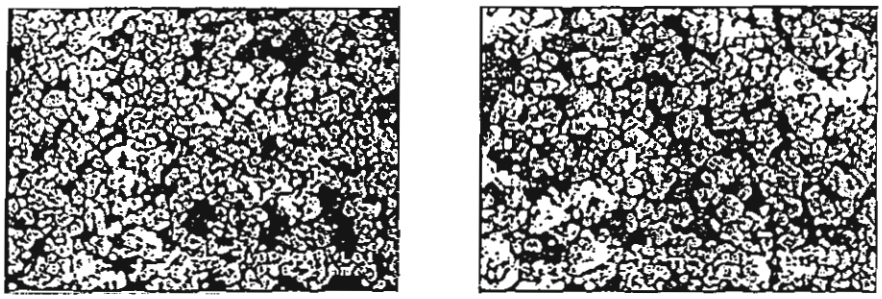

0.4%Pd/Cu/H-MFI

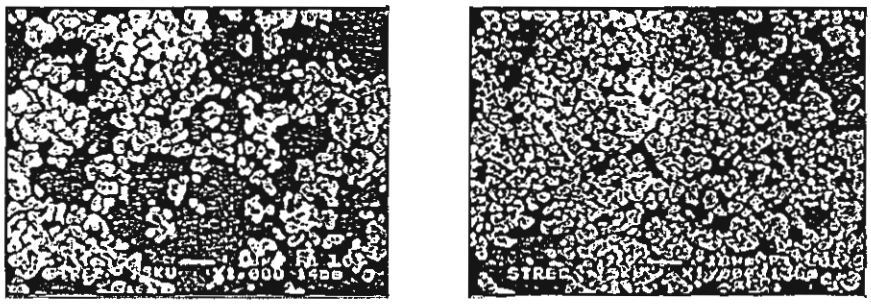

0.6%Pd/Cu/-MFI

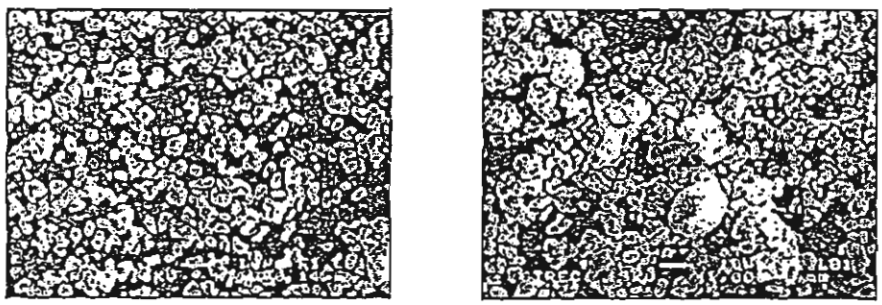

0.8%Pd/Cu/H-MFI

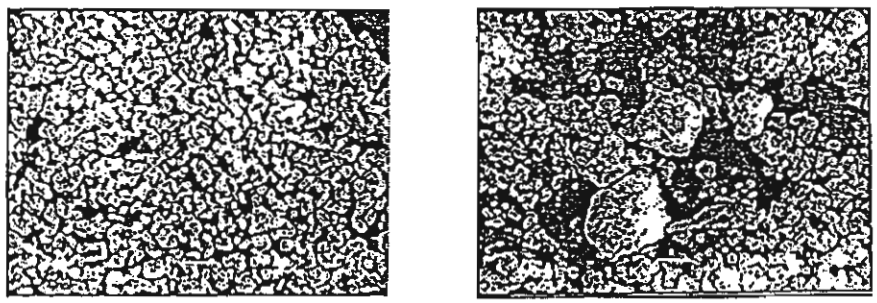

1.0%Pd/Cu/H-MFI

(a) (b)

Figure 3.2

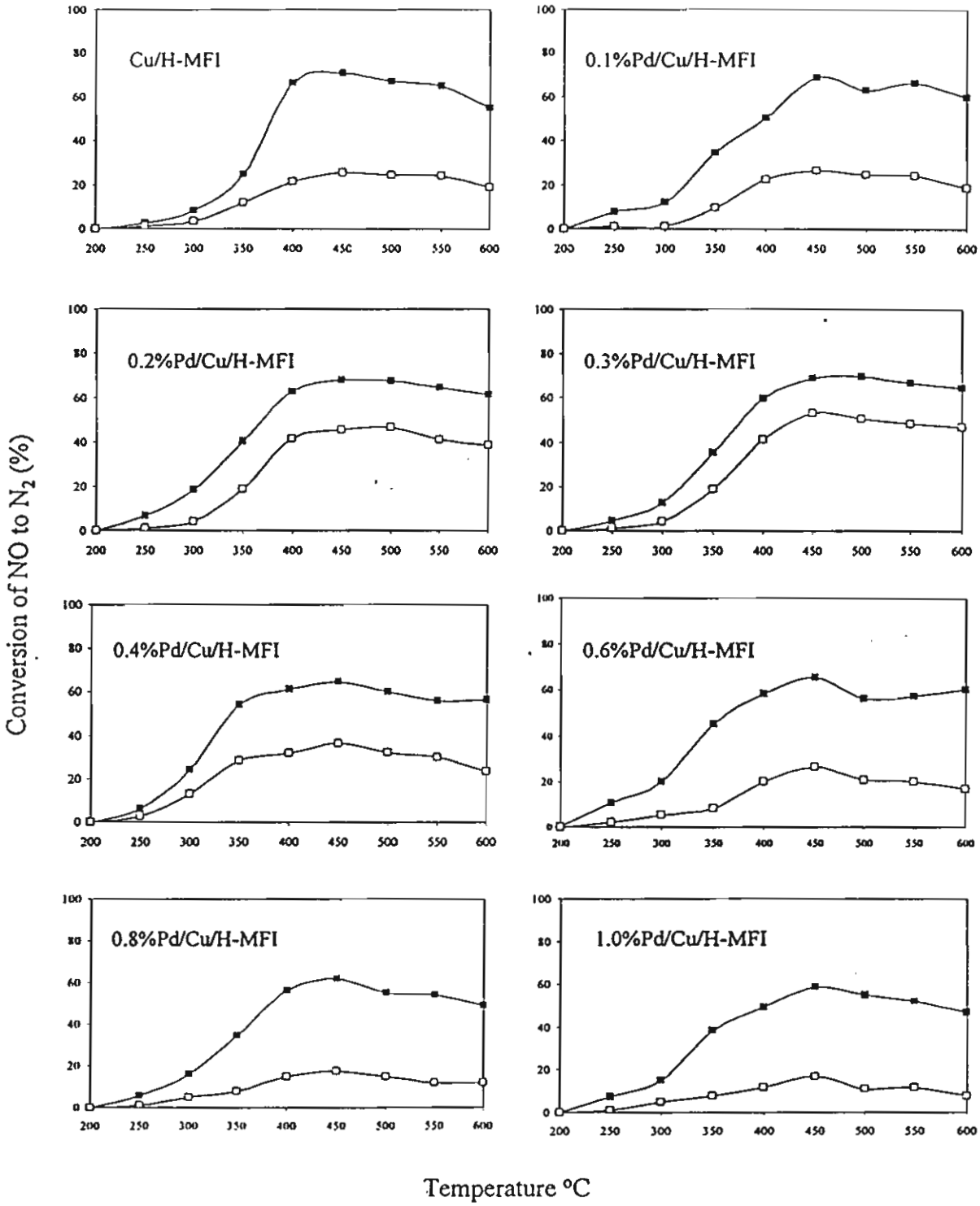
Cu/H-MFI
0.1%Pd/Cu/H-MFI
0.2%Pd/Cu/H-MFI
0.3%Pd/Cu/H-MFI
0.4%Pd/Cu/H-MFI
0.6%Pd/Cu/H-MFI
0.8%Pd/Cu/H-MFI
1.0%Pd/Cu/H-MFI
Conversion of NO to N_2 (%)
Temperature °C

Figure 4

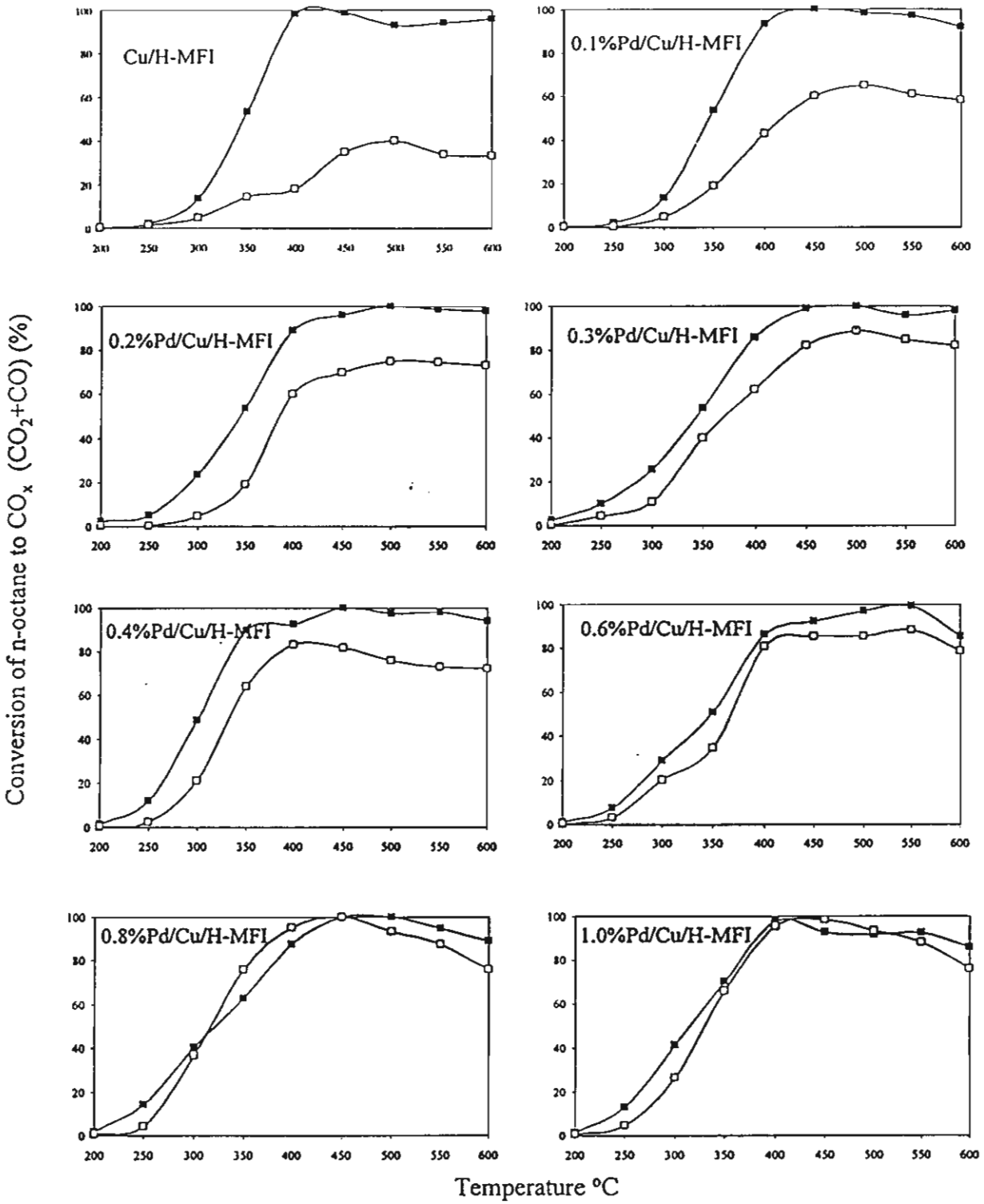
Cu/H-MFI
0.1%Pd/Cu/H-MFI
0.2%Pd/Cu/H-MFI
0.3%Pd/Cu/H-MFI
0.4%Pd/Cu/H-MFI
0.6%Pd/Cu/H-MFI
0.8%Pd/Cu/H-MFI
1.0%Pd/Cu/H-MFI
Conversion of n-octane to CO_x (CO_2+CO) (%)
Temperature °C

Figure 5

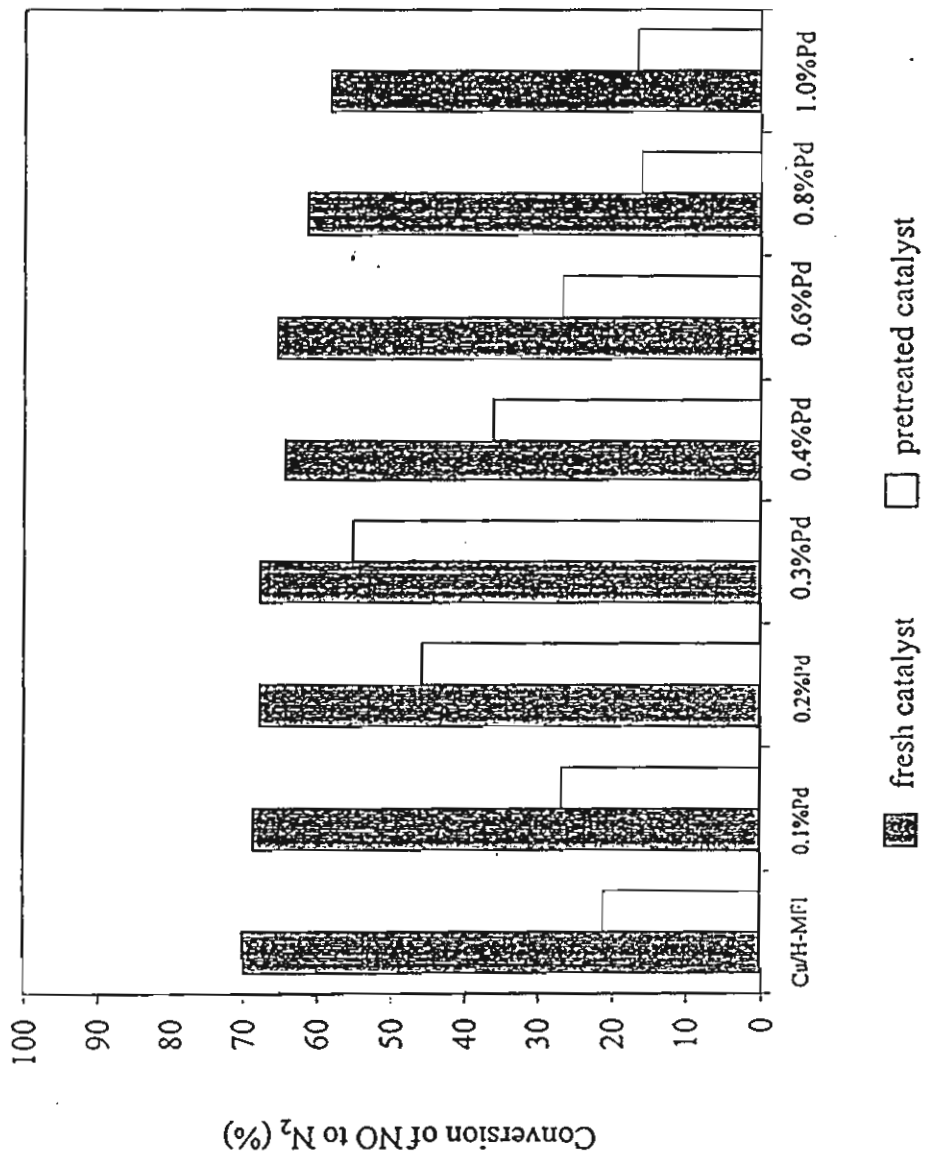
Conversion of NO to N_2 (%)
100
90
80
70
60
50
40
30
20
10
0
Cu/H-MFI
0.1%Pd
0.2%Pd
0.3%Pd
0.4%Pd
0.6%Pd
0.8%Pd
1.0%Pd
fresh catalyst
pretreated catalyst

Figure 6

Table 1. Data for bulk composition, BET surface area and crystallinity of catalysts

Figure 1 ^{27}Al MAS-NMR spectra of fresh (a) and severe steamed (b) catalysts.

Figure 2.1 ESR spectra of high spin Cu^{2+} of Cu/H-MFI and Pd/Cu/H-MFI with and without pretreatment at 800°C 10% H_2O a) fresh Cu/H-MFI, b) severe steamed Cu/H-MFI, c) fresh 0.1%Pd/Cu/H-MFI, d) severe steamed 0.1%Pd/Cu/H-MFI

Figure 2.2 ESR spectra of high spin Cu^{2+} of Cu/H-MFI and Pd/Cu/H-MFI with and without pretreatment at 800°C 10% H_2O a) fresh 0.2%Pd/Cu/H-MFI, b) severe steamed 0.2%Pd/Cu/H-MFI, c) fresh 0.3% Pd/Cu/H-MFI, d) severe steamed 0.3%Pd/Cu/H-MFI

Figure 2.3 ESR spectra of high spin Cu^{2+} of Cu/H-MFI and Pd/Cu/H-MFI with and without pretreatment at 800°C 10% H_2O a) fresh 0.4%Pd/Cu/H-MFI, b) severe steamed 0.4%Pd/Cu/H-MFI, c) fresh 0.6% Pd/Cu/H-MFI, d) severe steamed 0.6%Pd/Cu/H-MFI

Figure 2.4 ESR spectra of high spin Cu^{2+} of Cu/H-MFI and Pd/Cu/H-MFI with and without pretreatment at 800°C 10% H_2O a) fresh 0.8%Pd/Cu/H-MFI, b) severe steamed 0.8%Pd/Cu/H-MFI, c) fresh 1.0% Pd/Cu/H-MFI, d) severe steamed 1.0%Pd/Cu/H-MFI

Figure 3.1 Scanning electron micrograph of catalysts.(a) fresh and (b) severe steamed catalysts

Figure 3.2 Scanning electron micrograph of catalysts.(a) fresh and (b) severe steamed catalysts

Figure 4 The effect of hydrothermal-treatment on the activity of NO conversion of Cu/H-MFI, Pd/Cu/H-MFI. Close symbol: fresh catalysts, Open symbol: pretreated catalysts

Figure 5 The effect of hydrothermal-treatment on the activity of n-Octane conversion of Cu/H-MFI, Pd/Cu/H-MFI. Close symbol: fresh catalysts, Open symbol: pretreated catalysts

Figure 6 Maximum NO conversion of catalysts

Isomerization of n-Hexane over Platinum Ion-Exchanged Zeolite Beta

*S. Phatanasri, P. Praserthdam, S. Kularbkeaw , and S. Panichsarn

Petrochemical Engineering Laboratory, Department of Chemical Engineering, Faculty of Engineering, Chulalongkorn University, Bangkok 10330, Thailand Tel: +(662) 218-6890 Fax: +(662) 218-6877

Abstract - Zeolite Beta was synthesized from appropriate gels and crystallized under the controlled temperature and pressurized conditions. For isomerization of n-hexane, platinum ion-exchanged zeolite Beta exhibited high activity and selectivity for 2,2-Dimethylbutane (2,2-DMB), 2,3-dimethylbutane (2,3-DMB), 2-Methylpentane (2-MP) and 3-Methylpentane (3-MP). As high as 72% of n-hexane conversion and 98% of product selectivity were obtained at 250°C, 1600 h^{-1} for 20 min on stream. The influences of reaction temperature, space velocity, as well as the catalyst stability were also studied. Pt/H-Beta zeolite was recommended as one of the promising catalyst for n-hexane isomerization due to its high activity and stability. The combined effect of the stronger acidity possessed by H-Beta and the dehydrogenation role played by Pt was believed to be responsible for the good catalytic performance of Pt/H-Beta.

Key word: isomerization, n-hexane, zeolite beta, Pt-ion-exchanged zeolite beta

INTRODUCTION

Zeolite Beta is a 12-member ring (12MR) tridirectional zeolite, with two different types of channels having about 7.0 and 5.5 A°[1]. It can be synthesized within a wide range of silica-to-alumina ratio (12-200) [2]. This zeolite may offer interesting opportunities as a catalyst for the isomerization and transalkylation of xylenes[2,3], the alkylation of

* To whom correspondence should be made

toluene by methanol[4], and the condensation of benzene and formaldehyde[5]. Furthermore, the isomerization processes were run over bifunctional zeolite Beta consisting of highly dispersed metals[2,3].

Therefore, this work aims to investigate the synthesis of zeolite Beta and the performance of zeolite Beta for isomerization of n-hexane.

EXPERIMENTAL

Catalyst Preparation

Zeolite Beta was synthesized by hydrothermal technique under autogenous pressure following the procedure reported earlier [1]. The synthesis batch consists of K_2O : $2Na_2O$: 12.5 $(TEA)_2O$: $0.5Al_2O_3$: $40SiO_2$: $700H_2O$: 0-3HCl.

The crystallization period was for 40 hours at 135°C. After the crystallization the solid material thus obtained was separated by centrifugation and decantation, dried in an oven at 110°C overnight. The as-synthesized zeolite Beta was calcined at 773 K and repeatedly ion exchanged with 1 M ammonium nitrate solution. Another calcination again at 773 K converted the NH_4-Beta to its proton form, H-Beta. The Pt ion-exchange was conducted by adding 1 g of catalyst in 40 ml of distilled water. The mixture was heated from room temperature to 98°C, then $Pt(NH_3)_4Cl_2$ solution was added into the mixture and heated at 98°C for additional 6 h. The sample was dried overnight at 110 °C. Dry crystals were heated to 350°C in 50 ml/min of air stream with a constant heating rate of 3°C/min and maintained at that temperature for 10 min. The amount of Pt loading in the catalyst was 0.6 wt%. The catalysts were tableted, crushed and sieved to the range of 8-16 mesh to provide the reaction.

APPARATUS AND REACTION METHOD

The isomerization of n-hexane was carried out by using a conventional flow tubular reactor. A 0.3 g portion of the catalyst was packed in the quartz tubular reactor. The reaction was carried out under the following conditions: atmospheric pressure; gas hourly space velocities (GSHV), 380-3200 h^{-1}; reaction temperatures, 150-350°C.

RESULTS AND DISCUSSION

Effect of reaction temperatures

The reaction temperatures of n-hexane conversion were varied as 150, 200, 250, 300 and 350°C. The reaction was carried out over Pt/H-Beta (Si/Al = 40, 0.6%wt Pt loaded by ion exchange) at GHSV of 650 h^{-1} for 20 min on stream by using hydrogen as carrier gas.

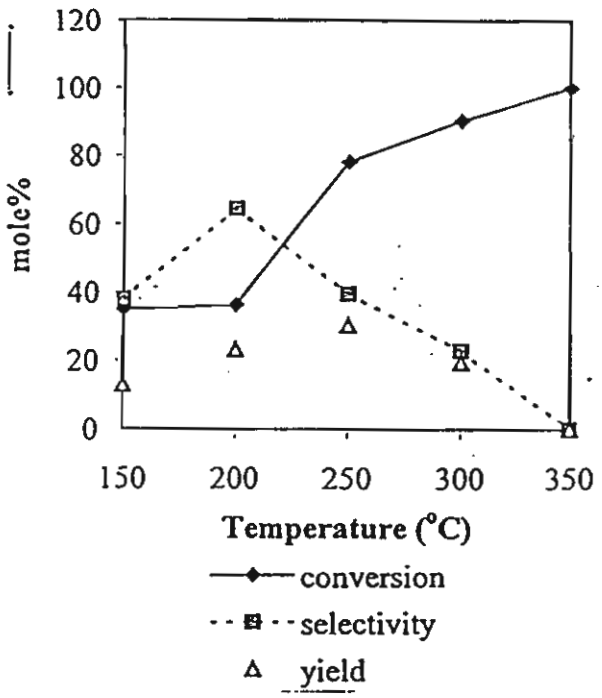

Fig.1 Isomerizationof n-hexane on Pt/H-Beta at various temperatures reaction conditions: 650 h^{-1}, 20 min on stream.

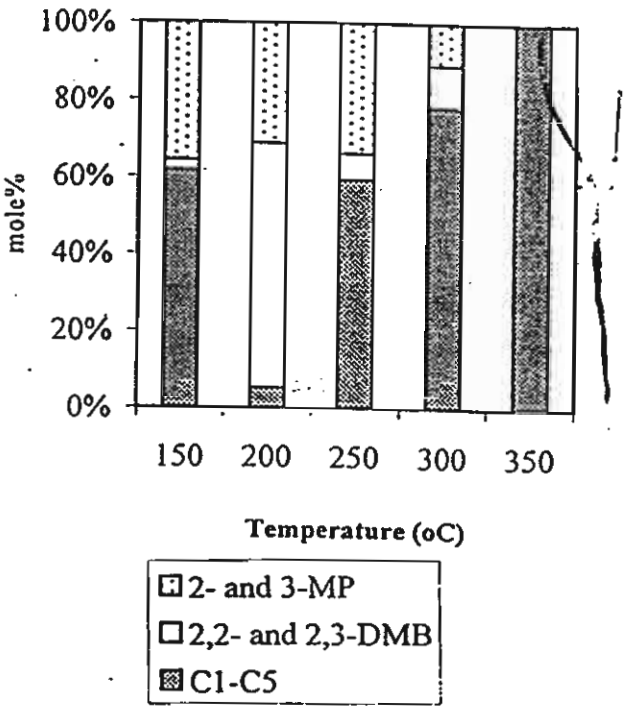

Fig.2 Product distribution of n-hexane isomerization of Pt/H-Beta.

The conversion and selectivity of n-hexane isomerization are shown in Figs. 1 and 2. It has been found that the hexane conversion increased with the increasing temperature and nearly complete conversion was obtained at 350°C. The isomers selectivity (2,2-DMB, 2,3-DMB, 2-MP, 3-MP) was high at the reaction temperatures of 200-250°C. The maximum yield, defined as the product of conversion and selectivity, was obtained at reaction temperature of 250°C. At temperatures higher than 250°C, much C_1-C_5 amount was formed probably due to the catalytic cracking.

Effect of GHSV

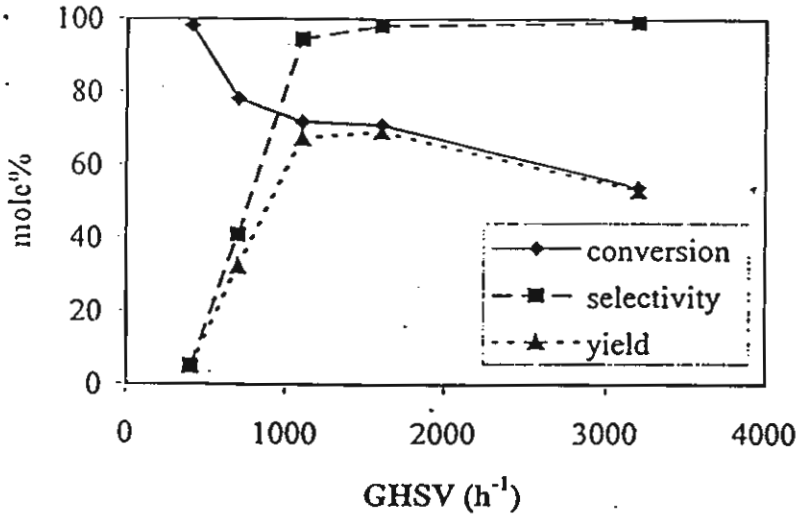

Fig.3 Isomerization of n-hexane on Pt/H-Beta at different space velocities reaction conditions: 250°C, 20 min on stream.

Figure 3 shows the conversion and selectivity of n-hexane isomerization over Pt/H-Beta with space velocities (GHSV) ranging from 400 to 3200h^{-1}. The reaction was carried out at 250°C for 20 minutes on stream by using hydrogen as carrier gas. At higher GHSV the contact time between hexane and catalyst was shortened and thus the conversion decreased; however, the amount of C_6 isomers (2,2-DMB, 2,3-DMB, 2-

MP, 3-MP) was markedly increased. It should be noted that at low GHSV especially 380 h^{-1}, the main product was C_1-C_5 fraction. It has been suggested that C_1-C_5 should be formed through catalytic cracking of C_6 isomer during the long contact time. Therefore at high GHSV, the formation of C_1-C_5 was substantially prevented and thus the high yield of isomer products was obtained.

Prolonged operation test

The catalyst stability was tested by prolonged operation at 250°C and GHSV of 1600 h^{-1} for 13 h as shown in Fig. 4. The conversion and selectivity of n-hexane isomerization were almost constant throughout the period. It has been generally accepted that Pt on the catalyst may act as hydrogen porthole to transfer hydrogen to the adsorbate species on the catalyst surface, and thus the coke formation was significantly suppressed.

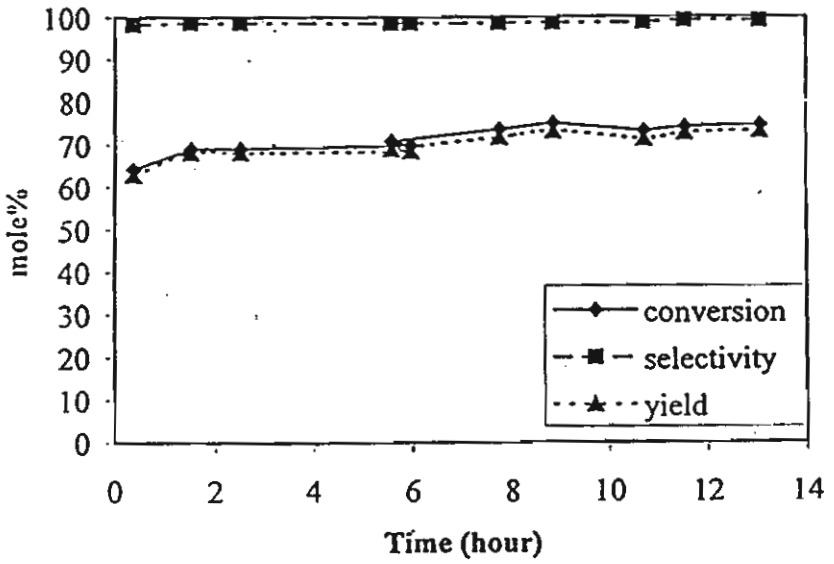

Fig.4 Prolonged operation of n-hexane isomerization on Pt/H-Beta
reaction conditions: 250°C, 1600 h^{-1}.

Comparison of Pt/H-Beta and Pt/H-Y

From Figs. 5 and 6, the conversion and selectivity of n-hexane isomerization was compared when using Pt/H-Beta and Pt/H-Y as the catalysts with the same amount of platinum loading (0.6%wt). It has been found that the Pt/H-Beta gave much higher conversion than did Pt/H-Y zeolite. It has been realized that Pt/H-Beta and Pt/H-Y have substantially

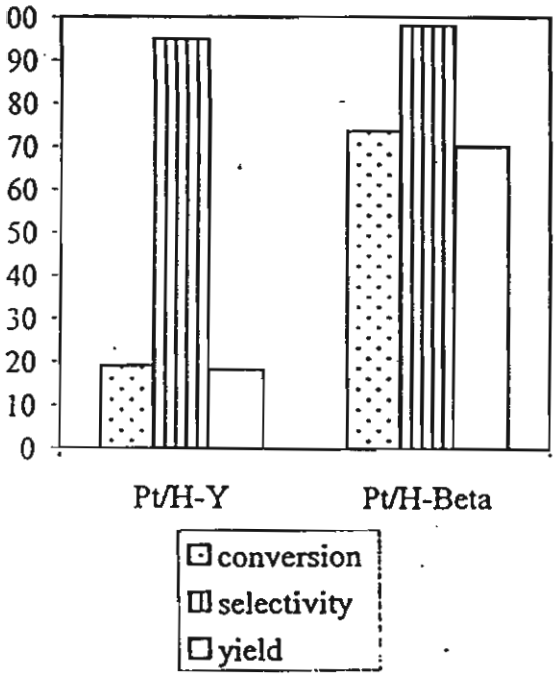

Fig. 5 Isomerization of n-hexane on Pt/H-Y and Pt/H-Beta
reaction conditions: 250°C, 1600 h^{-1}, 20 min on stream.

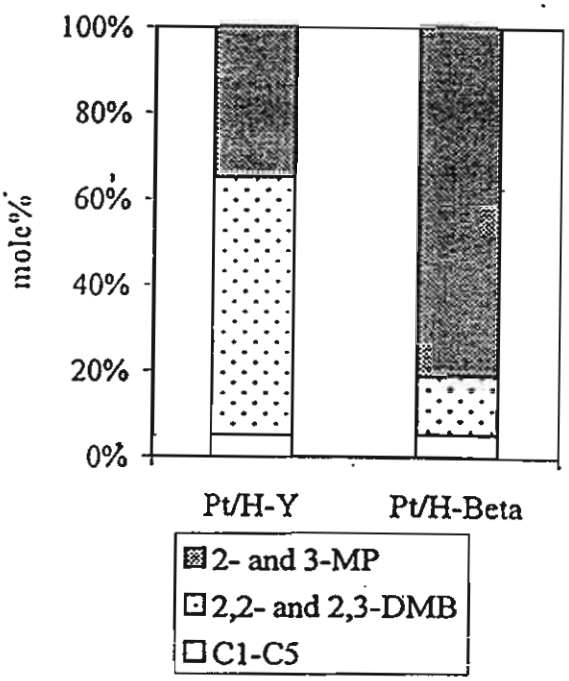

Fig.6 Product distribution of n-hexane isomerization on Pt/H-Y and Pt/H-Beta.

similar pore size and shape with the average pore diameters of 15.69 Å for Pt/H-Beta and 15.57 Å for Pt/H-Y [6,7]. To gain further insight, the pyridine adsorption technique on in-situ FTIR was adopted for the assessment of Brönsted and Lewis acidities. The bands at about 1540 cm^{-1} and 1450 cm^{-1}(not shown here) were reportedly assigned to pyridine adsorbed on Brönsted and Lewis acid sites, respectively [8,9,10]. The Brönsted and Lewis acid site concentrations, defined as A_B and A_L, of H-

Beta and H-Y were determined by measurement of peak areas of these bands at the reference temperature of 150°C while the relative acid strengths of Brönsted and Lewis types were determined by measurement of the temperature required for reduce a half of pyridine adsorbed, defined as $T_{B/2}$ and $T_{L/2}$, respectively. Thus, the higher temperature means the stronger acid strength. As shown in Table 1, H-Beta zeolite contains smaller amount of acid sites but stronger acid strengths than H-Y. Therefore, though the selectivities for C_6 isomers obtained on both catalysts were almost the same due to their similar pore size and shape, the stronger acidities possessed by Pt/H-Beta should be responsible for the higher n-hexane conversion.

Table 1: Brönsted and Lewis acidities on H-Beta and H-Y catalysts

Catalyst	A_B	A_L	$T_{B/2}$(°C)	$T_{L/2}$ (°C)
H-Beta	150.9	106.3	434.5	247.1
H-Y	206.0	287.4	369.3	156.3

CONCLUSIONS

Beta zeolite has been found to be a promising catalyst for n-hexane isomerization. The products obtained include 2,2-Dimethylbutane(2,2-DMB); 2,3-Dimethylbutane (2,3-DMB); 2-Methylpentane (2-MP); and 3-Methylpentane (3-MP). The optimum catalyst composition was zeolite Beta with Si/Al ratio of 40 loaded with 0.6 wt% of Pt by ion-exchange. The optimum reaction conditions were as follows: reaction temperature of 250°C; GHSV of 1600 h^{-1} with the presence of H_2.

ACKNOWLEDGEMENT

This research has been partly supported by the Thailand Research Fund (TRF). The authors would like to express their deep appreciation herein.

REFERENCES

1. R. L. Wadlinger, G. T. Keer, and E. J. Rosinski, US. Patent 3308069 (1967).
2. J. Perez-Pariente and E. Sastre: *Appl. Catal.*, **69**, 125 (1991).
3. P. Ratnasamy, R.N. Bhat, S.K. Pokhrrigal, S.G. Hegde, and R. Kumar: *J. Catal.*, 65, 199 (1989).
4. C. Marcilly, J. Deves, and F. Raatz, Eur. Pat. Appl., EP 278839 (1988).
5. M.J. Climent, A. Corma, H. Garcia, S. Iborra, and J. Primo, Heterogeneous Catalysis and Fine Chemicals II, *Studies in Surface Science and Catalysis*, **59**, 557 (1991).
6. Li-Jen Leu, L.Y. Hou, and B.C. Kang: *Appl. Catal.*, **69**, 49 (1991).
7. L. Beranek and M. Kraus, Comprehensive Chemical Kinetics (C.H., Banford and C.F.H., Tipper, eds.), VI. 20, Chapter 3, Elsevier, New York (1978).
8. J. Connerton, R. Joyner, and M. Padley: *J.C.S. Faraday*, **91**, 1841 (1995).
9. M. Campbell, M. Bibby, M. Coddington, F. Howe, and H. Meinhold: *J. Catal.*, **161**, 358 (1996).
10. H.G. Karge: *Microporous Materials*, **22**, 547 (1998).